Title
Role of IFN-beta in disease and characterization of the immune response following acute radiation exposure

Author
Boxx, Gayle

Publication Date
2016

Peer reviewed|Thesis/dissertation

UNIVERSITY OF CALIFORNIA

Los Angeles

Role of IFN-beta in disease and characterization of the immune response following acute radiation exposure

A dissertation submitted in partial satisfaction of the requirements for the degree Doctor of Philosophy in Microbiology, Immunology, and Molecular Genetics

by

Gayle Marie Boxx

2016

ABSTRACT OF THE DISSERTATION

Role of IFN-beta in disease and characterization of the immune response following acute radiation exposure

By

Gayle Marie Boxx

Doctor of Philosophy in Microbiology, Immunology, and Molecular Genetics

University of California, Los Angeles, 2016

Professor Genhong Cheng, Chair

Type I interferons (IFNs) are a group of pleiotropic of cytokines well known for their role in promoting an antiviral state through the induction of interferon stimulated genes (ISGs). Pathogen associated molecular patterns (PAMPs) expressed by bacteria such as lipid A induce type I IFNs. In macrophages we found induction by ISGs by lipid A was highly dependent on the signaling by the IFNβ subtype. Furthermore, IFNβ was required to positively regulate the feedback loop for induction of downstream ISGs. Identification of this major role led us to investigate the functional consequence of IFNβ signaling in two different bacterial infections. Both macrophages and IFNAR signaling are necessary to promote host defense against *Escherchia coli* peritonitis, however we found survival of *Ifnb*-/- mice was not drastically reduced. Next, we studied the role of IFNβ during post-influenza pneumonia since previous studies from our lab showed IFNAR signaling enhanced host susceptibility. We found IFNβ deficiency was not sufficient to protect the host from bacterial pneumonia. The results from both models led us to conclude additional subtypes of type I IFN must be cooperating with IFNβ to either promote host resistance or susceptibility.

To study the role of ISGs and IFNAR signaling in non-infectious disease we focused on three different models. In the first we examined the role of the interferon inducible protein,

CXCL10 in the progression of LPS induced endotoxic shock. We found CXCL10 deficiency increased survival of female mice, not males. Moreover, CXCL10 likely mediated its pathogenic effects by signaling through the canonical receptor CXCR3. In the second model, we studied the role of poly I:C induced type I IFN on the progression of chronic experimental autoimmune encephalitis (EAE), a mouse model of human multiple sclerosis. We found poly I:C transiently attenuated symptoms of EAE by signaling through toll like receptor 3 (TLR3) to induce type I IFNs. Finally, we measured the induction and expression of type I IFNs and ISGs in the mouse model of tuberous sclerosis complex disorder. Our results demonstrate *Tsc2*+/- mice express elevated levels of type I IFNs and ISGs following poly I:C treatment. This result points to a possible mechanism for the increased incident of neuropsychiatric disease in TSC haploinsufficient patients.

Finally, we monitored survival of mice treated with lethal doses of whole body irradiation to characterize response during acute radiation syndrome (ARS) and delayed effects of acute radiation syndrome (DEARE). We found both PAMPs and select small molecules were able to either protect or rescue mice from ARS. Among mice that survived ARS and were monitored for one year, we noticed specific symptoms were correlated with the type of radiomitigator administered during ARS. Moreover, we observed mice that were likely to die or develop disease had higher concentrations of serum cytokines, and gut microbial dysbiosis. Immunological challenge revealed disparities between mice, but also suggested that more comprehensive studies may lead to the development of biomarkers that will be useful to predict response to future vaccination or disease.

The dissertation of Gayle Marie Boxx is approved.

Peter J. Bradley

Robert L. Modlin

William H. McBride

Genhong Cheng, Committee Chair

UNIVERSITY OF CALIFORNIA, Los Angeles

2016

DEDICATION

To my family, especially my parents,

for their steadfast encouragement and loving support.

TABLE OF CONTENTS

LIST OF FIGURES AND TABLES

CHAPTER 3

CHAPTER 4

CHAPTER 5

ACKNOWLEDGEMENTS

I would like to thank my mentor, Dr. Genhong Cheng, for accepting me into his lab and for giving me the opportunity to work on so many different projects. Over the years, Genhong encouraged me to participate in the preparation of grants, progress reports and other writings, and I am grateful to have such a wealth of writing experience.

I would also like to thank members of my committee: Dr. Peter Bradley for his support and help with strategic planning of my graduate career, Dr. Robert Modlin for his advice and comments on my work and Dr. William McBride for his caring mentorship as both my committee member and as a collaborator. Thanks also to Dr. Kathleen Kelly who served briefly on my committee and as my mentor during my first rotation at UCLA.

My sincere gratitude to the members of the Cheng lab. I am especially grateful to Maxime Chapon who has been an amazing colleague to work with; always willing to discuss science, help out with big mouse experiments, or share a pot of coffee. Many thanks to Anna Reichardt for her encouragement, thoughtfulness and friendship. Thanks to Dr. Elisa Deriu, I sincerely enjoyed our collaboration and I look forward to working with her in the future. Much appreciation to Dr. Roghiyari (Saba) Aliyari for all of her efforts to keep the lab running efficiently. Also a big thanks to Drs. Kislay Parvatiyar, Jose Pindado Rodriguez, Natalie Quanquin, Shankar Iyer, Su-Yang Liu, Paul Dempsey for helpful discussions and comments. Thanks to Chinese visiting scholars and collaborators Drs. Zhengtao Hu, Aiping Wu and Daihai Zheng for their sharing their knowledge and insights.

I am also very thankful for the support from my collaborators. Thanks to Dr. Jane Deng and her team, Wing Lung and Cherise (Meyerson) Isserman for their help setting up the lung infection models. Thanks to the members of the Center for Medical Countermeasures against Radiation (CMCR) at ULCA especially Dr. Ewa Micewicz, Dr. Dorthe Schaue, Dr. Robert

Damoiseaux, and Josephine Ratikan. I am grateful to Dr. Manuel Lopez Aranda from Dr. Alcino Silva's lab for inviting me to work on the Tsc2 project.

Thanks also to all of my friends, colleagues, instructors and classmates at UCLA.

Finally, I am immensely thankful to Dr. Jan Mrazek who has been a close friend and colleague during my career at UCLA. His passion for science is infectious and it has led me to strike out on a new path into the world of business. I look forward to navigating the biotech world with him.

My work at UCLA would not have been possible without the amazing support staff. I am especially grateful for William Cage, Kayla Lynch, Lorena Cervantes, Tim March, Karla Perez, and Aulani Navarro-King from DLAM and to Bridget Wells and Weiling Chen from MIMG.

I would also like to acknowledge my funding: the Eugene V. Cota-Robles Fellowship for financial support during my first and fourth year, and the Microbial Pathogenesis Training Grant (5T32AI007323) for support during my second and third year.

I acknowledge the permission from Elsevier to reprint Gayle M. Boxx and Genhong Cheng. The Roles of Type I Interferon in Bacterial Infection. Cell Host & Microbe 2016 Jun 8; 19(6): 760-769 as Chapter 2 of my dissertation, and to reprint Ye Zhu,Janina Jiang,Najwane Said-Sadier,Gale Boxx,Cheryl Champion,Ashley Tetlow,Valerie A. Kickhoefer,Leonard H. Rome,David M. Ojcius,Kathleen A. Kelly. Activation of the NLRP3 inflammasome by vault nanoparticles expressing a chlamydial epitope. 2015 Jan 3; 33(2): 298-306 as Appendix A. I acknowledge permission granted by the Creative Commons Attribution (CC BY) license to reprint Deriu, Elisa, Boxx, Gayle M, He, Xuesong, Pan, Calvin, Benavidez, Sammy David, Cen, Lujia, Rozengurt, Nora, Shi, Wenyuan, and Cheng, Genhong. Influenza Virus Affects Intestinal Microbiota and Secondary Salmonella Infection in the Gut through Type I Interferons. 2016 May 5; 12(5): e1005572 as Appendix B.

BIOGRAPHICAL SKETCH

EDUCATION

9/2010 to present	University of California Los Angeles, Los Angeles, CA Ph.D., Microbiology, Immunology and Molecular Genetics
8/2003 to 5/2005	California State University Long Beach, Long Beach, CA M.S., Microbiology
8/1999 to 8/2003	California State University Chico, Chico, CA B.S, Biological Sciences, minor in Chemistry

RESEARCH EXPERIENCE

9/2010 to present	Genhong Cheng, University of California Long Beach, Los Angeles, CA Graduate Student Researcher Researcher
6/2005 to 8/2010	Mason Zhang, California State University Long Beach, Long Beach, CA Research Associate
8/2003 to 5/2005	Mason Zhang, California State University Long Beach, Long Beach, CA Graduate Student Researcher
9/2002 to 5/2003	Gordon Wolfe, California State University Chico, Chico, CA Undergraduate Student Researcher

PUBLICATIONS

1. Gayle M. Boxx and Genhong Cheng. 2016. The Roles of Type I Interferon in Bacterial Infection. Cell Host and Microbe 19, June 8. http://dx.doi.org/10.1016/j.chom.2016.05.016

2. Deriu Elisa, Gayle M. Boxx, Xuesong He, Calvin Pan, Sammy David Benavidez, Lujia Cen, Nora Rozengurt, Wenyuan Shi, Genhong Cheng. 2016. Influenza Virus Affects Intestinal Microbiota and Secondary Salmonella Infection in the Gut through Type I Interferons. Plos Pathogens. 12(5):e1005572.

3. Nishiya, C.T., Boxx G.M., Robison, K., Itatani, C., Kozel, T.R., Zhang, M.X. 2016. Influence of IgG Subclass on Human Antimannan Antibody-Mediated Resistance to Hematogenously Disseminated Candidiasis in Mice. Infection and Immunity. 84(2):386-94.

4. Zhu, Y., Jiang, J., Said-sadier, N., Boxx, G., Champion, C., Tetlow, A., Kelly, K.A. 2014. Activation of the NLRP3 inflammasome by vault nanoparticles expressing a chlamydial epitope. Vaccine, 33(2), 298–306.

5. Peltz, G., Zaas, A.K., Zheng, M., Solis, N.V., Zhang, M.X., Liu, H.H., Hu Y., Boxx, G.M., Phan, Q.T., Dill, D., Filler, S.G. 2011. Next-generation computational genetic analysis:

multiple complement alleles control survival after Candida albicans infection. Infection and Immunity. 79, 4472-4479.

6. Boxx, G.M., C.T Nishiya, T.R. Kozel, M.X. Zhang. 2010. Influence of mannan and glucan on complement activation and C3 binding by Candida albicans. Infection and Immunity. 78, 1250-1259.

7. Boxx, G.M., C.T. Nishiya, T.R. Kozel, M.X. Zhang. 2009. Characteristics of Fc-independent human antimannan antibody-mediated alternative pathway initiation of C3 deposition to Candida albicans. Molecular Immunology. 46, 473-480.

POSTERS

1. Gayle Boxx, Maxime Chapon, Ewa Micewicz, William McBride, and Genhong Cheng. 2014. Long term effects of radiation exposure on immune response to challenge. CMCR Workshop II: Mitigation and Treatment of Radiation Injury, Baltimore, MD.

2. Danilova, Nadia, Qinghua Zhang, Gayle Boxx, Genhong Cheng, and Shuo Lin. 2013. Zebrafish model for the evaluation and mechanistic studies of radio-mitigators. CMCR & RITN Workshop – Mitigation and Treatment of Radiation Injury, Baltimore, MD.

3. Zhu, Y., Champion, C., Said-Sadier, N., Boxx, G., Jiang, J., Tetlow, A., Kickhoefer,V., Rome, L.H., Ojcius, D.M., Kelly, K.A. 2013. Activation of the NLRP3 inflammasome by vault nanoparticles expressing a chlamydial epitope. 6th Biennial Meeting of the Chlamydia Basic Research Society, San Antonio, TX.

4. Boxx, G., N. Madfis, D. M. Ojcius, K.A. Kelly. 2011. Vault nanoparticles activate inflammasome formation by lysosome destabilization. 5th Biennial Meeting of the Chlamydia Basic Research Society, Redondo Beach, CA.

5. Liao, W. G.M. Boxx, M. Engevik, K. Ambert, G. Lee, MX Zhang. 2010. β-1,2-linked mannotriose is the epitope for the protective human recombinant antimannan antibody M1g1 and is reactive with natural antimannan antibody. 110th General Meeting of the American Society for Microbiology, San Diego, CA.

6. Johnson, N., G. Boxx, V. Perry, K. Robison, M. Zhang. 2010. Characteristics of complement activation and C3 binding by non-albicans Candida species. 110th General Meeting of the American Society for Microbiology, San Diego, CA.

7. Boxx, G.M., S.J. Chaves, T.R. Kozel, M.X. Zhang. 2005. Influence of subclass specificity on antimannan IgG antibody-mediated complement activation by Candida albicans. 105th General Meeting of the American Society for Microbiology, Atlanta, GA

CHAPTER 1

Introduction

Early detection of pathogens by the host innate immune cells is accomplished through the expression of pattern recognition receptors (PRRs), including membrane bound Toll-like receptors (TLRs) and cytosolic sensors. PRRs bind conserved pathogen associated molecular patterns (PAMPs). Ligation triggers signaling cascades that culminate in the expression of primary response genes that regulate the host anti-microbial, inflammatory, and immunoregulatory response [1,2].

Type I IFN is a group of closely related pleiotropic cytokines that are induced by PRR stimulation. In mice, there are a dozen IFNα subtypes, and a single IFNβ, IFNε, IFNκ, IFNδ, IFNτ, IFNω and IFNζ [3,4]. All type I IFNs bind and signal through the interferon alpha receptor heterodimeric complex (IFNAR), composed of IFNAR1 and IFNAR2. IFNAR ligation activates the JAK/STAT pathway. Activation by phosphorylation and oligomerization of different STAT transcription factor complexes induce a set of genes collectively known as interferon stimulated genes (ISGs). Many ISGs code for proteins that defend the host against viral infection, but several ISGs have a significant role in other microbial infections, cancer and autoimmune disease.

Type I IFN subtypes induce distinct and overlapping gene expression. Induction of specific subtypes is influenced by the transcription factors constitutively expressed by the cell type and the location and nature of the stimulating PAMP [5,6]. In most cells, including macrophages, the transcription factor interferon regulatory factor 3 (IRF3) is constitutively expressed and preferentially promotes IFNβ transcription [7,8]. In some cases, IFNα4, the only IFNα with a complete IRF3 binding site, may also be transcribed [9]. In specific cell types, such as plasmacytoid dendritic cells, expression of IFNαs is favored due to the constitutive expression of IRF7 [10]. PRR sensing also affects which subtype is induced. TLRs are more abundantly expressed by immune cells and surveil the extracellular and endocytic environments, whereas cytosolic sensors are more ubiquitously expressed, but surveil only the cytosol.

Macrophages are central to the innate immune response. Some macrophages are resident in the tissue, while others are recruited along with neutrophils, natural killer cells, dendritic cells and others to the sites of infection or damage. Early signaling by macrophages shapes the immune response. IFNβ is one of the primary response genes expressed by macrophages following stimulation with lipopolysaccharide (LPS) [1,11], a PAMP found on the cell wall of Gram negative bacteria that is recognized by TLR4 [11]. TLR4 ligation activates two downstream adapters, MyD88 and TRIF, and it is through the TRIF dependent pathway [12] leading to IRF3 activation that *Ifnb* is transcribed [13]. IFNβ signals in an autocrine and paracrine fashion.

Role of type I IFNs in infectious disease

Type I IFNs were first discovered by Isaacs and Lindenmann, as anti-viral factors[14]. A functional role for type I IFNs during bacterial infections was later observed with *Listeria monocytogenes*, where IFNAR1 signaling was found to enhance host susceptibility by suppressing anti-bacterial genes and inducing cell death and tissue damage [15–17]. A brief overview of relevant microbial diseases is discussed below with particular emphasis on the role of IFNβ; a thorough review of type I IFNs during bacterial infections is discussed in **Chapter 2**.

Type I IFNs are observed to execute distinct roles during viral [18] and bacterial infections. IFNβ signaling during chronic viral infection with lymphocytic choriomeningitis virus (LCMV) propagates excessive tissue damage, whereas IFNα does not [19]. Similarly, IFNβ signaling during bacterial infection with *Salmonella enterica* serovar Typhimurium [20], induces host cell death. The specific contribution of IFNβ signaling to the host response against other microbial infections, especially during infections where IFNAR signaling has been shown to play a role, is unknown.

The Gram negative bacterium, *Escherichia coli* (*E. coli*) is the most often recovered bacterial species in septic patients [21]. Deficiency in IFNAR1 [22] or IL-10, an anti-inflammatory

cytokine, increases mortality [23], whereas deficiency in TLR4 or MyD88 [24] protects mice against lethal *E. coli* sepsis. Increased survival is associated with decreased production of inflammatory cytokines, such as TNFα and IL-6 [24] by macrophages [25], likely through production of IL-10 [26] by other innate cells, such as neutrophils [27]. While it is clear IFNAR signaling promotes host resistance, it is not known whether protection is mediated solely by IFNβ or in concert with additional type I IFNs.

IFNAR signaling, in particular IFNβ signaling [28], promotes host resistance to lung infections by the bacterium *Streptococcus pneumoniae* [28,29]. However, prior lung infection by influenza turns IFNAR signaling pathogenic and promotes bacterial superinfection [30,31]. One mechanism may be through the induction of type I IFNs by alveolar macrophages during influenza infection [32] that upregulates the histone modifying protein Setdb2, a lysine methyltransferase, known to negatively regulate the expression of chemokines, KC and MIP2[2,33]. These chemokines recruit myeloid cells that are critical to bacterial clearance [30]. It is unclear whether IFNβ signaling during co-infection suppresses their expression or whether other type I IFN subtypes are involved.

Role of type I IFNs in non-infectious disease

The immune system evolved to combat replicating pathogens, but immune activation by PAMPs also shapes the development and progression of non-infectious disease, including autoimmune disease. Type I IFNs have been observed to have acute and long term effects on tissue architecture and function. Shortly after their discovery, an ameliorating role for type I IFNs in non-infectious disease was noted and type I IFNs were incorporated into therapeutic treatments for cancer [34] and the autoimmune disease, multiple sclerosis [35]. Here, the role of type I IFNs in three distinct models of non-infectious disease are discussed.

Endotoxic shock

The first model is that of LPS induced endotoxic shock. This model is often used to complement studies of bacterial sepsis and septic shock; yet, there is a striking dichotomy in how the host responds to LPS and to bacterial sepsis. IFNAR signaling during *E. coli* infection [22] or polymicrobial sepsis [36] promotes host defense, but in the mouse model of LPS induced endotoxic shock, signaling by IFNβ through the IFNAR1-TYK2 axis is lethal [36–38]. In both models, the ISG and anti-inflammatory cytokine, IL-10, is necessary for survival [23,39], however the ISGs driving pathogenesis are poorly defined. A possible mechanism by which IFNβ signaling leads to mortality is through CXCL10, a chemokine induced by IFNs. During polymicrobial sepsis treatment with the CXCL10 is sufficient to restore host resistance. Given IFNAR signaling plays opposite roles in bacterial sepsis and endotoxic shock, we investigated whether CXCL10 would also play an opposite role whereby its deficiency would improve survival or completely protect the host from LPS induced endotoxic shock.

Multiple sclerosis/Experimental autoimmune encephalitis

The second model is experimental autoimmune encephalitis (EAE), the mouse model of the autoimmune disease multiple sclerosis (MS). MS is an inflammatory autoimmune disease, driven by T cells, that damages the myelin sheath that coats the neurons of the central nervous system. Most patients experience alternating periods of symptoms and dormancy, classified as relapsing-remitting MS, but some develop secondary progressive MS which is defined by chronic and persistent symptoms. Most frequently occurring in females [40], MS typically affects people in young adulthood (20 to 40s) [41]. While infection may be trigger for MS, a definite cause is unknown; however, a similar disease, EAE, may be induced by immunizing mice with a mixture of a myelin sheath peptide and Complete Freund's adjuvant. Active or passive immunization of SJL/J mice results in RRMS-like EAE, whereas the same immunization given to C57Bl/6 mice leads to progressive EAE [42].

Treatment of MS includes corticosteroids to reduce inflammation and type I interferons or other drugs that modify the adaptive immune response [43]. In some cases, IFNβ plays a beneficial role in both MS and EAE. In MS patients, recombinant IFNβ has been used to treat patients with RRMS with a success rate of 30% [35]. In the EAE model, mice deficient in IFNβ [44] or its receptor, IFNAR exhibit exacerbated symptoms [45].

Endogenous IFNβ is produced following stimulation of membrane bound endocytic receptors, TLR3 and TLR4, and the cytosolic receptors, RIG-I and MDA5. Intraperitoneal administration of the TLR3/RIG-I ligand, poly I:C, reduces the symptoms of relapsing-remitting EAE [46]. Moreover, deletion of TRIF, the downstream adapter for TLR3 and TLR4, leads to more severe progressive EAE symptoms [45]. Deletion of TLR4, however, does not affect progressive EAE [47], however stimulation of TLR4 expressing CD4+ T cells and γδ T cells appears to contribute to disease onset and progression [48].

Previously, our lab found IFNAR signaling in macrophages suppressed Th17, and thereby reduced the severity of chronic EAE [45]. However, whether IFNAR signaling induced by treatment with the RNA ligand poly I:C attenuates chronic EAE is unknown. Furthermore, it is unclear whether which PRR is responsible for the induction of type I IFNs.

Autism

The final model focuses on the tuberous sclerosis complex (TSC) disorder. In humans, tuberous sclerosis results from a heterozygous autosomal dominant genetic mutation in either TSC1/TSC2 [49] and is strongly linked to the development of neuropsychiatric syndromes including autism spectrum disorder [50]. The TSC1/TSC2 complex negatively regulates the mammalian target of rapamycin (mTOR) pathway [51]. Though ubiquitously expressed among cells during early development, expression decreases in all adult tissues organs except for the brain [52].

Innate immune pathways and mTOR signaling are intimately linked; mTOR signaling augments the type I IFN pathway. Expression of interferon induced proteins, CXCL10 and ISG15, requires mTOR mediated deactivation of the translational repressor 4E-BP-1 [53]. In addition, rapamycin, a chemical inhibitor of the mTOR pathway that acts by destabilizing the mTORC1 complex [54], also inhibits plasmacytoid dendritic cells from transcribing type I IFN by preventing IRF7 activation and translocation [55]. Furthermore, deficiency in TSC1 or TSC2 licenses translation of CXCL10 and ISG15 [53], while transfection TSC1 deficient macrophages with poly I:C enhances the transcription of *Ifna* [56].

Clinically, there is a significant correlation between peak influenza season, late stage pregnancy, and the development of autism spectrum disorder in TSC haploinsufficient individuals. Modeling this maternal immune activation in *Tsc2*+/- mice reveaed that poly I:C treatment during pregnancy increased the likelihood of fetal abortion or lifelong social interaction deficiencies in the surviving pups [57]. The mechanism by which viral infection or poly I:C treatment induces neuropsychiatric symptoms is unknown, but recent, unpublished experiments IFNAR signaling is required for pathogenesis.

Irradiation and the immune response

At the population level, exposure to a lethal dose of radiation, results in two major waves of death. The first wave, called acute radiation syndrome (ARS), is due to hematopoietic failure and it occurs within the first 30 days of exposure. The second wave, called delayed effects of acute radiation exposure (DEARE), arises about 100 days after irradiation and is likely due to inflammation-mediated multiple organ dysfunction syndrome (MODS).

Symptoms of ARS includes failure of the hematopoietic, gastrointestinal and nervous systems and is caused by cell death from DNA damage. Increased cytokine expression following irradiation has been observed [58]. Interestingly, treatment with PAMPs, such as LPS, is radioprotective when administered prior to or immediately after irradiation [59]. Similarly, pre-

treatment with proinflammatory cytokines, IL-1 or TNFα [60], or granulocyte colony stimulating factor (G-CSF) [61] are also protective. Macrophages are key mediators of radioprotection as depletion reduces the level LPS induced IL-1β and TNFα rendering the host susceptible to ARS [25]. This suggests pathways leading to IL-1β and TNFα are important for radioprotection.

The Center for Medical Countermeasures against Radiation (CMCR) at UCLA is studying serveral radiomitgators that, when administered 24 hr after whole body irradiation (WBI), rescue mice from ARS. The lead radiomitigators include, 512, a compound identified that contains a 4-nitrophenylsulfonamide group, was identified from a high throughput screen [62] and granulocyte colony stimulating factor (G-CSF), a cytokine routinely used to treat chemotherapy induced neutropenia [63]. Both mitigators rescue mice from ARS, however little is known about health status of rescued mice in the months following ARS and whether mitigator treatment affects DEARE.

In other disease models, prior tissue damage can have lasting effects on the host that range from the formation of immunological memory to accelerate response to compromised organ function due to tissue remodeling. Survivors of whole body irradiation (WBI) have delayed and late effects of radiation damage that can manifest as cardiac and/or pulmonary toxicity [64]. A better understanding of DEARE will lead to the identification of biomarkers and better predict immune response to future vaccinations and disease.

Conclusion

Together each disease model provides insight into how the immune system orchestrates the response and resolution phases. Studies of the early immune activation foreshadow formation of immunological memory and scars that affect how the host deals with future threats. Experiments presented in the following dissertation strive to illuminate poorly understood roles and mechanisms, especially those contributed by type I IFNs.

REFERENCES

1. Tong, A. *et al.* A Stringent Systems Approach Uncovers Gene-Specific Mechanisms Regulating Inflammation. *Cell* **165,** 165–79 (2016).

2. Kroetz, D. N. *et al.* Type I Interferon Induced Epigenetic Regulation of Macrophages Suppresses Innate and Adaptive Immunity in Acute Respiratory Viral Infection. *PLoS Pathog.* **11,** 1–25 (2015).

3. Pestka, S., Krause, C. D. & Walter, M. R. Interferons, interferon-like cytokines, and their receptors. *Immunol. Rev.* **202,** 8–32 (2004).

4. Boxx, G. M. & Cheng, G. The Roles of Type I Interferon in Bacterial Infection. *Cell Host Microbe* **19,** 760–769 (2016).

5. Gao, J. J. *et al.* Bacterial LPS and CpG DNA differentially induce gene expression profiles in mouse macrophages. *J. Endotoxin Res.* **9,** 237–43 (2003).

6. Salkowski, C. A., Detore, G. R. & Vogel, S. N. Lipopolysaccharide and monophosphoryl lipid A differentially regulate interleukin-12 , gamma interferon , and interleukin-10 mRNA production in murine macrophages . Lipopolysaccharide and Monophosphoryl Lipid A Differentially Regulate Interleukin-12 , Gam. (1997).

7. Sakaguchi, S. *et al.* Essential role of IRF-3 in lipopolysaccharide-induced interferon-β gene expression and endotoxin shock. *Biochem. Biophys. Res. Commun.* **306,** 860–866 (2003).

8. Honda, K., Takaoka, A. & Taniguchi, T. Type I Inteferon Gene Induction by the Interferon Regulatory Factor Family of Transcription Factors. *Immunity* **25,** 349–360 (2006).

9. van Pesch, V., Lanaya, H., Renauld, J.-C. & Michiels, T. Characterization of the murine alpha interferon gene family. *J. Virol.* **78,** 8219–8228 (2004).

10. Kawai, T. *et al.* Interferon-alpha induction through Toll-like receptors involves a direct interaction of IRF7 with MyD88 and TRAF6. *Nat. Immunol.* **5,** 1061–1068 (2004).

11. Sing, A. *et al.* Bacterial induction of beta interferon in mice is a function of the lipopolysaccharide component. *Infect. Immun.* **68,** 1600–1607 (2000).

12. Yamamoto, M., Sato, S. & Hemmi, H. Role of Adaptor TRIF in the. *Science (80-.).* **301,** 640–643 (2003).

13. Doyle, S. *et al.* IRF3 mediates a TLR3/TLR4-specific antiviral gene program. *Immunity* **17,** 251–63 (2002).

14. Isaccs, A. & Lindenmann, J. Virus interference. I. The interferon. *Proc. R. Soc. Lond. B. Biol. Sci.* (1957).

15. O'Connell, R. M. *et al.* Type I interferon production enhances susceptibility to Listeria monocytogenes infection. *J. Exp. Med.* **200,** 437–45 (2004).

16. Carrero, J. a, Calderon, B. & Unanue, E. R. Type I interferon sensitizes lymphocytes to apoptosis and reduces resistance to Listeria infection. *J. Exp. Med.* **200,** 535–540 (2004).

17. Auerbuch, V., Brockstedt, D. G., Meyer-Morse, N., O'Riordan, M. & Portnoy, D. a. Mice lacking the type I interferon receptor are resistant to Listeria monocytogenes. *J. Exp.*

Med. **200,** 527–533 (2004).

18. Sheehan, K. C. F., Lazear, H. M., Diamond, M. S. & Schreiber, R. D. Selective Blockade of Interferon-α and -β Reveals Their Non-Redundant Functions in a Mouse Model of West Nile Virus Infection. *PLoS One* **10,** e0128636 (2015).

19. Ng, C. T. *et al.* Blockade of interferon Beta, but not interferon alpha, signaling controls persistent viral infection. *Cell Host Microbe* **17,** 653–61 (2015).

20. Robinson, N. *et al.* Type I interferon induces necroptosis in macrophages during infection with Salmonella enterica serovar Typhimurium. *Nat. Immunol.* **13,** 954–62 (2012).

21. Holzheimer, R. G., Muhrer, K. H., L'Allemand, N., Schmidt, T. & Henneking, K. Intraabdominal infections: classification, mortality, scoring and pathophysiology. *Infection* **19,** 447–52 (1991).

22. Mancuso, G. *et al.* Type I IFN Signaling Is Crucial for Host Resistance against Different Species of Pathogenic Bacteria. *J. Immunol.* **178,** 3126–3133 (2007).

23. Sewnath, M. E. *et al.* IL-10-deficient mice demonstrate multiple organ failure and increased mortality during Escherichia coli peritonitis despite an accelerated bacterial clearance. *J. Immunol.* **166,** 6323–31 (2001).

24. Roger, T. *et al.* Protection from lethal gram-negative bacterial sepsis by targeting Toll-like receptor 4. *Proc. Natl. Acad. Sci. U. S. A.* **106,** 2348–52 (2009).

25. Salkowski, C. a *et al.* Effect of liposome-mediated macrophage depletion on LPS-induced cytokine gene expression and radioprotection. *J. Immunol.* **155,** 3168–79 (1995).

26. Fiorentino, D. F., Zlotnik, A., Mosmann, T. R., Howard, M. & O'Garra, A. IL-10 inhibits cytokine production by activated macrophages. *J. Immunol.* **147,** 3815–22 (1991).

27. Ocuin, L. M. *et al.* Neutrophil IL-10 suppresses peritoneal inflammatory monocytes during polymicrobial sepsis. *J. Leukoc. Biol.* **89,** 423–432 (2011).

28. LeMessurier, K. S., Häcker, H., Chi, L., Tuomanen, E. & Redecke, V. Type I interferon protects against pneumococcal invasive disease by inhibiting bacterial transmigration across the lung. *PLoS Pathog.* **9,** e1003727 (2013).

29. Parker, D. *et al.* Streptococcus pneumoniae DNA initiates type I interferon signaling in the respiratory tract. *MBio* **2,** e00016–11 (2011).

30. Shahangian, A. *et al.* Type I IFNs mediate development of postinfluenza bacterial pneumonia in mice. *J. Clin. Invest.* **119,** 1910–20 (2009).

31. Cao, J. *et al.* Activation of IL-27 signalling promotes development of postinfluenza pneumococcal pneumonia. *EMBO Mol. Med.* **6,** 120–140 (2014).

32. Kumagai, Y. *et al.* Alveolar Macrophages Are the Primary Interferon-α Producer in Pulmonary Infection with RNA Viruses. *Immunity* **27,** 240–252 (2007).

33. Schliehe, C. *et al.* The methyltransferase Setdb2 mediates virus-induced susceptibility to bacterial superinfection. *Nat. Immunol.* **16,** 67–74 (2015).

34. Antonelli, G., Scagnolari, C., Moschella, F. & Proietti, E. Twenty-five years of type I interferon-based treatment: a critical analysis of its therapeutic use. *Cytokine Growth*

Factor Rev. **26,** 121–31 (2015).

35. Interferon beta-1b is effective in relapsing-remitting multiple sclerosis. I. Clinical results of a multicenter, randomized, double-blind, placebo-controlled trial. The IFNB Multiple Sclerosis Study Group. *Neurology* **43,** 655–61 (1993).

36. Kelly-Scumpia, K. M. *et al.* Type I interferon signaling in hematopoietic cells is required for survival in mouse polymicrobial sepsis by regulating CXCL10. *J. Exp. Med.* **207,** 319–26 (2010).

37. Karaghiosoff, M. *et al.* Central role for type I interferons and Tyk2 in lipopolysaccharide-induced endotoxin shock. *Nat. Immunol.* **4,** 471–7 (2003).

38. de Weerd, N. a *et al.* Structural basis of a unique interferon-β signaling axis mediated via the receptor IFNAR1. *Nat. Immunol.* 1–9 (2013). doi:10.1038/ni.2667

39. Berg, D. J. *et al.* Interleukin-10 is a central regulator of the response to LPS in murine models of endotoxic shock and the Shwartzman reaction but not endotoxin tolerance. *J. Clin. Invest.* **96,** 2339–2347 (1995).

40. Whitacre, C. C., Reingold, S. C. & O'Looney, P. A. A gender gap in autoimmunity. *Science* **283,** 1277–8 (1999).

41. Mayr, W. T. Incidence and prevalence of multiple sclerosis in Olmsted County, Minnesota, 1985-2000. *Neurology* **61,** 1373–1377 (2003).

42. McCarthy, D. P., Richards, M. H. & Miller, S. D. Mouse models of multiple sclerosis: experimental autoimmune encephalomyelitis and Theiler's virus-induced demyelinating disease. *Methods Mol. Biol.* **900,** 381–401 (2012).

43. Damal, K., Stoker, E. & Foley, J. F. Optimizing therapeutics in the management of patients with multiple sclerosis: a review of drug efficacy, dosing, and mechanisms of action. *Biologics* **7,** 247–258 (2013).

44. Teige, I. *et al.* IFN-beta gene deletion leads to augmented and chronic demyelinating experimental autoimmune encephalomyelitis. *J. Immunol.* **170,** 4776–84 (2003).

45. Guo, B., Chang, E. Y. & Cheng, G. The type I IFN induction pathway constrains Th17-mediated autoimmune inflammation in mice. *J. Clin. Invest.* **118,** 1680–90 (2008).

46. Touil, T., Fitzgerald, D., Zhang, G.-X., Rostami, A. & Gran, B. Cutting Edge: TLR3 stimulation suppresses experimental autoimmune encephalomyelitis by inducing endogenous IFN-beta. *J. Immunol.* **177,** 7505–9 (2006).

47. Miranda-Hernandez, S. *et al.* Role for MyD88, TLR2 and TLR9 but not TLR1, TLR4 or TLR6 in experimental autoimmune encephalomyelitis. *J. Immunol.* **187,** 791–804 (2011).

48. Reynolds, J. M., Martinez, G. J., Chung, Y. & Dong, C. Toll-like receptor 4 signaling in T cells promotes autoimmune inflammation. *Proc. Natl. Acad. Sci. U. S. A.* **109,** 13064–9 (2012).

49. Slegtenhorst, M. v. Identification of the Tuberous Sclerosis Gene TSC1 on Chromosome 9q34. *Science (80-.).* **277,** 805–808 (1997).

50. Curatolo, P., Moavero, R. & de Vries, P. J. Neurological and neuropsychiatric aspects of tuberous sclerosis complex. *Lancet Neurol.* **14,** 733–745 (2015).

51. Inoki, K., Li, Y., Zhu, T., Wu, J. & Guan, K.-L. TSC2 is phosphorylated and inhibited by Akt and suppresses mTOR signalling. *Nat. Cell Biol.* **4,** 648–57 (2002).

52. Murthy, V. *et al.* Developmental expression of the tuberous sclerosis proteins tuberin and hamartin. *Acta Neuropathol* **101,** 202–210 (2001).

53. Kaur, S. *et al.* Regulatory effects of mammalian target of rapamycin-activated pathways in type I and II interferon signaling. *J. Biol. Chem.* **282,** 1757–68 (2007).

54. Ehninger, D. & Silva, A. J. Rapamycin for treating Tuberous sclerosis and Autism spectrum disorders. *Trends Mol. Med.* **17,** 78–87 (2011).

55. Cao, W. *et al.* Toll-like receptor-mediated induction of type I interferon in plasmacytoid dendritic cells requires the rapamycin-sensitive PI(3)K-mTOR-p70S6K pathway. *Nat. Immunol.* **9,** 1157–64 (2008).

56. Pan, H., Brien, T. F. O. & Zhang, P. The Role of TSC1 in Regulating Innate Immunity. (2013). doi:10.4049/jimmunol.1102187

57. Ehninger, D. *et al.* Gestational immune activation and Tsc2 haploinsufficiency cooperate to disrupt fetal survival and may perturb social behavior in adult mice. *Mol. Psychiatry* **17,** 62–70 (2012).

58. Fedorocko, P., Egyed, A. & Vacek, A. Irradiation induces increased production of haemopoietic and proinflammatory cytokines in the mouse lung. *Int. J. Radiat. Biol.* **78,** 305–13 (2002).

59. SMITH, W. W., ALDERMAN, I. M. & GILLESPIE, R. E. Increased survival in irradiated animals treated with bacterial endotoxins. *Am. J. Physiol.* **191,** 124–30 (1957).

60. Neta, R., Perlstein, R., Vogel, S. N., Ledney, G. D. & Abrams, J. Role of interleukin 6 (IL-6) in protection from lethal irradiation and in endocrine responses to IL-1 and tumor necrosis factor. *J. Exp. Med.* **175,** 689–94 (1992).

61. Uckun, F. M., Souza, L., Waddick, K. G., Wick, M. & Song, C. W. In vivo radioprotective effects of recombinant human granulocyte colony-stimulating factor in lethally irradiated mice. *Blood* **75,** 638–45 (1990).

62. Kim, K. *et al.* High throughput screening of small molecule libraries for modifiers of radiation responses. *Int. J. Radiat. Biol.* **87,** 839–45 (2011).

63. Scholz, M., Ackermann, M., Emmrich, F., Loeffler, M. & Kamprad, M. Effectiveness of cytopenia prophylaxis for different filgrastim and pegfilgrastim schedules in a chemotherapy mouse model. *Biologics* **3,** 27–37 (2009).

64. Carver, J. R. *et al.* American Society of Clinical Oncology clinical evidence review on the ongoing care of adult cancer survivors: cardiac and pulmonary late effects. *J. Clin. Oncol.* **25,** 3991–4008 (2007).

CHAPTER 2

The Roles of Type I Interferon in Bacterial Infection

CellPress

Cell Host & Microbe
Review

The Roles of Type I Interferon in Bacterial Infection

Gayle M. Boxx[1] and Genhong Cheng[1,*]
[1]Department of Microbiology, Immunology, and Molecular Genetics, University of California, Los Angeles, Los Angeles, CA 90095, USA
*Correspondence: gcheng@mednet.ucla.edu
http://dx.doi.org/10.1016/j.chom.2016.05.016

Type I interferons (IFNs) are pleiotropic cytokines well recognized for their role in the induction of a potent antiviral gene program essential for host defense against viruses. They also modulate innate and adaptive immune responses. However, the role of type I IFNs in host defense against bacterial infections is enigmatic. Depending on the bacterium, they exert seemingly opposite and capricious functions. In this review, we summarize the effect of type I IFNs on specific bacterial infections and highlight the effector mechanisms regulated by type I IFNs in an attempt to elucidate new avenues to understanding their role.

Introduction

The innate immune system is the first line of defense against invading bacteria. Germline-encoded pattern recognition receptors (PRRs) bind bacterial components and initiate an antibacterial inflammatory gene program that promotes immune cell recruitment and directs antibacterial activities. Engagement of select PRRs also leads to the induction of what is classically considered an antiviral gene program. The role of these antiviral genes in the context of bacterial infections is unclear.

Antiviral gene expression is directed by type I interferons (IFNs), a group of small, inducible cytokines that were discovered to "interfere" with the ability of a virus to successfully replicate (Isaacs and Lindenmann, 1957). Type I IFNs are one of three families of IFNs. They include IFNβ, IFNω, IFNκ, IFNε, IFNζ, IFNδ, IFNτ, and 14 IFNα subtypes. Among them, IFNβ and the IFNαs are the most abundant and well-studied; thus, all subsequent reference to type I IFNs herein will mainly refer to these two types. Type II IFN is composed of single IFNγ, while type III IFN includes IFNλ1 (IL-29), IFNλ2 (IL-28A), IFNλ3 (IL-28B), and IFNλ4. Unlike type II and type III IFNs, type I IFNs are broadly expressed. They signal through the heterodimeric IFN α/β receptor (IFNAR) and induce over 300 IFN-stimulated genes (ISGs). These ISGs directly inhibit key steps of the viral life cycle (Yan and Chen, 2012), stimulate host cell death, activate innate immune cells, and promote the development of the adaptive immune response (Crouse et al., 2015).

Although early investigations focused on the antiviral properties of type I IFNs, several groups studying the intracellular bacteria *Chlamydia* observed that type I IFNs were induced by the bacterium (Sueltenfuss and Pollard, 1963) and that, in turn, they restricted bacterial growth (de la Maza et al., 1985). Much later, studies with another intracellular bacteria, *Listeria monocytogenes* (*L. monocytogenes*), substantiated a functional role for type I IFNs in directing the outcome of bacterial infections. Using mice deficient in IFNAR signaling, three groups revealed type I IFNs enhanced the susceptibility of mice to *Listeria* infection. Taken together, these seminal studies illustrated that type I IFN signaling plays a decisive role in *Listeria* infection by (1) reducing the efficiency of bacterial clearance, (2) decreasing the abundance of proinflammatory myeloid cells, (3) promoting the expression of proapoptotic genes, and (4) enhancing T cell sensitivity to apoptotic cell death (Auerbuch et al., 2004; Carrero et al., 2004; O'Connell et al., 2004).

These striking results encouraged further investigation into how type I IFNs modulated the outcome of other bacterial infections. Studies conducted for more than a decade have revealed a paradoxical role for type I IFNs. They play an adverse role in certain bacterial infections, while in others they are critical for host defense. In this review, we will focus on how type I IFNs function to direct disparate outcomes in a spectrum of bacterial infections.

Pathways of Recognition and Response

Expression of type I IFNs is driven by the IFN regulatory factor (IRF) family of transcription factors, namely, IRF3 and IRF7. In most cells, IRF3 is the dominant transcription factor during early type I IFN expression. Later, IRF7, which is also an ISG, is expressed and amplifies type I IFN transcription (Honda et al., 2006). In specific cell types, however, other IRFs direct early expression of type I IFNs. For example, in plasmacytoid dendritic cells (pDCs), constitutive expression of IRF7 makes it the preferred IRF (Honda et al., 2006; Prakash et al., 2005). Interestingly, IRF5 appears to play a more dominant role in the induction of type I IFNs in response to bacterial pathogens (Bergstrøm et al., 2015; Castiglia et al., 2016; Gratz et al., 2011; Pandey et al., 2009; Parker et al., 2014), and to a lesser extent against viruses (Lazear et al., 2013). Following PRR stimulation, IRFs are activated in a phosphorylation-dependent manner. PRR ligation recruits a signaling adaptor molecule that further recruits and activates the IRF kinases TBK1, IKKε, IRAK, and IKKα. There are five classes of PRRs that detect bacterial components to activate IRFs. Toll-like receptors (TLRs) are membrane-bound PRRs, while RIG-I-like receptors (RLRs), nucleotide-binding and oligomerizing domain (NOD)-like receptors (NLRs), DNA sensors, and AIM-like receptors (ALRs) are found in the cytoplasm (Figure 1).

TLRs are a family of 14 transmembrane receptors that are anchored in the cytoplasmic and endosomal membranes. Ligation of TLRs predominately induces proinflammatory and antibacterial genes; however, a subset of TLRs also induces the expression of type I IFNs. Initially located at the plasma membrane, TLR4, and to a much lesser extent TLR2, induce type I

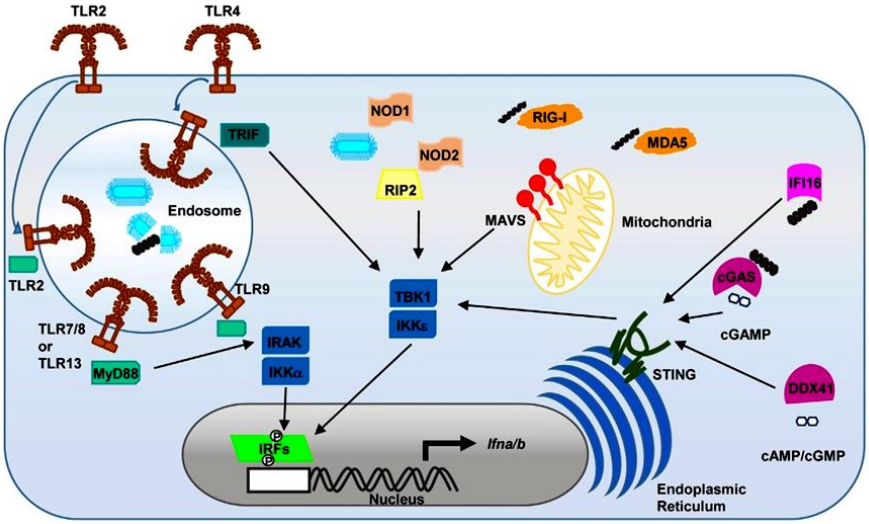

Figure 1. Signaling Pathways Leading to the Induction of Type I IFNs

Recognition of components derived from bacteria occurs at the membrane and in the cytosol. Ligand binding of TLRs recruits the signaling adaptor molecule MyD88 to TLR2/7/8/9/13, leading to activation of IRF kinases IRAK and IKKα. TLR4 recruits the adaptor TRIF, and together they activate the IRF kinases TBK1 and IKKε. Engagement of cytosolic sensors leads to the recruitment of the signaling adaptor molecule MAVS to the RLRs (RIG-I and MDA-5), STING to the DNA sensors (cGAS, DDX41, and IFI16), and RIP2 to the NLRs (NOD1 and NOD2). Like TRIF, cytosolic signaling adapters all activate TBK1 and IKKε. IRF kinases activate IRFs by phosphorylation-dependent dimerization, allowing them to translocate into the nucleus and drive type I IFN expression.

IFNs following endocytosis by ligating components derived from the bacterial cell surface (Barbalat et al., 2009; Kagan et al., 2008). In immune cells, such as dendritic cells (DCs), endosomal membrane anchored TLR9 is activated by bacterial DNA, whereas single-stranded RNA is sensed by TLR7 (Mancuso et al., 2009), TLR8 (Eigenbrod et al., 2015), and TLR13 (Castiglia et al., 2016) to activate type I IFN expression. All TLRs, except TLR3, activate the downstream signaling adaptor, MyD88. TLR4, however, activates both MyD88 and TRIF, but induces type I IFNs only through TRIF-dependent signaling (Kawai and Akira, 2011).

In the cytoplasm, RNA is recognized by the RLRs, RIG-I and MDA-5. Ligand binding promotes association with the mitochondrial signaling adaptor MAVS/Cardif/IPS/VISA (Kawai and Akira, 2011). Peptides derived from the bacterial cell wall elicit type I IFNs by engaging the NLRs, NOD1 (Watanabe et al., 2010) and NOD2, which in turn recruit the signaling adaptor RIP2 (Pandey et al., 2009). Finally, DNA sensing is primarily carried out by cyclic GMP-AMP synthase (cGAS), an enzyme that has been recognized for its critical role in catalyzing the formation of cyclic-GMP-AMP (cGAMP) (Sun et al., 2013). Other DNA sensors include the DExD/H box helicase DDX41, which binds cyclic-di-GMP and cyclic-di-AMP, secondary metabolites unique to bacteria (Parvatiyar et al., 2012), and IFI16 (murine, IFI204), an ALR that binds double-stranded DNA (Unterholzner et al., 2010). The adaptor for the DNA sensors, as well as for cGAMP, is the stimulator of IFN genes (STING), a transmembrane protein that resides in the endoplasmic reticulum (Ishikawa and Barber, 2008).

Unlike bacteria, viruses parasitize the host translation machinery to replicate, and, as a consequence, the major pathways of recognition leading to type I IFNs are initiated by cytosolic PRRs. RLRs are engaged by viral RNAs, while viral DNA is sensed by STING-dependent cGAS (Sun et al., 2013) and IFI16 (Unterholzner et al., 2010). Distinguishing viral and host nucleic acids is predicated on the detection of nucleotide sequence motifs and secondary structure formations unique to viruses (Kell et al., 2015; Sanchez et al., 2008). In the endosome, viral nucleic acids stimulate TLR3, TLR7, TLR8, and TLR9. TLR3 detects viral double-stranded RNA, and like TLR4, signals through the TRIF signaling adaptor. Lastly, contributing to a lesser extent, TLR2 and TLR4 ligation of viral proteins also triggers type I IFN induction (Kawai and Akira, 2011).

All type I IFNs signal in an autocrine and paracrine fashion through IFNAR, the heterodimeric transmembrane receptor composed of IFNAR1 and IFNAR2. Once crosslinked, the cytoplasmic tails of the IFNAR1/2 heterodimer activate Janus kinase 1 (JAK1) and tyrosine kinase 2 (TYK2), which in turn phosphorylate members of the STAT family, allowing them to dimerize and translocate to the nucleus. Formation of different transcription factor complexes is determined, in part, by the abundance and type of STAT produced by the cell (Miyagi et al., 2007), but also by positive and negative regulators (Ivashkiv and Donlin, 2014). Most cells express STAT1, STAT2, and IRF9, the canonical type I IFN transcription factors. STAT1/2 heterodimers recruit IRF9 to form the IFN-stimulated gene factor 3 (ISGF3) complex. This complex binds to IFN-stimulated response elements (ISREs) located in the promoters of antiviral

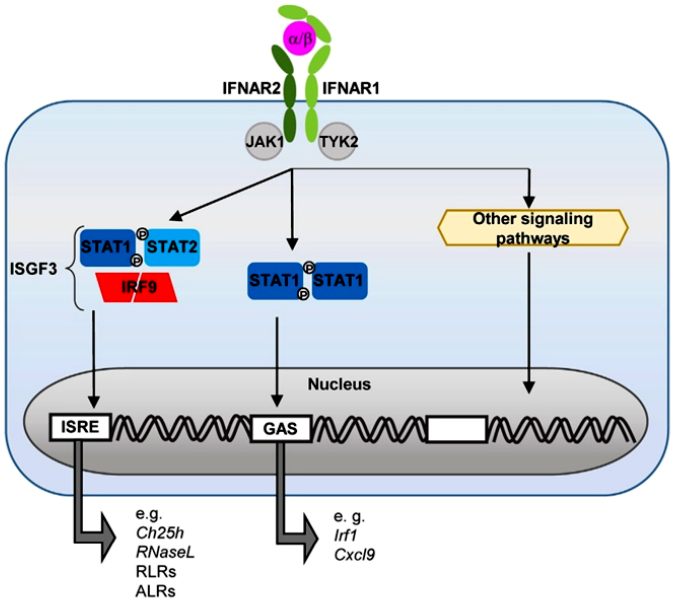

Figure 2. Type I IFNs Induce ISG Expression through JAK/STAT Signaling
Binding of type I IFNs to the IFNAR1-IFNAR2 heterodimer activates Janus kinases, JAK1 and TYK2, to phosphorylate STAT transcription factors. Dimerization of activated STAT1 and STAT2 further recruits IRF9 and forms the ISGF3 complex, which promotes expression of genes containing an ISRE sequence in their promoter. Homodimerization of activated STAT1 drives the expression of genes containing a γ-activated sequence (GAS) in their promoter.

genes. In addition, both type I and type II IFNs can activate STAT1 homodimers, which bind γ-activated sequences that lead to the transcription of genes such as IRF1. STAT-independent pathways are also activated by type I IFN, and they contribute to the induction and expression of ISGs, reviewed elsewhere (Platanias, 2005) (Figure 2). Taken together, type I IFNs induce a diverse set of ISGs that extend beyond antiviral genes to include genes involved in modulating cellular activation and death pathways.

Disparate Roles of Type I IFNs during Bacterial Infection

How type I IFNs direct the outcome of bacterial infections hinges on many factors including, but not limited to, the bacterial replication strategy and virulence factors, as well as the route and site of the infection. These factors influence which type of host cell is activated, the magnitude of induction, the timing, and the duration of the response. Here we will present a vignette of different bacterial infections that, from the host perspective, are either negatively or positively affected by type I IFNs (also see Table 1).

Type I IFN Exacerbates Bacterial Infections

Widely used to study bacterial pathogenesis, *Listeria*, in humans, causes meningitis and sepsis in immunocompromised individuals and fetal infections in pregnant women. Infection by *Listeria* induces a strong type I IFN response that promotes host susceptibility, as deficiency in either IFNAR1 or IRF3 protects mice from *Listeria* infection (O'Connell et al., 2005). Listeriolysin O (LLO), a cytolysin secreted by *Listeria* to disrupt the integrity of the vacuole, allows the bacteria to escape into the cytoplasm. Escape is critical for bacterial replication, and it also exposes bacterial DNA to detection by cGAS, and to a lesser extent by IFI16 (Hansen et al., 2014) and bacterial RNA to RIG-I (Abdullah et al., 2012). Activation of these cytoplasmic sensors leads to type-I-IFN-dependent induction of the proapoptotic genes such as *Daxx* (*Dap6*) and *Trail*, which promote macrophage (O'Connell et al., 2004) and lymphocyte (Carrero et al., 2004) apoptosis, ultimately promoting dissemination and proliferation of the bacteria. Consequently, *Listeria* is cleared more rapidly in the absence of IFNAR signaling (Auerbuch et al., 2004; Carrero et al., 2004; O'Connell et al., 2004). In addition, type I IFNs have been observed to attenuate expression of the IFNγ receptor (IFNRG1) (Rayamajhi et al., 2010), likely through the recruitment of gene-silencing proteins by the early growth response transcription factor 3 (ERG3) in complex with NGFI-A binding protein 1 (NAB1), culminating in decreased *Ifnrg1* transcription (Kearney et al., 2013). Finally, type I IFNs inhibit the expression of IL-17A by γδ T cells, a type of innate immune lymphocyte, to suppress neutrophil recruitment (Henry et al., 2010).

Francisella tularensis is responsible for tularemia, a highly contagious and life-threatening respiratory disease. Expression of genes in the *Francisella* pathogenicity island triggers the escape of the bacteria from the phagosome to the cytoplasm, and once in the cytoplasm the bacteria induce type I IFN through cGAS- and IFI204-STING-IRF3-dependent pathways (Henry et al., 2007; Storek et al., 2015). Type I IFNs suppress the innate antibacterial response by inhibiting expression of IL-17A by γδ T cells. As in *Listeria* infections, elevated expression of IL-17A in IFNAR1-deficient mice enhances splenic neutrophil recruitment and is correlated with both improved bacterial clearance and survival (Henry et al., 2010). Interestingly, though deficiency in cGAS, STING, IFNAR1, or IRF3 renders mice resistant to infection by *Francisella* (Henry et al., 2007; Storek et al., 2015), deletion of AIM2, an ALR induced by type I IFNs, is detrimental to host defense (Jones et al., 2010; Rathinam et al., 2010). Yet while type I IFNs potentiate AIM2 expression and indirectly its antibacterial activity, simultaneously AIM2 suppresses induction of type I IFNs by negatively regulating the cGAS-STING-IRF3 pathway (Corrales et al., 2016).

The Gram-negative, intracellular bacterium *Salmonella enterica* serovar Typhimurium causes acute gastroenteritis in humans and, if uncontrolled, may disseminate and cause a more

Table 1. Role of Type I IFNs in Different Bacterial Infections

Pathogen	Gram Reaction	Location	IFNα/β Signaling	Key Mechanisms	Citations
Listeria monocytogenes	(+)	intracellular	detrimental	Promotion of apoptosis. Suppression of type II IFN and IL-17.	Auerbuch et al., 2004; Carrero et al., 2004; Henry et al., 2010; O'Connell et al., 2004; Rayamajhi et al., 2010
Francisella tularensis	(–)	intracellular	detrimental	Suppression of IL-17A.	Henry et al., 2007, 2010; Jones et al., 2010; Storek et al., 2015
Salmonella enterica serovar Typhimurium	(–)	intracellular	detrimental	Promotion of necroptosis. Suppression of innate cell recruitment and proinflammatory response.	Perkins et al., 2015; Robinson et al., 2012; Schmolke et al., 2014
Staphylococcus aureus	(+)	extracellular	detrimental	Suppression of innate cell recruitment and proinflammatory response.	Martin et al., 2009; Parker et al., 2014
Legionella pneumophilia	(–)	intracellular	protective	Promotion of IRG1 (itaconic acid).	Lippmann et al., 2011; Naujoks et al., 2016; Plumlee et al., 2009
Streptococcus pyogenes	(+)	extracellular	protective	Suppression of excessive proinflammatory response.	Castiglia et al., 2016; Gratz et al., 2011; Mancuso et al., 2007, 2009
Streptococcus pneumoniae	(+)	extracellular	protective	Promotion of tissue integrity.	Damjanovic et al., 2014; LeMessurier et al., 2013; Parker et al., 2011
Helicobacter pylori	(+)	extracellular	protective	Promotion of Cxcl10-mediated cell recruitment.	Flach et al., 2012; Watanabe et al., 2010
Polymicrobial sepsis	(+) and (–)	extracellular	protective	Promotion of Cxcl10-mediated cell recruitment.	Kelly-Scumpia et al., 2010
Post-influenza bacterial pneumonia	(+) or (–)	extracellular	detrimental	Suppression of proinflammatory response.	Lee et al., 2015; Shahangian et al., 2009
Mycobacterium tuberculosis	(+)	intracellular	detrimental	Promotion of IL-10 anti-inflammatory response.	Berry et al., 2010; Manca et al., 2001; Mayer-Barber et al., 2014
Mycobacterium leprae	(+)	intracellular	detrimental	Promotion of IL-10 and IL-27 anti-inflammatory response.	Liu et al., 2012; Teles et al., 2013, 2015

life-threatening disease. RIG-I detection of *Salmonella* mRNA induces type I IFNs in non-phagocytic cells, whereas recognition of *Salmonella* LPS by TLR4 drives type I IFN induction in phagocytic cells (Schmolke et al., 2014). During systemic infection, IFNAR1-deficient mice accumulate less bacteria in the spleen and liver, and have marked survival compared to wild-type (WT) mice. Enhanced survival and defense noted in IFNAR1- and IFNβ-deficient mice are associated with increased antibacterial proinflammatory responses (Perkins et al., 2015). Moreover, induction of type I IFNs during *Salmonella* infection promotes macrophage death by necroptosis (Henry et al., 2007; Robinson et al., 2012). Necroptosis is a type of programmed cell death that, unlike TRAIL-mediated apoptosis, proceeds in a caspase-independent manner. Here IFNβ, not IFNα, promotes necroptosis (Robinson et al., 2012), illustrating an exclusive effector function for IFNβ.

Infections caused by the Gram-positive, extracellular bacterium *Staphylococcus aureus* (*S. aureus*) are also exacerbated by type I IFNs. *S. aureus* is a common etiological agent of local skin infections, but it is also a primary cause of severe lung pneumonia and bloodstream infections. Type I IFNs are induced by protein A, a virulence factor (Martin et al., 2009), and via TLR9-IRF1 or NOD2-IRF5 (Parker et al., 2014). In vivo, IFNAR1 deficiency confers resistance to lethal pneumonia. Survival is associated with increased CD11c$^+$ DCs in the lungs and reduced TNFα in the bronchoalveolar lavage fluid (Martin et al., 2009). Interestingly, while IFNβ expression is inducible in cultured lung epithelial cells (Martin et al., 2009; Parker et al., 2014), transcript for IFNα is not detected (Martin et al., 2009). This suggests strain-specific effects, as well as host-specific capacities, for differences between hematopoietic and non-hematopoietic cells are also noted (Parker et al., 2014).

Type I IFNs Protect against Bacterial Infections

Legionella pneumophilia is responsible for Legionnaires' disease, a severe lung pneumonia. Its type IV secretion system, Dot/Icm, is required for entry into and replication within the macrophage cytosol (Lippmann et al., 2011). It has been reported that the host detects *Legionella* in the cytosol by a STING-dependent pathway (Lippmann et al., 2011), leading to IRF3-dependent type I IFN expression (Plumlee et al., 2009). While in a mouse model of pulmonary *Legionella* infection, IFNAR2-deficient mice did not reveal a role for type I IFNs (Ang et al., 2010), proliferation of *Legionella* in macrophages is inhibited by type I IFNs (Lippmann et al., 2011; Plumlee et al., 2009). Moreover, type I IFN, along with type II IFN, promotes host defense likely through induction of cell-intrinsic ISGs such as immune-responsive gene 1 (IRG1) (Naujoks et al., 2016).

Type I IFNs also fortify the host against infections caused by Gram-positive Streptococci. *Streptococcus pyogenes*, the group A streptococcus, causes superficial and deep tissue

infections that can develop into necrotizing fasciitis. Both group A streptococci and group B streptococci (*Streptococcus agalactiae*) activate the STING-TBK1-IRF3 pathway in macrophages (Gratz et al., 2011), while in cDCs, TLR7-Myd88-IRF5 and, to a lesser extent, IRF1 both play a role (Castiglia et al., 2016; Gratz et al., 2011; Mancuso et al., 2009). In a mouse model of *S. pyogenes* cellulitis, survival of WT mice is significantly greater than IFNAR1-deficient mice (Gratz et al., 2011). Enhanced survival is linked to the anti-inflammatory properties conferred by type I IFN signaling (Castiglia et al., 2016). Likewise, systemic infection of adult or neonatal mice with group B streptococci also requires IFNAR signaling to protect the host, and while IFNα4 was induced in WT group B streptococci-infected mice, IFNβ plays a dominant role in conferring protection, as *Ifnβ* KO (knockout) mice are more susceptible than WT mice (Mancuso et al., 2007).

Streptococcus pneumoniae causes life-threatening pneumonia. Host detection of *S. pneumoniae* is facilitated by the expression of autolysin and pneumolysin, two virulence factors that cooperate to introduce bacterial DNA into the cytosol. In epithelial cells, bacterial DNA activates STING to induce IFNβ (Parker et al., 2011). In two independent studies, it was observed that in the absence of IFNAR1, even though immune cell recruitment was enhanced, more bacteria were found in the lungs (Parker et al., 2011) or escaping from the lungs into the bloodstream (LeMessurier et al., 2013). Exogenous IFNβ decreases transmigration into the bloodstream by promoting the expression of genes encoding tight junction proteins and, simultaneously, downregulating the expression of platelet-activating receptor, the receptor by which the bacteria enter the cell (LeMessurier et al., 2013). Moreover, treatment of mice with an IFNα-expressing adenoviral vector led to decreased immunopathology and enhanced antibacterial activity in macrophages, resulting in an overall increase in survival (Damjanovic et al., 2014).

The Gram-negative bacterium *Helicobacter pylori* is the etiological agent of acute gastric infections, as well as chronic gastric ulcers and cancer. In non-hematopoietic cells, NOD1 sensing of a peptide derived from *H. pylori* peptidoglycan induces type I IFN expression in an IRF7-dependent manner. IFNAR1- or NOD1-deficient mice fail to restrict *H. pylori* proliferation. Concurrently, a significant reduction in expression of the chemotactic ISG, *Cxcl10*, suggests type-I-IFN-induced *Cxcl10* is critical for the control of *H. pylori* proliferation (Watanabe et al., 2010), and it is further supported by elevated CXCL10 levels observed in vaccinated mice (Flach et al., 2012) and patients that are asymptomatic carriers (Jafarzadeh et al., 2013).

Type-I-IFN-induced CXCL10 also promotes host resistance during polymicrobial sepsis. Using a model of cecal ligation and puncture (CLP) in mice, investigators found the absence of IFNAR signaling led to increased mortality. Although the chemokine CXCL1 was elevated in IFNAR1-deficient mice, decreased levels CXCL10 were also noted. Administration of CXCL10 to IFNAR1-deficient mice restored hematopoietic cell recruitment and antibacterial activity, which led to enhanced bacterial clearance and host resistance to polymicrobial sepsis (Kelly-Scumpia et al., 2010).

Type I IFNs Are Detrimental to Secondary Bacterial Infections

High mortality rates associated with seasonal and pandemic influenza are driven by the development of secondary bacterial pneumonia caused by *S. pneumoniae* or *S. aureus*, and, at a lower incidence, other bacteria (McCullers, 2014). This enhanced susceptibility is transient, limited by the initiation and the duration of type I IFN expression. As discussed, type I IFNs promote host defense against *S. pneumoniae* infection, yet preceding expression of type I IFNs has detrimental effects. First, prior induction of type I IFNs attenuates the expression of neutrophil chemokines (Shahangian et al., 2009). Neutrophil recruitment is restored by deletion of either IFNAR1 (Shahangian et al., 2009) or the type I IFN responsive methyltransferase, Setdb2, which culminates in bacterial clearance (Schliehe et al., 2015; Shahangian et al., 2009). Second, prior expression of type I IFNs suppresses production of IL-17 by T cells (Cao et al., 2014; Kudva et al., 2011). In the absence of IL-17, diminished secretion of antibacterial peptides lipocalin 2 and BPIFA1 is associated with increased bacterial growth (Lee et al., 2015). Lastly, the duration of type I IFN expression dictates sensitivity to secondary bacterial infection, as superinfections do not develop if initiated 14 days after influenza infection (Lee et al., 2015).

Type I IFN Promotes Chronic Bacterial Infections

Mycobacteria comprise a group of highly contagious pathogens that establish chronic infections of the lungs (*M. tuberculosis*) or skin (*M. leprae*). The host relies on cGAS sensing of bacterial DNA (Collins et al., 2015; Wassermann et al., 2015; Watson et al., 2015), as well as NOD2 sensing of cell-wall-associated muramyl dipeptides (Pandey et al., 2009), to detect *M. tuberculosis*. Virulent strains provoke higher IFNα expression in the lungs compared to less virulent strains. IFNAR signaling suppresses IL-12 and IFNγ, thereby arresting the development of the antibacterial adaptive T cell (Th1) response and reducing host survival (Manca et al., 2001; Mayer-Barber et al., 2014). Similar results have been reported in human patients. Examination of the gene expression pattern of whole blood revealed a distinct gene expression signature defined by type I IFN and downstream ISGs in patients with active tuberculosis that was not present in patients with latent tuberculosis (Berry et al., 2010). Likewise, ex vivo studies with *M. leprae* demonstrate IFNβ-sinduced anti-inflammatory cytokines drive the progression to chronic leprosy by inhibiting the development of Th1 immunity (Teles et al., 2013, 2015).

Disparate Effector Mechanisms of Type I IFNs

Given their pleotropic nature, type I IFNs have the capacity to influence multiple host defense mechanisms. Productive host response to acute bacterial infection requires secretion of proinflammatory cytokines and chemokines that recruit and activate innate immune cells. Herein, we will explore the effect of type I IFN on key antibacterial mechanisms.

Suppression of Type II IFN Responses by Type I IFN

Like type I IFN, type II IFN is expressed during microbial infections and exerts antiviral and immunomodulatory activities. Type II IFN, solely consisting of IFNγ, is induced by IL-12 and IL-18, with natural killer (NK) and T cells being the dominant producers. Type I and type II IFNs activate distinct and overlapping gene programs by signaling through their respective canonical JAK-STAT pathways. IFNγ preferentially induces phosphorylation and dimerization of STAT1 to promote expression of the γ-activated, sequence-dependent genes. Type I IFNs favor the

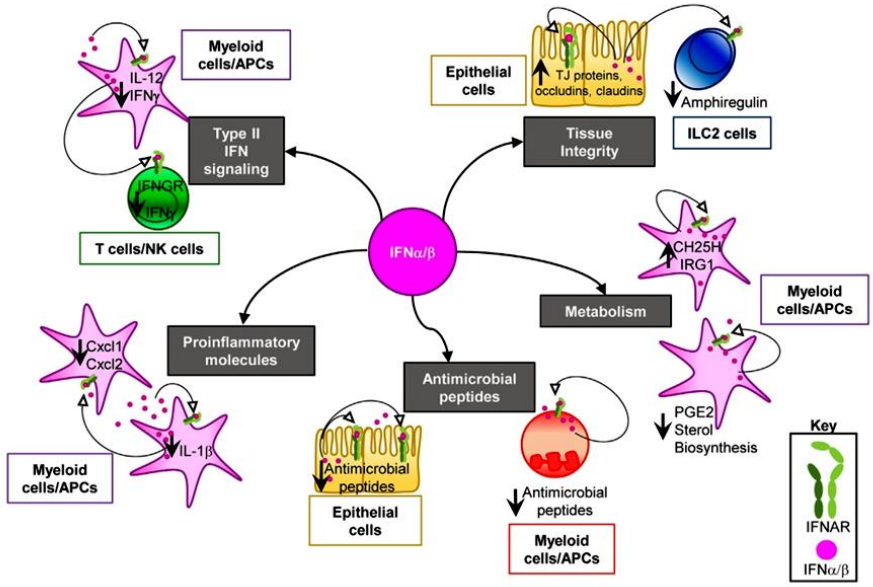

Figure 3. Effector Mechanisms Mediated by Type I IFNs during Bacterial Infection
Autocrine and paracrine signaling of type I IFNs suppress type II IFN signaling, proinflammatory responses, and production of antimicrobial peptides to contribute to overall detrimental host outcomes. Modulation of metabolism by type I IFNs also exerts negative effects by either suppressing sterol biosynthesis and PGE2 or by upregulating CH25H, but may also promote host defense by inducing expression of IRG1. Tissue integrity is strengthened by type I IFNs through the induction of tight junction (TJ) proteins, claudins and occludins, yet suppressive effects on ILC2s and amphiregulin are also observed. See text for details.

assembly of the ISGF3 transcription factor complex, which drives ISRE-controlled genes, but also activate STAT1 dimerization (Manca et al., 2001). Intriguingly, NK cells express high basal levels of STAT4, which enables rapid induction of IFNγ following type I IFN stimulation. However, in the absence of IL-12 signaling, IFNγ expression is transient as STAT4 is displaced by STAT1, thus negatively regulating the production of type II IFN (Mack et al., 2011; Miyagi et al., 2007). IFNγ is critical for defense against many bacterial pathogens (Harty and Bevan, 1995; Lippmann et al., 2011; Teles et al., 2013). Despite numerous studies, it is still not clear how type I and type II IFN play opposite roles in host defense against certain bacteria and which downstream effector genes are responsible for such differences. In addition to regulating downstream effector genes, type I IFNs also suppress IFNγ expression by attenuating the transcription of its inducer, IL-12 (Berry et al., 2010; Carrero et al., 2004; Manca et al., 2001), and its receptor, IFNRG1 (Kearney et al., 2013; Rayamajhi et al., 2010) (Figure 3). Insufficient IFNγ expression can have drastic consequences. *M. leprae* infections that manifest as "self-healing" leprosy provoke an IFNγ-driven Th1 response, while a type I IFN signature dominates during chronic, disseminated infections (Liu et al., 2012; Teles et al., 2013). Further, hypervirulent strains of *M. tuberculosis* promote the expression of type I IFNs and concurrently attenuate IL-12 and IFNγ (Manca et al., 2001), further reinforcing that induction of type I IFNs is favorable for bacterial pathogenesis.

Anti-inflammatory Responses by Type I IFN

Productive host antibacterial response relies on the coordination and balance of proinflammatory molecules to clear bacteria, and anti-inflammatory molecules to limit tissue damage. Type I IFNs propagate the anti-inflammatory response by upregulating the expression of *Il10* and *Il27*. IL-10 is a type I IFN inducible immunosuppressive and anti-inflammatory cytokine. Induction of IL-10 has been described to occur through both IL-27-dependent (Iyer et al., 2010) and IL-27-independent mechanisms (McNab et al., 2014). IL-10 inhibits the acute phase cytokines, TNFα and IL-1 (Bogdan et al., 1992), thereby attenuating expression of adhesion molecules and chemokines required for leukocyte recruitment (Yarilina et al., 2008). Downregulation of the proinflammatory response is essential to protect against tissue-damage-induced mortality, as observed during *Escherichia coli* sepsis (Sewnath et al., 2001), but it is detrimental to the clearance of other bacterial infections (Auerbuch et al., 2004; Di Paolo et al., 2015; Mayer-Barber et al., 2014; McNab et al., 2014). Similarly, IL-27 protects against tissue damage during acute influenza infection (Liu et al., 2014), but compromises the host response to both secondary (Cao et al., 2014; Robinson et al., 2015) and chronic bacterial infections (Teles et al., 2015). The delicate balance between proinflammatory and anti-inflammatory responses is further illustrated by chemokine recruitment. Type-I-IFN-mediated suppression of proinflammatory chemokines, CXCL1 and CXCL2, reduces myeloid recruitment and

may protect against excessive tissue damage (Ellis et al., 2015), but may also compromise myeloid-mediated bacterial clearance (Perkins et al., 2015; Schliehe et al., 2015; Shahangian et al., 2009) (Figure 3).

Inhibition of Antimicrobial Peptides by Type I IFN

One consequence of the anti-inflammatory action mediated by type I IFNs is the suppression of several antimicrobial peptides (Figure 3). Antimicrobial peptides exert non-enzymatic activities that inhibit microbial functions by directly inhibiting the pathogen or host-specific targets. Cathelicidin (CAMP) and beta-defensin 2 (DEFB4) are two antimicrobial peptides induced by IL-1β and cytochrome P450 family 27 subfamily B member 1 (CYP27B1), an enzyme in the vitamin D pathway. They are indirectly downregulated by IFNβ-IL-10 (Teles et al., 2013) through the induction of *hsa-mir-21*, an ISG that inhibits the translation of *IL1B* and *CYP27B1* transcripts (Liu et al., 2012). Type I IFNs also negatively regulate the expression antimicrobial peptides induced by IL-22, such as lipocalin 2 and BPIFA1 (Lee et al., 2015). Downregulation of these antimicrobial peptides also occurs indirectly, as type I IFNs target IL-23, the cytokine that induces IL-22 (Kudva et al., 2011).

Regulation of Metabolic Pathways by Type I IFN

There is a growing appreciation for the role of cellular metabolism in the coordination of immune response. TLR signaling and microbial infections have been observed to redirect the metabolic strategy of macrophage and DCs. Type I IFNs downregulate sterol biosynthesis, triggering a shift away from de novo cholesterol synthesis (Blanc et al., 2011) and toward cholesterol import. This shift, by an unknown mechanism, drives spontaneous STING-IRF3-dependent IFNβ expression (York et al., 2015). Type I IFNs also promote key antiviral responses such as upregulation of cholesterol-25 hydroxylase (*Ch25h*), an ISG that inhibits viral entry (Liu et al., 2013). During *Listeria* infection, however, *Ch25h* expression increases the susceptibility of mice to bacterial infection by negatively regulating capase-1 and IL-1β maturation (Reboldi et al., 2014). Other metabolic pathways are also influenced by type I IFNs. Prostaglandin E2 (PGE2), an arachidonic-acid-derived lipid mediator that promotes host defense against *Mycobacterium*, is negatively regulated by type I IFN suppression of IL-1β but, at the same time, negatively regulates type I IFN expression (Mayer-Barber et al., 2014). Conversely, type I IFNs induce *Irg1*, an ISG that generates itaconic acid, an antimicrobial metabolite that effectively restricts the growth of intracellular bacteria (Naujoks et al., 2016) (Figure 3).

Regulation of Tissue Integrity by Type I IFN

Tissue integrity is maintained by the expression of tight junction proteins such as cadherins and claudins, and the peripheral scaffolding proteins such as occludins. The arrangement and density of these proteins determine the permeability of the epithelial barrier and act to confine local tissue infections (LeMessurier et al., 2013; Long et al., 2014). Type I IFNs, augmented by *RNase-L*, an ISG that mediates induction of type I IFNs, promote the expression of tight junction proteins (LeMessurier et al., 2013). RNase-L deficiency reduces IFNβ expression and, subsequently, diminishes tissue integrity (Long et al., 2013). This promotes host susceptibility to opportunistic (Long et al., 2013) and acquired bacterial infections (Li et al., 2008). In addition, group 2 innate lymphoid cells (ILC2s) have recently emerged as the key tissue resident cell type orchestrating tissue repair (Monticelli et al., 2011). ILC2s foster tissue integrity by upregulating expression of amphiregulin, an epithelial growth factor that promotes sustained signaling. Type I IFNs attenuate the expression of amphiregulin and stunt ILC2 proliferation (Monticelli et al., 2011) (Figure 3). This has been observed to confer long-lasting deficiencies to the integrity of the mesenteric adipose tissue and the mesenteric lymph nodes (Fonseca et al., 2015).

Conclusion and Future Outlook

Type I IFNs direct a potent antiviral response through the induction of a diverse set of ISGs. Some ISGs have evolved to exert broad antiviral activities, while others act to specifically target different classes of viruses. Over the past few decades, numerous studies have uncovered a pivotal role for type I IFNs in dictating host response to bacterial infections. Unlike their role in viral infections, type I IFNs play an unpredictable role in bacterial infections. Their pleiotropic nature leads not only to the induction of antiviral genes, but also to genes that modulate innate and adaptive immune responses. While some of the immunomodulatory genes are beneficial to host defense against bacterial infections, many are detrimental to the formation of an antibacterial inflammatory response.

Given the disparate role of type I IFNs among different bacterial infections, it is clear that the field will benefit from more comprehensive analyses of the type I IFN response. Crucially, the current state of our knowledge does not allow us to determine whether type I IFNs will be beneficial or detrimental based on the biology of the pathogen. Studies of the role of type I IFNs during viral infections have shown that a short, strong type I IFN response is generally beneficial to clearing the infection. However, sustained expression seems to be detrimental to the clearance of persistent viral infections (Wilson et al., 2013). Recently, it has been demonstrated that IFNβ and IFNα exert discrete functions during chronic viral infection: in early stages IFNβ promotes disorganization of the spleen, whereas IFNα limits viral dissemination (Ng et al., 2015). Thus, it is becoming increasingly apparent that type I IFNs are not redundant, but that they have overlapping and distinct functions.

Furthermore, functional differences may result not only from preferential expression of IFNα or IFNβ by different cell types (Honda et al., 2006; Prakash et al., 2005) or from their difference in affinity for IFNAR (de Weerd et al., 2013), but also from the route of infection. *Listeria* administered by oral gavage enhances host resistance, whereas infection initiated by intraperitoneal injection leads to host susceptibility (Kernbauer et al., 2013). Both routes elicit type I IFN expression by inflammatory myeloid cells; however, differences in hepatic colonization appear to shape the response (Kernbauer et al., 2013; Stockinger et al., 2009). Few have undertaken comprehensive studies of route, even though it has been shown to play a role in both host response and pathogen biology (Fitzgeorge et al., 1983; Kernbauer et al., 2013; Martins et al., 2013).

Extending these observations to the role of type I IFNs on the outcome of bacterial infections, we suggest that more detailed examinations of the composition, magnitude, and duration of type I IFN expression will complement mechanistic investigations

into the effector functions of specific type I IFNs and lead to more precise management of infections.

ACKNOWLEDGMENTS

We thank Kislay Parvatiyar, Maxime Chapon, and Elisa Deriu for helpful discussions and editing of this manuscript. We apologize, but due to space limitations, we were unable to cite all relevant studies. Work in the G.C. laboratory is supported by the NIH grants AI056154 and AI069120.

REFERENCES

Abdullah, Z., Schlee, M., Roth, S., Mraheil, M.A., Barchet, W., Böttcher, J., Hain, T., Geiger, S., Hayakawa, Y., Fritz, J.H., et al. (2012). RIG-I detects infection with live Listeria by sensing secreted bacterial nucleic acids. EMBO J. *31*, 4153–4164.

Ang, D.K.Y., Oates, C.V.L., Schuelein, R., Kelly, M., Sansom, F.M., Bourges, D., Boon, L., Hertzog, P.J., Hartland, E.L., and van Driel, I.R. (2010). Cutting edge: pulmonary Legionella pneumophila is controlled by plasmacytoid dendritic cells but not type I IFN. J. Immunol. *184*, 5429–5433.

Auerbuch, V., Brockstedt, D.G., Meyer-Morse, N., O'Riordan, M., and Portnoy, D.A. (2004). Mice lacking the type I interferon receptor are resistant to Listeria monocytogenes. J. Exp. Med. *200*, 527–533.

Barbalat, R., Lau, L., Locksley, R.M., and Barton, G.M. (2009). Toll-like receptor 2 on inflammatory monocytes induces type I interferon in response to viral but not bacterial ligands. Nat. Immunol. *10*, 1200–1207.

Bergstrøm, B., Aune, M.H., Awuh, J.A., Kojen, J.F., Blix, K.J., Ryan, L., Flo, T.H., Mollnes, T.E., Espevik, T., and Stenvik, J. (2015). TLR8 senses Staphylococcus aureus RNA in human primary monocytes and macrophages and induces IFN-β production via a TAK1-IKKβ-IRF5 signaling pathway. J. Immunol. *195*, 1100–1111, http://dx.doi.org/10.4049/jimmunol.1403176.

Berry, M.P.R., Graham, C.M., McNab, F.W., Xu, Z., Bloch, S.A., Oni, T., Wilkinson, K.A., Banchereau, R., Skinner, J., Wilkinson, R.J., et al. (2010). An interferon-inducible neutrophil-driven blood transcriptional signature in human tuberculosis. Nature *466*, 973–977.

Blanc, M., Hsieh, W.Y., Robertson, K.A., Watterson, S., Shui, G., Lacaze, P., Khondoker, M., Dickinson, P., Sing, G., Rodríguez-Martín, S., et al. (2011). Host defense against viral infection involves interferon mediated down-regulation of sterol biosynthesis. PLoS Biol. *9*, e1000598.

Bogdan, C., Paik, J., Vodovotz, Y., and Nathan, C. (1992). Contrasting mechanisms for suppression of macrophage cytokine release by transforming growth factor-beta and interleukin-10. J. Biol. Chem. *267*, 23301–23308.

Cao, J., Wang, D., Xu, F., Gong, Y., Wang, H., Song, Z., Li, D., Zhang, H., Li, D., Zhang, L., et al. (2014). Activation of IL-27 signalling promotes development of postinfluenza pneumococcal pneumonia. EMBO Mol. Med. *6*, 120–140.

Carrero, J.A., Calderon, B., and Unanue, E.R. (2004). Type I interferon sensitizes lymphocytes to apoptosis and reduces resistance to Listeria infection. J. Exp. Med. *200*, 535–540.

Castiglia, V., Piersigilli, A., Ebner, F., Janos, M., Goldmann, O., Damböck, U., Kröger, A., Weiss, S., Knapp, S., Jamieson, A.M., et al. (2016). Type I interferon signaling prevents IL-1β-driven lethal systemic hyperinflammation during invasive bacterial infection of soft tissue. Cell Host Microbe *19*, 375–387.

Collins, A.C., Cai, H., Li, T., Franco, L.H., Li, X.-D., Nair, V.R., Scharn, C.R., Stamm, C.E., Levine, B., Chen, Z.J., and Shiloh, M.U. (2015). Cyclic GMP-AMP synthase is an innate immune DNA sensor for mycobacterium tuberculosis. Cell Host Microbe *17*, 820–828.

Corrales, L., Woo, S.-R., Williams, J.B., McWhirter, S.M., Dubensky, T.W., Jr., and Gajewski, T.F. (2016). Antagonism of the STING pathway via activation of the AIM2 inflammasome by intracellular DNA. J. Immunol. *196*, 3191–3198, http://dx.doi.org/10.4049/jimmunol.1502538.

Crouse, J., Kalinke, U., and Oxenius, A. (2015). Regulation of antiviral T cell responses by type I interferons. Nat. Rev. Immunol. *15*, 231–242.

Damjanovic, D., Khera, A., Medina, M.F., Ennis, J., Turner, J.D., Gauldie, J., and Xing, Z. (2014). Type 1 interferon gene transfer enhances host defense against pulmonary Streptococcus pneumoniae infection via activating innate leukocytes. Mol. Ther. Methods Clin. Dev. *1*, 5.

de la Maza, L.M., Peterson, E.M., Goebel, J.M., Fennie, C.W., and Czarniecki, C.W. (1985). Interferon-induced inhibition of Chlamydia trachomatis: dissociation from antiviral and antiproliferative effects. Infect. Immun. *47*, 719–722.

de Weerd, N.A., Vivian, J.P., Nguyen, T.K., Mangan, N.E., Gould, J.A., Braniff, S.J., Zaker-Tabrizi, L., Fung, K.Y., Forster, S.C., Beddoe, T., et al. (2013). Structural basis of a unique interferon-β signaling axis mediated via the receptor IFNAR1. Nat. Immunol. *14*, 901–907.

Di Paolo, N.C., Shafiani, S., Day, T., Papayannoupoulou, T., Russell, D.W., Iwakura, Y., Sherman, D., Urdahl, K., and Shayakhmetov, D.M. (2015). Interdependence between interleukin-1 and tumor necrosis factor regulates TNF-dependent control of mycobacterium tuberculosis infection. Immunity *43*, 1125–1136.

Eigenbrod, T., Pelka, K., Latz, E., Kreikemeyer, B., and Dalpke, A.H. (2015). TLR8 senses bacterial RNA in human monocytes and plays a nonredundant role for recognition of Streptococcus pyogenes. J. Immunol. *195*, 1092–1099.

Ellis, G.T., Davidson, S., Crotta, S., Branzk, N., Papayannopoulos, V., and Wack, A. (2015). TRAIL+ monocytes and monocyte-related cells cause lung damage and thereby increase susceptibility to influenza-Streptococcus pneumoniae coinfection. EMBO Rep. *16*, 1203–1218.

Fitzgeorge, R.B., Baskerville, A., Broster, M., Hambleton, P., and Dennis, P.J. (1983). Aerosol infection of animals with strains of Legionella pneumophila of different virulence: comparison with intraperitoneal and intranasal routes of infection. J. Hyg. (Lond.) *90*, 81–89.

Flach, C.-F., Mozer, M., Sundquist, M., Holmgren, J., and Raghavan, S. (2012). Mucosal vaccination increases local chemokine production attracting immune cells to the stomach mucosa of Helicobacter pylori infected mice. Vaccine *30*, 1636–1643.

Fonseca, D.M., Hand, T.W., Han, S.-J., Gerner, M.Y., Glatman Zaretsky, A., Byrd, A.L., Harrison, O.J., Ortiz, A.M., Quinones, M., Trinchieri, G., et al. (2015). Microbiota-dependent sequelae of acute infection compromise tissue-specific immunity. Cell *163*, 354–366.

Gratz, N., Hartweger, H., Matt, U., Kratochvill, F., Janos, M., Sigel, S., Drobits, B., Li, X.D., Knapp, S., and Kovarik, P. (2011). Type I interferon production induced by Streptococcus pyogenes-derived nucleic acids is required for host protection. PLoS Pathog. *7*, e1001345.

Hansen, K., Prabakaran, T., Laustsen, A., Jørgensen, S.E., Rahbæk, S.H., Jensen, S.B., Nielsen, R., Leber, J.H., Decker, T., Horan, K.A., et al. (2014). Listeria monocytogenes induces IFNβ expression through an IFI16-, cGAS- and STING-dependent pathway. EMBO J. *33*, 1654–1666.

Harty, J.T., and Bevan, M.J. (1995). Specific immunity to Listeria monocytogenes in the absence of IFN gamma. Immunity *3*, 109–117.

Henry, T., Brotcke, A., Weiss, D.S., Thompson, L.J., and Monack, D.M. (2007). Type I interferon signaling is required for activation of the inflammasome during Francisella infection. J. Exp. Med. *204*, 987–994.

Henry, T., Kirimanjeswara, G.S., Ruby, T., Jones, J.W., Peng, K., Perret, M., Ho, L., Sauer, J.D., Iwakura, Y., Metzger, D.W., and Monack, D.M. (2010). Type I IFN signaling constrains IL-17A/F secretion by gammadelta T cells during bacterial infections. J. Immunol. *184*, 3755–3767.

Honda, K., Takaoka, A., and Taniguchi, T. (2006). Type I interferon [corrected] gene induction by the interferon regulatory factor family of transcription factors. Immunity *25*, 349–360.

Isaacs, A., and Lindenmann, J. (1957). Virus interference. I. The interferon. Proc. R. Soc. Lond. B Biol. Sci. *147*, 258–267.

Ishikawa, H., and Barber, G.N. (2008). STING is an endoplasmic reticulum adaptor that facilitates innate immune signalling. Nature *455*, 674–678.

Ivashkiv, L.B., and Donlin, L.T. (2014). Regulation of type I interferon responses. Nat. Rev. Immunol. *14*, 36–49.

Iyer, S.S., Ghaffari, A.A., and Cheng, G. (2010). Lipopolysaccharide-mediated IL-10 transcriptional regulation requires sequential induction of type I IFNs and IL-27 in macrophages. J. Immunol. *185*, 6599–6607.

Jafarzadeh, A., Nemati, M., Rezayati, M.T., Khoramdel, H., Nabizadeh, M., Hassanshahi, G., and Abdollahi, H. (2013). Lower circulating levels of chemokine CXCL10 in Helicobacter pylori-infected patients with peptic ulcer: influence of the bacterial virulence factor CagA. Iran. J. Microbiol. *5*, 28–35.

Jones, J.W., Kayagaki, N., Broz, P., Henry, T., Newton, K., O'Rourke, K., Chan, S., Dong, J., Qu, Y., Roose-Girma, M., et al. (2010). Absent in melanoma 2 is required for innate immune recognition of Francisella tularensis. Proc. Natl. Acad. Sci. USA *107*, 9771–9776.

Kagan, J.C., Su, T., Horng, T., Chow, A., Akira, S., and Medzhitov, R. (2008). TRAM couples endocytosis of Toll-like receptor 4 to the induction of interferon-beta. Nat. Immunol. *9*, 361–368.

Kawai, T., and Akira, S. (2011). Toll-like receptors and their crosstalk with other innate receptors in infection and immunity. Immunity *34*, 637–650.

Kearney, S.J., Delgado, C., Eshleman, E.M., Hill, K.K., O'Connor, B.P., and Lenz, L.L. (2013). Type I IFNs downregulate myeloid cell IFN-γ receptor by inducing recruitment of an early growth response 3/NGFI-A binding protein 1 complex that silences ifngr1 transcription. J. Immunol. *191*, 3384–3392.

Kell, A., Stoddard, M., Li, H., Marcotrigiano, J., Shaw, G.M., and Gale, M., Jr. (2015). Pathogen-associated molecular pattern recognition of hepatitis C virus transmitted/founder variants by RIG-I is dependent on U-core length. J. Virol. *89*, 11056–11068.

Kelly-Scumpia, K.M., Scumpia, P.O., Delano, M.J., Weinstein, J.S., Cuenca, A.G., Wynn, J.L., and Moldawer, L.L. (2010). Type I interferon signaling in hematopoietic cells is required for survival in mouse polymicrobial sepsis by regulating CXCL10. J. Exp. Med. *207*, 319–326.

Kernbauer, E., Maier, V., Rauch, I., Müller, M., and Decker, T. (2013). Route of infection determines the impact of type I interferons on innate immunity to Listeria monocytogenes. PLoS ONE *8*, e65007, http://dx.doi.org/10.1371/journal.pone.0065007.

Kudva, A., Scheller, E.V., Robinson, K.M., Crowe, C.R., Choi, S.M., Slight, S.R., Khader, S.A., Dubin, P.J., Enelow, R.I., Kolls, J.K., and Alcorn, J.F. (2011). Influenza A inhibits Th17-mediated host defense against bacterial pneumonia in mice. J. Immunol. *186*, 1666–1674.

Lazear, H.M., Lancaster, A., Wilkins, C., Suthar, M.S., Huang, A., Vick, S.C., Clepper, L., Thackray, L., Brassil, M.M., Virgin, H.W., et al. (2013). IRF-3, IRF-5, and IRF-7 coordinately regulate the type I IFN response in myeloid dendritic cells downstream of MAVS signaling. PLoS Pathog. *9*, e1003118.

Lee, B., Robinson, K.M., McHugh, K.J., Scheller, E.V., Mandalapu, S., Chen, C., Di, Y.P., Clay, M.E., Enelow, R.I., Dubin, P.J., and Alcorn, J.F. (2015). Influenza-induced type I interferon enhances susceptibility to gram-negative and gram-positive bacterial pneumonia in mice. Am. J. Physiol. Lung Cell. Mol. Physiol. *309*, L158–L167.

LeMessurier, K.S., Häcker, H., Chi, L., Tuomanen, E., and Redecke, V. (2013). Type I interferon protects against pneumococcal invasive disease by inhibiting bacterial transmigration across the lung. PLoS Pathog. *9*, e1003727.

Li, X.-L., Ezelle, H.J., Kang, T.-J., Zhang, L., Shirey, K.A., Harro, J., Hasday, J.D., Mohapatra, S.K., Crasta, O.R., Vogel, S.N., et al. (2008). An essential role for the antiviral endoribonuclease, RNase-L, in antibacterial immunity. Proc. Natl. Acad. Sci. USA *105*, 20816–20821.

Lippmann, J., Müller, H.C., Naujoks, J., Tabeling, C., Shin, S., Witzenrath, M., Hellwig, K., Kirschning, C.J., Taylor, G.A., Barchet, W., et al. (2011). Dissection of a type I interferon pathway in controlling bacterial intracellular infection in mice. Cell. Microbiol. *13*, 1668–1682.

Liu, P.T., Wheelwright, M., Teles, R., Komisopoulou, E., Edfeldt, K., Ferguson, B., Mehta, M.D., Vazirnia, A., Rea, T.H., Sarno, E.N., et al. (2012). MicroRNA-21 targets the vitamin D-dependent antimicrobial pathway in leprosy. Nat. Med. *18*, 267–273.

Liu, S.-Y., Aliyari, R., Chikere, K., Li, G., Marsden, M.D., Smith, J.K., Pernet, O., Guo, H., Nusbaum, R., Zack, J.A., et al. (2013). Interferon-inducible cholesterol-25-hydroxylase broadly inhibits viral entry by production of 25-hydroxycholesterol. Immunity *38*, 92–105.

Liu, F.D.M., Kenngott, E.E., Schröter, M.F., Kühl, A., Jennrich, S., Watzlawick, R., Hoffmann, U., Wolff, T., Norley, S., Scheffold, A., et al. (2014). Timed action of IL-27 protects from immunopathology while preserving defense in influenza. PLoS Pathog. *10*, e1004110, http://dx.doi.org/10.1371/journal.ppat.1004110.

Long, T.M., Chakrabarti, A., Ezelle, H.J., Brennan-Laun, S.E., Raufman, J.P., Polyakova, I., Silverman, R.H., and Hassel, B.A. (2013). RNase-L deficiency exacerbates experimental colitis and colitis-associated cancer. Inflamm. Bowel Dis. *19*, 1295–1305.

Long, T.M., Nisa, S., Donnenberg, M.S., and Hassel, B.A. (2014). Enteropathogenic Escherichia coli inhibits type I interferon- and RNase L-mediated host defense to disrupt intestinal epithelial cell barrier function. Infect. Immun. *82*, 2802–2814.

Mack, E.A., Kallal, L.E., Demers, D.A., and Biron, C.A. (2011). Type 1 interferon induction of natural killer cell gamma interferon production for defense during lymphocytic choriomeningitis virus infection. MBio *2*, e00169–e11.

Manca, C., Tsenova, L., Bergtold, A., Freeman, S., Tovey, M., Musser, J.M., Barry, C.E., 3rd, Freedman, V.H., and Kaplan, G. (2001). Virulence of a Mycobacterium tuberculosis clinical isolate in mice is determined by failure to induce Th1 type immunity and is associated with induction of IFN-alpha /beta. Proc. Natl. Acad. Sci. USA *98*, 5752–5757.

Mancuso, G., Midiri, A., Biondo, C., Beninati, C., Zummo, S., Galbo, R., Tomasello, F., Gambuzza, M., Macrì, G., Ruggeri, A., et al. (2007). Type I IFN signaling is crucial for host resistance against different species of pathogenic bacteria. J. Immunol. *178*, 3126–3133.

Mancuso, G., Gambuzza, M., Midiri, A., Biondo, C., Papasergi, S., Akira, S., Teti, G., and Beninati, C. (2009). Bacterial recognition by TLR7 in the lysosomes of conventional dendritic cells. Nat. Immunol. *10*, 587–594.

Martin, F.J., Gomez, M.I., Wetzel, D.M., Memmi, G., O'Seaghdha, M., Soong, G., Schindler, C., and Prince, A. (2009). Staphylococcus aureus activates type I IFN signaling in mice and humans through the Xr repeated sequences of protein A. J. Clin. Invest. *119*, 1931–1939.

Martins, N.E., Faria, V.G., Teixeira, L., Magalhães, S., and Sucena, É. (2013). Host adaptation is contingent upon the infection route taken by pathogens. PLoS Pathog. *9*, e1003601, http://dx.doi.org/10.1371/journal.ppat.1003601.

Mayer-Barber, K.D., Andrade, B.B., Oland, S.D., Amaral, E.P., Barber, D.L., Gonzales, J., Derrick, S.C., Shi, R., Kumar, N.P., Wei, W., et al. (2014). Host-directed therapy of tuberculosis based on interleukin-1 and type I interferon crosstalk. Nature *511*, 99–103.

McCullers, J.A. (2014). The co-pathogenesis of influenza viruses with bacteria in the lung. Nat. Rev. Microbiol. *12*, 252–262.

McNab, F.W., Ewbank, J., Howes, A., Moreira-Teixeira, L., Martirosyan, A., Ghilardi, N., Saraiva, M., and O'Garra, A. (2014). Type I IFN induces IL-10 production in an IL-27-independent manner and blocks responsiveness to IFN-γ for production of IL-12 and bacterial killing in Mycobacterium tuberculosis-infected macrophages. J. Immunol. *193*, 3600–3612.

Miyagi, T., Gil, M.P., Wang, X., Louten, J., Chu, W.-M., and Biron, C.A. (2007). High basal STAT4 balanced by STAT1 induction to control type 1 interferon effects in natural killer cells. J. Exp. Med. *204*, 2383–2396.

Monticelli, L.A., Sonnenberg, G.F., Abt, M.C., Alenghat, T., Ziegler, C.G., Doering, T.A., Angelosanto, J.M., Laidlaw, B.J., Yang, C.Y., Sathaliyawala, T., et al. (2011). Innate lymphoid cells promote lung-tissue homeostasis after infection with influenza virus. Nat. Immunol. *12*, 1045–1054.

Naujoks, J., Tabeling, C., Dill, B.D., Hoffmann, C., Brown, A.S., Kunze, M., Kempa, S., Peter, A., Mollenkopf, H.J., Dorhoi, A., et al. (2016). IFNs modify the proteome of legionella-containing vacuoles and restrict infection Via IRG1-derived itaconic acid. PLoS Pathog. *12*, e1005408.

Ng, C.T., Sullivan, B.M., Teijaro, J.R., Lee, A.M., Welch, M., Rice, S., Sheehan, K.C.F., Schreiber, R.D., and Oldstone, M.B. (2015). Blockade of interferon beta, but not interferon alpha, signaling controls persistent viral infection. Cell Host Microbe *17*, 653–661.

O'Connell, R.M., Saha, S.K., Vaidya, S.A., Bruhn, K.W., Miranda, G.A., Zarnegar, B., Perry, A.K., Nguyen, B.O., Lane, T.F., Taniguchi, T., et al. (2004). Type I interferon production enhances susceptibility to Listeria monocytogenes infection. J. Exp. Med. *200*, 437–445.

O'Connell, R.M., Vaidya, S.A., Perry, A.K., Saha, S.K., Dempsey, P.W., and Cheng, G. (2005). Immune activation of type I IFNs by Listeria monocytogenes occurs independently of TLR4, TLR2, and receptor interacting protein 2 but involves TNFR-associated NF kappa B kinase-binding kinase 1. J. Immunol. *174*, 1602–1607.

Pandey, A.K., Yang, Y., Jiang, Z., Fortune, S.M., Coulombe, F., Behr, M.A., Fitzgerald, K.A., Sassetti, C.M., and Kelliher, M.A. (2009). NOD2, RIP2 and IRF5 play a critical role in the type I interferon response to Mycobacterium tuberculosis. PLoS Pathog. *5*, e1000500.

Parker, D., Martin, F.J., Soong, G., Harfenist, B.S., Aguilar, J.L., Ratner, A.J., Fitzgerald, K.A., Schindler, C., and Prince, A. (2011). Streptococcus pneumoniae DNA initiates type I interferon signaling in the respiratory tract. MBio *2*, e00016–e11.

Parker, D., Planet, P.J., Soong, G., Narechania, A., and Prince, A. (2014). Induction of type I interferon signaling determines the relative pathogenicity of Staphylococcus aureus strains. PLoS Pathog. *10*, e1003951, http://dx.doi.org/10.1371/journal.ppat.1003951.

Parvatiyar, K., Zhang, Z., Teles, R.M., Ouyang, S., Jiang, Y., Iyer, S.S., Zaver, S.A., Schenk, M., Zeng, S., Zhong, W., et al. (2012). The helicase DDX41 recognizes the bacterial secondary messengers cyclic di-GMP and cyclic di-AMP to activate a type I interferon immune response. Nat. Immunol. *13*, 1155–1161, http://dx.doi.org/10.1038/ni.2460.

Perkins, D.J., Rajaiah, R., Tennant, S.M., Ramachandran, G., Higginson, E.E., Dyson, T.N., and Vogel, S.N. (2015). Salmonella Typhimurium co-opts the host type I IFN system to restrict macrophage innate immune transcriptional responses selectively. J. Immunol. *195*, 2461–2471, http://dx.doi.org/10.4049/jimmunol.1500105.

Platanias, L.C. (2005). Mechanisms of type-I- and type-II-interferon-mediated signalling. Nat. Rev. Immunol. *5*, 375–386.

Plumlee, C.R., Lee, C., Beg, A.A., Decker, T., Shuman, H.A., and Schindler, C. (2009). Interferons direct an effective innate response to Legionella pneumophila infection. J. Biol. Chem. *284*, 30058–30066.

Prakash, A., Smith, E., Lee, C.K., and Levy, D.E. (2005). Tissue-specific positive feedback requirements for production of type I interferon following virus infection. J. Biol. Chem. *280*, 18651–18657.

Rathinam, V.A., Jiang, Z., Waggoner, S.N., Sharma, S., Cole, L.E., Waggoner, L., Vanaja, S.K., Monks, B.G., Ganesan, S., Latz, E., et al. (2010). The AIM2 inflammasome is essential for host defense against cytosolic bacteria and DNA viruses. Nat. Immunol. *11*, 395–402.

Rayamajhi, M., Humann, J., Penheiter, K., Andreasen, K., and Lenz, L.L. (2010). Induction of IFN-alphabeta enables Listeria monocytogenes to suppress macrophage activation by IFN-gamma. J. Exp. Med. *207*, 327–337.

Reboldi, A., Dang, E.V., McDonald, J.G., Liang, G., Russell, D.W., and Cyster, J.G. (2014). Inflammation. 25-Hydroxycholesterol suppresses interleukin-1-driven inflammation downstream of type I interferon. Science *345*, 679–684.

Robinson, N., McComb, S., Mulligan, R., Dudani, R., Krishnan, L., and Sad, S. (2012). Type I interferon induces necroptosis in macrophages during infection with Salmonella enterica serovar Typhimurium. Nat. Immunol. *13*, 954–962.

Robinson, K.M., Lee, B., Scheller, E.V., Mandalapu, S., Enelow, R.I., Kolls, J.K., and Alcorn, J.F. (2015). The role of IL-27 in susceptibility to post-influenza Staphylococcus aureus pneumonia. Respir. Res. *16*, 10.

Sanchez, D.J., Miranda, D., Jr., Arumugaswami, V., Hwang, S., Singer, A.E., Senaati, A., Shahangian, A., Song, M.J., Sun, R., and Cheng, G. (2008). A repetitive region of gammaherpesvirus genomic DNA is a ligand for induction of type I interferon. J. Virol. *82*, 2208–2217.

Schliehe, C., Flynn, E.K., Vilagos, B., Richson, U., Swaminathan, S., Bosnjak, B., Bauer, L., Kandasamy, R.K., Griesshammer, I.M., Kosack, L., et al. (2015). The methyltransferase Setdb2 mediates virus-induced susceptibility to bacterial superinfection. Nat. Immunol. *16*, 67–74.

Schmolke, M., Patel, J.R., de Castro, E., Sánchez-Aparicio, M.T., Uccellini, M.B., Miller, J.C., Manicassamy, B., Satoh, T., Kawai, T., Akira, S., et al. (2014). RIG-I detects mRNA of intracellular Salmonella enterica serovar Typhimurium during bacterial infection. MBio *5*, e01006–e01014.

Sewnath, M.E., Olszyna, D.P., Birjmohun, R., ten Kate, F.J., Gouma, D.J., and van Der Poll, T. (2001). IL-10-deficient mice demonstrate multiple organ failure and increased mortality during Escherichia coli peritonitis despite an accelerated bacterial clearance. J. Immunol. *166*, 6323–6331.

Shahangian, A., Chow, E.K., Tian, X., Kang, J.R., Ghaffari, A., Liu, S.Y., Belperio, J.A., Cheng, G., and Deng, J.C. (2009). Type I IFNs mediate development of postinfluenza bacterial pneumonia in mice. J. Clin. Invest. *119*, 1910–1920.

Stockinger, S., Kastner, R., Kernbauer, E., Pilz, A., Westermayer, S., Reutterer, B., Soulat, D., Stengl, G., Vogl, C., Frenz, T., et al. (2009). Characterization of the interferon-producing cell in mice infected with Listeria monocytogenes. PLoS Pathog. *5*, e1000355.

Storek, K.M., Gertsvolf, N.A., Ohlson, M.B., and Monack, D.M. (2015). cGAS and Ifi204 cooperate to produce type I IFNs in response to Francisella infection. J. Immunol. *194*, 3236–3245.

Sueltenfuss, E.A., and Pollard, M. (1963). Cytochemical assay of interferon produced by duck hepatitis virus. Science *139*, 595–596.

Sun, L., Wu, J., Du, F., Chen, X., and Chen, Z.J. (2013). Cyclic GMP-AMP synthase is a cytosolic DNA sensor that activates the type I interferon pathway. Science *339*, 786–791.

Teles, R.M.B., Graeber, T.G., Krutzik, S.R., Montoya, D., Schenk, M., Lee, D.J., Komisopoulou, E., Kelly-Scumpia, K., Chun, R., Iyer, S.S., et al. (2013). Type I interferon suppresses type II interferon-triggered human anti-mycobacterial responses. Science *339*, 1448–1453.

Teles, R.M.B., Kelly-Scumpia, K.M., Sarno, E.N., Rea, T.H., Ochoa, M.T., Cheng, G., and Modlin, R.L. (2015). IL-27 suppresses antimicrobial activity in human leprosy. J. Invest. Dermatol. *135*, 2410–2417.

Unterholzner, L., Keating, S.E., Baran, M., Horan, K.A., Jensen, S.B., Sharma, S., Sirois, C.M., Jin, T., Latz, E., Xiao, T.S., et al. (2010). IFI16 is an innate immune sensor for intracellular DNA. Nat. Immunol. *11*, 997–1004.

Wassermann, R., Gulen, M.F., Sala, C., Perin, S.G., Lou, Y., Rybniker, J., Schmid-Burgk, J.L., Schmidt, T., Hornung, V., Cole, S.T., and Ablasser, A. (2015). Mycobacterium tuberculosis differentially activates cGAS- and inflammasome-dependent intracellular immune responses through ESX-1. Cell Host Microbe *17*, 799–810.

Watanabe, T., Asano, N., Fichtner-Feigl, S., Gorelick, P.L., Tsuji, Y., Matsumoto, Y., Chiba, T., Fuss, I.J., Kitani, A., and Strober, W. (2010). NOD1 contributes to mouse host defense against Helicobacter pylori via induction of type I IFN and activation of the ISGF3 signaling pathway. J. Clin. Invest. *120*, 1645–1662.

Watson, R.O., Bell, S.L., MacDuff, D.A., Kimmey, J.M., Diner, E.J., Olivas, J., Vance, R.E., Stallings, C.L., Virgin, H.W., and Cox, J.S. (2015). The cytosolic sensor cGAS detects Mycobacterium tuberculosis DNA to induce type I interferons and activate autophagy. Cell Host Microbe *17*, 811–819.

Wilson, E.B., Yamada, D.H., Elsaesser, H., Herskovitz, J., Deng, J., Cheng, G., Aronow, B.J., Karp, C.L., and Brooks, D.G. (2013). Blockade of chronic type I interferon signaling to control persistent LCMV infection. Science *340*, 202–207.

Yan, N., and Chen, Z.J. (2012). Intrinsic antiviral immunity. Nat. Immunol. *13*, 214–222.

Yarilina, A., Park-Min, K.-H., Antoniv, T., Hu, X., and Ivashkiv, L.B. (2008). TNF activates an IRF1-dependent autocrine loop leading to sustained expression of chemokines and STAT1-dependent type I interferon-response genes. Nat. Immunol. *9*, 378–387.

York, A.G., Williams, K.J., Argus, J.P., Zhou, Q.D., Brar, G., Vergnes, L., Gray, E.E., Zhen, A., Wu, N.C., Yamada, D.H., et al. (2015). Limiting cholesterol biosynthetic flux spontaneously engages type I IFN signaling. Cell *163*, 1716–1729.

CHAPTER 3

Induction of type I IFNs and role of IFN-beta signaling during bacterial infections

ABSTRACT

Type I interferons (IFN) are a family of small, pleiotropic cytokines that regulate the expression of a broad set of interferon stimulated genes (ISGs). Well known for their role in directing the host antiviral response, type I IFNs also play an important role in modulating host defense against bacterial infections. All type I IFNs signal through the type I IFN receptor (IFNAR) and induce an almost identical set of ISGs. Lipid A, a cell wall component of Gram negative bacteria stimulates the induction of type I IFNs and downstream ISGs. To examine the requirement for IFNβ signaling following lipid A treatment, bone marrow derived macrophages (BMMs) from mice with a genetic deficiency in IFNβ were compared to BMMs derived from wild type or IFNAR1 deficient mice. Gene expression was measured by RNASeq and quantitative PCR (qPCR). *Ifnb* was the primary type I IFN induced by the macrophages and IFNβ signaling was necessary for ISG expression. Furthermore, treatment with recombinant IFNβ or IFNα4 revealed induction of ISGs by IFNα4 was enhanced by IFNβ signaling. The role of IFNβ signaling was studied using two mouse models, acute *E. coli* peritonitis and post-influenza bacterial pneumonia. In the peritonitis model, IFNAR signaling is required to protect the host, thus we hypothesized that IFNβ was necessary for host resistance. There was only a modest decrease in the survival of IFNβ KO mice, indicating that additional pathways contributed and/or compensated for the loss of IFNβ signaling. In the post-influenza model, deficiency in IFNAR signaling was previously found to enhance bacterial clearance and promote host defense, so we hypothesized that IFNβ would promote bacterial pneumonia. Surprisingly, IFNβ deficient mice were as susceptible as wild type mice to pneumonia. From this we conclude that IFNβ is not acting alone, other type I IFNs, likely one or more of the IFNαs, contribute to enhanced host susceptibility.

INTRODUCTION

Induction of type I IFNs and ISGs

Macrophages are one of the first responders to an immunological threat. Due to their active role in early host defense, they are widely used to study innate immune gene regulation. Microarray analysis of macrophages stimulated with lipid A, a purified component of lipopolysaccharide (LPS) constituent of the Gram negative bacterial cell wall, revealed that more than 300 genes were IFNAR1 dependent [1]. *Ifnb* is considered a signature gene of LPS stimulation [2], however, microarray analysis of LPS stimulated IFNβ sufficient and deficient primary and ex vivo derived macrophages identified only 62 LPS regulated genes to be IFNβ dependent [3]. To investigate this discrepancy, we used RNA-Seq and qPCR to compared gene expression levels from WT, IFNAR1 KO and IFNβ KO BMMs stimulated with lipid A. We were interested to know whether expression of ISGs by BMMs requires IFNβ signaling.

Type I IFNs have distinct and overlapping functions [4–6]. ISG expression requires autocrine and paracrine signaling for maximal expression [7]. This is achieved by the induction of ISGs that function in the type I IFN signaling pathway, such as the transcription factors *Irf7* [8] and *Stat1* [9]. Interestingly, specific subtypes of type I IFN are preferentially administered to treat disease. For example, several subtypes of IFNα are used to treat cancer and chronic viral infection [10], while IFNβ is used to treat multiple sclerosis [11]. To study the requirement for IFNβ in ISG expression, we examined the magnitude of ISG induction following treatment of WT, IFNAR1 KO and IFNβ KO BMMs with recombinant IFNβ or IFNα4.

How type I IFNs contribute to host defense against bacteria is poorly understood. Differential activation of downstream ISGs suggests type I IFNs may mediate distinct functional outcomes during bacterial infections. To test this, we used two mouse models of bacterial infection: primary *Escherichia coli* (*E. coli*) peritonitis and secondary *Streptococcus pneumoniae* pneumonia.

IFNAR signaling protects the host against lethal *E. coli* peritonitis [12]. Once the pattern recognition receptor (PRR), TLR4, detects LPS on the *E. coli* cell wall it associates with two downstream adapter molecules, MyD88 and TRIF. TRIF dependent signaling leads to induction of type I IFN and is required to protect the host against *E. coli* peritonitis [13]. A possible mechanism for type I IFN mediated host defense against *E. coli* peritonitis is through the induction of the anti-inflammatory cytokine, IL-10 [14–16]. IL-10 signaling is critical to limit bystander tissue damage associated with the host proinflammatory response during *E. coli* infection [17]. To determine whether IFNβ is necessary and sufficient to defend the host against *E. coli* peritonitis, we measured survival of WT, IFNAR1 KO and IFNβ KO mice.

Influenza is an acute viral infection that is highly associated with the development of life-threatening secondary bacterial pneumonia [18]. The host response to influenza infection is characterized by the generation of a type I interferon response and infiltration of inflammatory cells into the lungs. During acute sub-lethal infections, inflammatory cell infiltration is observed 2 – 14 days post-infection and corresponds to viral clearance [19,20]. Both IFNβ and IFNα have been implicated in lung pathology [21], however in some viral infections, IFNβ alone mediates tissue damage [4].

Our lab previously demonstrated that IFNAR signaling during influenza lung infection promotes bacterial superinfection in the lung and leads to life threatening bacterial pneumonia [22]. To determine whether IFNβ signaling enhances host susceptibility to pneumonia, we infected WT, IFNβ KO and IFNAR1 KO with either influenza PR8 and *Streptococcus pneumoniae* (*S. pneumoniae*) or *S. pneumoniae* alone to elucidate the contribution of IFNβ signaling to disease progression and severity.

RESULTS

Lipid A induced ISG expression in macrophages primarily depends on IFNβ

Using RNAseq, we compared the level of gene induction in WT, IFNAR1 knockout (KO) and IFNβ KO BMMs, 4 and 12 hours after lipid A stimulation. Many of the genes induced by WT mice at both 4 and 12 hours depended on IFNAR1 signaling (Figure 3.1 A and B, left most panels). Likewise, a similar proportion of genes induced by lipid A stimulation of WT BMMs depended on IFNβ signaling (Figure 3.1 A and B, middle panels). Gene expression in IFNAR1 KO was then compared to gene expression in IFNβ KO BMMs. We found the expression of interferon stimulated genes was highly dependent on IFNβ signaling as gene expression patterns from macrophages lacking either IFNAR1 or IFNβ positively correlated at both 4 and 12 hours post stimulation (Figure 3.1).

In fact, *Ifnb* was the only type I IFN expressed by macrophages in response to lipid A. This observation was confirmed by qPCR (Figure 3.2, A). To examine whether the intact Gram negative bacteria elicited a similar response, we infected macrophages with *E. coli* bacteria grown to mid-log phase. Like purified lipid A, *E. coli* infected macrophages expressed *Ifnb*, not *Ifna4* (Figure 3.2, B). We further showed that the absence of transcripts for other type I IFNs was not an intrinsic defect of the macrophages but rather a consequence of the ligand-receptor signaling pathways activated, as *Ifna4* was induced following stimulation of cytosolic sensors by the RNA virus vesicular somatitis virus (VSV) (Figure 3.2, C).

To measure the expression profile of *Ifnb* and *Ifna4* in other immune cell types, bone marrow was differentiated to either conventional dendritic cells (cDCs) or plasmacytoid dendritic cells (pDCs). Stimulation of cDCs with LPS did not lead to induction of type I IFNs, while infection with *E. coli*, mildly induced *Ifnb* at 16 hours, but failed to induce *Ifna4*. *Ifnb* and *Ifna4* were induced by VSV infection of cDCs at both 4 and 16 hours, and the induction of *Ifna4* was comparable or slightly more in IFNβ KO cDCs than in WT (Supplementary figure 3.1, A). In

pDCs, LPS mildly stimulated Ifnb transcription, whereas the classic pDC ligand, CpGA, induced transcription of both *Ifnb* and *Ifna4* (Supplementary figure 3.1, B).

Maximal ISG induction requires IFNβ signaling

Next, we examined the induction of downstream ISGs to characterize the functional outcome of type I IFN expression. As anticipated, ISGs such as *Mx1* were transcribed by WT BMMs following lipid A or E. coli treatment (Figure 3.3, A and B). Since VSV infection led IFNβ KO BMMs to transcribe IFNα4 (Figure 3.2, C), we measured induction of downstream ISGs. Surprisingly, we found that were not transcribed by BMMs lacking IFNβ (Figure 3.3, C). This led us to explore the ISG signature following treatment of BMMs with purified IFNβ and IFNα.

BMMs were exposed to either rIFNβ or rIFNα, equivalent in unit activity, for 4 hours. Gene expression was measured by RNASeq and validated by qPCR. In WT BMMs, expression of downstream ISGs was almost comparable observed. However, in the absence of IFNβ signaling, IFNα4 induced ISG expression that was roughly 50% of the maximum induced by WT BMMs or IFNβ stimulated IFNβ KO BMMs (Figure 3.4, A – C). Thus, IFNβ signaling is crucial maintenance of the positive feedback loop for maximal ISG expression by BMMs.

IFNβ signaling promotes host defense during *E. coli* peritonitis

To study the functional consequence of the IFNβ bias by macrophages, we turned to in vivo models of bacterial infection. IFNAR signaling during *E. coli* peritonitis protects the host against lethal sepsis [12]. In macrophages, IFNβ induces IL-10 [14,15], a key anti-inflammatory cytokine that protects against *E. coli* peritonitis [17]. To determine whether IFNβ was required to mediate the protective response, an *E. coli* peritonitis model was established. Using this model, 10^5 CFU of *E. coli* O18:K1:H7, a clinical isolate was introduced by intraperitoneal injection. At this dose, all of the WT mice survive, while IL-10 deficient mice show a survival of 60% over 5 days. IFNβ deficiency increased mortality by 20% compared to WT when infected with either 10^5 or 10^7 CFU (Figure 3.5, A). Overall, however, there was no significant difference in bacterial

burden in the blood or peritoneal cavity of WT and IFNβ KO mice (Figure 3.5, B). Likewise, the gene expression pattern of the peritoneal exudate cells also showed no difference (Figure 3.4, C). Serum ALT, a marker of liver damage was elevated in IFNβ KO mice compared to WT, but both were still significantly lower than in IL-10 KO mice (Figure 3.5, D). Surprisingly, more IL-10 protein was found in the peritoneal lavage fluid of IFNβ KO mice (Figure 3.5, E), indicating other pathways leading to IL-10 production were activated.

Role of IFNβ during post-influenza bacterial pneumonia

Macrophages are one of the key type I IFN producers during influenza infection [23]. Given the preference for ex vivo differentiated macrophage cells to produce IFNβ, we established a mouse model of Influenza lung infection to characterize the production of type I IFNs and progression of a sub-lethal influenza infection. The dose required to achieve a sublethal infection was found to be 200 PFU of mouse adapted Influenza PR8 (Supplementary figure 3.2). At this dose, mice exhibited incremental weight loss beginning at day 3, reaching a maximum loss by day 10 and regaining to the pre-infection weight by day 17 (Figure 3.6, A). Viral load peaked at day 3 and by day 12 replicating virus was undetectable (Figure 3.6, B and C). The kinetics of polymorphonuclear (PMN) cell infiltration followed viral load and peaked at day 3 (Figure 3.6, D). Measurement of type I IFN gene expression in the lung revealed temporal differences in the expression of *Ifnb* and *Ifna*s; *Ifnb* peaked on day 5 whereas *Ifna4* and *Ifna5* on day 7 (Figure 3.5, E). Moreover, there was a difference in the expression magnitude; peak *Ifnb* was about 3-fold higher than peak *Ifna4* or *Ifna5*. Finally, at the tissue level, viral infiltration of alveolar cells precedes the disappearance of these cells, likely due to virus mediated cell death (Figure 3.5, F). This results in disruption of the tissue architecture of the alveolar lining.

Using this model, we tested whether development of post-influenza pneumonia is solely due to IFNβ signaling. WT, IFNAR1 KO and IFNβ KO mice were infected on day 0 with a sub-lethal dose of Influenza PR8, then 5 days later PR8 infected and naïve mice were challenged

with a sub-lethal dose of *S. pneumoniae* A66a. Co-infected WT mice experienced more weight loss than IFNAR1 KO mice. Unexpectedly, the weight change of IFNβ KO mice followed a pattern similar to WT mice, not IFNAR1 KO mice (Figure 3.7, A). Likewise, bacterial burden in the lungs of co-infected WT and IFNβ KO mice was higher than in the lungs of IFNAR1 KO (Figure 3.7, B), while viral load was similar (Figure 3.6, C). There was no significant difference in the induction of type I IFNs, *Ifna4* and *Ifna5*, or type III IFN, *Ifnl2/3*, between co-infected WT, IFNAR1 KO and IFNβ KO mice at day 7 (Figure 3.7, D). Interestingly, absence of IFNβ signaling compromised the induction of ISGs in the lung. Transcription of *Mx1* and *Cxcl10* was reduced in IFNβ KO mice compared to WT. In addition, chemokines, *Mip2* and *Kc*, were similarly reduced (Figure 3.7, F). These results show that while IFNβ signaling contributes, it is not sufficient to drive bacterial superinfection in the lung.

DISCUSSION

ISG induction by BMMs stimulated with bacterial ligand lipid A depends on IFNβ signaling (Figure 3.1). Indeed, in macrophages, IFNβ is categorized as a primary response gene, induced 35 min after lipid A stimulation [24]. The IFNα4 promoter is the only IFNα promoter that has an intact IRF3 binding site [25], yet bacterial ligands that induce *Ifnb* do not lead to *Ifna4* transcription (Figure 3.2, A and B). It is not clear why *Ifna* is not transcribed, but it is not general defect in macrophages as viral infection with VSV leads to its induction (Figure 3.2, C). Therefore, expression of type I IFNs and downstream ISGs depends on the stimulating ligand and the activating receptor.

We also show IFNβ signaling is required for maximum ISGs expression (Figure 3.3 and 3.4). The JAK-STAT pathway is the dominant signaling pathway involved in the induction of interferon stimulated genes (ISGs). Interestingly, TYK2 appears to be an accessory kinase augmenting STAT1 and STAT2 phosphorylation during IFNβ stimulation and it does not play a role when IFNα is the ligand [26]. Thus, it would be interesting to measure the level of STAT phosphorylation to further elucidate the reason for the weak induction of ISGs by IFNαs.

The inherent bias of macrophages to produce IFNβ after stimulation with bacterial ligands led us to examine the contribution of IFNβ signaling to host defense in two different models of bacterial infection. In the *E. coli* peritonitis model, IFNAR signaling bolsters host resistance [12]. Absence of IFNβ modestly decreases survival (Figure 3.4, A). Though we have previously published IFNβ is necessary for IL-10 induction in macrophages, other pathways also lead to IL-10 [27].The presence of more IL-10 protein in the peritoneal cavity of IFNβ KO mice (Figure 3.4, E) suggests these other pathways contribute and/or compensate when IFNβ signaling is absent.

Previously, we have shown that influenza infection promotes bacterial superinfection by signaling through IFNAR [22]. Here we show IFNAR1 KO mice are protected but IFNβ KO are not

(Figure 3.6). This result suggests another type I IFN subtype may mediate the pathogenic activity. This could be one or more of the IFNα subtypes. IFNβ has been reported to promote tissue damage in a manner distinct from other type I IFNs [4,5]. Others have observed IFNβ and IFNαs are functionally redundant during influenza infection, both promoting more severe tissue damage and are expendable for antiviral response [21]. An alternate explanation could be that constitutive expression of IFNε is enhanced and/or sufficient to support superinfection. IFNε [28] and IFNω [29] have been described to elicit antiviral activities in a manner similar to IFNα/β, however activity potency is dictated by their nuanced binding to IFNAR [30].

Though we did not find an exclusive role for IFNβ in promoting lung bacterial superinfection, we recently observed influenza induced type I IFNs exert detrimental effects on the homeostasis of a distant organ (Appendix B) [31]. IFNAR dependent intestinal microbiota dysbiosis was observed following sub-lethal lung infection with influenza. In addition, IFNAR signaling also promoted gut infection by *Salmonella* (Appendix B) [31]. During single infection with Salmonella, IFNβ signaling contributes to pathogenesis by initiating a cell death process called necroptosis [5]. Using IFNβ KO mice we will examine the role of influenza induced IFNβ on gut microbiota and *Salmonella* infection.

Further studies are necessary to appreciate the dynamics of type I IFNs during bacterial infection. IFNβ is preferentially induced by macrophages and IFNβ signaling is required to amplify ISG expression. Yet, during infections where IFNAR signaling enhances host defense, IFNβ deficiency is less detrimental than IFNAR1 deficiency. Moreover, during post-influenza pneumonia where IFNAR signaling is detrimental, loss of IFNβ signaling does not promote host resistance.

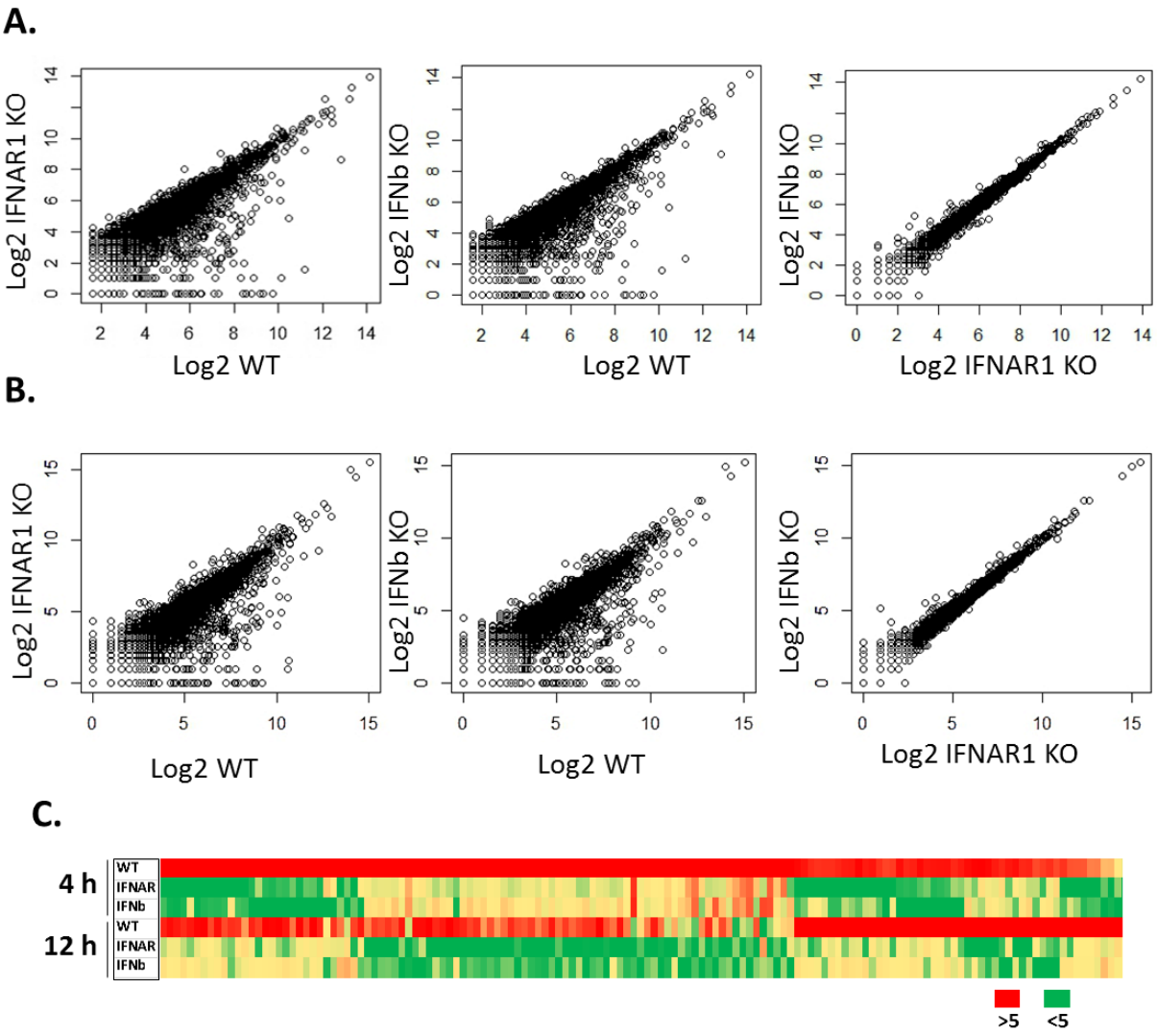

Figure 3.1. Lipid A induced gene expression in WT, IFNAR1 KO and IFNβ KO BMMs.

Scatter plots of gene expression level measured by RPKM after 4 (A) or 12 hours (B) incubation with lipid A. Heat map of type I IFN stimulated genes (C).

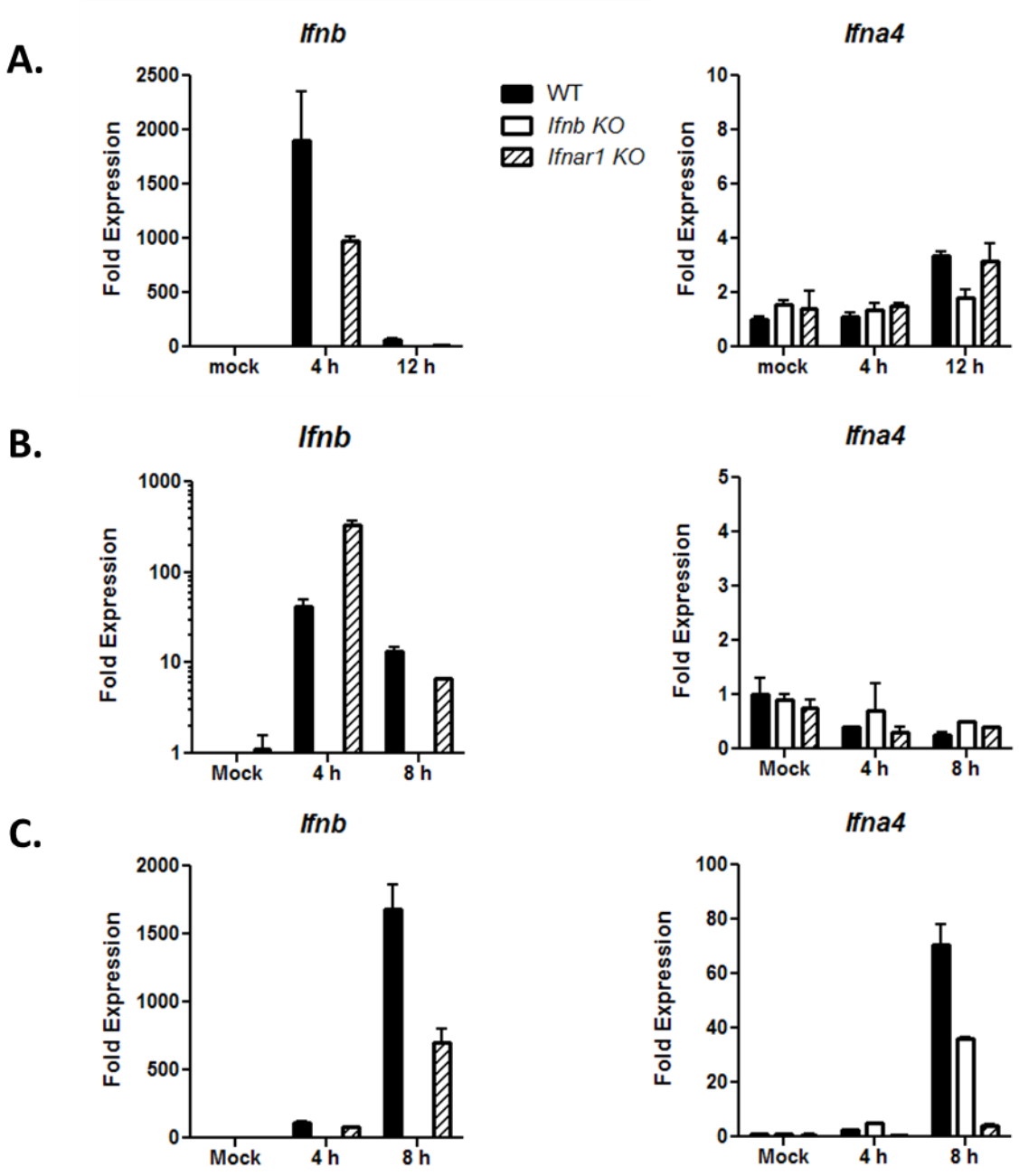

Figure 3.2. Expression of type I IFNs by BMMs is ligand dependent. WT, IFNAR1 KO and IFNβ KO BMMs were stimulated with lipid A for 4 and 12 hours (A), *E. coli* bacteria for 4 and 8 hours (B) or VSV virus for 4 and 8 hours (C).

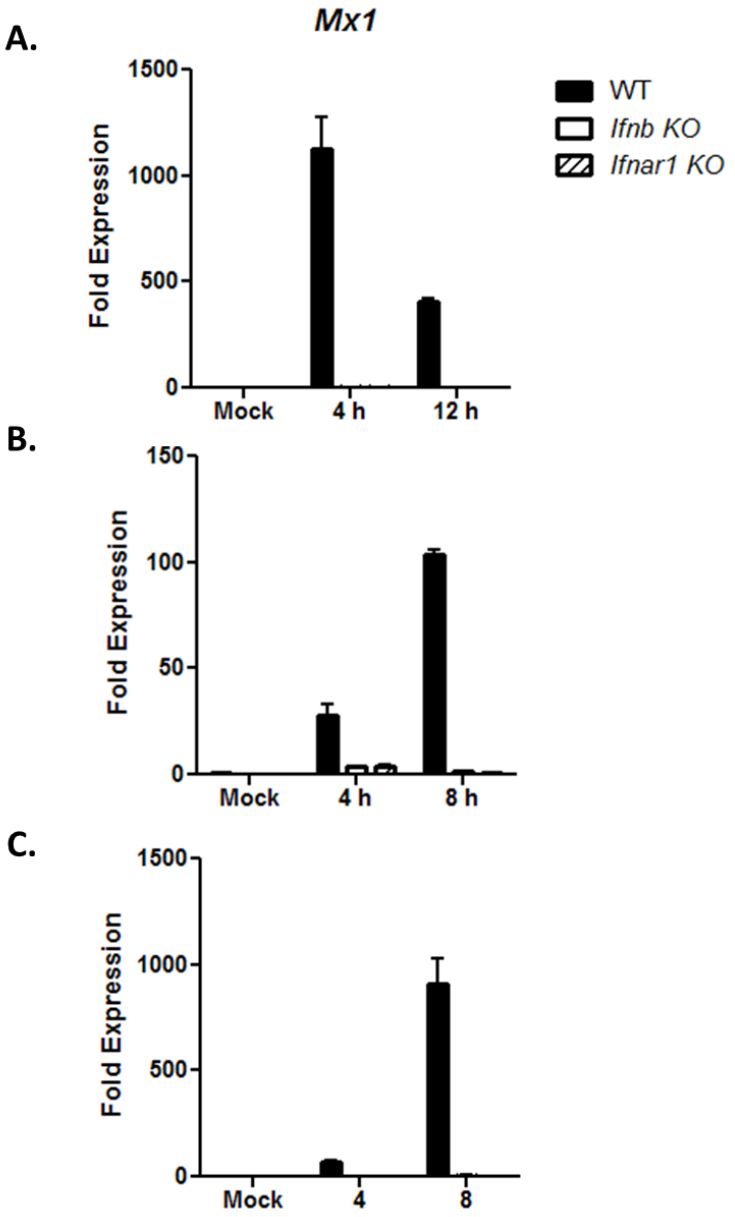

Figure 3.3. IFNβ signaling is required for induction of downstream ISG *Mx1*. WT, IFNAR1 KO and IFNβ KO BMMs were stimulated with lipid A (A) or infected with either E. coli (B) or VSV (C) and gene expression was measured by qPCR.

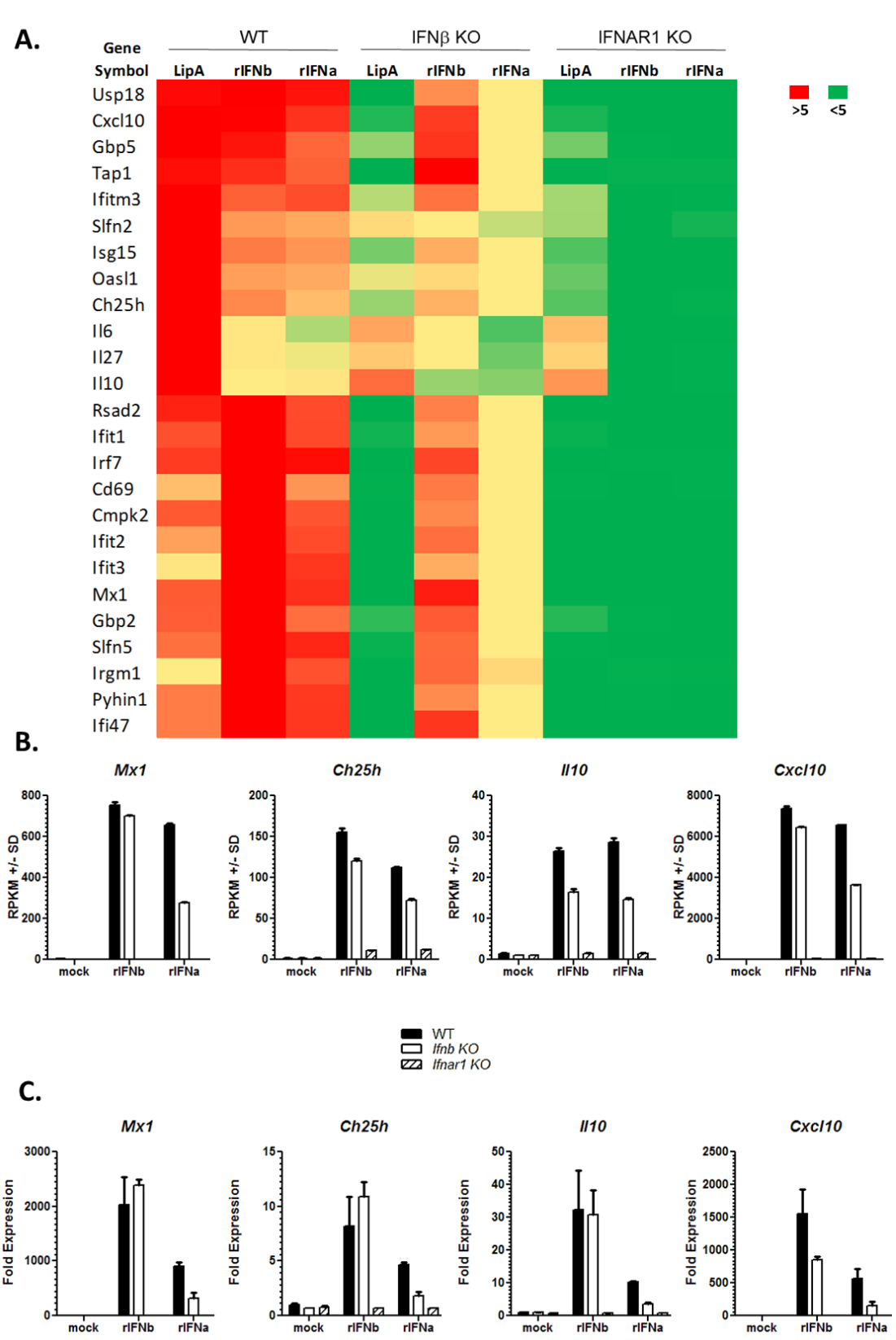
A.
Gene Symbol
WT
IFNβ KO
IFNAR1 KO
LipA
rIFNb
rIFNa
Usp18
Cxcl10
Gbp5
Tap1
Ifitm3
Slfn2
Isg15
Oasl1
Ch25h
Il6
Il27
Il10
Rsad2
Ifit1
Irf7
Cd69
Cmpk2
Ifit2
Ifit3
Mx1
Gbp2
Slfn5
Irgm1
Pyhin1
Ifi47
>5
<5
B.
Mx1
Ch25h
Il10
Cxcl10
RPKM +/- SD
mock
rIFNb
rIFNa
WT
Ifnb KO
Ifnar1 KO
C.
Fold Expression

Figure 3.4. Recombinant IFNβ and IFNα4 treatment elicit different magnitudes of ISG expression. BMMs from WT, IFNAR1 KO and IFNβ KO were stimulated with lipid A or incubated with 500 U of rIFNβ or rIFNα4 for 4 hours. Heat map of select ISGS (A). Gene expression measured by RPKM (B) and quantitative PCR (C) of different ISGs.

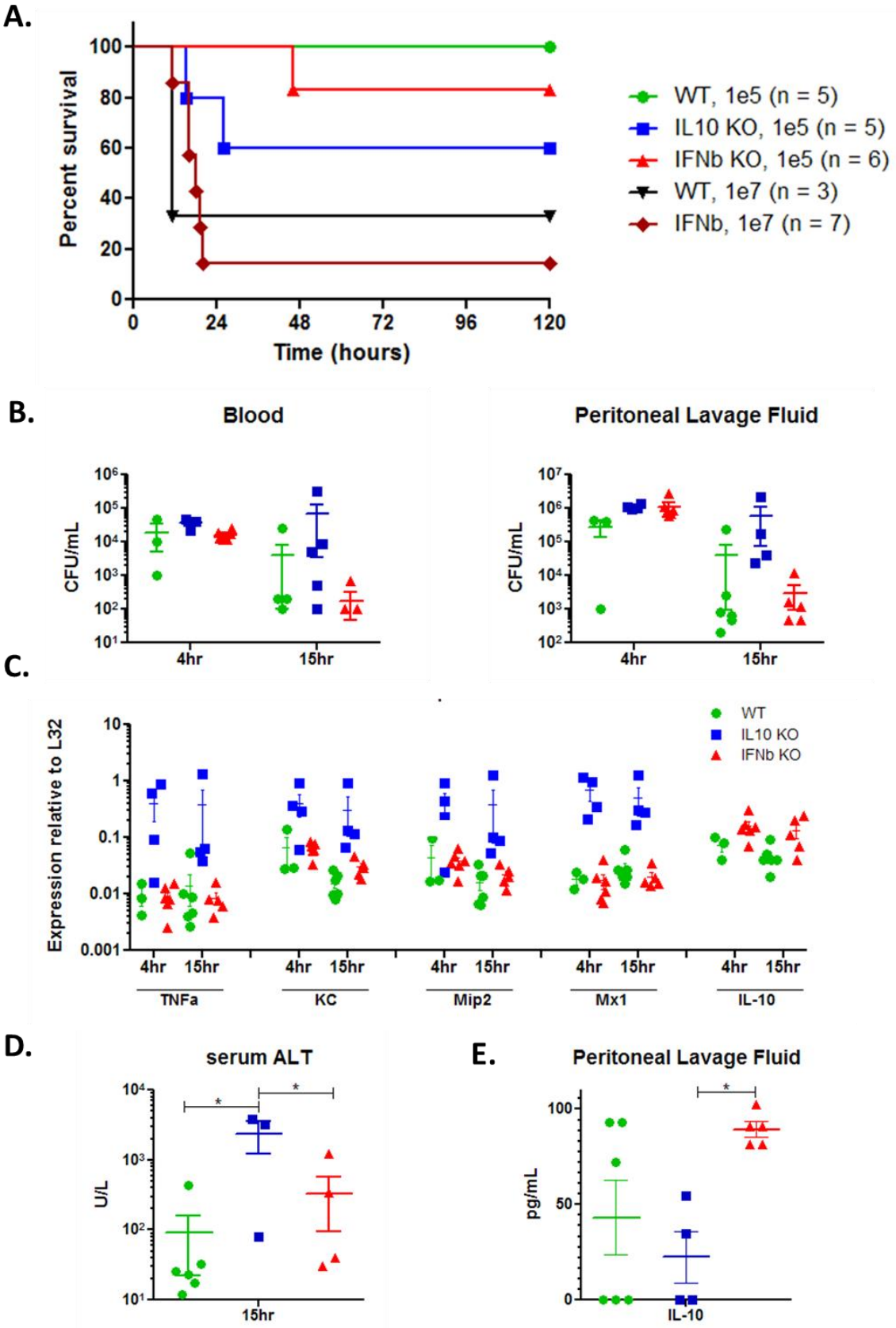
A.
Percent survival
Time (hours)
WT, 1e5 (n = 5)
IL10 KO, 1e5 (n = 5)
IFNb KO, 1e5 (n = 6)
WT, 1e7 (n = 3)
IFNb, 1e7 (n = 7)
B.
Blood
Peritoneal Lavage Fluid
CFU/mL
4hr
15hr
C.
Expression relative to L32
WT
IL10 KO
IFNb KO
TNFa
KC
Mip2
Mx1
IL-10
D.
serum ALT
U/L
E.
Peritoneal Lavage Fluid
pg/mL

Figure 3.5. IFNβ signaling contributes to host survival during *E. coli* peritonitis. WT, IL-10 KO and IFNβ KO mice were infected by intraperitoneal injection with 10^5 CFU of *E. coli* bacteria grown to mid-log phase and a separate cohort of WT and IFNβ KO mice were infected with 10^7 CFU of *E. coli* bacteria; survival was monitored (A). Cohorts of mice infected with 10^5 CFU of *E. coli* bacteria were euthanized at 4 and 15 hours; bacterial burden in the blood and peritoneal lavage fluid was quantified (B), gene expression in peritoneal exudate cells was measured by quantitative PCR, serum ALT was determined by colorimetric assay (D) and IL-10 protein in the peritoneal lavage fluid was measured by ELISA (E).

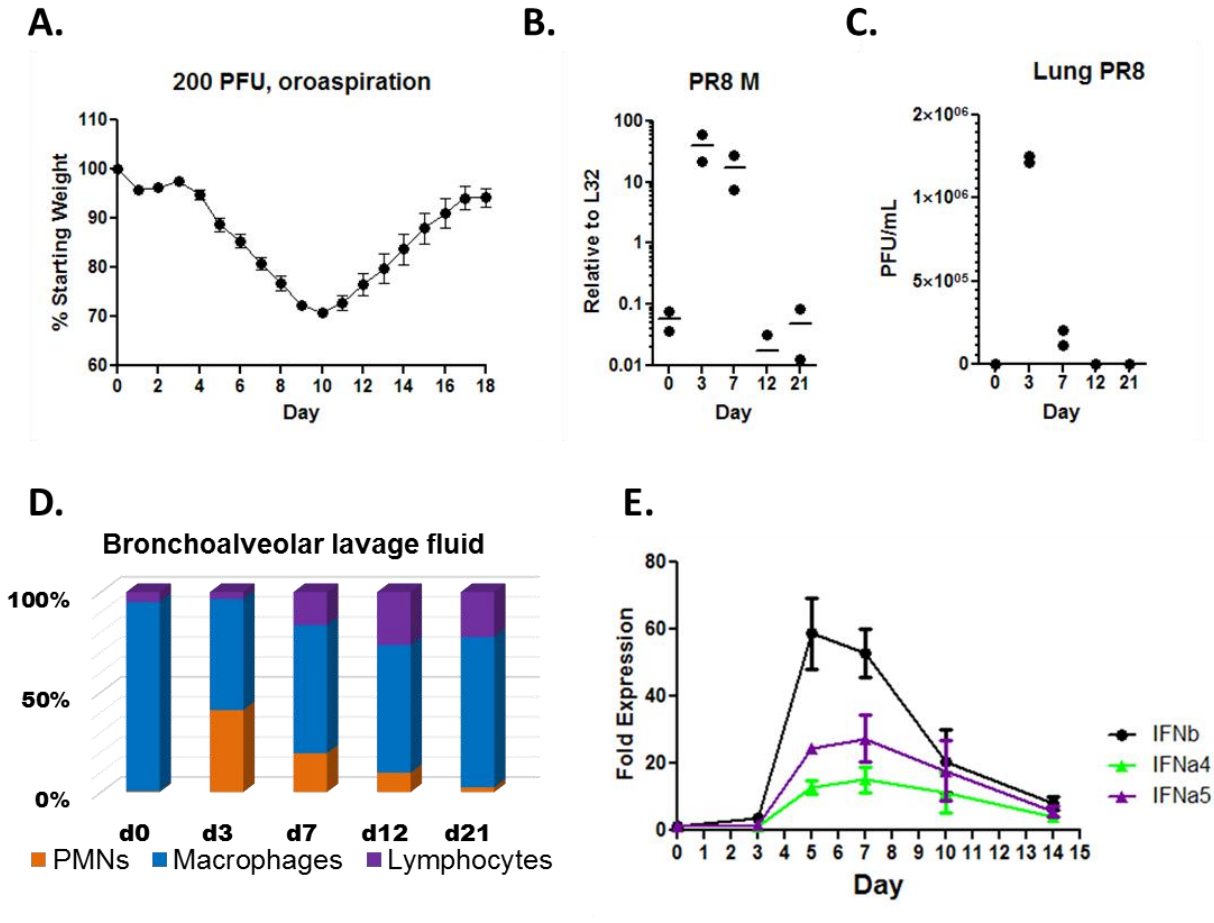
A.
200 PFU, oroaspiration
% Starting Weight
Day
B.
PR8 M
Relative to L32
Day
C.
Lung PR8
PFU/mL
Day
D.
Bronchoalveolar lavage fluid
100%
50%
0%
d0
d3
d7
d12
d21
PMNs
Macrophages
Lymphocytes
E.
Fold Expression
Day
IFNb
IFNa4
IFNa5
F.
CCSP NS1
DAPI SPC
Day 0
Day 3
Day 7
Day 12
Day 21

Figure 3.6. Temporal progression of a sublethal Influenza PR8 infection initiated by non-surgical intratracheal instillation. Mice were infected with 200 PFU of mouse adapted Influenza PR8 and weight change was monitored for 18 days (A). Lung viral load was quantified by qPCR (B) and plaque assay (C). Cellular infiltration was quantified in the bronchoalveolar lavage fluid by QuikDiff staining and microscopy (D). Transcription of type I IFNs in lung homogenate (E). Micrographs of lung sections stained for non-structural protein 1(NS1) of influenza, Clara cell specific protein (CCSP), surfactant protein C (SPC), an alveolar type II cell marker, and nuclei (DAPI).

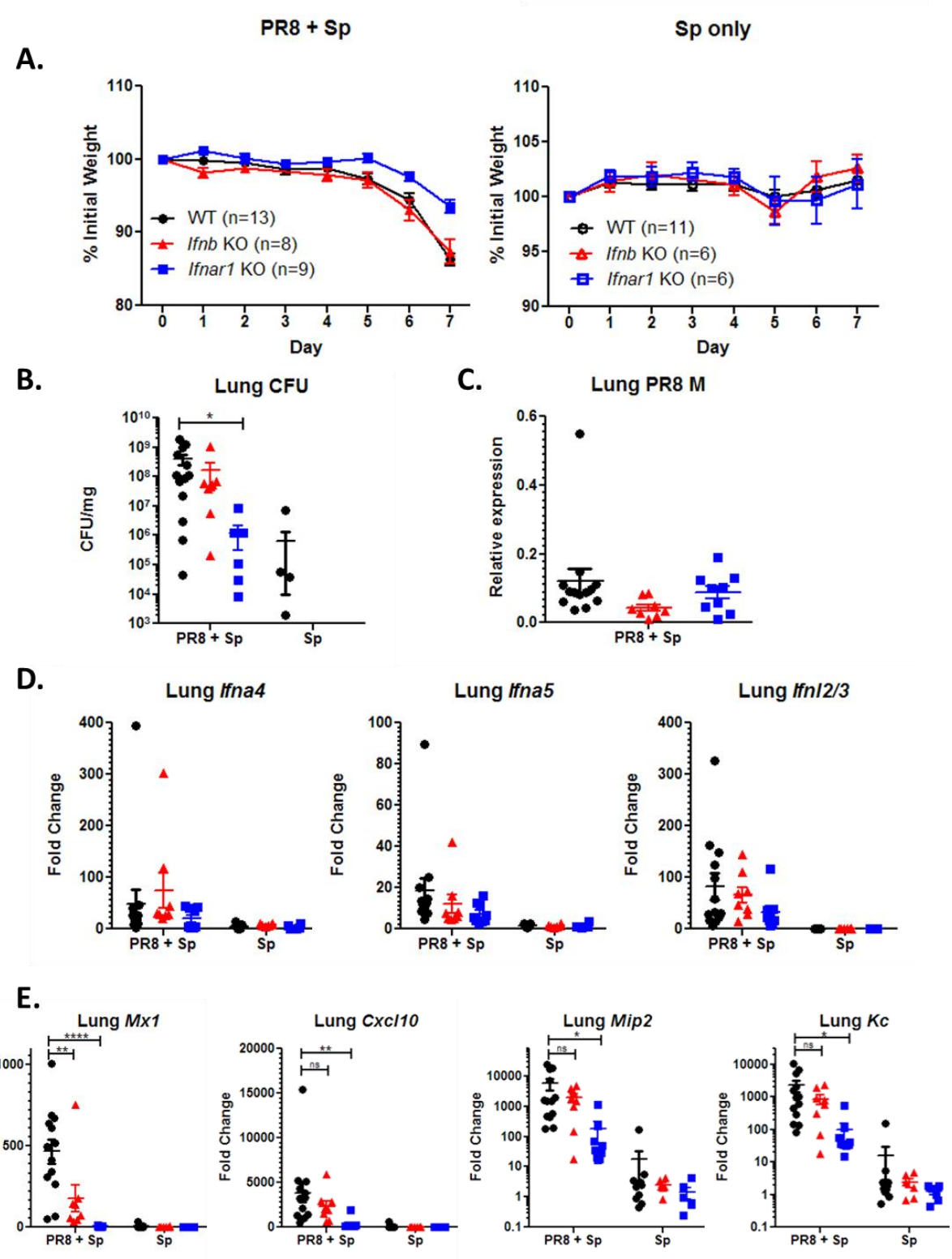
A.
PR8 + Sp
Sp only
% Initial Weight
Day
WT (n=13)
Ifnb KO (n=8)
Ifnar1 KO (n=9)
WT (n=11)
Ifnb KO (n=6)
Ifnar1 KO (n=6)
B.
Lung CFU
CFU/mg
PR8 + Sp
Sp
C.
Lung PR8 M
Relative expression
D.
Lung Ifna4
Lung Ifna5
Lung Ifnl2/3
Fold Change
E.
Lung Mx1
Lung Cxcl10
Lung Mip2
Lung Kc

Figure 3.7. IFNβ deficient mice are not protected against post-influenza pneumonia. WT, IFNβ KO and IFNAR1 KO mice were infected by non-surgical intratracheal instillation with 200 PFU Influenza PR8 on day 0 and/or with 10^4 CFU S. pneumoniae A66a on day 5. Mice were monitored daily and weight was recorded (A). Mice were euthanized on day 7. Bacterial burden in the lungs was determined by CFU assay (B). Lung viral load was quantified by relative gene expression of influenza M gene using qPCR (C). Induction of type I and type III IFNs (D) and ISGs (E) were also measured by qPCR as the fold change over uninfected WT and normalized to the housekeeping gene, L32.

Gene Symbol	Ch25h	Cd69	Irf7
Irgm1	Iigp1	Ifi203	Enpp4
Ifi35	Pmepa1	Mx2	Mov10
Irgm2	Flrt2	Nt5c3	Ddx60
Eif2ak2	Ptgdr2	Il15	Epsti1
Batf2	Nlgn2	Trim21	Mlkl
Trim30d	Gm10865	Sp140	Dusp5
Nmi	Spdya	Papd7	Slc25a22
Setdb2	Cxcl10	Sp110	Nme9
Mitd1	Rsad2	Socs1	Tgif2
Prnp	Ifit1	Nlrc5	Mndal
Tagap	Cmpk2	Fam26f	Atp10a
Slfn3	Oasl1	Zufsp	Slfn1
Phf11c	Ifit2	Tmem171	Zbp1
Mtfr2	Il27	Slfn9	Lgals3bp
Igtp	Ifit3	Gbp7	Stat2
Daxx	Mx1	Bambi-ps1	Mthfr
Tap1	Gbp2	Pcgf5	Herc6
Tor3a	Slfn5	Il18	Ccl7
Parp12	Ifi204	Tnfsf10	Pydc3
Gm12250	Usp18	Casp7	Slc28a2
Etnk1	Ifi47	Cdk6	Frmd4a
Pml	Ifi205	Gnb4	Pnp2
Mxd1	Slfn8	Mier3	Gbp9
Tlr3	Gbp3	Tmem67	Gm7030
Rbl1	Ddx58	Pyhin1	Lrp11
Ppm1k	Parp10	Stat1	Tpbg
Gca	Isg20	Cxcl9	Tnfaip6
Spsb1	Slamf9	Gm14446	Gem
Prr5l	Xaf1	Slfn4	Zeb1
Gcnt2	Gm5431	Oas1b	Shf
Cish	Pydc4	Oas1a	Tmem26
Lipg	Oas1g	Fcgr4	Rgcc
Ifnb1	Rgs14	Phf11d	Mcmdc2
Serpina3g	Ccl12	Tgtp2	Nos2
Plekha4	Il15ra	Phf11a	Ms4a4c
Ccne1	Oaf	Hmga1	Ms4a6b
Tex12	Samhd1	Oasl2	Dhx58

Supplementary Table 3.1. ISGs induced by IFNAR1 and IFNβ signaling.

qPCR	Forward: 5’ -> 3’	Reverse: 5’ -> 3’
L32	AAGCGAAACTGGCGGAAAC	TAACCGATGTTGGGCATCAG
Ifnb	CAGCTCCAAGAAAGGACGAAC	GGCAGTGTAACTCTTCTGCAT
Ifna4	CCTGTGTGATGCAGGAACC	TCACCTCCCAGGCACAGA
Ifna5	TGACCTCAAAGCCTGTGTGATG	AAGTATTTCCTCACAGCCAGCAG
Mx1	AAACCTGATCCGACTTCACTTCC	TGATCGTCTTCAAGGTTTCCTTGT
Tnfa	GGTGCCTATGTCTCAGCCTCTT	CGATCACCCCGAAGTTCAGTA
Il1b	GAGCTGAAAGCTCTCCACCTCA	TCGTTGCTTGGCTCCTTGTAC
Cxcl10	CCTGCCCA CGTGTTGAGAT	TGATGGTCTTAGATTCCGGATTC
Kc	CAAGAACATCCAGAGCTTGAAGGT	GTGGCTATGACTTCGGTTTGG
Mip2	AGCTACATCCCACCCACACAG	AAAGCCATCCGACTGCATCT
Il10	TCATCGATTTCTCCCCTGTGA	GACACCTTGGTCTTGGAGCTTATT
Il27p28	CTCTGCTTCCTCGCTACCAC	GGGGCAGCTTCTTTTCTTCT
Ch25h	TGCTACAACGGTTCGGAGC	AGAAGCCCACGTAAGTGATGAT
M gene (influenza)	CATGGAATGGCTAAAGACAAGACC	CCATTAAGGGCATTTTGGACA
Genotyping		
Ifnb	ATGAACAACAGGTGGATCCTCCA	TTGAGGACATCTCCCACGTC
Neomycin	AGAGGCTATTCGGCTATGAC	GATGCTCTTCGTCCAGATC

Supplementary Table 3.2. Primer pairs for qPCR and genotyping.

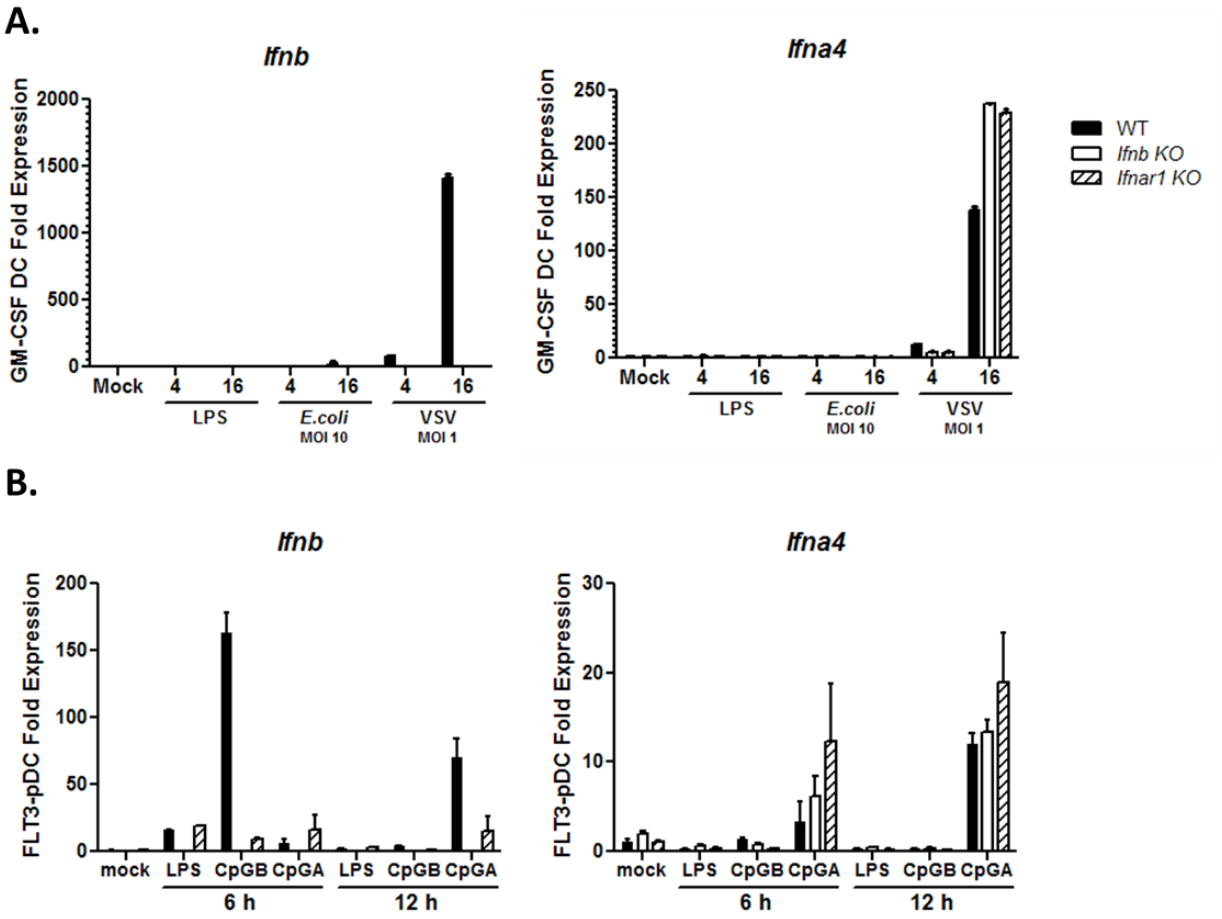

Supplementary figure 3.1. Induction of type I IFNs by ex vivo differentiated cDCs and Flt3l-pDCs. Induction of *Ifnb* and *Ifna4* by cDCs after stimulation with LPS, *E. coli*, or VSV for 4 or 16 hours (A). Induction of *Ifnb* and *Ifna4* by Flt3l-pDCs after stimulation with LPS, CpG-B, or CpG-B for 4 or 12 hours (B).

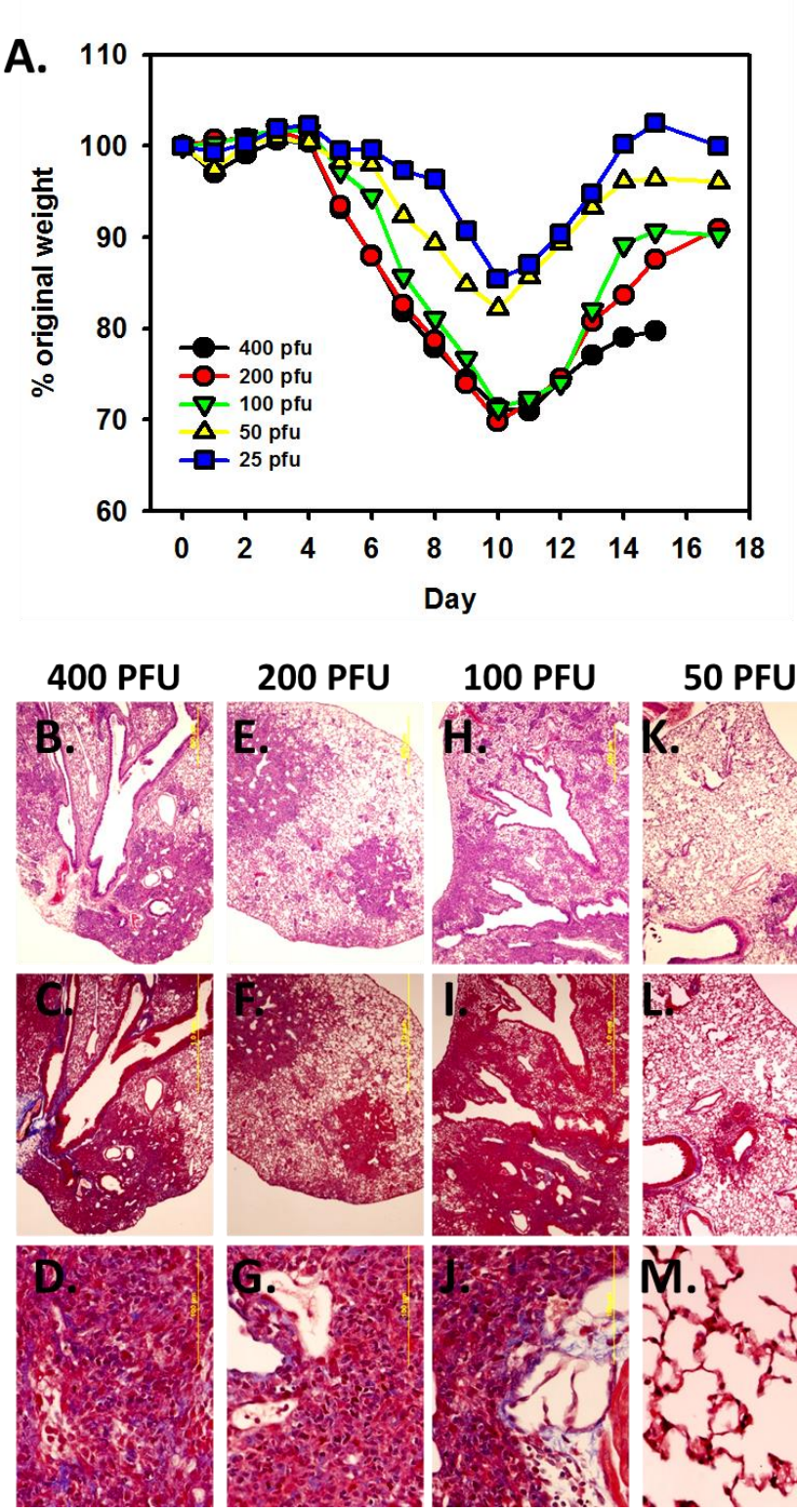
A.
110
100
90
80
70
60
% original weight
400 pfu
200 pfu
100 pfu
50 pfu
25 pfu
0
2
4
6
8
10
12
14
16
18
Day
400 PFU
200 PFU
100 PFU
50 PFU
B.
E.
H.
K.
C.
F.
I.
L.
D.
G.
J.
M.

Supplementary Figure 3.2. Response of WT mice to incremental doses of mouse adapted influenza PR8. Mean weight change for WT mice (n = 4, per dose) infected by non-surgical intra-tracheal injection with incremental doses of PR8 (A). Representative micrographs of lung sections isolated from mice infected with incremental doses of PR8, collected on day 15: H&E stained, magnified 25X (B, E, H and K), and Masson's trichrome stained, magnified 25X (C, F, I and L) and magnified 400X (D, G, J, and M).

MATERIALS AND METHODS

Animals and Cell Culture

All mice were bred and maintained in specific pathogen free facilities managed by the Department of Laboratory Animal Medicine at UCLA in strict accordance with protocols approved by the UCLA Animal Research Committee. Mouse experiments were carried out with age and sex matched WT, IFNAR1 KO, IFNβ KO, and/or IL-10 KO mice following UCLA Animal Research Committee approved experimental protocols. Mice were euthanized at experimental endpoints or if the animal met the defined criteria for euthanasia by CO_2 asphyxiation, followed by confirmatory pneumothorax.

Bone marrow derived macrophages (BMMs) were differentiated from bone marrow collected from wild type C57Bl/6 (WT), IFNAR1 KO backcrossed 9 generations onto C57Bl/6 [32] and IFNβ KO, a gift from Dr. Eleanor Fish. All mice were bred and maintained in specific pathogen free facilities managed by the Department of Laboratory Animal Medicine at UCLA in strict accordance with protocols approved by the UCLA Animal Research Committee.

Bone marrow was flushed from four leg bones, pooled, and treated with ACK lysing buffer, a hypotonic solution for the removal of red blood cells. The remaining cells were counted and plated at 0.5 x 10^6/mL per well in 6-well tissue culture treated dishes containing macrophage differentiating medium (DMEM, 10% fetal bovine serum, 100 U/mL penicillin, 100 µg/mL streptomycin, and 2% macrophage colony stimulating factor (MCSF) conditioned medium, collected from L929 cells overexpressing MCSF).

Bone marrow derived plasmacytoid dendritic cells (Flt3l-pDCs) were differentiated by plating bone marrow collected from WT, IFNAR1 KO and IFNβ KO mice into sterile petri dishes containing pDC differentiating medium (RPMI, 10% fetal bovine serum, 100 U/mL penicillin, 100 µg/mL streptomycin, and 100 ng/mL murine Flt3-ligand (R&D Systems, 427-FL-.025)) and culturing for 7 days [33]. Conventional dendritic cells (BMDCs) were differentiated by plating bone

marrow cells into cDC differentiating medium (DMEM, 100 U/mL penicillin, 100 µg/mL streptomycin, and 10 ng/mL GM-CSF) and culturing for 6 days [33,34].

In vitro stimulations and infections

Adherent BMMs were stimulated or infected on day 7. Stimulations were accomplished by spiking in 100 ng/mL Lipid A purified from *Eshcherichia coli* O57 (Sigma). *Escherichia coli* O18ac:K1:H7 was inoculated from frozen glycerol stock into 4 mL trypticase soy broth and incubated overnight at 37°C, 250 rpm. The following day the culture was passaged 1:10 and grown to mid-log phase, ~2.5 hours. Bacteria cell concentration was determined by optical density at 600 nm and a previously established growth curve, then verified by colony forming unit (CFU) analysis by plating serial dilutions on trypticase soy agar. Bacteria were pelleted, re-suspended in DPBS, then added to BMMs at a multiplicity of infection (MOI) of 10. Vesicular stomatitis virus (VSV) was prepared and tittered by by Dr. Roghiyari (Saba) Aliyari. Briefly, VSV virus was amplified by infecting VERO cells; resulting virions in the supernatant were collected, filtered through 0.2 µm filter, aliquoted, then frozen at -80°C. Activity of frozen stock was measured by plaque assay. For in vitro infection, frozen VSV stocks were thawed on ice and used directly at a MOI of 1.

Differentiated BMDCs were collected from untreated sterile petri dishes, counted and re-plated at 0.5 x 10^6 per well in a 24-well plate. Cells were stimulated with 100 ng/ml LPS or infected with *E. coli*, MOI 10 or VSV, MOI 1, for 4 and 16 hours. Differentiated Flt3l-pDCs were pooled, counted, re-plated at 0.5 x 10^6 per well in a 6-well plate, and then stimulated with either 5 µg/mL LPS, 75 nM CpG B 1826, or 75 nM CpG A ODN 1585, for 6 and 12 hours.

RNA Isolation and quantitative RNA measurement

Total RNA was isolated using Trizol Reagent (Invitrogen) according to the manufacturer's protocol. RNA was quantified using NanoDrop 2000 and 0.5 or 1 µg was used to make complementary DNA (cDNA) templates using iScript™ cDNA Synthesis Kit (Bio Rad)

according to the manufacturer's instructions and oligo-dT primers. Real time quantitative PCR (qPCR) was carried out using iTaq™ SYBR® Green Supermix reagent (Bio Rad) and measured using MyiQ™ Single-Color Real-Time PCR Detection System (Bio Rad). Gene specific primers are listed in Supplementary Table 3.2. Amplification was carried out with the following conditions: 95.0°C for 3:00 min, 95.0°C for 0:03 sec, 60.0°C for 0:20 sec; repeated 39 times followed by a melt curve from 65.0°C to 95.0°C, at 0.5°C increments, each 0:05 sec. Cycle threshold values for the gene of interest were normalized to the housekeeping gene, L32, and fold expression was normalized to the untreated, wild type control. For detection of Influenza M protein gene expression, relative expression was determined by standard curve method and normalized to L32. Lung PR8 was also measured by RT-PCR with primers specific for the influenza M gene.

Samples for RNASeq analysis were prepared by Dr. Shankar Iyer and analyzed by Dr. Aiping Wu. Briefly, BMMs differentiated from WT, IFNAR1 KO, IFNβ KO were unstimulated or stimulated with 100 ng/mL lipid A for 4 or 12 h. RNA-seq Library Construction, Sequencing Mapping and Analysis Strand-specific libraries were generated using 500ng RNA input according to "deoxyuridine triphosphate (dUTP) method using TruSeq library preparation kit (Illumina, San Diego, CA). Illumina HiSeq2000 was used for sequencing with a single end sequencing length of 100 nucleotides. All bioinformatics analyses were conducted using the Galaxy platform (Goecks et al. 2010). Reads were aligned to the mouse mm9 reference genome with Tophat (Trapnell et al. 2010) using default parameters. Alignments were restricted to uniquely mapping reads, with up to 2 mismatches permitted. The reads counts were calculated with HTSeq (Anders et al. 2014) and further used to generate RPKM for all mm9 RefSeq genes (Pruit et al. 2005). Differential analyses for WT vs. IFNAR vs. IFNb were performed using DEseq2 (Love et al. 2014) with default parameters for three conditions.

Significance was corrected for multiple testing models using standard Benjami-Hochberg tests. Differential expressed genes had a p(adj)<0.05.

E. coli peritonitis

E. coli bacteria were prepared as described above in “In vitro sitmulations and infections”. Mice were infected by intraperitoneal injection, monitored at least twice a day for signs of illness, and euthanized if displaying signs of morbidity or at the experimental end point of 5 days. To establish the non-lethal dose, wild type mice were infected with incremental amounts of *E. coli* and monitored for survival. In most experiments, mice were infected with 10^5 CFU mid-log phase *E. coli*. Mice were monitored for survival and cohorts were euthanized 4 and 15 hours post-infection to determine the bacterial load and assay the immune response. Mice were euthanized by CO_2 asphyxiation. Blood was collected by cardiac puncture; one drop (~50 µl) was placed into an EDTA coated tube and placed on ice while the remaining was allowed to clot at RT for 30 min, centrifuged and the resulting serum fraction was transferred to a clean tube. The peritoneal cavity was lavaged by injecting 5 ml ice cold DPBS+2% FBS into the peritoneal cavity using a 27-Gauge needle and massaging the peritoneal cavity. The peritoneal lavage fluid (PLF) was collected by tenting the peritoneum with forceps, making a small cut, and then inserting a 20-Gauge needle and aspirating the fluid containing the cells. Similar volumes were recovered from each mouse. To measure IL-10 levels in the PLF, a portion of the PLF was clarified by centrifugation then analyzed by ELISA according to the manufacturer’s protocol (R&D Systems, DY417). To measure gene transcription in the peritoneal exudate cells (PECs), PECs were pelleted and RNA was isolated using TRIzol Reagent (Invitrogen). The blood and PLF was serially dilution and plated on blood agar plates to determine the number of colony forming units. Serum inflammatory marker, alanine transferase (ALT) was measured using the Vet Axcel Chemistry Analyzer (Alfa Wassermann) (UCLA DLAM Diagnostics Lab).

In vivo infections by non-surgical intratracheal instillation

Influenza PR8 virus, a kind gift from Dr. Su-Yang Liu, was diluted to 200 plaque forming units (PFU) in a final volume of 60 µl in pharmaceutical grade PBS. *Streptococcus pneumonia* A66a, a generous gift from Dr. Jane Deng, M.D., was inoculated from frozen glycerol stock into Todd Hewitt broth and incubated for 6 h in a static 37°C incubator containing 5% CO_2. The concentration of the resulting culture was quantified by absorbance at 600 nm and adjusted to 10^4 CFU in final 60 µl pharmaceutical grade PBS.

Infection was accomplished by anesthetizing mice with an intraperitoneal injection of a ketamine-xylazine mixture (100 mg/10 mg/kg), then individually suspended and secured an angled stand. Using forceps covered with polypropylene tubing, the tongue and lower jaw were held and 60 µl of the virus solution was instilled into the back of the throat. Following aspiration of the inoculum, the mouse was monitored for signs of rapid breathing, an indicator of successful pulmonary instillation, then gently removed from the stand and placed on warming pads until completely ambulatory. Mice were observed daily and weight was recorded.

Influenza infection time course

Mice were infected as described above with 200 PFU Influenza PR8. On day 0, 3, 7, 12 and 21 cohorts of four mice were euthanized and organs were collected. Blood was collected by cardiac puncture, allowed to clot at room temperature, then serum was isolated by centrifugation, transferred to a sterile tube and stored at -80˚C until further analysis. The lungs from 2 mice were excised, lobes were separated and placed in a 2 mL FastPrep homogenization tube containing lysing matrix D. Sterile DPBS was added to give a final 20% w/v suspension and homogenized using a FastPrep-24 Instrument, 6 m/s, 45 s (MP Biomedicals, Santa Ana, CA). Lung homogenate was diluted 1:10 in TRIzol Reagent (Life Technologies, Grand Island, NY) for analysis of gene expression; and serially diluted for quantification of viral titer by plaque assay. Viral titer was determined by plating a monolayer of MDCK cells in 6-well tissue culture treated plates, then incubating cells lung homogenate,

serially diluted in virus dilution buffer (PBS with 1% Penicillin/Streptomycin, 0.2% BSA, 0.005% DEAE Dextran, 1X $CaCl_2/MgCl_2$), for 1 h at 37˚C. Extracellular virus was removed by gently washing the monolayer, then an overlay containing 2% low melting point agarose in virus growth medium (MEM containing BME vitamins, 10 mM HEPES, 1% Penicillin/Streptomycin, 0.15% NaHCO3, 0.2% BSA, 0.0015% DEAE Dextran, 0.7 mg/ml TPCK-treated Trypsin) was applied and plates were incubated for 2 days at 37°C. The overlay was gently aspirated, then the plates were incubated with 0.3% crystal violet in 20% ethanol and plaque forming units were enumerated.

The lungs from the remaining two mice were lavaged with 5 mM EDTA-DPBS to collect infiltrating white blood cells, then sequentially perfused with 5mM EDTA-DPBS and paraformaldehyde, and paraffin embedded for histological analysis. H&E staining was performed by the Translational Pathology Core Laboratory (UCLA) and the Masson's trichrome staining was completed by the Division of General Histology (UCLA). 5 µm sections mounted on glass slides were de-paraffinized using standard techniques, then treated with Proteinase K solution (20 mg/ml Proteinase K (Sigma), in 50mM Tris-Cl, 1mM EDTA, pH 8.0) for 20 min in a humid chamber at 37°C, to expose antigens. Sections were incubated with blocking buffer (3% (m/v) BSA in 1x PBS, containing 0.2% (v/v) Triton X-100) for 1 h in a humid chamber at room temperature (RT). Primary antibodies were diluted in blocking buffer as indicated: 1:100 for monoclonal mouse anti-Influenza A NS1 antibody (Santa Cruz Biotechnology, sc-130568), 1:200 for polyclonal rabbit anti-CCSP antibody (US Biological, C5828), and 1:100 for goat anti-pro-SPC (Santa Cruz Biotechnology, sc-7706). The primary antibody master mix was laid over the section and incubated in humid chamber under 4°C, overnight. Sections were gently washed 3x with PBS, then a master mix of secondary antibodies, donkey anti-mouse Alexa 488, donkey anti-rabbit Alexa 555, donkey anti-goat Alex 647 (Life Technologies), each diluted 1:100 in blocking buffer was applied, then incubated in a darkened humid chamber for 2 h, at RT.

Sections were gently washed and SlowFade® Gold Antifade Reagent with DAPI (Life Technologies, S36938) was applied with a cover slip. Sections were imaged with a Zeiss Axio Observer.Z1 microscope and AxioVision software (Zeiss).

Secondary bacterial pneumonia

Mice were infected with 200 PFU Influenza PR8 on day 0, then with 10^4 CFU *S. pneumonia* on day 5, or singly infected with 10^4 CFU *S. pneumonia*. All mice were euthanized 48 hours after infection with *S. pneumonia*. Blood was collected by cardiac puncture; one drop (~50 µl) was placed into an EDTA coated tube and placed on ice, while the remaining was transferred to a sterile tube and processed for serum isolation as described above. Lungs were separated and collected into a 2 mL FastPrep homogenization tube containing lysing matrix D containing 1 ml 5 mM EDTA-DPBS. Lungs were homogenized used for CFU assay or diluted 1:10 into Trizol Reagent for RNA extraction and processed as described above. EDTA treated blood and lung homogenate were serially diluted in 5 mM EDTA-DPBS and plated on blood agar plates and incubated overnight in a static 37°C incubator containing 5% CO_2.

REFERENCES

1. Liu, S.-Y., Sanchez, D. J., Aliyari, R., Lu, S. & Cheng, G. Systematic identification of type I and type II interferon-induced antiviral factors. *Proc. Natl. Acad. Sci. U. S. A.* **109,** 4239–44 (2012).

2. Toshchakov, V. *et al.* TLR4, but not TLR2, mediates IFN-beta-induced STAT1alpha/beta-dependent gene expression in macrophages. *Nat. Immunol.* **3,** 392–8 (2002).

3. Thomas, K. E., Galligan, C. L., Newman, R. D., Fish, E. N. & Vogel, S. N. Contribution of interferon-beta to the murine macrophage response to the toll-like receptor 4 agonist, lipopolysaccharide. *J. Biol. Chem.* **281,** 31119–30 (2006).

4. Ng, C. T. *et al.* Blockade of interferon Beta, but not interferon alpha, signaling controls persistent viral infection. *Cell Host Microbe* **17,** 653–61 (2015).

5. Robinson, N. *et al.* Type I interferon induces necroptosis in macrophages during infection with Salmonella enterica serovar Typhimurium. *Nat. Immunol.* **13,** 954–62 (2012).

6. Sheehan, K. C. F., Lazear, H. M., Diamond, M. S. & Schreiber, R. D. Selective Blockade of Interferon-α and -β Reveals Their Non-Redundant Functions in a Mouse Model of West Nile Virus Infection. *PLoS One* **10,** e0128636 (2015).

7. Doyle, S. *et al.* IRF3 mediates a TLR3/TLR4-specific antiviral gene program. *Immunity* **17,** 251–63 (2002).

8. Prakash, A., Smith, E., Lee, C. K. & Levy, D. E. Tissue-specific positive feedback requirements for production of type I interferon following virus infection. *J. Biol. Chem.* **280,** 18651–18657 (2005).

9. Kim, H. S. *et al.* STAT1 deficiency redirects IFN signalling toward suppression of TLR response through a feedback activation of STAT3. *Sci. Rep.* **5,** 13414 (2015).

10. Antonelli, G., Scagnolari, C., Moschella, F. & Proietti, E. Twenty-five years of type I interferon-based treatment: a critical analysis of its therapeutic use. *Cytokine Growth Factor Rev.* **26,** 121–31 (2015).

11. Interferon beta-1b is effective in relapsing-remitting multiple sclerosis. I. Clinical results of a multicenter, randomized, double-blind, placebo-controlled trial. The IFNB Multiple Sclerosis Study Group. *Neurology* **43,** 655–61 (1993).

12. Mancuso, G. *et al.* Type I IFN Signaling Is Crucial for Host Resistance against Different Species of Pathogenic Bacteria. *J. Immunol.* **178,** 3126–3133 (2007).

13. Cuenca, A. G. *et al.* TRIF-Dependent Innate Immune Activation Is Critical for Survival to Neonatal Gram-Negative Sepsis. *J. Immunol.* **194,** 1169–77 (2015).

14. McNab, F. W. *et al.* Type I IFN induces IL-10 production in an IL-27-independent manner and blocks responsiveness to IFN-γ for production of IL-12 and bacterial killing in Mycobacterium tuberculosis-infected macrophages. *J. Immunol.* **193,** 3600–12 (2014).

15. Iyer, S. S., Ghaffari, A. A. & Cheng, G. Lipopolysaccharide-mediated IL-10 transcriptional regulation requires sequential induction of type I IFNs and IL-27 in macrophages. *J. Immunol.* **185,** 6599–607 (2010).

16. Chang, E. Y., Guo, B., Doyle, S. E. & Cheng, G. Cutting edge: involvement of the type I

IFN production and signaling pathway in lipopolysaccharide-induced IL-10 production. *J. Immunol.* **178,** 6705–9 (2007).

17. Sewnath, M. E. *et al.* IL-10-deficient mice demonstrate multiple organ failure and increased mortality during Escherichia coli peritonitis despite an accelerated bacterial clearance. *J. Immunol.* **166,** 6323–31 (2001).

18. Rynda-Apple, A., Robinson, K. M. & Alcorn, J. F. Influenza and Bacterial Superinfection: Illuminating the Immunologic Mechanisms of Disease. *Infect. Immun.* **83,** 3764–70 (2015).

19. Kumar, P. A. *et al.* Distal Airway Stem Cells Yield Alveoli In Vitro and during Lung Regeneration following H1N1 Influenza Infection. *Cell* **147,** 525–38 (2011).

20. Buchweitz, J. P., Harkema, J. R. & Kaminski, N. E. Time-dependent airway epithelial and inflammatory cell responses induced by influenza virus A/PR/8/34 in C57BL/6 mice. *Toxicol. Pathol.* **35,** 424–35 (2007).

21. Davidson, S., Crotta, S., McCabe, T. M. & Wack, A. Pathogenic potential of interferon αβ in acute influenza infection. *Nat. Commun.* **5,** 3864 (2014).

22. Shahangian, A. *et al.* Type I IFNs mediate development of postinfluenza bacterial pneumonia in mice. *J. Clin. Invest.* **119,** 1910–20 (2009).

23. Kallfass, C., Lienenklaus, S., Weiss, S. & Staeheli, P. Visualizing the beta interferon response in mice during infection with influenza A viruses expressing or lacking nonstructural protein 1. *J. Virol.* **87,** 6925–30 (2013).

24. Tong, A. *et al.* A Stringent Systems Approach Uncovers Gene-Specific Mechanisms Regulating Inflammation. *Cell* **165,** 165–79 (2016).

25. van Pesch, V., Lanaya, H., Renauld, J.-C. & Michiels, T. Characterization of the murine alpha interferon gene family. *J. Virol.* **78,** 8219–8228 (2004).

26. Prchal-Murphy, M. *et al.* TYK2 kinase activity is required for functional type I interferon responses in vivo. *PLoS One* **7,** e39141 (2012).

27. Ouyang, W., Rutz, S., Crellin, N. K., Valdez, P. a & Hymowitz, S. G. Regulation and Functions of IL-10 Family Cytokines in Inflammation and Diseases. *Annu. Rev. Immunol.* (2010). doi:10.1146/annurev-immunol-031210-101312

28. Peng, F.-W. *et al.* Purification of recombinant human interferon-ε and oligonucleotide microarray analysis of interferon-ε-regulated genes. *Protein Expr. Purif.* **53,** 356–362 (2007).

29. Škorvanová, L., Švančarová, P., Svetlíková, D. & Betáková, T. Protective efficacy of IFN-ω AND IFN-λs against influenza viruses in induced A549 cells. *Acta Virol.* **59,** 413–7 (2015).

30. Thomas, C. *et al.* Structural Linkage between Ligand Discrimination and Receptor Activation by Type I Interferons. *Cell* **146,** 621–632 (2011).

31. Deriu, E. *et al.* Influenza Virus Affects Intestinal Microbiota and Secondary Salmonella Infection in the Gut through Type I Interferons. *PLoS Pathog.* **12,** e1005572 (2016).

32. O'Connell, R. M. *et al.* Type I interferon production enhances susceptibility to Listeria

monocytogenes infection. *J. Exp. Med.* **200,** 437–45 (2004).

33. Oganesyan, G. *et al.* IRF3-dependent type I interferon response in B cells regulates CpG-mediated antibody production. *J. Biol. Chem.* **283,** 802–8 (2008).

34. Madaan, A., Verma, R., Singh, A. T., Jain, S. K. & Jaggi, M. A stepwise procedure for isolation of murine bone marrow and generation of dendritic cells. *J. Biol. Methods* **1,** 8–10 (2014).

CHAPTER 4

Type I IFNs in non-infectious disease

ABSTRACT

Ligation of pattern recognition receptors (PRRs) is a hallmark of innate immune activation. Type I IFNs are pleiotropic cytokines produced during the early host response that, through the induction of interferon stimulated genes (ISGs), can cause transient and long term alterations to the immune response and homeostasis of non-immune tissue. CXCL10, an ISG that recruits immune cells such as natural killer (NK) cells and T cells, contributes to the pathogenesis of non-infectious disease. Here, we examined the contribution of CXCL10 to LPS induced endotoxic shock. We found CXCL10 promotes host susceptibility, but only among female mice. There was no significant difference between male and female mice in the number of cells expressing CXCR3, the receptor for CXCL10, but there is evidence to suggest CXCR3 is required for CXCL10 pathogenesis. Next, we examined innate immune activation by poly I:C in experimental autoimmune encephalitis (EAE), the mouse model of multiple sclerosis (MS). Previously, we found deficiency of adapter proteins upstream of type I IFN exacerbated EAE. Here, we show poly I:C transiently attenuates symptoms of chronic EAE, likely through ligation of TLR3. Finally, we investigated the role of IFNAR signaling in social behavior in mice with *Tsc2* haploinsufficiency, a model of human tuberous sclerosis disorder. We found, expression of type I IFNs and ISGs are enhanced in *Tsc2*+/- mice treated with poly I:C. Moreover, we discovered that while dysregulation at the gene level is transient, treatment with poly I:C during early development confers lasting social behavior defects.

INTRODUCTION

Several non-infectious diseases have chronic or re-occurring symptoms or produce seemingly irreversible phenotypes. In some cases, these types of diseases arise as a side effect of the host response to an immune stimulating event. Pathogen associated molecular patterns (PAMPs) or host response to infectious pathogens may promote autoimmune disease [1] or alter fetal development [2,3]. Type I IFNs and downstream ISGs contribute to the pathogenesis of non-infectious disease. The pleiotropic nature of type I IFNs not only leads to the development of the host antiviral response, but also regulates inflammation [4], induces cell death [5,6] and alters tissue architecture [7].

To explore the role of ISGs and type I IFN signaling we examined three models of non-infectious disease: LPS induced endotoxic shock; EAE, the mouse model of MS; and tuberous sclerosis disorder.

LPS induced endotoxic shock

In the mouse model of LPS induced endotoxic shock, signaling by IFNβ through the IFNAR1-TYK2 axis is lethal. Mice deficient in the IFNβ [8], IFNAR complex [9], IFNAR1 [10], or TYK2 [8] survive LPS challenge. CXCL10/IP-10, is a chemokine upregulated by type I IFN that is often used as a biomarker of septic shock [11]. CXCL10 and the closely related CXCL9 and CXCL11, all signal through CXCR3, a receptor predominately expressed on natural killer (NK) cells, NK T cells, and CD8+ T cells. The role of CXCL10 in disease is contradictory. CXCL10 has been reported to ameliorate EAE symptoms [12], protect against sepsis [9,13] and protect against virus mediated tissue damage [14]. Yet, CXCL10 has also been reported to enhance the pathogenesis of influenza [15] and bronchiolitis-like inflammation [16], block crypt regeneration [17,18] and promote autoimmunity [19,20]. Interestingly, some studies have found CXCL10 mediates detrimental effects such as apoptotic cell death through a non-canonical pathway involving ligation of TLR4 and that leads to sustained signaling through Akt and JNK [21,22].

To determine whether CXCL10 is involved in the pathogenesis of LPS induced endotoxic shock, CXCL10 deficient mice were injected with LPS and survival was compared to similarly injected WT mice.

Multiple sclerosis/Experimental autoimmune encephalitis

IFNβ is clinically used to treat multiple sclerosis [23]. 30% of patients with relapsing and remitting multiple sclerosis (RRMS) benefit from IFNβ treatment. Furthermore, in the mouse model of relapsing and remitting EAE (RR-EAE), deficiency in IFNβ exacerbates the disease [24], whereas treatment with an inducer of type I IFNs, poly I:C, alleviates symptoms [25]. In the RR-EAE, TLR3 sensing of poly I:C leads to IFNβ [25].

Previously, our lab found TRIF, the adapter for TLR3 that leads to induction of type I IFNs, is necessary for reducing symptom of chronic EAE[26] In this study we investigated whether poly I:C induced type I IFNs attenuate chronic EAE. Furthermore, we examine the pathway activated by poly I:C that leads to production of IFNβ.

Tuberous sclerosis complex and Autism

Mutations in the tuberous sclerosis complex (TSC), TSC1 or TSC2, manifests as autosomal dominant disorder. Patients with tuberous sclerosis complex disorder are more likely to experience neuropsychiatric disorders such as autism spectrum disorder than patients with WT TSC1 and TSC2. Yet, not all patients will exhibit symptoms suggesting that additional factors contribute to the development of autism spectrum disorder.

Gestational immune activation by poly I:C confers long term social deficits to *Tsc2*+/- pups [3]. Social defects, permanent and transient, are also noted when pups or adults are treated with poly I:C (unpublished data). To understand how poly I:C may be differentially experienced by Tsc2+/- mice, we examined the gene expression pattern in the spleen and in the brain at different time points after intraperitoneal injection with poly I:C. In addition, we measured the

expression of type I IFNs and ISGs in adult mice that were recently injected with poly I:C or injected as pups.

RESULTS

CXCL10 deficiency enhances survival of female mice from LPS induced endotoxic shock

We set up a model of LPS induced endotoxic shock to investigate the effect of CXCL10. To our surprise, we found *Cxcl10*-/- females were more resistant to endotoxic shock than *Cxcl10*-/- males or WT mice, either gender (Figure 4.1, A). We examined the cell population in the peritoneal cavity, 6 hours after the administration of LPS, using flow cytometry and fluorescently labeled antibodies specific for F4/80, a macrophage marker, NK1.1, a natural killer cell marker, and CD3ε, a T cell marker. Compared to WT females or *Cxcl10*-/- males, there was no significant difference in the type or abundance of immune cell recruitment to the peritoneal cavity (Figure 4.1, B). Measurement of tissue damage markers in the serum revealed survival was associated with decreased concentrations of serum ALT, AST and LDH in the *Cxcl10*-/- female (Figure 4.1, C-E).

Sex hormones are known to modulate the immune response [27,28] and influence disease susceptibility [29,30]. Estradiol, in particular, has been found to attenuate production of the pro-inflammatory cytokine, TNFα [28], a key mediator of endotoxic shock [31]. To determine whether estradiol alters the gene expression of inflammatory cytokines, splenocytes from male and female WT and *Cxcl10*-/- mice were collected. Flow cytometric analysis of cells labeled with fluorescent antibodies against NK and T cells revealed no significant difference in the basal abundance of CXCR3+ cells (Figure 4.2, A). Ex vivo treatment of the splenocytes with 17-β-estradiol followed by LPS for 6 hours showed no significant difference between estradiol treated and untreated cells (Figure 4.2, B). Similar treatment of bone marrow derived macrophages (BMMs) from these same mice, also showed no difference in LPS induced transcription of *Tnfa* or *Il6* between estradiol treated and untreated cells (Figure 4.2, C and D).

CXCL10 has been found to promote pathogenesis by signaling through a non-canonical pathway that requires ligation of TLR4 [21,32]. To determine whether the canonical receptor

contributes to the pathogenesis and mortality of WT females, we injected *Cxcr3*-/- with LPS. A similar trend was observed; survival was increased *Cxcr3*-/- females compared to *Cxcr3*-/- males. In this experiment, however, the *Cxcl10*-/- controls did not show the phenotype previous observed (Figure 4.2, E). One variable that may account for the loss of the phenotype is the age of the mouse. In this experiment, the mice were one month older than in all previous experiments.

Poly I:C treatment transiently attenuates chronic EAE

Poly I:C, has been shown to reduce symptoms of relapsing and remitting EAE, but inducing the expression of IFNβ. To determine whether treatment with poly I:C would attenuate symptoms of chronic EAE, we induced EAE in WT mice and one week later a cohort was treated with poly I:C, every other day for a total of three times. Mice were weighed and scored daily for at least 30 days. As the disease progressed, poly I:C treated mice displayed a similar weight loss trend as WT mice, but between days 12 and 19 poly I:C treated mice experienced a less dramatic percent weight loss than WT mice (Figure 4.3, A). The reduced weight loss was accompanied by a delay in symptom onset and a lower overall clinical score (Figure 4.3, B). Yet, beyond day 30, there was no significant difference in weight change or clinical score (data not shown). At the tissue level, we did not find a substantial difference in the inflammatory cell infiltration (Figure 4.3, C – F) or in demyelination (Figure 4.3, G).

Poly I:C can signal through the cytosolic RIG-I pathway that uses the adaptor CARDIF (also known as IPS-1, MAVS, VISA) to induce type I IFNs [33], as well as through the TLR3-TRIF pathway [34]. To determine which receptor was responsible for the mild attenuation of symptoms mediated by poly I:C treatment, chronic EAE was induced in TLR3 KO and TLR3/CARDIF double KO mice. TLR3 KO mice experienced more weight loss (Figure 4.4, A) and more severe clinical symptoms than TLR3/CARDIF double KO (Figure 4.4, B), yet severity was less than that observed in WT mice (Figure 4.3, A and B). This result was unexpected, we anticipated that

TLR3 deficient mice would display more severe symptoms than WT mice, yet here we find little difference.

Type I IFNs and downstream ISGs are elevated in *Tsc2*+/- mice

During early development and in the nervous system, the heterodimeric TSC1/TSC2 complex negatively regulates the mTOR pathway. To determine whether type I IFN expression is dysregulated in Tsc2+/- mice, we measured its magnitude and kinetics of expression in mice treated with a single intraperitoneal injection of poly I:C. A distinct and progressive type I IFN signature was observed in the spleen. *Ifnb*, and to a lesser extent, *Ifna4* were upregulated in both WT and Tsc2+/- splenocytes at 2 hours, while the ISG, *Mx1*, was elevated at 2 hours, peaked at 4 hours was diminishing by 12 hours (Figure 4.5, A). The type I IFN signature was less prominent in the hippocampus, a modest increase in *Ifnb*, not *Ifna4*, was observed at 2 hours and *Mx1* peaked at 4 hours (Figure 4.5, B). The magnitude of *Ifnb* transcription was moderately elevated in Tsc2+/- compared to WT and this translated into significantly higher IFNβ protein expression in the serum, $p < 0.0001$ (Figure 4.5, C). Translation of the ISG CXCL10 is negatively regulated by TSC2 [35], so we measured the level of CXCL10 in the serum. Our results suggest CXCL10 was elevated in the serum in the serum of *Tsc2*+/- mice, however the variance was too large to determine whether the increase was significant (Figure 4.5, D).

Poly I:C treatment of *Tsc2*+/- pups leads to long lasting behavioral defects, whereas treatment of adults results in transient behavioral defects. To investigate whether the behavioral defects were due to altered gene expression, we measured gene expression in the spleen of adult mice that were either injected with a series of 4 doses of poly I:C as pups or as adults. Genes associated with a type I IFN response were upregulated in mice injected as adults, but not in mice injected as pups (Figure 4.6). Contrary to the kinetics experiment (Figure 4.5), WT and *Tsc2*+/- mice exhibited similar levels of *Ifnb* transcript when adult mice were injected 2 hours prior to organ harvest (Figure 4.6, A). However, expression of Irf7 and Il27p28 was

enhanced in *Tsc2*+/- mice, but the increase was not significant, $p = 0.224$ and $p = 0.145$, respectively.

DISCUSSION

Surprisingly, we found a sex effect in mice deficient for CXCL10 during LPS induced endotoxic shock that favored the survival of females, not males (Figure 4.1, A). There was no difference in the distribution of the cell types recruited to the peritoneal cavity in WT and CXCL10 KO females (Figure 4.1, B), but we did find females deficient in CXCL10 had less tissue damage as measured by serum ALT, AST and LDH (Figure 4.1, C – E).

Sex effects have previously been observed in rats LPS endotoxic shock, however the mechanism was not determined [36]. To explore the mechanism, we examined the effect of estradiol on the immune response to LPS. Splenocytes and BMMs from WT and CXCL10 KO were pretreated with estradiol then stimulated with LPS. We did not find a difference in the transcription of pro-inflammatory cytokines (Figure 4.2, B – D), however that does not eliminate the possibility that estradiol treatment had an effect at the protein level.

Finally, we conducted a pilot study to determine whether CXCL10 pathogenesis was mediated by the canonical receptor, CXCR3, or through the non-canonical receptor TLR4 [21,32]. Previously, CXCL10 ligation of TLR4 was shown to promote apoptosis in a mouse model of diabetes [22]. Here however, we found survival of CXCR3 KO females was greater which suggests CXCL10-CXCR3 signaling contributes to pathogenesis. Unfortunately, in this experiment all of the CXCL10 KO females in this experiment died (Figure 4.2, E). This result was unexpected. Retrospective analysis shows the CXCL10 KO females were older than those used in previous experiments and older than the CXCR3 KO females in the current experiment. This suggests that while gender is a factor in survival, age may also play a role.

In the EAE model, treatment of WT mice with poly I:C transiently attenuates disease severity (Figure 4.4, A and B). The benefits, however, were not as striking as in the RR-EAE model [25]. In trying to determine which pathway is responsible for the modest protection conferred by poly I:C we found that without the endocytic TLR3 or the cytosolic adapter,

CARDIF, mice experience less severe symptoms (Figure 4.3, H and I). Treatment, however, of TLR3 KO mice with poly I:C exacerbated symptoms which suggest TLR3 signaling is beneficial (Figure 4.4, C and D).

In examination of the type I IFN response in WT and *Tsc2*+/- mice, we find there is no difference in the kinetics of expression, but rather a difference in magnitude (Figure 4.5, A). The spleen (Figure 4.5, A) was more reactive than the hippocampus (Figure 4.5, B) to treatment with poly I:C. Induction of higher amounts of type I IFNs in *Tsc2*+/- mice was accompanied by elevated levels of IFNβ in the serum (Figure 4.5, C). This suggests circulating type I IFNs may induce changes in the brain. Indeed, distant expression of virus induced type I IFNs is observed to activate IFNAR signaling in the brain [2].

Finally, we examined the type I IFN signature in WT and *Tsc2*+/- mice immediately following social behavior testing. These mice were either injected multiple times with poly I:C as pups and tested as adults, or injected multiple times as adults and tested two hours after the final injection. Though both groups exhibit social behavior deficits (data not shown), only the acutely injected adults express a type I IFN gene signature (Figure 4.6). This result suggests the long lasting effects of poly I:C are not at the mRNA level.

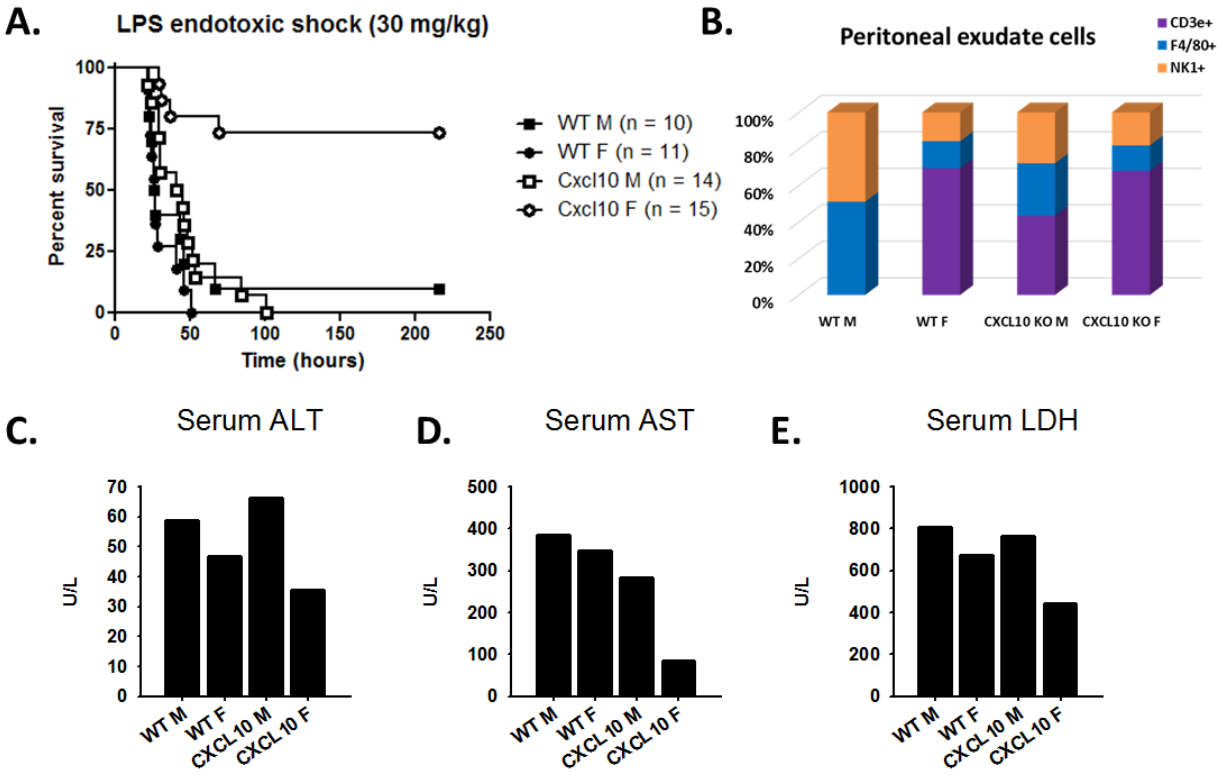

Figure 4.1. CXCL10 deficiency in female mice attenuates LPS induced endotoxic shock. Survival proportions of male and female, WT and Cxcl10-/- mice following intraperitoneal injection of 30 mg/kg *E. coli* 055:B5 LPS (A). Identify and distribution of peritoneal exudate cells by fluorescent antibody staining and flow cytometry 6 hours after LPS injection (B). Concentration of tissue damage biomarkers, ALT (C), AST (D) and LDH (E), in the serum 6 hours after LPS injection.

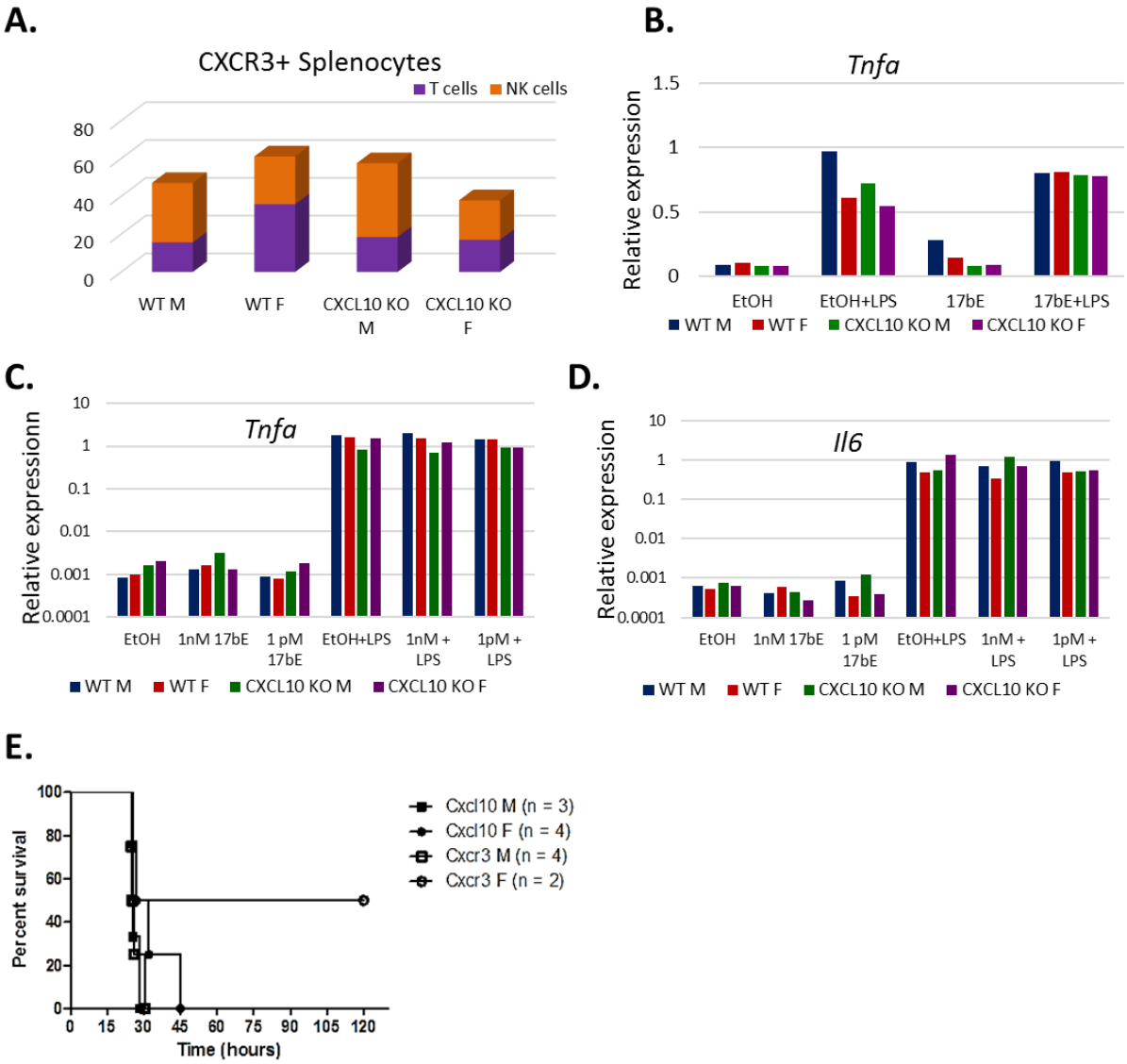

Figure 4.2. Role of estradiol and CXCR3 in LPS induced endotoxic shock. Expression of CXCR3 on naïve splenic T cells and NK cells from 1 male and female, WT and Cxcl10-/- mouse (A). Expression of *Tnfa* by splenocytes (B) or *Tnfa* (C) and *Il6* (D) by BMMs treated overnight with 17-β-estradiol, followed by a 6 hour stimulation with LPS. Survival curve of male and female Cxcl10-/- and Cxcr3-/- treated with 30 mg/kg *E. coli* 055:B5 LPS (E).

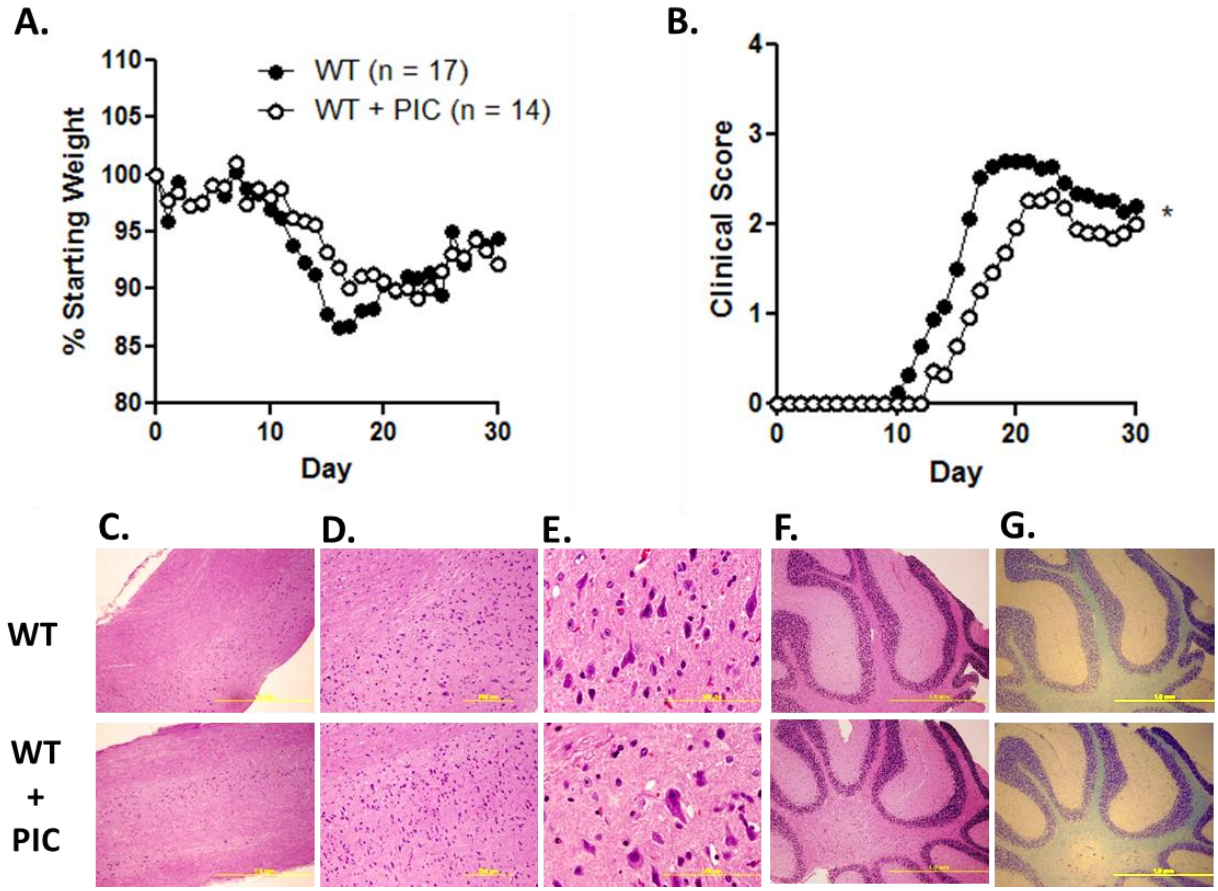

Figure 4.3. Chronic EAE is transiently attenuated by poly I:C treatment. Mean percent weight change (A) and mean clinical score (B) for WT untreated or treated with poly I:C one week after the induction of chronic EAE. H&E stained longitudinal spinal sections magnified 25X (C), 100X (D), and 400X (E). H&E stained (F) and luxol fast blue (G) stained cerebellum magnified 25X. All tissues were collected on day 44 and are representative of 3 independent experiments.

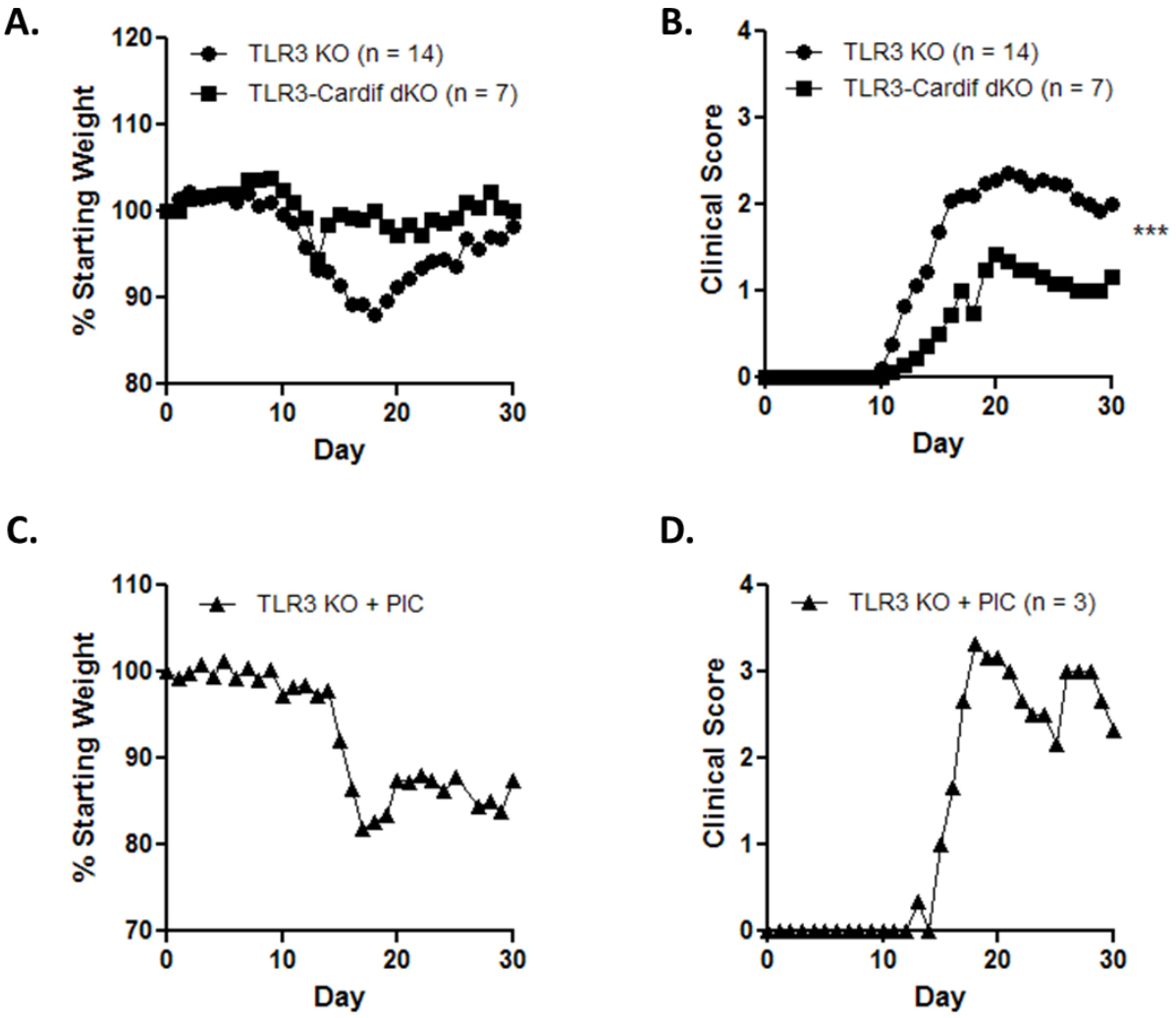

Figure 4.4. Contribution of TLR3 and Cardif signaling to EAE progression. Mean percent weight change (A) and mean clinical score (B) of TLR3 KO and TLR3/Cardif double KO mice. Mean percent weight change (C) and mean clinical score (D) of TLR3 KO treated with 100 µg poly I:C.

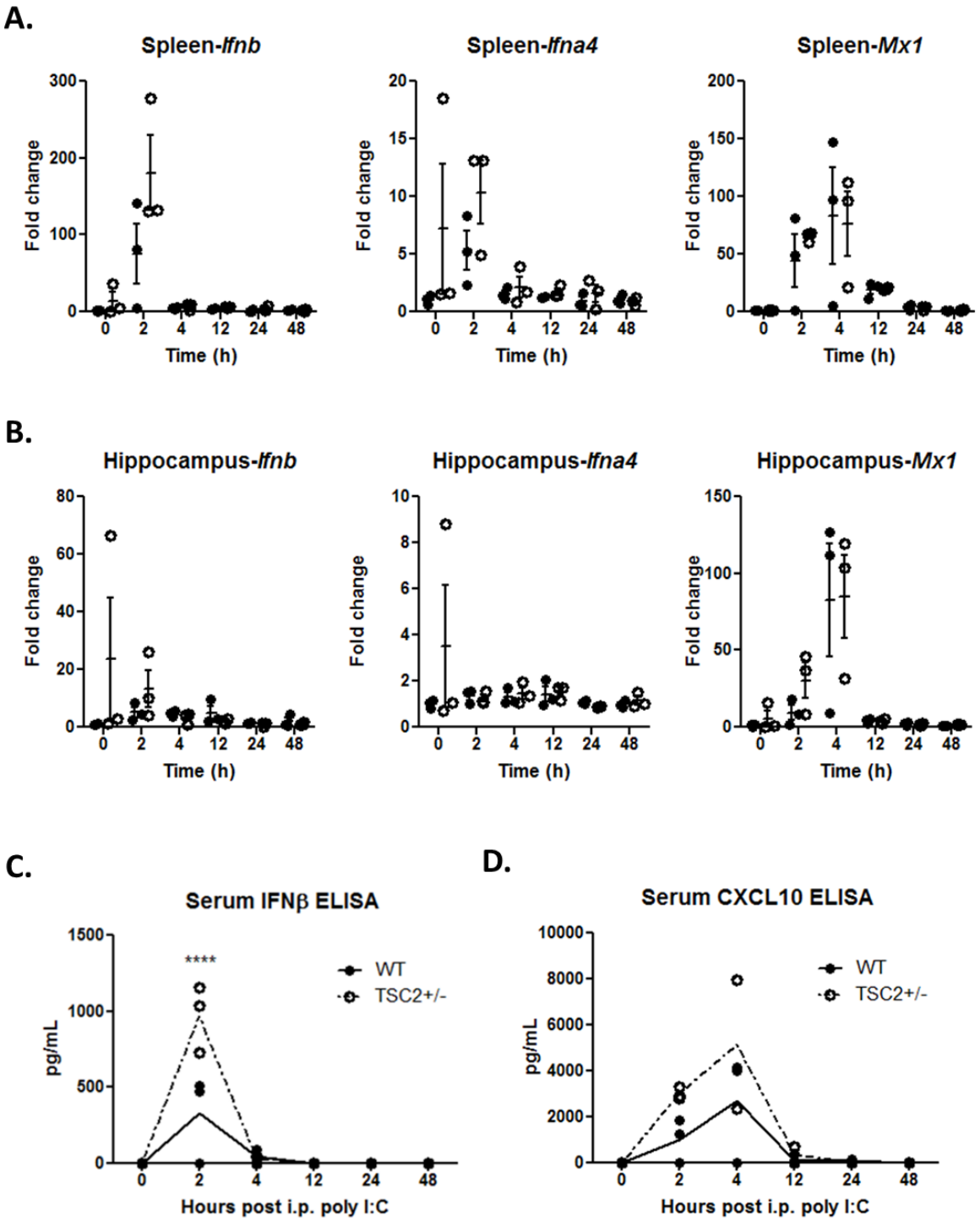
A.
Spleen-Ifnb
Spleen-Ifna4
Spleen-Mx1
Fold change
Time (h)
0
2
4
12
24
48
B.
Hippocampus-Ifnb
Hippocampus-Ifna4
Hippocampus-Mx1
C.
Serum IFNβ ELISA
pg/mL
****
WT
TSC2+/-
Hours post i.p. poly I:C
D.
Serum CXCL10 ELISA

Figure 4.5. Kinetics of type I IFNs in *Tsc2+/-* mice. WT and *Tsc2*+/- mice were treated with 50 µg poly I:C by intraperitoneal injection. At 0 (mock treated), 2, 4, 12, 24 and 48 hours post injection, a cohort of 3 mice of each genotype were euthanized. Expression of type I IFNs and ISGs was measured by qPCR in the spleen (A) and hippocampus (B). Protein levels of IFNβ (C) and CXCL10 (D) in the serum were measured by ELISA.

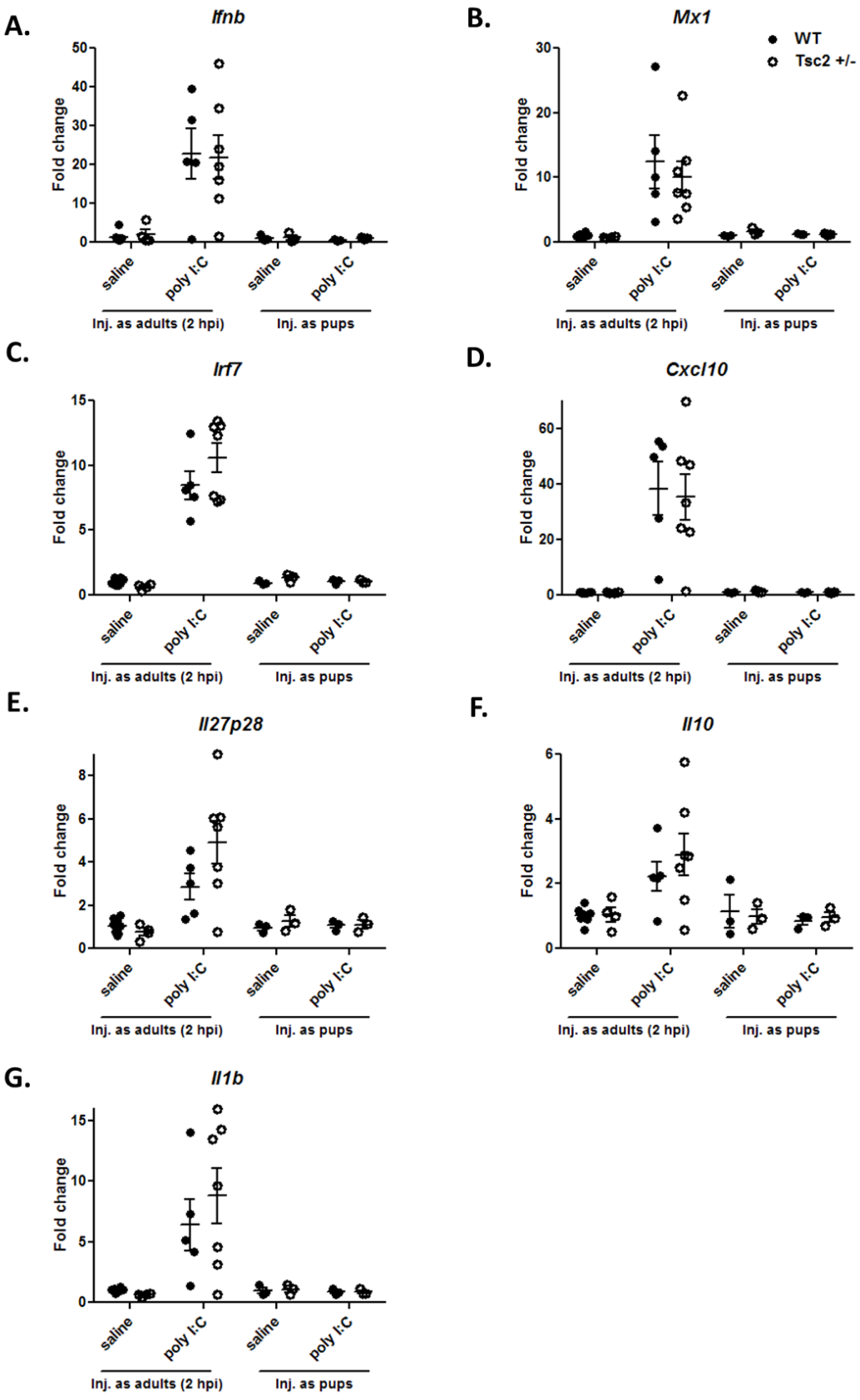
A.
Ifnb
Fold change
50
40
30
20
10
0
saline
poly I:C
saline
poly I:C
Inj. as adults (2 hpi)
Inj. as pups
B.
Mx1
WT
Tsc2 +/-
Fold change
30
20
10
0
saline
poly I:C
saline
poly I:C
Inj. as adults (2 hpi)
Inj. as pups
C.
Irf7
Fold change
15
10
5
0
saline
poly I:C
saline
poly I:C
Inj. as adults (2 hpi)
Inj. as pups
D.
Cxcl10
Fold change
60
40
20
0
saline
poly I:C
saline
poly I:C
Inj. as adults (2 hpi)
Inj. as pups
E.
Il27p28
Fold change
8
6
4
2
0
saline
poly I:C
saline
poly I:C
Inj. as adults (2 hpi)
Inj. as pups
F.
Il10
Fold change
6
4
2
0
saline
poly I:C
saline
poly I:C
Inj. as adults (2 hpi)
Inj. as pups
G.
Il1b
Fold change
15
10
5
0
saline
poly I:C
saline
poly I:C
Inj. as adults (2 hpi)
Inj. as pups

Figure 4.6. Poly I:C induced gene signature is transient. Spleens from WT and Tsc2+/- mice injected with four consecutive doses of 50 µg poly I:C, as pups or as adults were collected. Induction of *Ifnb* (A), *Mx1* (B), *Cxcl10* (C), *Irf7* (D), *Il27p28* (E), *Il10* (F) and *Il1b* (G) was measured by qPCR. WT: n = 5, Tsc2+/-: n = 7.

	Forward: 5’ -> 3’	Reverse: 5’ -> 3’
L32	AAGCGAAACTGGCGGAAAC	TAACCGATGTTGGGCATCAG
Ifnb	CAGCTCCAAGAAAGGACGAAC	GGCAGTGTAACTCTTCTGCAT
Ifna4	CCTGTGTGATGCAGGAACC	TCACCTCCCAGGCACAGA
Irf7	ACAGGGCGTTTTATC TTGCG	TCCAAGCTCCCGGCTAAGT
Mx1	AAACCTGATCCGACTTCACTTCC	TGATCGTCTTCAAGGTTTCCTTGT
Tnfa	GGTGCCTATGTCTCAGCCTCTT	CGATCACCCCGAAGTTCAGTA
Il1b	GAGCTGAAAGCTCTCCACCTCA	TCGTTGCTTGGCTCCTTGTAC
Il6	CACAGAGGATACCACTCCCAACA	TCCACGATTTCCCAGAGAACA
Cxcl10	CCTGCCCA CGTGTTGAGAT	TGATGGTCTTAGATTCCGGATTC
Il10	TCATCGATTTCTCCCCTGTGA	GACACCTTGGTCTTGGAGCTTATT
Il27p28	CTCTGCTTCCTCGCTACCAC	GGGGCAGCTTCTTTTCTTCT

Supplementary Table 4.1. Primer pairs for qPCR.

MATERIALS AND METHODS

Animals

All mice were bred and maintained in specific pathogen free facilities managed by the Department of Laboratory Animal Medicine at UCLA in strict accordance with protocols approved by the UCLA Animal Research Committee. Male and female mice were used for experimental autoimmune encephalitis experiments, while only male mice were used for experiments studying the type I IFN signature in *Tsc2* heterozygous mice.

Bone marrow derived macrophages

Bone marrow was flushed from four leg bones, pooled, and treated with ACK lysing buffer, a hypotonic solution for the removal of red blood cells. The remaining cells were counted and plated at 0.5 x 10^6/mL per well in 6-well tissue culture treated dishes containing macrophage differentiating medium (DMEM, 10% fetal bovine serum, 100 U/mL penicillin, 100 µg/mL streptomycin, and 2% macrophage colony stimulating factor (MCSF) conditioned medium, collected from L929 cells overexpressing MCSF)

RNA Isolation and quantitative RNA measurement

Total RNA was isolated using Trizol Reagent (Invitrogen) according to the manufacturer's protocol. RNA was quantified using NanoDrop 2000 and 0.5 or 1 µg was used to make complementary DNA (cDNA) templates using iScript™ cDNA Synthesis Kit (Bio Rad) according to the manufacturer's instructions and oligo-dT primers. Real time quantitative PCR (qPCR) was carried out using iTaq™ SYBR® Green Supermix reagent (Bio Rad) and measured using MyiQ™ Single-Color Real-Time PCR Detection System (Bio Rad). Gene specific primers are listed in Supplementary Table 4.1. Amplification was carried out with the following conditions: 95.0°C for 3:00 min, 95.0°C for 0:03 sec, 60.0°C for 0:20 sec; repeated 39 times followed by a melt curve from 65.0°C to 95.0°C, at 0.5°C increments, each 0:05 sec. The cycle

threshold values for the gene of interest were normalized to the housekeeping gene, L32, and fold expression was normalized to untreated, wild type control.

LPS Induced Endotoxic Shock

LPS from *E. coli* 055:B5 (Sigma, L2637-25MG) was brought into solution with sterile saline, final 10 mg/ml. The solution was sonicated for 5 min in an immersion bath sonicator on LOW setting. Mice were weighed, then injected via the intraperitoneal route with 30 mg/kg. For survival studies, mice were monitor twice daily and any mouse showing signs of morbidity was euthanized immediately. For mechanism studies, mice were injected with 30 mg/kg LPS and euthanized 6 hours later. Blood was collected by cardiac puncture, allowed to clot at RT for 30 min, centrifuged and the resulting serum fraction was transferred to a clean tube. Serum inflammatory markers, ALT and AST were measured using the Vet Axcel Chemistry Analyzer (Alfa Wassermann) (UCLA DLAM Diagnostics Lab). Peritoneal exudate cells (PECs) were dislodged by injecting 5 ml ice cold DPBS+2% FBS into the peritoneal cavity using a 27-Gauge needle and massaging the peritoneal cavity to release the resident and infiltrating immune cells. The PECs were collected by tenting the peritoneum with forceps, making a small cut, and then inserting a 20-Gauge needle and aspirating the fluid containing the cells. Similar volumes were recovered from each mouse. The PECs were washed and quantified by trypan blue exclusion on a hemocytometer. PEC composition and distribution was determined by fluorescent antibody staining and flow cytometry. 1×10^5 cells were stained with a master mix containing anti-mouse F4/80-FITC (eBioscience, 11-4801-81), anti-mouse NK1.1-PE (eBioscience, 12-5941-83) and anti-mouse CD3e-APC (BD, 553066) for 20 min at 4°C. Unbound antibodies were removed by washing 3x with DPBS-2% FBS. Cells were fixed with 2% formaldehyde in PBS, analyzed using the BD FACSVerse and data was analyzed with FlowJo software (Tree Star, Inc.).

Immune cell distribution and ex vivo stimulations were carried out with splenocytes and BMMs. The spleen was collected from naïve mice, gently dissociated and single cells were

collected by passing the homogenate through a 70 µm nylon mesh strainer. The cells were centrifuged then re-suspended in 1ml ACK lysing buffer and incubated on ice for 5 min. Cell were rescued with DPBS-2% FBS, washed and suspended in DPBS-2% FBS. To analyze spleen cell composition, an aliquot of cells was plated at a density of 1 x 10^6 cells per 10 cm dish for 1 hour to selectively remove macrophage cells. Unattached cells were collected, centrifuged and quantified by trypan blue exclusion. Cells were stained with anti-mouse CXCR3-PE (Biolegend, 126505), anti-mouse CD3e-FITC (Biolegend, 100306), and anti-mouse NK1-APC for 20 min at 4°C. Cells were washed and fixed with 2% para-formaldehyde-DPBS.

Ex vivo stimulations were carried out by directly plating 0.5 x 10^6 splenocytes per well in a 12-well tissue culture plate or by differentiating bone marrow cells to macrophages with 2% MCSF for 7 days. To study the effect of 17-β-estradiol (Sigma E2257-1mg) on LPS induced gene transcription or on CXCR3 expression, splenocytes were treated overnight with 1 pM or 1 nM of 17-β-estradiol or its solvent, ethanol. LPS was added and incubated for 11 hours. To quantify gene expression, adherent and non-adherent cells were collected and pooled in Trizol reagent. RNA was extracted according to manufacturer's protocol (Invitrogen). To measure CXCR3 expression, non-adherent cells were collected, stained and analyzed as described above for naïve cell analysis. BMMs were treated overnight with similarly 1 pM or 1 nM of 17-β-estradiol or its solvent, ethanol, the next day 100 ng/ml LPS was added and incubated for 6 hours, and then collected into Trizol for RNA extraction.

Experimental Autoimmune Encephalitis

A mixture containing 100 µg myelin oligodendrocyte peptide (MOG), 35 – 55 (Anaspec, 60130-5), 100 µl Complete Freund's adjuvant (Sigma, F5881), and 200 µg heat killed, lyophilized Mycobacterium, per mouse was prepared by passing it through an 18-Gauge emulsification adapter connecting 2, 3 mL glass syringes, 50X. Mice were anesthetized with isofluorane using an induction chamber and maintained using a nose cone. On day 0, 50 µl of

the MOG-CFA emulsification was injected subcutaneously above the hind and fore leg of the same side of the body. On both day 0 and day 2, 250 ng of pertussis toxin was administered by intraperitoneal injection. On day 7, MOG-CFA was applied as described, but on the opposite side of the body. In some experiments, 100 µg solution of polyinosinic-polycytosinic acid (Poly I:C) in water was given by intraperitoneal injection on days 5, 7 and 9.

TSC2+/- in vivo

For time course experiment, mice were treated with 20 mg/kg of polyinosinic-polycytosinic acid (Poly I:C) by a single intraperitoneal injection. Mice were euthanized and blood was collected by retro-orbital puncture. Serum was separated from clotted blood by centrifugation and stored -80°C until further analysis. The mouse was decapitated and the brain was dissected to isolate the hippocampus which was further divided in half for histological analysis and RNA extraction. The spleen was extracted, cut in half and the halves were snap frozen in liquid nitrogen, separately. Serum IFNβ was measured using the Verikine^{TM} Mouse IFN-Beta ELISA (PBL Assay Science) and serum CXCL10 was measured using the Duoset ELISA (R&D Systems).

Pups were treated with 20 mg/kg poly I:C by intraperitoneal injection at P3, P7, and P14. 6 week old adult mice were given 4 injections with 20 mg/kg poly I:C on day 0, 4, 11 and 2 hours prior to behavioral testing.

REFERENCES

1. Hansen, B. S., Hussain, R. Z., Lovett-Racke, A. E., Thomas, J. a & Racke, M. K. Multiple toll-like receptor agonists act as potent adjuvants in the induction of autoimmunity. *J. Neuroimmunol.* **172,** 94–103 (2006).

2. van den Pol, A. N., Ding, S. & Robek, M. D. Long-distance interferon signaling within the brain blocks virus spread. *J. Virol.* **88,** 3695–704 (2014).

3. Ehninger, D. *et al.* Gestational immune activation and Tsc2 haploinsufficiency cooperate to disrupt fetal survival and may perturb social behavior in adult mice. *Mol. Psychiatry* **17,** 62–70 (2012).

4. Sewnath, M. E. *et al.* IL-10-deficient mice demonstrate multiple organ failure and increased mortality during Escherichia coli peritonitis despite an accelerated bacterial clearance. *J. Immunol.* **166,** 6323–31 (2001).

5. O'Connell, R. M. *et al.* Type I interferon production enhances susceptibility to Listeria monocytogenes infection. *J. Exp. Med.* **200,** 437–45 (2004).

6. Robinson, N. *et al.* Type I interferon induces necroptosis in macrophages during infection with Salmonella enterica serovar Typhimurium. *Nat. Immunol.* **13,** 954–62 (2012).

7. Wilson, E. B. *et al.* Blockade of chronic type I interferon signaling to control persistent LCMV infection. *Science* **340,** 202–7 (2013).

8. Karaghiosoff, M. *et al.* Central role for type I interferons and Tyk2 in lipopolysaccharide-induced endotoxin shock. *Nat. Immunol.* **4,** 471–7 (2003).

9. Kelly-Scumpia, K. M. *et al.* Type I interferon signaling in hematopoietic cells is required for survival in mouse polymicrobial sepsis by regulating CXCL10. *J. Exp. Med.* **207,** 319–26 (2010).

10. de Weerd, N. a *et al.* Structural basis of a unique interferon-β signaling axis mediated via the receptor IFNAR1. *Nat. Immunol.* 1–9 (2013). doi:10.1038/ni.2667

11. Chen, H.-L., Hung, C.-H., Tseng, H.-I. & Yang, R.-C. Plasma IP-10 as a predictor of serious bacterial infection in infants less than 4 months of age. *J. Trop. Pediatr.* **55,** 103–8 (2009).

12. Narumi, S. *et al.* Neutralization of IFN-inducible protein 10/CXCL10 exacerbates experimental autoimmune encephalomyelitis. *Eur. J. Immunol.* **32,** 1784–91 (2002).

13. Cuenca, A. G. *et al.* Critical role for CXC ligand 10/CXC receptor 3 signaling in the murine neonatal response to sepsis. *Infect. Immun.* **79,** 2746–54 (2011).

14. Shen, F.-H. *et al.* Absence of CXCL10 aggravates herpes stromal keratitis with reduced primary neutrophil influx in mice. *J. Virol.* **87,** 8502–10 (2013).

15. Wang, W. *et al.* Monoclonal antibody against CXCL-10/IP-10 ameliorates influenza A (H1N1) virus induced acute lung injury. *Cell Res.* **23,** 577–80 (2013).

16. Jiang, D. *et al.* Long-term exposure of chemokine CXCL10 causes bronchiolitis-like inflammation. *Am. J. Respir. Cell Mol. Biol.* **46,** 592–8 (2012).

17. Sasaki, S. *et al.* Blockade of CXCL10 protects mice from acute colitis and enhances crypt

cell survival. *Eur. J. Immunol.* **32,** 3197–205 (2002).

18. Suzuki, K. *et al.* Blockade of interferon-gamma-inducible protein-10 attenuates chronic experimental colitis by blocking cellular trafficking and protecting intestinal epithelial cells. *Pathol. Int.* **57,** 413–20 (2007).

19. Antonelli, A. *et al.* Chemokine (C-X-C motif) ligand (CXCL)10 in autoimmune diseases. *Autoimmun. Rev.* **13,** 272–80 (2014).

20. Ito, T. *et al.* CXCL10 produced from hair follicles induces Th1 and Tc1 cell infiltration in the acute phase of alopecia areata followed by sustained Tc1 accumulation in the chronic phase. *J. Dermatol. Sci.* **69,** 140–7 (2013).

21. Sahin, H. *et al.* Pro-apoptotic effects of the chemokine CXCL10 are mediated by the non-cognate receptor TLR4 in hepatocytes. *Hepatology* 1–36 (2012). doi:10.1002/hep.26069

22. Schulthess, F. T. *et al.* CXCL10 impairs beta cell function and viability in diabetes through TLR4 signaling. *Cell Metab.* **9,** 125–39 (2009).

23. Interferon beta-1b is effective in relapsing-remitting multiple sclerosis. I. Clinical results of a multicenter, randomized, double-blind, placebo-controlled trial. The IFNB Multiple Sclerosis Study Group. *Neurology* **43,** 655–61 (1993).

24. Teige, I. *et al.* IFN-beta gene deletion leads to augmented and chronic demyelinating experimental autoimmune encephalomyelitis. *J. Immunol.* **170,** 4776–84 (2003).

25. Touil, T., Fitzgerald, D., Zhang, G.-X., Rostami, A. & Gran, B. Cutting Edge: TLR3 stimulation suppresses experimental autoimmune encephalomyelitis by inducing endogenous IFN-beta. *J. Immunol.* **177,** 7505–9 (2006).

26. Guo, B., Chang, E. Y. & Cheng, G. The type I IFN induction pathway constrains Th17-mediated autoimmune inflammation in mice. *J. Clin. Invest.* **118,** 1680–90 (2008).

27. Pioli, P. a *et al.* Estradiol attenuates lipopolysaccharide-induced CXC chemokine ligand 8 production by human peripheral blood monocytes. *J. Immunol.* **179,** 6284–90 (2007).

28. Liu, L. *et al.* Estrogen-induced nongenomic calcium signaling inhibits lipopolysaccharide-stimulated tumor necrosis factor α production in macrophages. *PLoS One* **8,** e83072 (2013).

29. Markle, J. G. & Fish, E. N. SeXX matters in immunity. *Trends Immunol.* **35,** 97–104 (2014).

30. Taylor, L. C., Puranam, K., Gilmore, W., Ting, J. P.-Y. & Matsushima, G. K. 17Beta-Estradiol Protects Male Mice From Cuprizone-Induced Demyelination and Oligodendrocyte Loss. *Neurobiol. Dis.* **39,** 127–37 (2010).

31. Berg, D. J. *et al.* Interleukin-10 is a central regulator of the response to LPS in murine models of endotoxic shock and the Shwartzman reaction but not endotoxin tolerance. *J. Clin. Invest.* **96,** 2339–2347 (1995).

32. Schulthess, F. T. *et al.* CXCL10 impairs beta cell function and viability in diabetes through TLR4 signaling. *Cell Metab.* **9,** 125–39 (2009).

33. Kawai, T. *et al.* IPS-1, an adaptor triggering RIG-I- and Mda5-mediated type I interferon induction. *Nat. Immunol.* **6,** 981–988 (2005).

34. Yamamoto, M., Sato, S. & Hemmi, H. Role of Adaptor TRIF in the. *Science (80-.).* **301,** 640–643 (2003).

35. Kaur, S. *et al.* Regulatory effects of mammalian target of rapamycin-activated pathways in type I and II interferon signaling. *J. Biol. Chem.* **282,** 1757–68 (2007).

36. Losonczy, G. *et al.* Male gender predisposes to development of endotoxic shock in the rat. *Cardiovasc. Res.* **47,** 183–91 (2000).

CHAPTER 5

Long term effects of acute radiation exposure

ABSTRACT

Ionizing radiation causes well defined, dose dependent symptoms within the first 30 days collectively referred to as acute radiation syndrome (ARS). Treatment with pathogen associated molecular patterns (PAMPs) prior to exposure protects against ARS. We explored the mechanism of LPS induced radioprotection and found LPS and irradiation synergize to upregulate specific serum cytokines. Moreover, LPS radioprotection depended on MyD88 signaling. Non-routine exposures to radiation have prompted the development of radiomitigators, molecules that protect against ARS when administered after an exposure event. As part of the Center for Medical Countermeasures against Radiation (CMCR) at UCLA, we have participated in the study of novel radiomitigators with particular focus on the long term effects of radiation exposure on the immune system. Mice that survived ARS were observed daily for over a year. Weight, illness, serum cytokines and gut microbiota were monitored. Mice treated with the CMCR mitigators, 512 or G-CSF, were more likely to develop penile prolapse or anemia, respectively. In many cases, elevated serum cytokine levels were indicative of morbidity or moribundity. Analysis of gut microbiota at the phylum level revealed a difference in the overall distribution between mice treated with irradiation and those not exposed, but further analysis is required. Finally, immune response to vaccination with the chicken ovalbumin protein, OVA, and either poly I:C, a TLR3 agonist or CpG B, a TLR9 agonist, was performed to assess the response of radiation survivors to an immunological challenge. Following immunization, mice treated with certain mitigators showed enhanced cytokine response compared with un-irradiated or irradiated only mice. In one experiment, a distinct difference in the development of the humoral response was noted, but not a second experiment. Moreover, in a single experiment, the distribution of myeloid cells, CD4 central and effector memory was found to differ significantly between mice treated with the same mitigators, but different TLR agonists.

INTRODUCTION

Exposure to radiation causes cell death from DNA damage and, depending on the dose rate and exposure time, leads to the failure of the hematopoietic, gastrointestinal and nervous systems. Collectively known as ARS, damage can be prevented by pre-treatment with radioprotectants or post-treatment with radiomitigators.

Immune system activation by PAMPs mediates radioprotection. Ligation of TLR2 [1], TLR4 [2], TLR5 [3] and TLR9 [4] have all been found to promote host resistance to whole body irradiation (WBI). Macrophages are a key effector in TLR4 mediated protection [5]. TLR4 interacts with two downstream adapters, MyD88 and TRIF. The MyD88 dependent pathway predominately leads to activation of proinflammatory, NFkB dependent genes such as TNFα [6], while the TRIF dependent pathway leads leads to IRF3 dependent transcription of type I IFNs [7]. MyD88 is required for long term survival following irradiation [8], but its contribution to ARS is not well defined.

As part of the CMCR at UCLA, we have identified several molecules [9] that, when administered at least 24 hr after WBI, enhance survival and restore levels of circulating RBCs, WBCs and platelets. These radiomitigators are being studied for protection during ARS and long term effects on health in the following months. Our lead candidate is 512, a compound that contains a 4-nitrophenylsulfonamide group. Another lead radiomitigator is granulocyte colony stimulating factor (G-CSF). GSCF protects against irradiation [10] and is extensively used in the clinic to treat chemotherapy induced neutropenia [11]. In collaboration with GeneronBiomed Inc. of Shanghai, we are testing their bivalent G-CSF construct. It was designed to address some of the problems associated with repeated treatment with monovalent G-CSF including short half-life and immune exhaustion [11].Bivalent G-CSF is essentially two molecules of G-CSF linked together with the Fc domain found in antibodies.

The role of radiomitigators, if any, in delayed effects of acute radiation exposure (DEARE) is not known. In general, the long term effects of acute radiation have been poorly defined. This is in part due to the variation stemming from exposure type and dose as well as genetic predisposition. Some data from human survivors of accidental or non-routine exposures finds cataract and increased tumor incidence to be among the late effects [12]. In mice, one study reported long lasting effects of GI syndrome after partial body irradiation [13]. To further define DEARE, we observed mice in the months following ARS and noted any signs or symptom of illness. Furthermore, we collected blood and fecal samples for analysis of DEARE biomarkers.

Mice that survive ARS, appear healthy, however mice are maintained in specific pathogen free environments. We do not know whether they are able to generate a normal immune response when challenged or whether mitigators treatment has a long term effect on the ability of the immune system to respond to a challenge. Some have reported partial or full body irradiation compromises epithelial integrity, not the antiviral response, and host resistance to influenza infections in the future [14]. Likewise, others have shown the anti-bacterial response of irradiated mice to *E. coli* infection remains intact, even though cytokine levels are elevated and increased tissue damage is observed [15]. Combined treatment with LPS and irradiation may enhance susceptibility to future Gram negative infection by suppressing platelets and reducing organ mass [16].

To determine whether survivors of radiation exposure are able to mount a normal immune response we challenged mice. Rather than initiate an infection, we vaccinated mice with the prototypic protein antigen, ovalbumin, then studied the innate and adaptive response. Ovalbumin administered with poly I:C, a TLR3 agonist, or CpG, a TLR9 agonists, leads to the induction of specific cytokines act in concert to shape the formation of the adaptive response, particularly the humoral response [17,18]. Here, we measured cytokine response 24 hours after immunization and cell based response in the weeks following the last immunization.

RESULTS

Lipid A treatment prior to WBI alters platelet and cytokine levels

Cytokine signaling is an important component of the innate immune response to irradiation. Induction of cytokines following exposure has been observed [19] and prophylactic treatment with cytokines [10,20] or LPS [21] is radioprotective. To further examine the effect of PAMP prophylaxis on the immune landscape, WT C57Bl/6 mice were treated with lipid A 24 hours prior to irradiation and euthanized 4 hours after irradiation. Lipid A pre-treatment did not significantly alter the number of circulating RBCs (Figure 5.1, A), WBCs (Figure 5.1, B), or the hemoglobin level (Figure 5.1, D) in the blood when compared to mice receiving irradiation only. Platelets, however, were lower in mice treated with lipid A and irradiation than in mice exposed to either alone (Figure 5.1, C). This was not unexpected as a previous study observed LPS treatment 10 days after irradiation transiently suppressed circulating platelets [16].

Next, cytokine levels in the serum were measured. Interestingly, lipid A pre-treatment accentuated the expression of interferon inducible proteins, CXCL10 (Figure 5.1, E), IL-10 (Figure 5.1, F), and RANTES (Figure 5.1, G). Serum concentration of IL-1α, a protein that may be induced by LPS or released by dying cells [22], was increased only in mice exposed to irradiation.

MyD88 dependent signaling mediates radioprotection

LPS or llpid A ligation of TLR4 activates two downstream adapters, MyD88 and TRIF. Signaling through the TRIF dependent pathway leads to transcription of type I IFNs [7] which then induces interferon stimulated genes (ISGs). Synergistic upregulation of ISGs by lipid A and irradiation (Figure 5.1, E – G) suggests that TRIF dependent genes may be important for radioprotection. To examine the contribution of TRIF to radioprotection, WT C57Bl/6 and Ticam(Lps2) mice, which have a mutation in the Trif gene that renders it non-functional, were treated with LPS by intraperitoneal injection 1 hour or 24 hours prior to irradiation. WT C57Bl/6

mice were completely protected when LPS was administered 24 hours prior to irradiation, but only 75% were protected when LPS was given 1 hour before (Figure 5.2, A). Surprisingly, LPS treatment 24 hours before also led to 100% survival of the Ticam mice (Figure, 5.2, B). Overall, Ticam mice were more sensitive to radiation compared to WT, but LPS treatment 1 hour prior to irradiation increased survival by 20% compared to irradiated only (Figure 5.2, B).

Exogenous treatment with proinflammatory, MyD88 dependent [23] cytokines, IL-1β and TNFα [10,20], is radioprotective. To ascertain the role of MyD88 in LPS radioprotection, C57Bl/6, MyD88 and Ticam mice were treated with LPS 24 hours prior to irradiation. Similar survival curves were observed for C57Bl/6 and Ticam mice (Figure 5.2, C and D), however MyD88 KO mice were extremely radiosensitive, irrespective of LPS treatment (Figure 5.2, E). These studies illustrated MyD88 dependent pathway is required for LPS mediated radioprotection, while the TRIF pathway contributes to a lesser extent.

Radiomitigators promote survival during and after ARS

As part of the CMCR program at ULCA, novel radiomitigators have been identified from a high throughput screen of a small molecule library. It was found that compounds containing a 4-nitrophenylsulfonamide structure rescued radiation-induced apoptosis (unpublished data). The lead 4-nitrophenylsulfonamide containing compound, 512, was further tested and found to protect mice WT C3H mice from lethal ARS (Figure 5.3, A). Additional radiomitigators were also assessed. Monovalent G-CSF, commercially known as filgrastim, is known to have a short half-life and multiple treatments leads to immune exhaustion [11] and bivalent G-CSF, which has a longer half-life and requires fewer treatments to achieve results similar to monovalent G-CSF (unpublished data). Both G-CSF variants protected mice from lethal ARS, however bivalent G-CSF was less protective (Figure 5.3, B and C). Moreover, survival was also promoted when 512 was applied in combination with monovalent or bivalent G-CSF. Furthermore, we noticed a

similar pattern of survival emerged in the following 31 – 700 days. Compiled together, we find following ARS there are additional waves of death around 200 and 450 days after irradiation.

Symptoms associated with delayed and late effects of radiation

Following the mice in the months after radiation treatment, we noticed not only patterns of survival but also illness (Figure 5.3). Over the course of 12 months, symptoms ranging from anemia, hair loss, penile prolapse, diarrhea and tumors were observed (Figure 5.4, A). Breaking down the symptoms by mitigator treatment we found mice treated with 512, alone or in combination, were more likely to experience penile prolapse (Figure 5.4, B). Penile prolapse is often a symptom of urinary obstruction [24] or a more general malaise accompanied by increased contact of the penis with cage bedding. Curiously, treatment with either G-CSF, alone or in combination, had a higher incidence of anemia (Figure 5.4, C). Anemia is a hallmark of hematopoietic failure during ARS, however the trigger for late stage anemia is unknown.

Serum cytokines as DEARE biomarkers

To further evaluate the heath state of the mice, blood was collected by non-lethal retro-orbital puncture or by after euthanasia. Serum was isolated and cytokine concentration was measured. In one experiment, cytokine levels were compared between two or more collections from the same mouse and between mice from the same mitigators cohort. A heat map of expression of the levels showed that for some mice cytokine expression increased at or close to the time of death. For others, there was difference between earlier collections and collection at the time of death. Overall, there was no consistent change in cytokine levels between individuals given the same mitigators treatment (Figure 5.4).

In separate experiment, health state was also compared to circulating cytokine levels (Figure 5.5). Cytokine levels measured from a single blood collection were organized into a heat map by final health status. Elevated cytokine levels were more associated with illness and/or death, while lower levels more likely expressed by healthy, irradiated or non-irradiated mice

(Figure 5.5, A). Analysis by cytokine revealed mice that died in the months following exposure to WBI had significantly higher levels of GM-CSF, IL-12p40 and MIP-2 compared to either irradiated and non-irradiated mice. Moreover, irradiated mice displaying signs of illness expressed elevated levels of IFNγ and IP-10 (CXCL10) (Figure 5.5, B). These results suggest cytokine level may be predictive of mortality.

Fecal microbiota as DEARE biomarkers

Diarrhea was one symptom observed in mice that survived ARS (Figure 5.4, A). This led us to investigate whether diarrhea was accompanied by gut microbial dysbiosis. Feces were collected from individual mice and bacterial DNA was isolated. 16S libraries were constructed and sequenced. At the phylum level, mice that were never exposed to irradiation had a greater abundance of Firmicutes than mice treated with WBI + mitigator (Figure 5.7, A). Conversely, the abundance of TM7 was more likely to be increased in WBI + mitigator treated mice than in unexposed mice (Figure 5.7, A). With the exception of select WBI + mitigators treated mice, there was no difference in the abundance Proteobacteria. Next, we focused in on 3 individual mice for which 3 fecal samples had been collected at 5, 7, and 12 months after WBI. The phyla abundance in the unexposed mouse was consistent over a 7-month period (Figure 5.7, B). For WBI mice treated with a combination of AMD + 512, phyla abundance fluctuated. The cause of the dramatic increase in Firmicutes during month 5 for mouse 1 is unclear. For mouse 2, however, increase in Proteobacteria and decrease in Firmicutes during month 12 corresponded with the incidence of diarrhea and penile prolapse (Figure 5.7, B).

Immune response to OVA vaccination

To examine the effect of WBI and/or mitigator treatment on the host response immune challenge, we vaccinated mice with the ovalbumin (OVA) protein and measured the innate and adaptive immune response. Two independent vaccination experiments were conducted, each

with surviving mice from multiple ARS experiments, all 35 – 78 weeks after WBI. A schematic of the immunization schedule is presented in Figure 5.8, A.

Blood was collected before and 24 hours after each immunization for the measurement of serum cytokines and antibodies. Following immunization, the secretion of these cytokines was enhanced, and the degree of enhancement was dependent on the type of TLR agonist administered. WBI with or without mitigators treatment led to increased expression of certain cytokines. For example, G-CSF (Figure 5.8, B) and IL-17 (Figure 5.8, C) were elevated in naïve WBI. Following immunization, WBI mice that received CpG as the adjuvant expressed similar concentrations of G-CSF as mice that were not exposed to WBI, but WBI mice that received poly I:C expressed substantially more G-CSF than similarly treated controls (Figure 5.8, B). For IL-17, however, primer WBI predisposed the mice to higher serum IL-17 concentrations and these concentrations were not altered following immunization (Figure 5.8, C). Prior exposure to WBI did not other cytokines such as TNFα (Figure 5.8, D) or IL-5 (Figure 5.8, E), either before or after immunization. Cytokine expression shapes the formation of the adaptive response. We measured the B cell response as a function of production of OVA specific antibody. Greater differences were observed between mice not treated with WBI and mice that were later vaccinated with poly I:C, therefore we hypothesized the WBI mice treated with ovalbumin and poly I:C may develop variable antibody response. Indeed, mice vaccinated with OVA + poly I:C and exposed to WBI produced less OVA specific antibody compared to mice not exposed to WBI and to mice treated with OVA + CpG (Figure 5.8, F).

In the second experiment, mice were sacrificed one week after the 2nd immunization. Mice treated with radiation and GCSF, displayed splenomegaly after immunization with OVA-CpG (Figure 5.9, A) which was due to an increase in myeloid like cells (Figure 5.9, B). In contrast, end point analysis (day 28) of mice treated with 512 and/or GCSF showed no defect in production of total antibody (Figure 5.9, C) or in isotype switching (data not shown). Moreover,

mice treated with both 512 and GCSF then immunized with OVA had heightened production of total and IgG1 specific antibody compared to OVA only cohorts (Figure 5.9, B). In contrast to other cohorts, irradiated mice treated with both 512 and GCSF had greater immunogen dependent variation in CD4 T cell effector memory proliferation, and less variation in the CD4 central memory population (Figure 5.10, A and B). No difference was observed in the CD8 T cell populations (Figure 5.10, C and D).

DISCUSSION

Protection from ARS may be accomplished by administration of radioprotective or radiomitigator compounds. Radioprotection by LPS is associated with transient suppression of circulating platelets and synergistic activation of serum cytokine expression (Figure 5.1). Interferon dependent proteins were more likely to be enhanced by co-treatment with LPS and WBI (Figure 5.1, E – G) suggesting that radioprotection was mediated through LPS activation of the TRIF dependent pathway. This, however, was not the case. While TRIF dependent signaling did enhance survival (Figure 5.2, B and D), MyD88 deficient mice were more radiosensitive (Figure 5.2, E). This result, however, is in contrast with some published literature which found MyD88 signaling increased the incidence of apoptosis and decreased survival of colonic cypts [25]. However, another study found MyD88 deficiency enhanced long term development of lung fibrosis and death associated with thoracic irradiation [8].

Treatment with radiomitigators, 512 and G-CSF, rescue mice from ARS (Figure 5.3). In the long term, these mice experience symptoms of illness including anemia, diarrhea, penile prolapse, tumors and hair loss (Figure 5.3, A). Two distinct patterns emerged. Mice treated with 512, alone or in combination, with another mitigators were more likely to develop penile prolapse. Whereas mice treated with G-CSF, along or in combination, had a higher incidence of anemia. Ironically, G-CSF is used in the clinic to treat aplastic anemia [26]. Increased incidence may be attributed to G-CSF driven myeloid expansion [10].

In two independent experiments, the concentration of cytokines in the serum was measured to determine whether level or signatures correlated with health status and could be used in the future as a biomarker of DEARE. In one experiment, mice were monitored for over a year and cytokine expression was measured at least twice (Figure 5.5). A trend is not readily apparent, but will be further explored. In the other experiment, a single serum sample was collected, samples were grouped based on treatment and the final health state 43 days later

(Figure 5.6). Interestingly, mice that expressed radically altered basal cytokine profiles were more likely to die in the near future, suggesting that cytokines may be used as a biomarker to predict morbidity and mortality.

We also examined gut microbiota to determine whether any trends or signatures could be a biomarker. We found mice exposed to irradiation had a lower abundance of Firmicutes (Figure 5.7, A). Others have observed similar decreases in the abundance of Firmicutes following pelvic irradiation [27]. However, on closer inspection of individual mice taking into account disease symptoms we find an increased abundance of Firmicutes (Figure 5.7, B). Interestingly, WBI + mitigator treated mice were more likely to have a higher abundance of TM7 than untreated mice (Figure 5.7, A). TM7 is most often associated with the pathogenesis of inflammatory bowel diseases of which symptoms include diarrhea [28].

To measure the functional response of the immune system we used employed an immunization model that uses OVA co-injected with or without a TLR agonist (Figure 5.8, A). This model allows for the study of the innate immune response to either poly I:C RNA, a TLR3 ligand, or CpG DNA, a TLR9 ligand. We hypothesized that survivors of WBI would have alterations in their hematopoietic cells and/or immune compartments that would affect their ability to mount a normal response.

Prior to immunization, survivor mice had increased basal expression of serum cytokine and chemokines, yet there waas pronounced variance between individuals, but the levels were dramatically different from age matched mice not exposed to WBI (Figure 5.5 and 5.6). After immunization, cytokine expression was enhanced in irradiated mice, but in some cases the effect was adjuvant dependent (Figure 5.8, B – E).

Analysis of the adaptive response revealed more variation between mice treated with different mitigators than between irradiated and non-irradiated mice; mice treated with certain mitigators presented with defective OVA specific antibody production while mice treated with

other mitigators had disproportionate expansion of splenic myeloid and T cell subpopulations. Together these data indicate that there is a defect in the immunological response of the survivor mice and suggests that the type of mitigator used for treatment may influence subsequent responses, but that it is important to examine these responses at the level of the individual to better predict response outcome. WBI survivors rescued with P1, P2 or P3 showed depressed antibody production (Figure 5.8, F), but appropriate isostype switching indicating the signaling was appropriate but suggests the response was not amplified. Antibody production and isotype switching in 512 and/or GSCF treated mice closely resembled that observed in the unirradiated mice (Figure 5.9, C), however further study will need to be conducted to determine if the response is sustained.

Administration of the mitigator GCSF was associated with myeloid hyperplasia in the spleen when survivor mice were immunized with OVA-CpG (Figure 5.9, A and B). This suggests that the choice of mitigator may favor proliferation of specific populations. Overall there was not a significant difference in the expansion of CD8+ T cells populations following immunization regardless of mitigator treatment. However, irradiated mice treated with both 512 and GCSF had significant expansion of the CD4 T cell effector memory population after OVA only immunization, with a concurrent stagnation in the CD4 T cell central memory population (Figure 5.10).

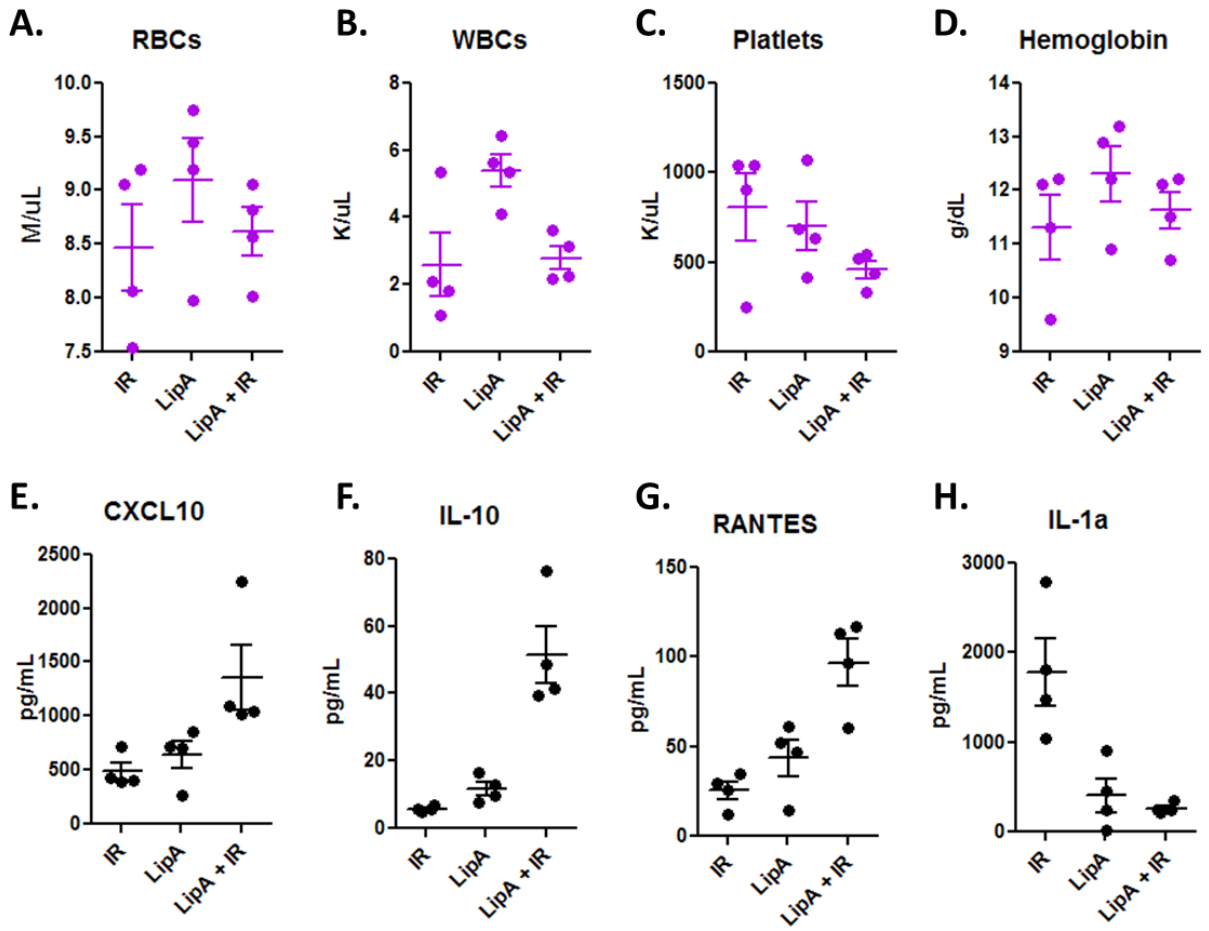

Figure 5.1. CBC and cytokine analysis following lipid A treatment and WBI. Mice were treated with saline or lipid A 24 by intraperitoneal injection 24 hours before performing WBI using an X-ray machine at a dose rate of 1.173 Gy/min. Concentration of circulating RBCs (A), WBCs (B), platelets (C) and hemoglobin (D) was measured using a Hemavet machine. Concentration of serum CXCL10 (E), IL-10 (F), RANTES (G) and IL-1α (H) proteins was measured by multiplex assay.

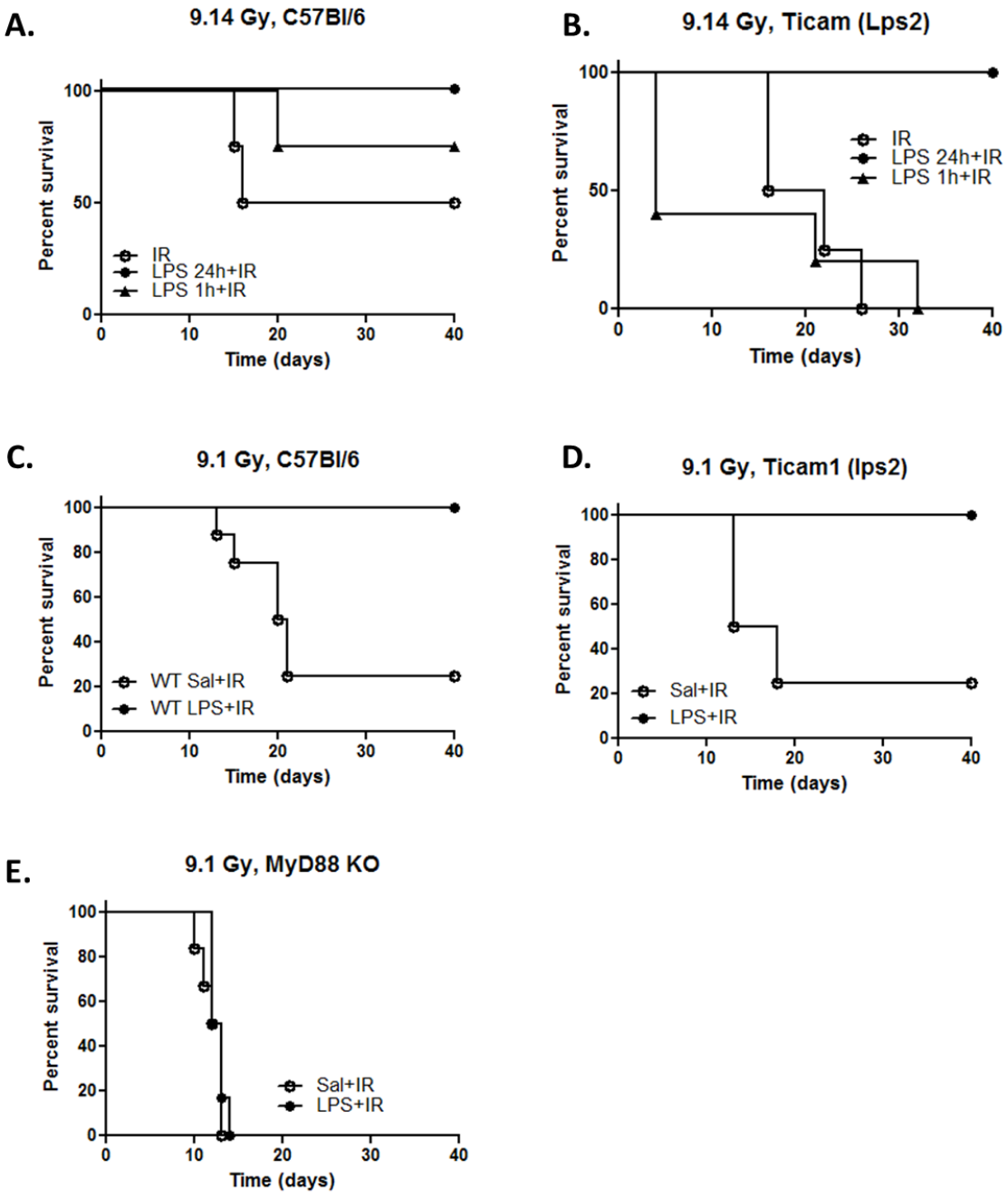

Figure 5.2. Radioprotection by LPS is primarily mediated by MyD88 dependent signaling. Survival curves for WT C57Bl/6 (A) and Ticam1(lps2) (B) treated with LPS 1 or 24 hours prior to WBI performed using a Cs^{137} source at a dose rate of 1.09 Gy/min. Survival curves for WT C57Bl/6 (C), Ticam1(lps2) (D) and MyD88 KO (E) mice treated with LPS 24 hours prior to WBI using a Cs^{137} source at a dose rate of 1.09 Gy/min.

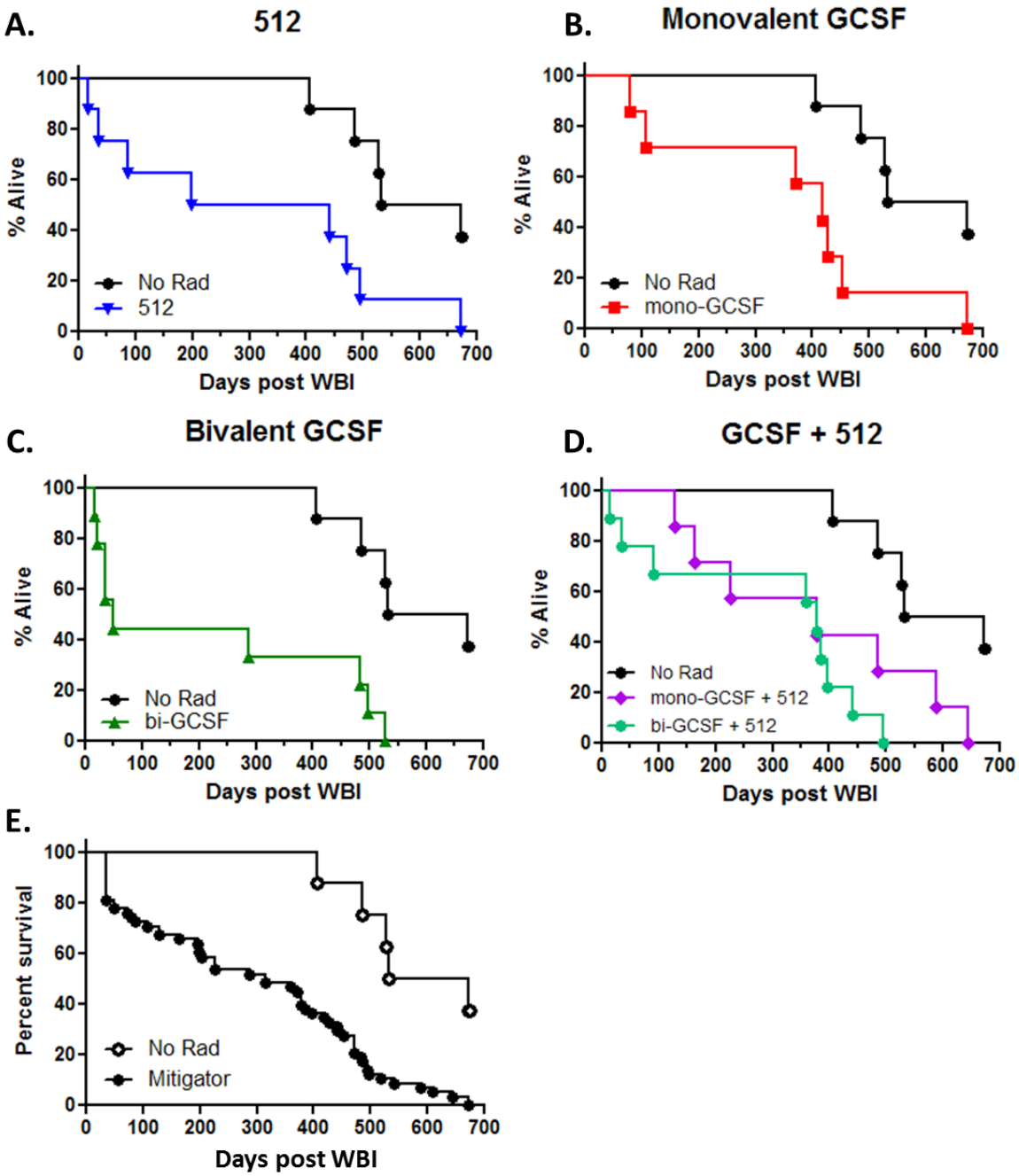

Figure 5.3. Survival curves of mice treated with radiomitigators that survived ARS. C3H mice were exposed to a Cs137 source at a dose rate of 62 cGy/min, then treated 24 hours later with either 512 (A), monovalent GCSF (B), bivalent GCSF (C), or combinations of 512 and GCSF (D). Survival of mice treated with WBI and radiomitigator(s) and no irradiation controls (E).

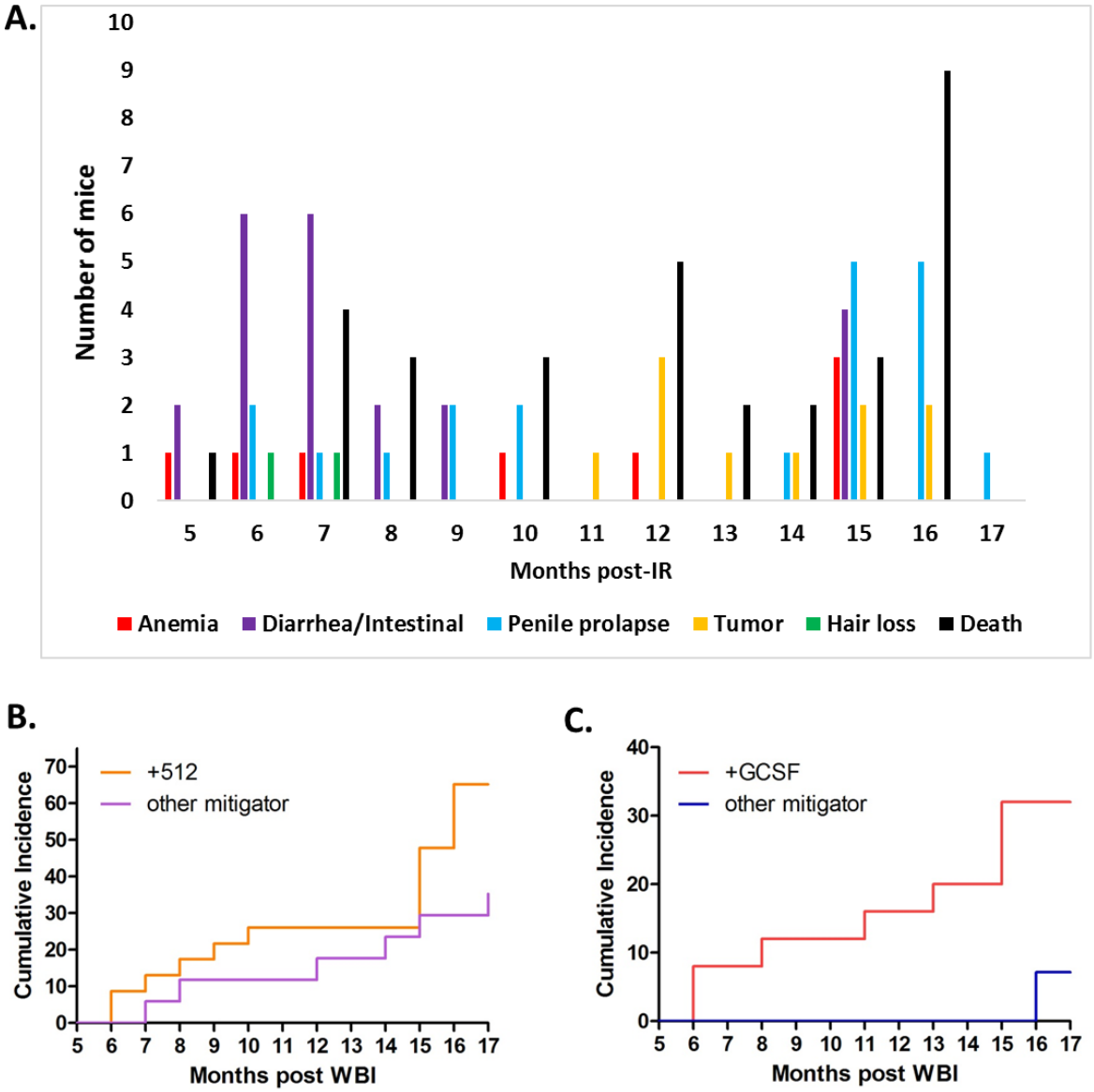

Figure 5.4. Incidence of symptoms and illness in mice following survival from ARS. Total number of mice treated with WBI and mitigators that displayed symptom or illness (A). Cumulative incidence of penile prolapse (B) and anemia (C).

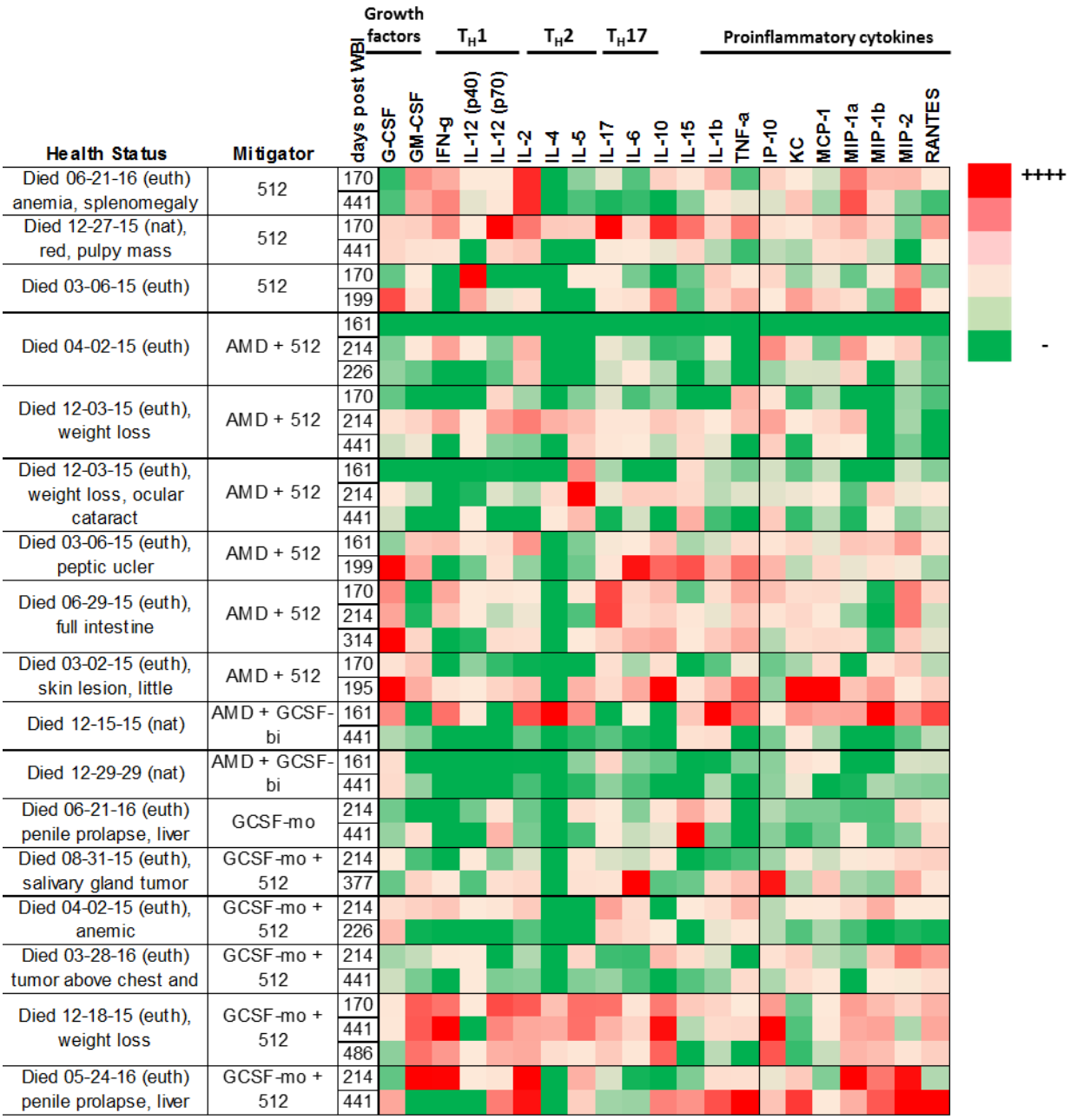

Figure 5.5. Serum cytokine levels measured over time in survivors of WBI.

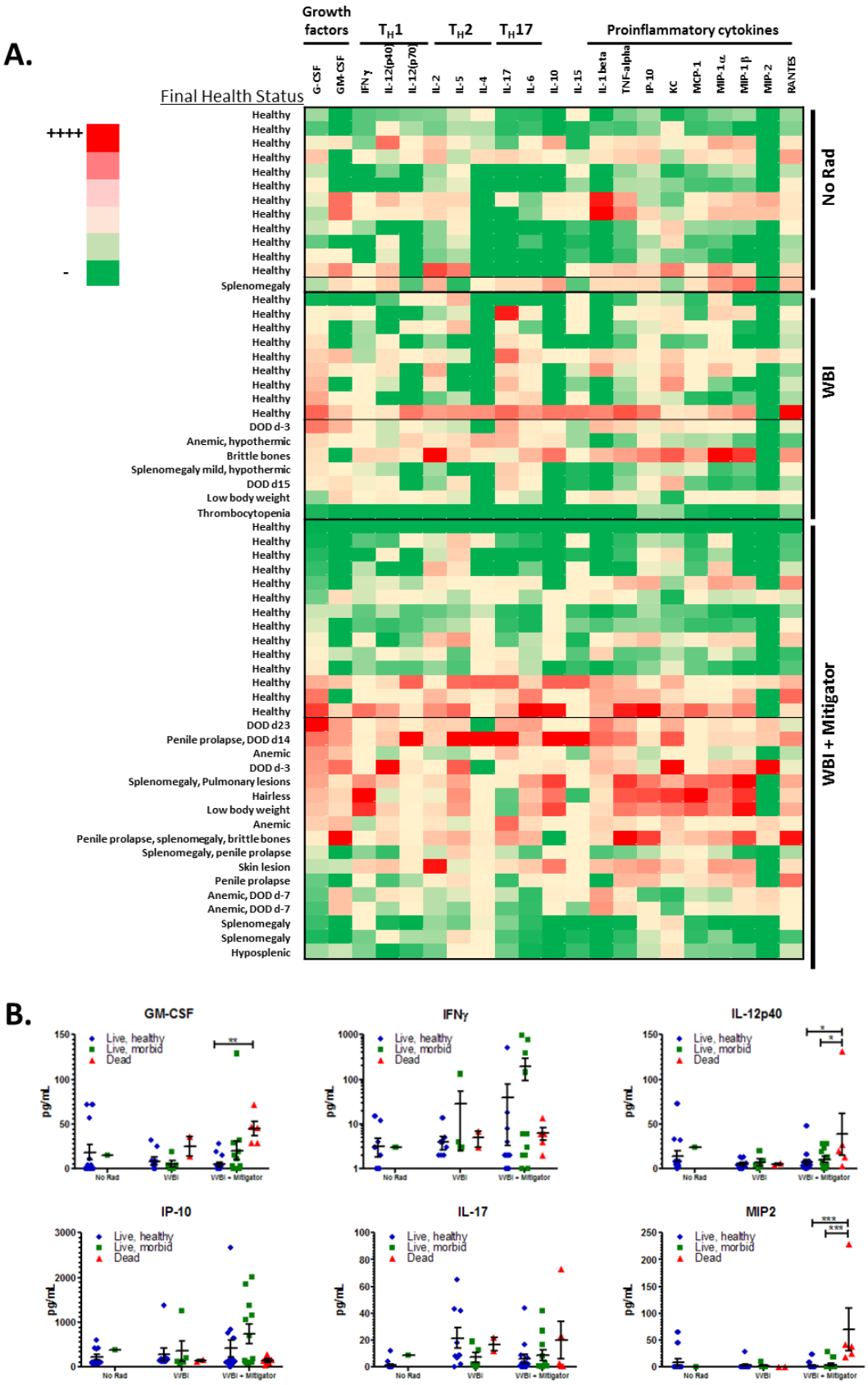
A.
Growth factors
T_H1
T_H2
T_H17
Proinflammatory cytokines
G-CSF
GM-CSF
IFN-γ
IL-12(p40)
IL-12(p70)
IL-2
IL-5
IL-4
IL-17
IL-6
IL-10
IL-15
IL-1 beta
TNF-alpha
IP-10
KC
MCP-1
MIP-1α
MIP-1β
MIP-2
RANTES
Final Health Status
++++
-
Healthy
Splenomegaly
DOD d-3
Anemic, hypothermic
Brittle bones
Splenomegaly mild, hypothermic
DOD d15
Low body weight
Thrombocytopenia
DOD d23
Penile prolapse, DOD d14
Anemic
DOD d-3
Splenomegaly, Pulmonary lesions
Hairless
Low body weight
Anemic
Penile prolapse, splenomegaly, brittle bones
Splenomegaly, penile prolapse
Skin lesion
Penile prolapse
Anemic, DOD d-7
Anemic, DOD d-7
Splenomegaly
Splenomegaly
Hyposplenic
No Rad
WBI
WBI + Mitigator
B.
GM-CSF
IFNγ
IL-12p40
IP-10
IL-17
MIP2
Live, healthy
Live, morbid
Dead
pg/mL
No Rad
WBI
WBI + Mitigator

Figure 5.6. Serum cytokine levels correlate with health state.

Blood was collected from C3H mice, 27 – 68 weeks after exposure to 8.5 Gy, an LD70/30 dose of ionizing radiation, by retro-orbital puncture. Cytokine and chemokine levels were measured using the mouse cytokine/chemokine magnetic bead panel from Millipore. Final healthy status was determined 35 days after blood collection unless the mouse met requirements for euthanasia or died before; illustrated by a heat map (A) and by grouped plots of select individual cytokines (B).

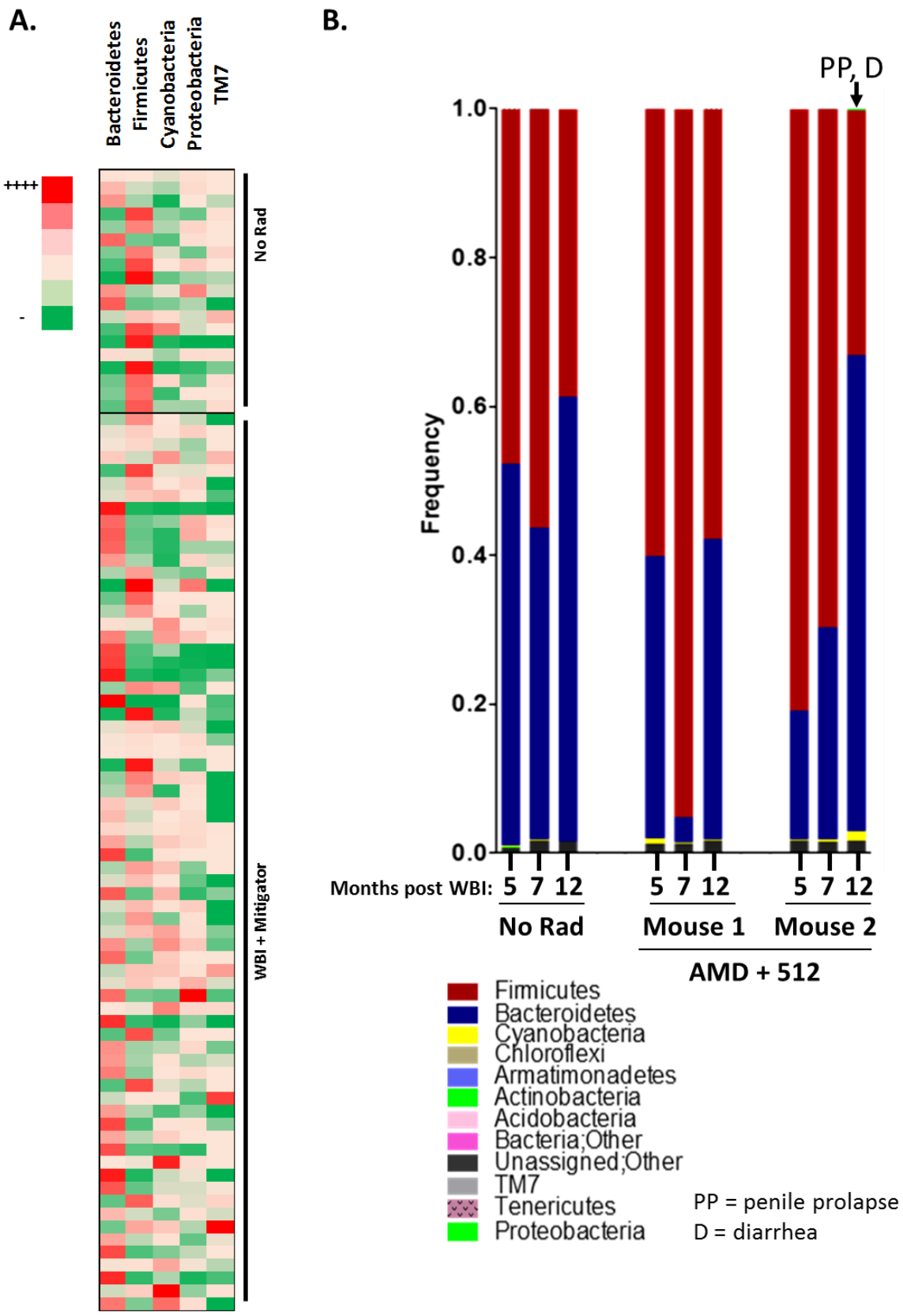
A.
Bacteroidetes
Firmicutes
Cyanobacteria
Proteobacteria
TM7
++++
-
No Rad
WBI + Mitigator
B.
PP, D
1.0
0.8
0.6
0.4
0.2
0.0
Frequency
Months post WBI: 5 7 12 5 7 12 5 7 12
No Rad
Mouse 1
Mouse 2
AMD + 512
Firmicutes
Bacteroidetes
Cyanobacteria
Chloroflexi
Armatimonadetes
Actinobacteria
Acidobacteria
Bacteria;Other
Unassigned;Other
TM7
Tenericutes
Proteobacteria
PP = penile prolapse
D = diarrhea

Figure 5.7. Abundance of fecal bacteria may be a biomarker for DEARE. A heat map of select bacterial phyla grouped by no irradiation and WBI + mitigators (A). Relative abundance of bacterial phyla in fecal samples collected 5, 7 and 12 months after WBI.

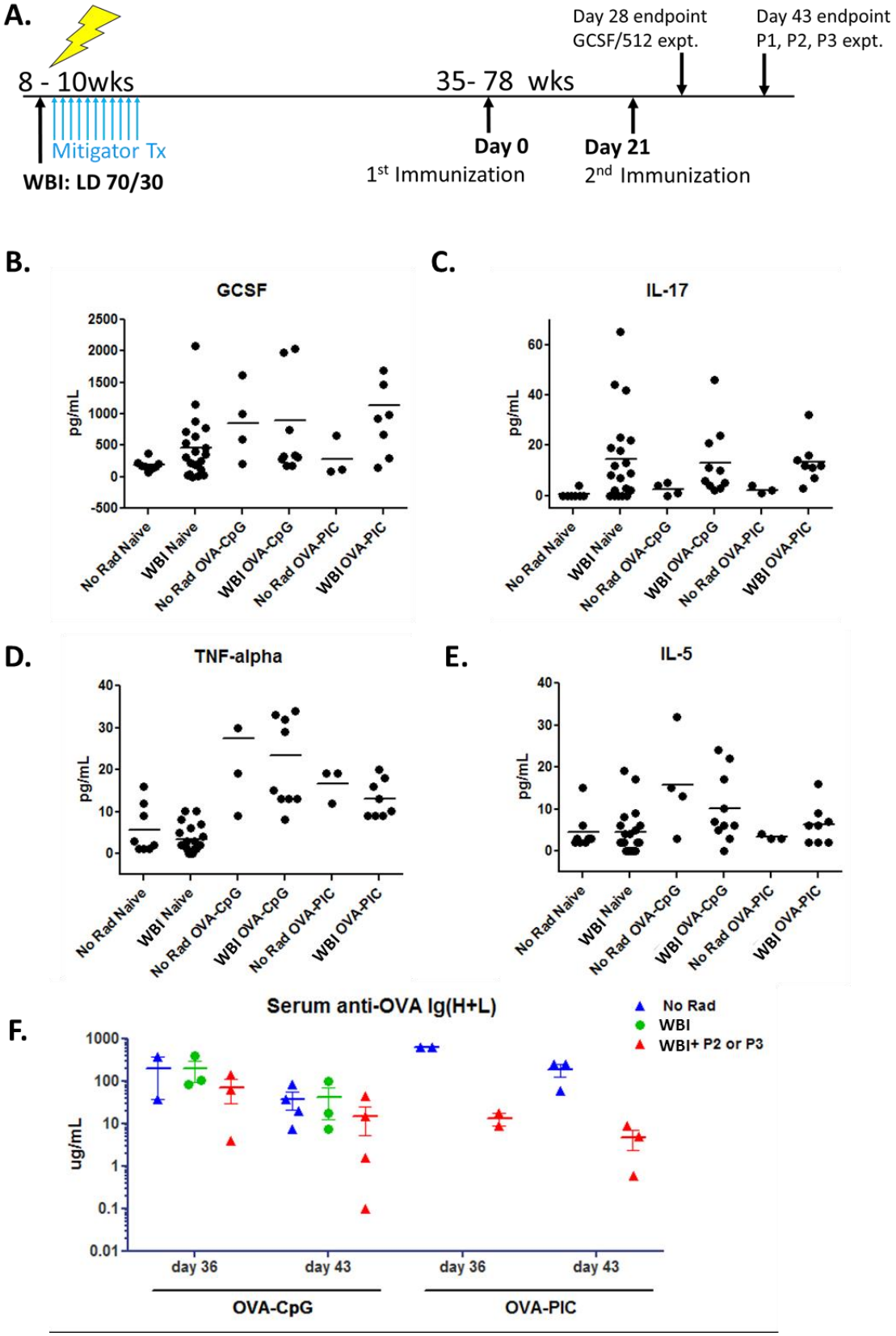
A.
8 - 10wks
Mitigator Tx
WBI: LD 70/30
35- 78 wks
Day 0
1st Immunization
Day 21
2nd Immunization
Day 28 endpoint
GCSF/512 expt.
Day 43 endpoint
P1, P2, P3 expt.
B.
GCSF
pg/mL
C.
IL-17
pg/mL
D.
TNF-alpha
pg/mL
E.
IL-5
pg/mL
No Rad Naive
WBI Naive
No Rad OVA-CpG
WBI OVA-CpG
No Rad OVA-PIC
WBI OVA-PIC
F.
Serum anti-OVA Ig(H+L)
ug/mL
No Rad
WBI
WBI+ P2 or P3
day 36
day 43
OVA-CpG
OVA-PIC

Figure 5.8. Immune response following vaccination with OVA is altered by WBI.

Schematic of OVA immunization schedule and experimental endpoints for two independent experiments (A). Serum cytokines levels prior to and 24 hours after the first OVA immunization in the P1/P2/P3 experiment: GCSF (B), IL-17 (C), TNF-alpha (D), IL-5 (E). Total antibody specific for OVA on day 36 and day 43, after vaccination (F).

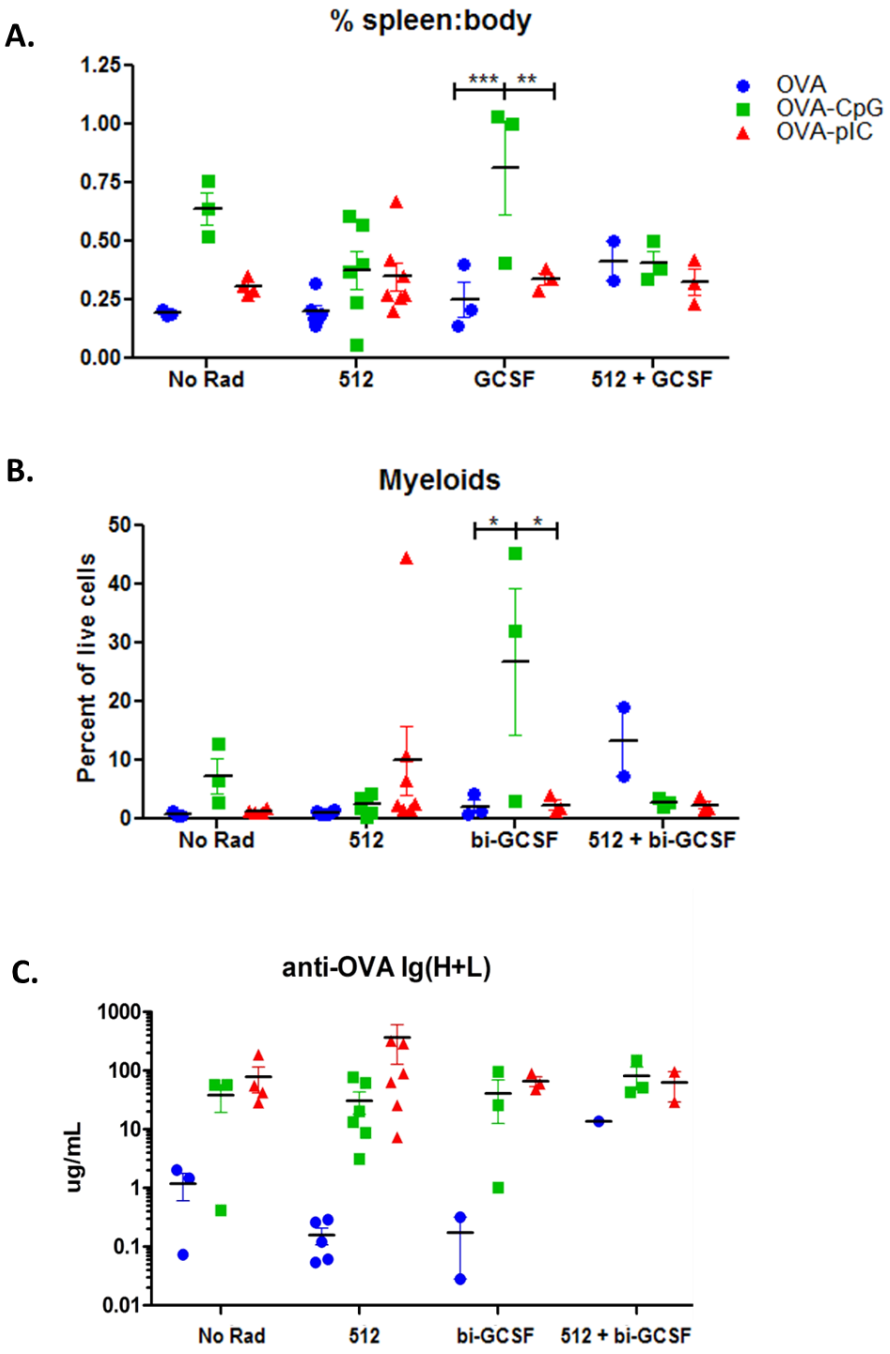

Figure 5.9. Radiomitigator treatment and vaccine adjuvants influence immune cell abundance. Immune response of mice from GCSF/512 experiment. Percent spleen weight of total body weight (A), myeloid cell abundance in the spleen and total OVA specific antibody (C) on day present on day 28.

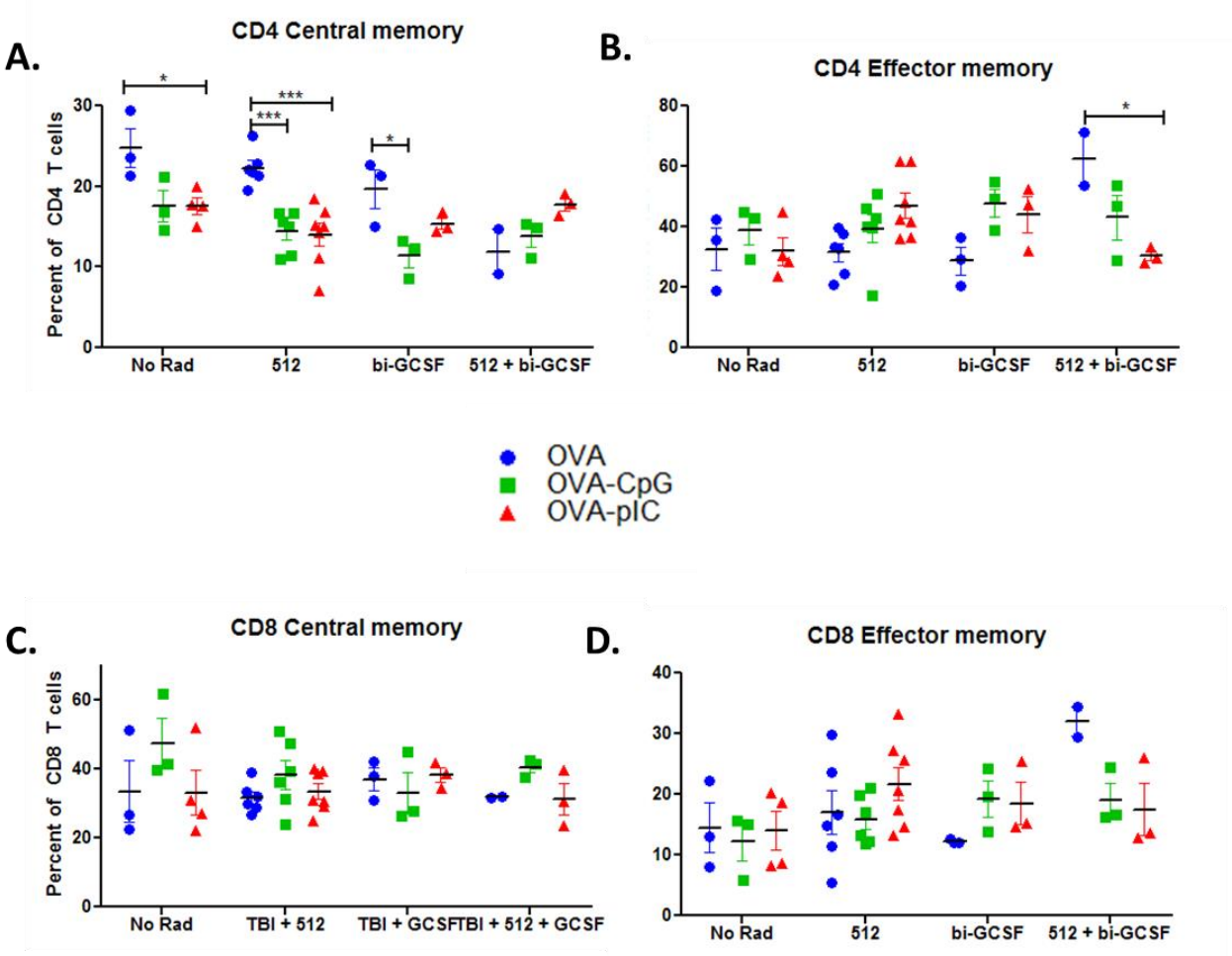

Figure 5.10. Distribution of CD4 and CD8 T cells in the spleen on day 28 of OVA immunization. Percent CD4 central (A) and effector (B) memory cells and CD8 central (C) and effector (D) memory cells.

MATERIALS AND METHODS

Animals and Irradiation

Male C3Hf/Sed//Kam were bred and maintained in the Radiation Oncology AAALAC-accredited facility, strictly adhering to all IACUC-approved protocols and NIH guidelines. WBI was performed on unanesthetized mice using a Gamma cell 40 irradiator (Cs^{137} source; Atomic Energy of Canada, Ltd.) at a dose rate of around 62 cGy/min, for a total dose of 7.725 Gy.

Male or female C57Bl/6, Ticam(Lps2) and MyD88 KO mice were either purchased directly from The Jackson Laboratory (Bar Harbor, Maine) or bred and maintained in specific pathogen free facilities managed by the Department of Laboratory Animal Medicine at UCLA in strict accordance with protocols approved by the UCLA Animal Research Committee. WBI was performed on unanesthetized mice, housed in an irradiation pie, using a Mark I - 68A irradiator (Cs^{137} source; JL Sheppard & Associates) at a dose rate of around 1.09 Gy/min, for a total dose of 9 – 9.14 Gy. In one experiment, WBI was performed on unanesthetized mice, housed in an irradiation pie, using a 300 kVp X-ray machine at dose rate of 1.173 Gy/min, for a total dose of 9.5 Gy.

Treatment with radioprotective and radiomitigative molecules

For radioprotection studies, mice were C57Bl/6, Ticam(Lps2) and MyD88 mice were given 0.5 mg/ml Baytril (Bayer), ad libitum for one week, then treated with 20 µg LPS from *E. coli* 055:B5 (Sigma, L2637-25MG) or 15 µg lipid A from *E. coli* serotype R515 (Enzo, ALX-581-200-L002) either 1 hour or 24 hours prior to WBI.

For radiomitigator studies, the ARS component of the experiments, including radiomitigator treatment, were designed and carried out by Dr. Ewa Micewiz. In one experiment, C3H mice were treated with Rad Only + H2O; Rad Only + PG carrier; P1, 5x 5mg/kg; P1 PG, 5x 5mg/kg; P2, 5x 5mg/kg; P2 PG, 5x 5mg/kg; P3, 5x 5mg/kg; or P3 PG (LD70/30); 5x 5mg/kg. P1 is a metabolite of the 4-nitrophenylpiperazine compound, 512, and P2 and P3 are structural

variants of 512. In another experiment, subcutaneous injections were started 24h after WBI; 150 ug/kg IL-22 or G-CSF was injected 3 times a week, for three weeks; 512 injections 5 times (daily). In the last experiment, the following radiomitigators were injected subcutaneously beginning 24 hours after WBI: 512: 5mg/kg; 5 x daily, GCSF-bi: 50 ug/kg; every other day; 9x, GCSF-mono: 125 ug/kg; every day; 16x, AMD3100: 3.5 mg/kg; every other day; 6x.

Non-lethal blood collection and analysis

Mice were anesthetized using isofluorane, then a microcapillary tube was inserted into the retro-orbital cavity puncturing the blood capillaries. Blood was dispensed into EDTA coated tubes and immediately mixed to prevent clotting. Plasma was isolated by centrifugation, transferred to a new clean tube and stored at -80°C. No more than 100 µl blood was collected per week from a single animal. Blood flow was stopped by applying pressure with sterile gauze, then an ophthalmic antibiotic ointment was applied to the eye. Mice were checked daily for signs of ocular distress or infection.

Complete blood count was measuring using the Hemavet blood analyzer (Drew Scientific) with blood into EDTA coated tubes. Serum cytokines were measured using multiplex Mouse Cytokine/Chemokine Panel kit (Millipore, MPXMCYTO-70K) and a Luminex machine.

Fecal microbiome analysis

Fecal pellets were collected directly from individual mice, into sterile 1.5 ml microcentrifuge tubes. Fecal pellets were snap frozen in liquid nitrogen and stored at -80°C. Dr. Elisa Deiru isolated DNA from fecal microbiota from thawed fecal pellets using QIAamp DNA stool kit (Qiagen), according to the manufacturer's instructions. Bacterial DNA was amplified by a two-step PCR enrichment of the 16S rDNA (V4 region) encoding sequences from each sample with primers modified by addition of barcodes for multiplexing. DNA was subsequently sequenced using the Personal Genome Machine (PGM™) System (Thermo Scientific).

OVA Immunization

C3H male mice, 35 – 78 weeks after WBI (7.725 Gy), were immunized by subcutaneous injection with 50 µg OVA protein (InvivoGen, vac-efova) alone or co-injection with either 100 µg Poly I:C (Invivogen, Tlrl-pic) or 100 µg CpG 1826 (Invivogen, tlrl-1826-5).

OVA specific antibody was measured by ELISA. Plates were coated with ovalbumin (InvivoGen, Vac-ova) diluted in PBS, 50 µg/ml per well and incubated overnight at 4°C. Wells were washed and blocked with 0.5% gelatin-PBS for 2 hours at room temperature. Serum was diluted in 0.5% gelatin-0.05% tween20-PBS and serially diluted two fold over 7 wells. For measurement of total OVA antibody, a mouse IgG2a Ovalbumin antibody, clone TOSGAA1 (Biolegend, 520401) was used as a standard. Bound anti-ovalbumin antibody was detected with goat anti-mouse Ig, human ads-HRP (Southern Biotech, 1010-05), developed with the colorimetric TMB substrate, and stopped with 0.16 M sulfuric acid.

Identity and distribution of splenocytes was determined by fluorescent antibody staining and flow cytometry in collaboration with Mr. Maxime Chapon. The spleen was collected from mice, gently dissociated and single cells were collected by passing the homogenate through a 70 µm nylon mesh strainer. The cells were centrifuged then re-suspended in 1ml ACK lysing buffer and incubated on ice for 5 min. Cell were rescued with DPBS-2% FBS, washed and suspended in DPBS-2% FBS. Cell viability was measured with Zombie Aqua (Biolegend, 423101) and cell identity was determined with the following antibody panel: CD3-FITC (Biolegend, 100204), CD4-PerCP (Biolegend, 100538), CD8-Alexa 700 (Biolegend, 100730), CD19-APC (BD Pharmingen, 561738), CD44-BV421 (Biolegend, 103039), and CD62L-BV605 (Biolegend, 104437). Unbound antibody was removed by washing 3x with DPBS-2% FBS. Cells were fixed with 2% formaldehyde in PBS, analyzed using the BD LSRII flow cytometer (UCLA Flow Cytometry Core) and data was analyzed with FlowJo software (Tree Star, Inc.).

REFERENCES

1. Shakhov, A. N. *et al.* Prevention and mitigation of acute radiation syndrome in mice by synthetic lipopeptide agonists of Toll-like receptor 2 (TLR2). *PLoS One* **7,** e33044 (2012).

2. Liu, C. *et al.* A critical role of toll-like receptor 4 (TLR4) and its' in vivo ligands in basal radio-resistance. *Cell Death Dis.* **4,** e649 (2013).

3. Burdelya, L. G. *et al.* An agonist of toll-like receptor 5 has radioprotective activity in mouse and primate models. *Science* **320,** 226–30 (2008).

4. Saha, S. *et al.* TLR9 agonist protects mice from radiation-induced gastrointestinal syndrome. *PLoS One* **7,** e29357 (2012).

5. Salkowski, C. a *et al.* Effect of liposome-mediated macrophage depletion on LPS-induced cytokine gene expression and radioprotection. *J. Immunol.* **155,** 3168–79 (1995).

6. Yamamoto, M. *et al.* TRAM is specifically involved in the Toll-like receptor 4-mediated MyD88-independent signaling pathway. *Nat. Immunol.* **4,** 1144–1150 (2003).

7. Doyle, S. *et al.* IRF3 mediates a TLR3/TLR4-specific antiviral gene program. *Immunity* **17,** 251–63 (2002).

8. Brickey, W. J. *et al.* MyD88 provides a protective role in long-term radiation-induced lung injury. *Int. J. Radiat. Biol.* **88,** 335–47 (2012).

9. Kim, K. *et al.* High throughput screening of small molecule libraries for modifiers of radiation responses. *Int. J. Radiat. Biol.* **87,** 839–45 (2011).

10. Uckun, F. M., Souza, L., Waddick, K. G., Wick, M. & Song, C. W. In vivo radioprotective effects of recombinant human granulocyte colony-stimulating factor in lethally irradiated mice. *Blood* **75,** 638–45 (1990).

11. Scholz, M., Ackermann, M., Emmrich, F., Loeffler, M. & Kamprad, M. Effectiveness of cytopenia prophylaxis for different filgrastim and pegfilgrastim schedules in a chemotherapy mouse model. *Biologics* **3,** 27–37 (2009).

12. Cardis, E. Epidemiology of accidental radiation exposures. *Environ. Health Perspect.* **104 Suppl ,** 643–9 (1996).

13. Booth, C., Tudor, G. L., Katz, B. P. & MacVittie, T. J. The Delayed Effects of Acute Radiation Syndrome: Evidence of Long-Term Functional Changes in the Clonogenic Cells of the Small Intestine. *Health Phys.* **109,** 399–413 (2015).

14. Manning, C. M. *et al.* Lung irradiation increases mortality after influenza A virus challenge occurring late after exposure. *Int. J. Radiat. Oncol. Biol. Phys.* **86,** 128–35 (2013).

15. Pecaut, M. J., Baqai, F. P. & Gridley, D. S. Impact of total-body irradiation on the response to a live bacterial challenge. *Int. J. Radiat. Biol.* **90,** 515–26 (2014).

16. Gridley, D. S., Miller, G. M. & Pecaut, M. J. Radiation and primary response to lipopolysaccharide: bone marrow-derived cells and susceptible organs. *In Vivo* **21,** 453–61 (2007).

17. Alignani, D. *et al.* Orally administered OVA/CpG-ODN induces specific mucosal and systemic immune response in young and aged mice. *J. Leukoc. Biol.* **77,** 898–905 (2005).

18. Hafner, A. M., Corthésy, B. & Merkle, H. P. Particulate formulations for the delivery of poly(I:C) as vaccine adjuvant. *Adv. Drug Deliv. Rev.* **65,** 1386–99 (2013).

19. Fedorocko, P., Egyed, A. & Vacek, A. Irradiation induces increased production of haemopoietic and proinflammatory cytokines in the mouse lung. *Int. J. Radiat. Biol.* **78,** 305–13 (2002).

20. Neta, R., Perlstein, R., Vogel, S. N., Ledney, G. D. & Abrams, J. Role of interleukin 6 (IL-6) in protection from lethal irradiation and in endocrine responses to IL-1 and tumor necrosis factor. *J. Exp. Med.* **175,** 689–94 (1992).

21. SMITH, W. W., ALDERMAN, I. M. & GILLESPIE, R. E. Increased survival in irradiated animals treated with bacterial endotoxins. *Am. J. Physiol.* **191,** 124–30 (1957).

22. Dagvadorj, J. *et al.* Lipopolysaccharide Induces Alveolar Macrophage Necrosis via CD14 and the P2X7 Receptor Leading to Interleukin-1α Release. *Immunity* **42,** 640–653 (2015).

23. Yamamoto, M. *et al.* Essential role for TIRAP in activation of the signalling cascade shared by TLR2 and TLR4. *Nature* **420,** 324–329 (2002).

24. Burkholder, T., Foltz, C., Karlsson, E., Linton, C. G. & Smith, J. M. Health Evaluation of Experimental Laboratory Mice. *Curr. Protoc. Mouse Biol.* **2,** 145–165 (2012).

25. Lai, X. Y. & Egan, L. J. Suppression of radiation-induced DNA double-strand break repair by MyD88 is accompanied by apoptosis and crypt loss in mouse colon. *Oncogenesis* **2,** e62 (2013).

26. Martínez-Jaramillo, G., Gómez-Morales, E. & Mayani, H. Effect of recombinant human granulocyte macrophage-colony stimulating factor in long-term marrow cultures from patients with aplastic anemia. *Am. J. Hematol.* **61,** 107–14 (1999).

27. Nam, Y.-D., Kim, H. J., Seo, J.-G., Kang, S. W. & Bae, J.-W. Impact of pelvic radiotherapy on gut microbiota of gynecological cancer patients revealed by massive pyrosequencing. *PLoS One* **8,** e82659 (2013).

28. Kuehbacher, T. *et al.* Intestinal TM7 bacterial phylogenies in active inflammatory bowel disease. *J. Med. Microbiol.* **57,** 1569–1576 (2008).

CHAPTER 6

Conclusion and Future Perspectives

Regulation and function of type I IFNs is still not clearly understood. Here we set out to understand how type I IFNs are induced in macrophages and what the requirements are for amplification of downstream ISGs. We found type I IFN expression by macrophages on the nature of the stimulating PAMP and that bacterial LPS preferentially led macrophages to induce IFNβ (Figures 3.1 and 3.2). Furthermore, IFNβ, irrespective of the PAMP, IFNβ was necessary to positively regulate IFNAR signaling and ISG induction (Figures 3.3 and 3.4). The functional implications are immense as IFNAR signaling is decisive in the outcome of many bacterial infections. In two different models of bacterial infection, we found IFNβ contributed, but was not sufficient to either completely protect against *E. coli* peritonitis (Figure 3.5) or enhance host susceptibility to post-influenza pneumonia (Figure 3.7). Further studies are needed to determine whether other subtypes of type I IFNs are involved. In addition, the role of IFNβ in post-influenza gut *Salmonella* infections will be examined. We recently found IFNAR signaling during influenza infection led to gut microbial dysbiosis and enhanced host susceptibility to *Salmonella* infection (Appendix B). We will conduct studies using *Ifnb*-/- mice to determine whether IFNβ signaling is required to promote host susceptibility.

ISGs and IFNAR signaling dictate the course of non-infectious diseases. IFNβ signaling during LPS induced endotoxic shock is lethal. We suspected CXCL10, an interferon induced chemokine, may be a pathogenic effector because it has been implicated in other diseases. We found deficiency in CXCL10 partially rescued survival, but only in female mice (Figure 4.1). Detrimental effects seemed to require CXCR3, the receptor for CXCL10, but not estradiol signaling (Figure 4.2). Gender effects are difficult to dissect and often observations in rodents do not translate to humans, thus these studies were discontinued.

We also sought to investigate the role of poly I:C treatment on the progression of EAE, the mouse model of human MS. Previous work in our laboratory showed TRIF, an adapter molecule in the poly I:C activated pathway, attenuated disease symptoms. Therefore, we

hypothesized that poly I:C treatment would alleviate disease. We observed a transient reduction in overall clinical score (Figure 4.3) that seemed to required poly I:C sensing by TLR3, not the cytosolic pathway (Figure 4.4). Though symptoms were mildly attenuating, the significance was border line and subsequent investigations were terminated.

In another study, we investigated IFNAR signaling during tuberous sclerosis complex disorder, that results from TSC1 or TSC2 halploinsufficiency and is highly associated with the development of autism spectrum disorder in humans. Measurement of gene and protein expression following poly I:C treatment of WT and *Tsc2*+/- mice revealed enhanced expression of type I IFNs and ISGs by *Tsc2*+/- mice (Figures 4.5 and 4.6). This results in combination with functional studies of social behavior strongly suggest IFNAR signaling is responsible for the increased incidence of autism spectrum disorder in tuberous sclerosis complex disorder. In the future, the contribution of IFNβ will be determined by crossing *Tsc2*+/- mice with *Ifnb*-/- mice.

ARS following exposure to a lethal dose of radiation can be mitigated by treatment with a number of radioprotective or radiomitigative molecules. These compounds promote survival (Figures 5.2 and 5.3), but their effects nor the effects of irradiation in the long term are not well understood. We undertook to monitor mice that survived ARS. Health status, periodic measurement of serum cytokines and of intestinal microbiota were collected and analyzed. We found trends among cohorts treated with the same radiomitigator as well as overarching trends among mice treated with WBI (Figures 5.4 – 5.7). Moreover, we found that in response to immune challenge, distinct differences were observed that appeared to be influenced by the radiomitigator administered during ARS and the nature of the immune challenge (Figures 5.8 – 5.10). Much work remains to be done. Future studies will continue to integrate multiple parameters to better understand DEARE.

APPENDIX A

Activation of the NLRP3 inflammasome by vault nanoparticles expressing a chlamydial epitope

Contents lists available at ScienceDirect

Vaccine

journal homepage: www.elsevier.com/locate/vaccine

Activation of the NLRP3 inflammasome by vault nanoparticles expressing a chlamydial epitope☆

Ye Zhu[a], Janina Jiang[b], Najwane Said-Sadier[a,1], Gale Boxx[b], Cheryl Champion[b], Ashley Tetlow[b], Valerie A. Kickhoefer[c], Leonard H. Rome[c], David M. Ojcius[a,*], Kathleen A. Kelly[b,**]

[a] Department of Molecular Cell Biology, and Health Sciences Research Institute, University of California, Merced, CA 95343, USA
[b] Department of Pathology and Laboratory Medicine, University of California, Los Angeles, CA 90095, USA
[c] Department of Biological Chemistry, University of California, Los Angeles, CA 90095, USA

ARTICLE INFO

Article history:
Received 11 June 2014
Received in revised form 4 November 2014
Accepted 15 November 2014
Available online 24 November 2014

Keywords:
Vaults
Inflammasomes
Chlamydia
Lysosomes

ABSTRACT

The full potential of vaccines relies on development of effective delivery systems and adjuvants and is critical for development of successful vaccine candidates. We have shown that recombinant vaults engineered to encapsulate microbial epitopes are highly stable structures and are an ideal vaccine vehicle for epitope delivery which does not require the inclusion of an adjuvant. We studied the ability of vaults which were engineered for use as a vaccine containing an immunogenic epitope of *Chlamydia trachomatis*, polymorphic membrane protein G (PmpG), to be internalized into human monocytes and behave as a "natural adjuvant". We here show that incubation of monocytes with the PmpG-1-vaults activates caspase-1 and stimulates IL-1β secretion through a process requiring the NLRP3 inflammasome and that cathepsin B and Syk are involved in the inflammasome activation. We also observed that the PmpG-1-vaults are internalized through a pathway that is transiently acidic and leads to destabilization of lysosomes. In addition, immunization of mice with PmpG-1-vaults induced PmpG-1 responsive CD4+ cells upon re-stimulation with PmpG peptide *in vitro*, suggesting that vault vaccines can be engineered for specific adaptive immune responses. We conclude that PmpG-1-vault vaccines can stimulate NLRP3 inflammasomes and induce PmpG-specific T cell responses.

1. Introduction

Chlamydia trachomatis is the most prevalent bacterial sexually transmitted disease (STD) in the United States. Chlamydial infections in women can cause pelvic inflammatory disease (PID) and result in infertility, ectopic pregnancy, and chronic pelvic pain [1–3]. Most *Chlamydia* infections are asymptomatic, increasing the risk of transmission of *Chlamydia* to unsuspecting females and result in PID [4–6]. Identification of protective responses is a key component of vaccine development. Intensive studies have been done in order to dissect immunity towards to resolution of primary chlamydial infection, and immunity to reinfection in mouse genital infection model. CD4+ T cells play major role in resolving primary genital infection [7], particularly IFN-γ secreting CD4+ T cells (Th1 cells) [8], with or without CD8+ T cells or antibody [9,10]. CD4+ T cells and/or antibody are also essential for resistance to reinfection. However, CD8+ T cells appear to be unnecessary against reinfection [10]. Development of a protective vaccine for prevention of *Chlamydia* PID is challenging due to difficulties in identifying and delivering relevant T cell antigens and developing a safe adjuvant that does not produce excessive inflammatory responses which can diminish the likelihood of public acceptance [11–13].

Abbreviations: *C. trachomatis*, *Chlamydia trachomatis*; PmpG, polymorphic membrane protein G; CARD, caspase recruitment domain; MOMP, major outer membrane protein; PAMPs, pathogen associated molecular patterns; DAMPs, danger associated molecular patterns; NLR, Nod-like receptor; MSU, monosodium urate; ASC, apoptosis-associated speck-like protein containing a CARD; Syk, spleen tyrosine kinase; PMA, phorbol 12-myristate 13-acetate.

☆ These studies were funded by NIH grant AI079004, Balance From Products, and a University of California Presidential Chair.

* Corresponding author at: Molecular Cell Biology, University of California, 5200 North Lake Road, Merced, CA 95343, USA. Tel.: +1 209 228 2948.
** Corresponding author.
E-mail addresses: david.ojcius@gmail.com (D.M. Ojcius), KKelly@mednet.ucla.edu (K.A. Kelly).
[1] Current address: Department of Immunology and Microbiology, Faculty of Medicine, Beirut Arab University, Beirut, Lebanon.

http://dx.doi.org/10.1016/j.vaccine.2014.11.028
0264-410X/

The full potential of vaccines relies on development of effective delivery systems and adjuvants and is critical for development of successful vaccine candidates. Vaults are large cytoplasmic ribonucleoprotein (RNP) particles consisting of three proteins and a small untranslated RNA [14,15]. Their function within cells has not been identified but reports have suggested their involvement with multidrug resistance, cell signaling and innate immunity [16–24]. *In vitro* expression of MVP in insect cell can form hollow vault-like particles identical to native vaults [25]. An MVP interaction domain (INT) associates non-covalently with MVP binding site and can be used to internally package other proteins of interests. We have shown that vaults can be engineered *in vitro* as a vaccine which effectively delivers antigen for generation of a protective immune response. However, we and others [26–28] also discovered that recombinant vaults can interact with host immune cells and display self-adjuvanting properties, distinguishing them from other vaccine preparations. Moreover, we reported that vaults engineered to contain a recombinant *Chlamydia* protein (MOMP-vault vaccine) induced strong protective anti-chlamydial immune responses without eliciting excessive inflammation as measured by TNF-α production [29]. We hypothesized that vaults vaccines act as "smart adjuvants" and can be engineered to produce a tailored immune response against specific antigens by housing proteins in the central cavity of the recombinant vault that is hollow and large enough to accommodate multiple copies of foreign epitopes [26,29]. Our data further suggested that the vault vaccine induced inflammasomes, an innate immune response that could possibly account for the self-adjuvanting property of vault-vaccines upon phagocytosis.

Inflammasomes serve as the first line of immune defense against inducers of cellular stress [30]. Following detection of stress inducers such as infection, inflammasomes promote maturation and secretion of IL-1β [31]. The inflammasome containing the Nod-like receptor (NLR) family member, NLRP3, is one of the best studied inflammasomes and can be activated by a wide range of stimuli, including membrane-damaging toxins, pathogen associated molecular patterns (PAMPs), and danger associated molecular patterns (DAMPs) [32–35]. The NLRP3 inflammasome can also be stimulated by large particles such as monosodium urate (MSU) crystals, silica, nanoparticles, and the adjuvant, alum, which can lead to lysosomal damage after engulfment by phagocytes and the release of lysosomal proteases such as cathepsin B [36–38]. When these stimuli are detected, NLRP3 interacts with the adaptor, ASC (apoptosis-associated speck-like protein containing a CARD), which in turn recruits the protease, pro-caspase-1. When pro-caspase-1 is assembled into the inflammasome, it becomes auto-activated and cleaved into a 20 kD fragment and induces caspase-1-dependent maturation and secretion of proinflammatory cytokines such as IL-1β [35,39–44]. Upon activation of the NLRP3 inflammasome, the mature IL-1β is secreted out of the cell. In many cells such as monocytes and macrophages, the activated 20 kD form of caspase-1 is also secreted.

In this report, we have used a different chlamydial protein, PmpG-1, and convincingly show that PmpG-1-vault vaccines induce NLRP3 inflammasome activation that differs from other particulate induces following phagocytosis *in vitro*. PmpG-1-vault vaccines also induce a T cell response against a PmpG-1 peptide demonstrating that vault-vaccines can be engineered for a tailored immune response.

2. Materials and methods

2.1. Assembly of PmpG-1-vaults vaults

Recombinant baculoviruses were generated using the Bac-to-Bac protocol (Invitrogen, Carlsbad, CA). The 17 amino acid coding region of PmpG-1 (ASPIYVDPAAAGGQPPA) was fused to the N-terminus of the INT domain derived from VPARP (amino acids 1563–1724) by PCR using the following primers: PmpG-1-INT Forward BamHI-5′GGGATCCATGGCAAGCCCAATTT-ATGTCGACCCAGCAGCAGCAGGTGGTCAACCACCAGCATGCACACA-ACACTGGCAGGA-3′ and INT Reverse XhoI-5′-GCTCGAGTTAGCC-TTGACTGTAATGGAGGA-3′ using INT in pET28 as the template. The resultant PCR product containing the fused PmpG-1-mINT was purified on a Qiagen column (Qiagen, Germantown, MD), digested with BamHI and XhoI, gel purified, and ligated to pFASTBAC to form PmpG-1-mINT pFASTBAC. Construction of cp-MVP-z in pFASTBAC has been described previously [25]. All primers used in this study were purchased from Invitrogen (Carlsbad, CA). Sf9 cells were infected with cp-MVP-z, and PmpG-1-INT recombinant baculoviruses at a multiplicity of incubation (MOI) of 0.01 for approximately 72 h and then pelleted and stored at −80 °C until needed. PmpG-1-INT and cp-MVP-z pellets were lysed on ice in buffer A [50 mM Tris–HCl (pH 7.4), 75 mM NaCl, and 0.5 mM $MgCl_2$] with 1% Triton X-100, 1 mM dithiothreitol, 0.5 mM chymostatin, 5 μM leupeptin, 5 μM pepstatin) (Sigma, St. Louis, MO). Lysates containing PmpG-1-vaults were mixed with lysates containing PmpG-1-INT and incubated on ice for 30 min to allow the INT fusion proteins to package inside of vaults. As a control, another lysate of cp-MVP-z pellets was prepared without PmpG-1-INT. Recombinant vaults were purified as previously described and resuspended in sterile RPMI media [25,45,46]. The protein concentration was determined using the BCA assay (Pierce) and sample integrity was analyzed by negative stain electron microscopy and SDS-PAGE with Coomassie staining.

The PmpG-1 was cloned in frame with the INT (interaction domain amino acids 1563–1724 of VPARP ref) protein by PCR ligation, resulting in a ~20 kD fusion protein. Addition of this fusion protein to vaults results in packaging inside the particle [47]. An IgG binding domain (the Z domain) was engineered to the C-terminus of MVP to enhance immunity [29] and a cysteine-rich peptide was added to the N-terminus of MVP to enhance particle stability [47]. These vaults are referred to as cp-MVP-z and following packaging of the PmpG-1-INT fusion protein they are designated cp-MVP-z/PmpG-1-INT (and abbreviated PmpG-1-vaults).

2.2. Cell culture and inhibitor treatment

THP-1 cells were grown in RPMI 1640 (Sigma–Aldrich) with 10% FBS (Invitrogen) and 10 μg/ml gentamicin. A total of 1×10^6 cells per well in a 6-well plate were differentiated with 500 nM PMA for 3 h. Differentiated THP-1 cells were washed with 1×PBS 3 times and incubated for 24 h at 37 °C with 5% CO_2. Z-WEHD (100 nM) and CA-074 Me (10 μM) were used 1.5 h before treatment with vaults. Syk-inhibitor (10 μM) was used 30 min prior to addition of vaults. PmpG-1-vaults (250 nM) were incubated with cells, and after 6 h post-incubation, we collected the supernatant from the treated cells.

2.3. Gene product depletion by RNA interference

THP-1 stably expressing shRNA against NRLP3, ASC, Syk and caspase-1 were obtained by transducing THP-1 cells with lentiviral particles containing shRNAs. The sequences 5′-CCGGGCGTTAGAAACACTTCAGAACTCGAGTTCTTGAAGTGTTTCTA-ACGCTTTTTG-3′ for human NLRP3 (Sigma; catalog number NM_004895), 5′-CCGGCGGAAGCTCTTCAGTTTCACACTCGAGTGTG-AAACTGAAGATTCCGTTTTTG-3′ for human ASC (Sigma; catalog number NM_013248), 5′-CCGGGCAGGCCATCATCAGTCAGAACTC-GAGTTCTGACTGATGATGGCCTGCTTTTT-3′ for human spleen tyrosine kinase (Syk) (Sigma; catalog number NM-003177), and five sequences for caspase-1 (Sigma; catalog number NM-001223):

5′-CCGGGAAGAGTTTGAGGATGATGCTCTCGAGAGCATCATCCTCAA-ACTCTTCTTTTT-3′,5′CCGGTGTATGAATGTCTGCTGGGCACTCGAGT-GCCCAGCAGACATTCATACATTTTT3′,5′CCGGCACACGTCTTGCTCTC-ATTATCTCGAGATAATGAGAGCAAGACGTGTGTTTTT3′,5′CCGGCTA-CAACTCAATGCAATCTTTCTCGAGAAAGATTGCATTGAGTTGTAGTTT-TT3′,5′CCGGCCAGATATACTACAACTCAATCTCGAGATTGAGTTGTA-GTATATCTGGTTTTT-3′ were used separately to silence gene expression following the manufacturer's instructions. Nontarget shRNA control cells were also generated using an irrelevant sequence (Sigma; catalog number SHC002 V). Cells (3×10^5) were plated at 35% confluency 24 h prior to transduction and then the corresponding lentiviral transduction particles were added at an moi of 3 overnight. Fresh media were added the next day, and transduced cells were selected by addition of media containing 2 μg/ml puromycin (Sigma). The knockdown (KD) efficiency was tested by qPCR. mRNA was isolated from cells after indicated treatments or incubations using the Qiagen RNeasy Kit (Qiagen, Valencia, VA) following the manufacturer's instruction.

2.4. IL-1β and TNF-α ELISA assay

Supernatant from vaults-treated cells was collected after 6 h post-incubation and stored at −80° C until ready for use in the assay. Measurement of IL-1β was carried out using human IL-1β ELISA kit (eBioscience, San Diego, CA), following manufacturer's instructions.

2.5. Western blotting

Supernatants from vaults-treated cells were collected and precipitated with TCA. Samples were lysed using 1× RIPA Lysis Buffer (Millipore) with 1× protease inhibitor cocktail (Biovision) and loaded onto a 12% SDS-polyacrylamide gel and then transferred to a polyvinylidene difluoride membrane (Millipore). For detection of the active caspase-1 subunit (p20), the blot was probed with 1 mg/ml rabbit anti-human caspase-1 antibody (Millipore), and then incubated again with conjugated 1:10,000 dilution of anti-rabbit IgG horseradish peroxidase (Millipore). To detect mature IL-1β, the blot was probed with IL-1β antibody (Cell Signaling) at a 1:1000 dilution, and then incubated again with 1:10,000 dilution of anti-mouse secondary antibody (Santa Cruz Biotechnology). Western blotting detection reagents (Amersham Biosciences) were used following manufacturer's instructions and chemiluminescence was detected using a gel doc system (Bio-Rad).

2.6. Fluorescence-activated cell sorting (FACS)

THP-1 cells (2×10^6/well) were plated in 6-well plates and primed for 3 h with 0.5 μM Phorbol 12-myristate 13-acetate (PMA) (Sigma–Aldrich, St. Louis, MO). Recombinant PmpG-1-vaults were dual-labeled with the fluorescent dyes FITC and TRITC by primary amine reaction following manufacturer's instructions (Pierce, Thermo Scientific, Rockford, IL). Unconjugated dye was removed by filtration on a PD-10 column (GE Healthcare, Piscataway, NJ). Primed THP-1 cells were incubated in duplicate with FITC-TRITC dual-labeled vaults for 6, 18, 24 or 48 h. Half of the treatments were incubated with bafilomycin (Sigma-Aldrich, St. Louis, MO), an ATPase inhibitor, for 30 min to neutralize all subcellular compartments. Cells were collected by trypsinization, washed and immediately analyzed by flow cytometry using a BD FACSCalibur (BD Biosciences, Franklin Lakes, New Jersey) and data was analyzed using Flowjo software (Tree Star, Inc., Ashland, OR). A total of 10^5 cells were analyzed.

For FACS analysis of lymphocytes, the spleen was harvested from individual mice, and single cell suspensions were prepared by dissociating the lymphocytes through a 40 μm cell strainer (BD Falcon). Individual cells were washed with 1% PBS followed by red blood cell lysis treatment. Lymphocytes were re-suspended in RPMI 1640 at 4°C until used. For intracellular cytokine staining, lymphocytes isolated from spleen were incubated in RPMI 1640 in the presence of PmpG-$1_{303–311}$ peptide for 6–8 h. Brefeldin A (Sigma) was added 4 h before the end of culture. Cells were directly stained with fluorochrome-labeled antibodies against CD3 (clone 145-2C11) or CD4 (clone GK1.5). After washing, the cells were incubated with Cytofix/Cytoperm (BD Biosciences) for 1 h and stained with fluorochrome-conjugated anti-IFN-γ (clone XMG1.2), washed again, re-suspended in Cell Fix solution, and analyzed on a SORP BD LSR II (Beckman Dickinson, Franklin Lakes, NJ). FACS data were analyzed by Flowjo (Tree Star, Oregon).

2.7. Chlamydiae, immunization and challenge of mice

Chlamydia muridarum (MoPn) was grown on confluent McCoy cell monolayers, purified on Renograffin gradients and stored at −80°C in SPG buffer (sucrose-phosphate-glutamine) as previously described [48]. Female C57BL/6 mice, 5–6 weeks old were housed according to American Association of Accreditation of Laboratory Animal Care guidelines [48]. Mice receiving vaults were anesthetized with a mixture of 10% ketamine plus 10% xylazine and immunized i.n. with 100 μg PmpG-1-vaults in 20 μl saline for a total of 3 times every two weeks. Mice were hormonally synchronized by subcutaneous injection with 2.5 mg of medroxyprogesterone acetate (Depo Provera, Upjohn, Kalamazoo, MI) in 100 μl saline 7 days prior to a vaginal challenge with 1.5×10^5 IFU of *C. muridarum* and infection was monitored by measuring infection forming units (IFU) from cervical–vaginal swabs (Dacroswab Type 1, Spectrum Labs, Rancho Dominguez, CA) as previously described [48].

2.8. Colocalization studies

The following antibodies were used for immunofluorescence at the indicated dilutions: anti-early endosome antigen 1 (EEA1, G-4; 1:100; Santa Cruz Biotechnology, Dallas, TX), anti-lysosomal-associated membrane protein1 (LAMP1, clone H4A3; 1:100; Biolegend, San Diego, CA), anti-microtubule-associated protein 1 light chain 3 (LC3, clone 166AT1234; 1:100; Abgent, San Diego, CA), and AF488-goat anti-mouse immunoglobulin G (IgG; 1:400; Invitrogen, Carlsbad, CA). For colocalization studies, THP-1 cells (1.5×10^5) were seeded onto 18 mm glass coverslips and incubated at 37°C (with 5% CO_2) for 72 h in the presence of 10 ng/ml PMA. Purified PmpG-1-vaults vaults were labeled with DyLight 650 according to the manufacturer's instructions (Pierce, Thermo Scientific, Rockford, IL). Coverslips containing primed THP-1 cells were incubated with 30 μg of DyLight 650-labeled PmpG-1-vaults vaults for 15 min, 30 min, and 1 h. Cells were fixed in 3.7% paraformaldehyde in 1X PHEM buffer (60 mM Pipes, 25 mM Hepes, 10 mM EGTA, 2 mM $MgCl_2$) for 15 min at room temperature. Cells were washed 3 times in 1× PHEM buffer before permeabilization for 10 min in 0.25% Triton X-100 in 1× PHEM buffer. Following permeabilization, the cells were washed 3 times in 1× PHEM buffer prior to incubation in blocking solution (10% normal goat serum in 1× PHEM buffer) for 1 h at room temperature. Cells were further incubated with the appropriate primary antibody diluted in blocking solution for 1 h at room temperature, rinsed 3 times in 1× PHEM buffer and further incubated for 1 h in secondary antibody prepared in blocking solution. Following staining with the secondary antibody, the cells were washed 3 times with 1× PHEM buffer and mounted in VectaShield Hard Mount with DAPI (Vector Labs, Inc., Burlingame, CA) and visualized using a Yokagawa CSU-22 spinning disc confocal scanner and a Hamamatsu C9100-13 EMCCD camera mounted on a Zeiss Axiovert 200m stand. The images were captured using Slidebook 5 software (Intelligent Imaging Innovations, Inc.,

Denver, CO). The optimal conditions including the number of vault particles used for each experiment were determined empirically. Images were acquired with a 100× oil immersion objective and were processed using ImageJ (http://rsb.info.nih.gov/ij/). In addition, 10 images were used to determine colocalization by applying the Pearson's correlation coefficient located in the JACoP Plugin module.

3. Results

3.1. PmpG-1-vault-vaccines stimulate secretion of IL-1β and activated caspase-1 from monocytes

Treatment of THP-1 monocytes with PMA (phorbol-12-myristate-13-acetate) stimulates their differentiation into macrophages. PMA-primed THP-1 cells also synthesize pro-IL-1β, making them good models for studying inflammasome activation. To evaluate whether PmpG-1-vault-vaccines could affect inflammasome activation, we measured IL-1β secretion from PMA-primed THP-1 cells incubated with recombinant vaults containing the chlamydial epitope, PmpG. A significantly higher level of IL-1β was detected in the supernatants after 6 h of incubation with the PmpG-1-vaults "vaults" than from cells without vaults (Fig. 1A). The empty vaults (without any epitope) were also tested but do not induce an immune response (data not shown) [29], and therefore were not tested further here. To determine whether the IL-1β secretion is dependent on caspase-1 activation, we incubated the cells with a caspase-1 inhibitor, zWEHDfmk [49]. This inhibitor also blocks caspase-4 and caspase-5, which could potentially modulate inflammasome activity [50]. When cells are pre-treated with the caspase inhibitor before adding the vaults, a dramatic decrease in IL-1β secretion and processing was observed (Fig. 1A). ELISA of secreted (activated) caspase-1 and Western blot analysis confirmed that the inhibitor also blocked caspase-1 activation (Fig. 1C), as expected.

3.2. Incubation of cells with PmpG-1-vaults activates the NLRP3 inflammasome

The NLRP3 inflammasome can be activated by a broad range of stimuli, including nanoparticles and crystals [51]. We therefore examined whether PmpG-1-vaults may induce IL-1β secretion and caspase-1 activation through the NLRP3 inflammasome. We focused on several representative NLRP3 components such as the adaptor ASC, the NLR family member NLRP3, the protease caspase-1, and the mediators Syk and cathepsin B. To test whether these components may play a role in vault-induced IL-1β secretion, we applied inhibitors of each component and also depleted some components by RNA interference.

When CA-074 Me, an inhibitor of cathepsin B, was incubated with cells 1.5 h before incubation with the PmpG-1-vaults, there was a large inhibition of IL-1β secretion (Fig. 1A). The inhibitor alone had no effect on IL-1β secretion (data not shown). Similarly, pre-incubation with a Syk inhibitor for 30 min significantly decreased PmpG-1-vault-induced IL-1β secretion (Fig. 1A). These results suggest that both Syk recruitment and lysosomal destabilization are involved in vault-induced inflammasome activation.

To confirm NLRP3 inflammasome activation by the PmpG-1-vault vaccine, we also depleted ASC and NLRP3 using shRNA method delivered using lentiviral particles. THP-1 cells were treated with a non-target shRNA control, and lentiviral particles to deplete ASC, Syk, caspase-1, and NLRP3 individually. The efficiency of ASC reduction was evaluated by qPCR (Supplementary Fig. S1), which also confirmed specificity of the depletion. When cells were incubated with PmpG-1-vaults, IL-1β secretion decreased dramatically in each depleted cell line, compared to the control group (Fig. 1B). These results further strengthen the conclusion that PmpG-1-vaults activate the NLRP3 inflammasome.

Supplementary material related to this article can be found, in the online version, at http://dx.doi.org/10.1016/j.vaccine.2014.11.028.

We next measured caspase-1 activation in the presence of inhibitors against upstream mediators of the NLRP3 inflammasome. The cathepsin B inhibitor, CA-074 Me, dampened PmpG-1-vault activation by approximately half, suggesting that lysosomal disruption may be involved in this process. The Syk inhibitor also strongly decreased caspase-1 activation (Fig. 1A).

The effects of the inhibitors were confirmed by depleting the respective target genes by RNA interference (data not shown). Thus, there was significantly less vault-induced caspase-1 activation when THP-1 cells were depleted of ASC, NLRP3 or Syk. As expected, there was also less caspase-1 activation when the cells were depleted of caspase-1.

The results of processed IL-1β and activated caspase-1 secretion obtained by ELISA (Fig. 1) were confirmed by measuring mature IL-1β and activated caspase-1 in the supernatant by Western blot (Fig. 2). Incubation of THP-1 cells with vaults stimulated secretion of mature IL-1b in the supernatant, which could be inhibited by pre-incubation with the caspase-1 inhibitor zWEHDfmk (Fig. 2A and B). Similarly, activated caspase-1 could be observed in the supernatant of vault-stimulated THP1 cells, and secretion of activated caspase-1 could be inhibited by zWEHDfmk (Fig. 2C and D).

To confirm the functional specificity of the shRNA depletion of caspase-1, ASC, NLRP3 or Syk, the THP-1 cell lines were primed with 10 μg/ml LPS, and TNF-γ secretion was measured. Secretion of this cytokine takes place through an inflammasome-independent pathway, and the results demonstrated that depletion of inflammasome-associated components had no effect (Fig. 3). These results showed that depletion of caspase-1, ASC, NLRP3 and Syk by shRNA affected caspase-1 activation and IL-1 secretion, but not cytokine secretion through inflammasome-independent pathways. Taken together, these results imply that the PmpG-1-vault vaccines can activate caspase-1 and stimulate IL-1β secretion through a process involving the NLRP3 inflammasome.

3.3. Internalized vaults co-localize with lysosomes

PmpG-1-vaults were labeled with FITC (green) and TRITC (red) (Fig. 4A) in order to study their intracellular trafficking by flow cytometry (Fig. 4B). The fluorescence of FITC is sensitive to pH, which allowed us to determine whether the particles entered acidic compartments after internalization. One group of cells was treated with bafilomycin (to prevent re-acidification of vesicles) before incubation with PmpG-1-vaults. The results indicated that the majority of PmpG-1-vaults were in acidic compartments after 6 h of incubation, but most were at neutral pH after 24 h (Fig. 4C). These experiments suggest that following phagocytosis, the majority of PmpG-1-vaults are internalized initially into acidic compartments (endolysosomes or phagolysosomes), from which they escape into the cytosol.

This possibility was also addressed by confocal fluorescence microscopy, using DyLight650-labeled PmpG-1-vaults and antibodies against EEA1 (early endosomal marker), Lamp1 (marker of lysosomes), and LC3 (marker of autophagosomes) (Fig. 5). The results showed that after 15 min, 30 min and 60 min, approximately 40% of PmpG-1-vaults co-localized extensively with lysosomes (Fig. 5), with a significant Pearson's coefficient. This indicates that the majority of PmpG-1-vaults were internalized into lysosomes, which led to lysosomal disruption. These results are consistent with previous results showing that inhibitors of cathepsin B block NLRP3 inflammasome activation in cells incubated with vaults.

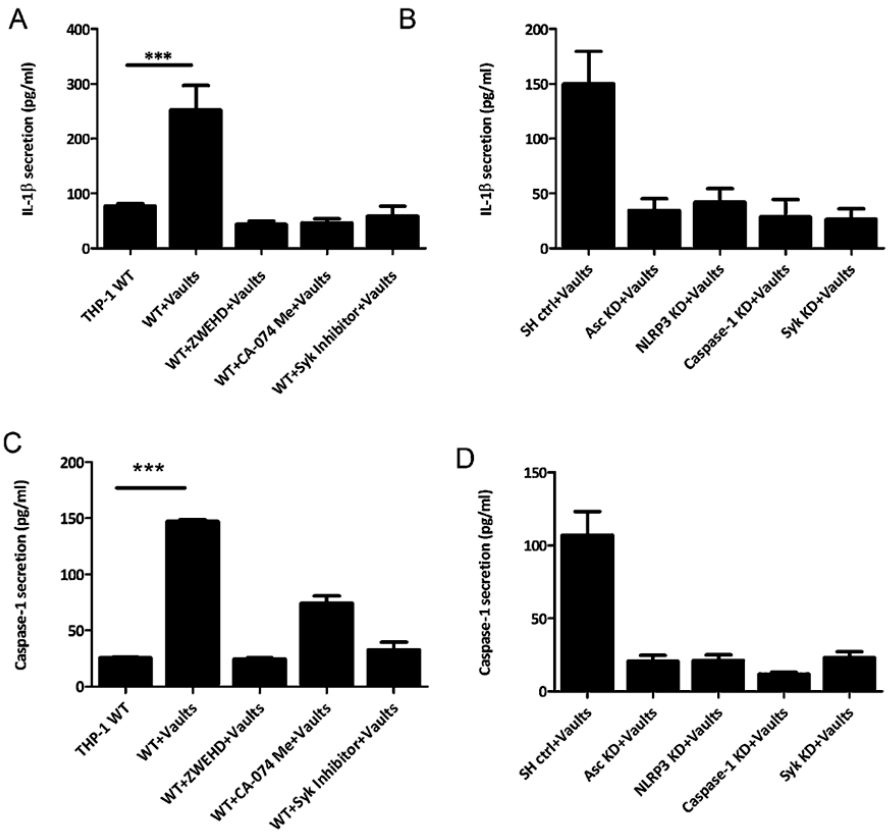

Fig. 1. PmpG-1-vaults activate the NLRP3 inflammasome and induce IL-1β secretion, as measured by an ELISA assay. THP-1 (1×10^6) wild type (WT) cells (A) were incubated in 6-well plates with RPMI 1640 media. Inhibitors of caspase-1 (ZWEHD) or cathepsin B (CA-074) were added individually 1.5 h prior to incubation with PmpG-1-vaults, and the Syk inhibitor was added 0.5 h prior to incubation with PmpG-1-vaults. THP-1 knockdown (KD) cells (B) were incubated with media alone, and 500 μg of PmpG-1-vaults were added to each well, except the WT control. Culture supernatants were collected 6 h post-incubation and IL-1β was measured by ELISA. IL-1β levels secreted by cells with inhibitors *vs* cells without inhibitors and by WT *vs* KD cells was significantly different ($p < 0{,}001$). (C) THP-1 (1×10^6) WT cells were incubated in 6-well plates, ZWEHD or CA-074 was added individually 1.5 h prior to incubation with PmpG-1-vaults, and the Syk inhibitor was added 0.5 h prior to incubation with PmpG-1-vaults. (D) THP-1 knockdown (KD) cells were incubated with media alone, and 500 μg of PmpG-1-vaults were added to each well, except the WT control. Culture supernatants were collected 6 h post-incubation and caspase-1 was measured by ELISA kit. The mean ± SD of a representative experiment from six times was analyzed by ANOVA. Caspase-1 levels secreted by cells with inhibitors *vs* cells without inhibitors and by WT *vs* KD cells was significantly different ($p < 0.001$). In all cases, cell supernatants were measured in triplicate.

3.4. Immunization with PmpG-1-vaults induces an immune response in vivo

We examined the immune response of mice vaccinated vaginally with the PmpG-1-vault vaccine. Spleen cells were harvested from naïve mice as well as from mice immunized with PmpG-1-vaults three times. Two weeks after the last immunization, all mice were sacrificed and the lymphocytes were isolated from spleens and stimulated *in vitro* overnight. Single-cell suspensions were analyzed by flow cytometry for expression of CD3, CD4, and IFN-γ, which are markers for TH1 helper cells, and gated on cells that are specific for MHC-peptide tetramers containing a peptide derived from PmpG-1 (Fig. 6). We observed that the cells from immunized mice have a larger percentage of specific TH1 cells within the $CD4^+$ cell compartment, compared to cells from naïve mice. Taken together, these results show that the immune system can recognize the foreign epitope incorporated into the PmpG-1-vault vaccine which could be used in a subsequent immune response to antigen-expressing *Chlamydia*.

4. Discussion

Vaccines that prevent significant infection of the female genital tract are essential to reduce the incidence of PID following *C. trachomatis* infection. We have shown that vaults containing a chlamydial protein (MOMP) markedly reduces infection early after infection suggesting that the self-adjuvanting vault vaccine is activating innate immunity while not producing excessive inflammation as measured by TNF-α production [29]. In this study, we characterized this innate immunity as involving inflammasome activation. The results demonstrate that incubation of PMA-primed THP-1 cells with PmpG-1-vaults can activate caspase-1 and stimulate IL-1β secretion through a process requiring the NLRP3 inflammasome. We found that the cathepsin B inhibitor CA-074

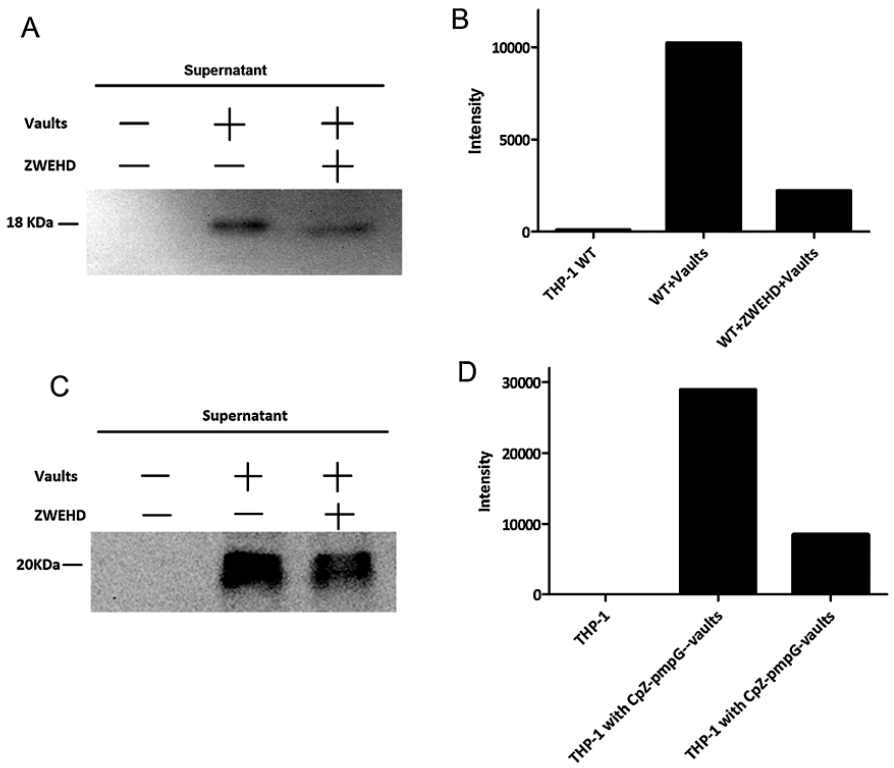

Fig. 2. PmpG-1-vaults activate the NLRP3 inflammasome and caspase-1, as measured by Western blot. THP-1 (1×10^6) wild type (WT) cells (A) were incubated in 6-well plates with RPMI 1640 media. ZWEHD was added 1.5 h prior to incubation with PmpG-1-vaults. THP-1 knockdown (KD) cells (B) were incubated with media alone, and 500 μg of PmpG-1-vaults were added to each well, except the WT control. Culture supernatants were collected 6 h post-incubation and IL-1β or caspase-1 were detected by Western blot. (A) Western blot of the supernatant probed for IL-1β. (B) Histogram showing the intensity of the bands in the Western blots. (C) Western blot of the supernatant probed caspase-1. (D) Histogram showing the intensity of the bands in the Western blots.

Me could partially inhibit this process. Interestingly, when internalized PmpG-1-vaults were visualized in cells, we found that the vaults co-localize at early times with lysosomes. The lysosomal permeabilization assay showed that the PmpG-1-vaults are in acidic compartments at early times, but then transfer to an environment with neutral pH. Once lysosomes are ruptured, they release proteases such as cathepsin B, which have been previously shown to activate the NLRP3 inflammasome.

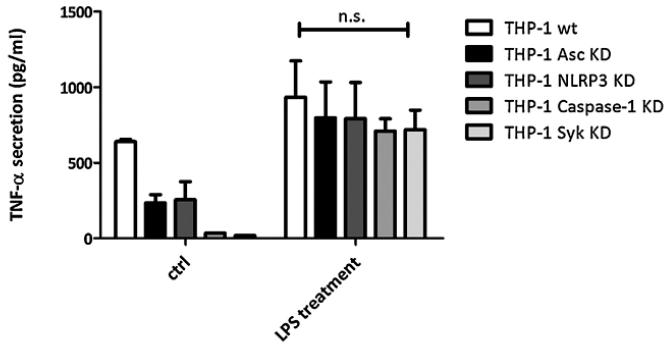

Fig. 3. TNF-α levels were not affected by depletion of inflammasome-related genes. THP-1 (1×10^6) knockdown (KD) cells were incubated in 6-well plates with RPMI 1640 media. LPS (100 ng/ml) was added as stimulator. Culture supernatants were collected 24 h post-incubation, and TNF-α was measured by ELISA. TNF-α levels from WT cells were compared to KD cells stimulated by LPS. The values for the WT and KD cells were not statistically significant: $p < 0.5$ for WT *vs* caspasd-1 KD, and $p < 0.5$ for WT *vs* Syk KD cells.

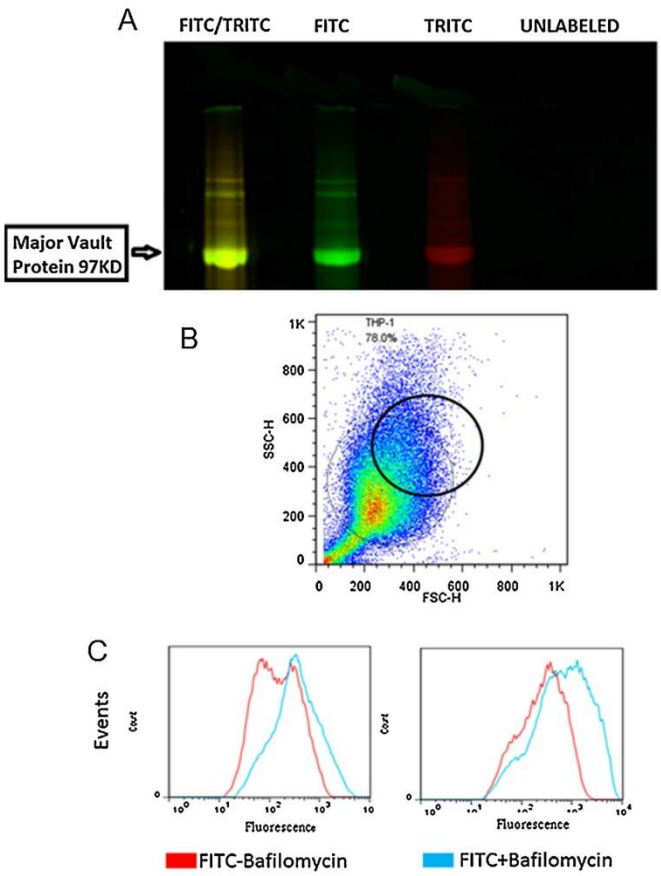

Fig. 4. PmpG-1-vaults are internalized into an acidic compartment. (A) PmpG-1-vaults dual-labeled with FITC and TRITC fluorophores and incubated with PMA-activated THP-1 cells. (B) Gating scheme (black circle) showing the dot plot of PMA-activated THP-1 cells after PmpG-1-vaults incubation. FITC can only fluoresence when inside acidified chambers and fluorescence can be modified with bafilomycin which prevents re-acidification of vesicles while TRITC constitutively fluoresces. (C) Overlay histogram of FITC-labeled vault fluorescence ± bafilomycin after 6 h and 24 h post vault exposure.

Syk also modulates vault-mediated inflammasome activation. While the mechanism for this dependence is not yet known, the Syk kinase is known to be recruited into lipid rafts when phagosomes form [52]. It had also been proposed that MVP is involved in intracellular transport and concentrated in lipid rafts [24]. Considering that vaults are phagocytosed by cells during incubation, we speculate that PmpG-1-vaults might enter the cells though lipid rafts and then interact with Syk kinase and, simultaneously, lysosomes, in order to activate the NLRP3 inflammasome. Alternatively, the PmpG-1-vaults were engineered with a 33 amino acid–peptide called the "Z" domain. This peptide was derived from a staphylococcal binding domain that can bind the Fc portion of IgG at a site distinct from the binding site for the Fc receptor (FcR). It was also previously shown that vaults with a "Z" domain increase binding of mouse IgG [29]. We expected that these vaults would be internalized through the FcR, which also stimulates the Syk pathway [53]. Further studies should elucidate the mechanisms whereby PmpG-1-vaults can stimulate Syk- and cathepsin B-dependent NLRP3 inflammasome activation.

Taken together, these findings support a model whereby *in vivo* administered vault-vaccines are phagocytosed by antigen presenting cells as we have shown *in vitro* using BMDC [47]. Following internalization, we showed in this study, that incubation of monocytes with PmpG-1-vaults can activate caspase-1 and stimulate IL-1β secretion through a process requiring the NLRP3 inflammasome. Inhibitors of the lysosomal protease, cathepsin B, prevented inflammasome activation, implying that lysosomal disruption likely plays a role in caspase-1 activation. This interpretation is consistent with the observation that the PmpG-1-vaults are internalized through a pathway that is transiently acidic and leads to destabilization of lysosomes. PmpG-1-vault interaction within cells are unique from other reported activators of NLRP3 inflammasomes, in that Syk was also shown to be involved in PmpG-1-vault-induced inflammasome activation, which may be due to vault interactions with lipid rafts. Vault vaccines can also be engineered to induce specific adaptive immunity, as we have shown here that immunization of mice with PmpG-1-vaults induces generation of PmpG-1-responsive $CD4^+$ cells immune cells. Vaults can also be engineered to deliver drugs and promote

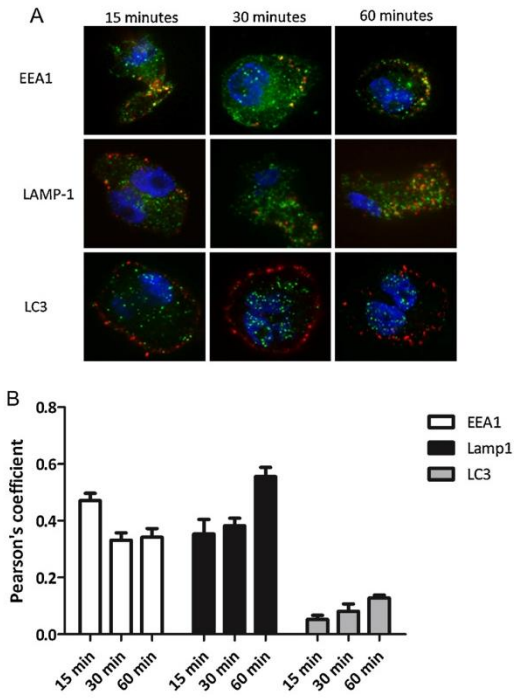

Fig. 5. Uptake of PmpG-1-vaults and colocalization within the endocytic pathway. (A) THP-1 cells were grown on 18 mm glass cover slips and treated with 30 μg of DyLight 650 labeled PmpG-1-vaults for 15, 30, and 60 min and imaged by confocal microscopy. For immunofluorescence staining, THP-1 cells were reacted with either anti-EEA1 mouse mAb, anti-Lamp1 mouse mAb, or anti-LC3 mouse mAb followed by Alexa Fluor 488-conjugated goat anti-mouse to identify endocytic compartments. (B) Colocalization of PmpG-1-vaults within each compartment was determined by calculation of the Pearson's correlation coefficient of the red and green channels using ImageJ. (For interpretation of the references to color in this figure legend, the reader is referred to the web version of this article.)

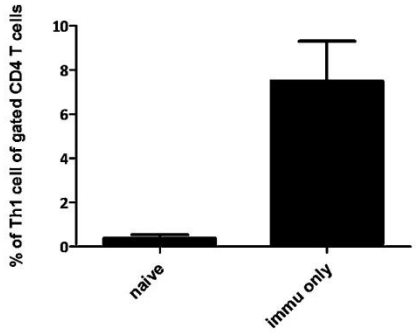

Fig. 6. PmpG-1-vaults immunization induces a cellular immune response *in vivo*. Spleen cells were harvested from naïve mice as well as mice immunized with PmpG-1-vaults containing a total of 15 μg PmpG-1 peptide, 7 days after challenge. Bars indicate percentage of $CD3^+CD4^+IFN\gamma^+$ (Th1) cells out of $CD4^+$ cells following *in vitro* stimulation with PmpG-peptide (mean % ± SEM). $n = 4$, $p < 0.001$ by Student's *t*-test.

anti-tumor responses [26,27,29]. These studies define vault-vaccines as unique among other vaccines that induce NLRP3 inflammasomes, such as alum, as they are also able to induce specific marked T cell responses against antigens incorporated in the vault body.

Acknowledgements

We thank Guangchao Liu (Dept. of Pathology and Laboratory Medicine, UCLA) for testing the vault-vaccine preparations *in vivo* and Hedi Roseboro (Dept Biological Chemistry, UCLA) for making the vault-vaccine preparations.

Conflict of interest: The authors declare that they have no conflict of interest.

References

[1] Haggerty CL, Gottlieb SL, Taylor BD, Low N, Xu F, Ness RB. Risk of sequelae after *Chlamydia trachomatis* genital infection in women. J Infect Dis 2010;201. S134-S155.
[2] Westrom L. Effect of acute pelvic inflammatory disease on fertility. Obstet Gynecol Surv 1975;30:552–3.
[3] Westrom L, Joesoef R, Reynolds G, Hagdu A, Thompson SE. Pelvic inflammatory disease and fertility: a cohort study of 1,844 women with laparoscopically verified disease and 657 control women with normal laparoscopic results. Sex Transm Dis 1992;19:185–92.
[4] Heinonen PK, Miettinen A. Laparoscopic study on the microbiology and severity of acute pelvic inflammatory disease. Eur J Obstet Gynecol Reprod Biol 1994;57:85–9.
[5] Taylor BD, Haggerty CL. Management of *Chlamydia trachomatis* genital tract infection: screening and treatment challenges. Infect Drug Resist 2011;4:19–29.
[6] Wiesenfeld HC, Sweet RL, Ness RB, Krohn MA, Amortegui AJ, Hillier SL. Comparison of acute and subclinical pelvic inflammatory disease. Sex Transm Dis 2005;32:400–5.
[7] Morrison RP, Feilzer K, Tumas DB. Gene knockout mice establish a primary protective role for major histocompatibility complex class II-restricted responses in *Chlamydia trachomatis* genital tract infection. Infect Immun 1995;63:4661–8.
[8] Ito JI, Lyons JM. Role of gamma interferon in controlling murine chlamydial genital tract infection. Infect Immun 1999;67:5518–21.
[9] Morrison SG, Morrison RP. Resolution of secondary *Chlamydia trachomatis* genital tract infection in immune mice with depletion of both CD4+ and CD8+ T cells. Infect Immun 2001;69:2643–9.
[10] Morrison SG, Su H, Caldwell HD, Morrison RP. Immunity to murine *Chlamydia trachomatis* genital tract reinfection involves B cells and CD4(+) T cells but not CD8(+) T cells. Infect Immun 2000;68:6979–87.
[11] Karunakaran KP, Yu H, Foster LJ, Brunham RC. Development of a *Chlamydia trachomatis* T cell vaccine. Hum Vaccin 2010;6:676–80.
[12] Su H, Feilzer K, Caldwell HD, Morrison RP. *Chlamydia trachomatis* genital tract infection of antibody-deficient gene knockout mice. Infect Immun 1997;65:1993–9.
[13] Ramsey KH, Soderberg LS, Rank RG. Resolution of chlamydial genital infection in B-cell-deficient mice and immunity to reinfection. Infect Immun 1988;56:1320–5.
[14] Kickhoefer VA, Poderycki MJ, Chan EKL, Rome LH. The La RNA-binding protein interacts with the vault RNA and is a vault-associated protein. J Biol Chem 2002;277:41282–6.
[15] Kedersha NL, Rome LH. Isolation and characterization of a novel ribonucleoprotein particle: large structures contain a single species of small RNA. J Cell Biol 1986;103:699–709.
[16] Kolli S, Zito CI, Mossink MH, Wiemer EA, Bennett AM. The major vault protein is a novel substrate for the tyrosine phosphatase SHP-2 and scaffold protein in epidermal growth factor signaling. J Biol Chem 2004;279:29374–85.
[17] Yu Z, Fotouhi-Ardakani N, Wu L, Maoui M, Wang S, Banville D, et al. PTEN associates with the vault particles in HeLa cells. J Biol Chem 2002;277:40247–52.
[18] Yi C, Li S, Chen X, Wiemer EA, Wang J, Wei N, et al. Major vault protein, in concert with constitutively photomorphogenic 1, negatively regulates c-Jun-mediated activator protein 1 transcription in mammalian cells. Cancer Res 2005;65:5835–40.
[19] Steiner E, Holzmann K, Pirker C, Elbling L, Micksche M, Sutterluty H, et al. The major vault protein is responsive to and interferes with interferon-gamma-mediated STAT1 signals. J Cell Sci 2006;119:459–69.
[20] Kim E, Lee S, Mian MF, Yun SU, Song M, Yi KS, et al. Crosstalk between Src and major vault protein in epidermal growth factor-dependent cell signalling. FEBS J 2006;273:793–804.
[21] Scheffer GL, Wijngaard PL, Flens MJ, Izquierdo MA, Slovak ML, Pinedo HM, et al. The drug resistance-related protein LRP is the human major vault protein. Nat Med 1995;1:578–82.
[22] Scheffer GL, Schroeijers AB, Izquierdo MA, Wiemer EA, Scheper RJ. Lung resistance-related protein/major vault protein and vaults in multidrug-resistant cancer. Curr Opin Oncol 2000;12:550–6.

[23] Gopinath SC, Matsugami A, Katahira M, Kumar PK. Human vault-associated non-coding RNAs bind to mitoxantrone, a chemotherapeutic compound. Nucleic Acids Res 2005;33:4874–81.
[24] Kowalski MP, Dubouix-Bourandy A, Bajmoczi M, Golan DE, Zaidi T, Coutinho-Sledge YS, et al. Host resistance to lung infection mediated by major vault protein in epithelial cells. Science 2007;317:130–2.
[25] Stephen AG. Assembly of vault-like particles in insect cells expressing only the major vault protein. J Biol Chem 2001;276:23217–20.
[26] Kar UK, Jiang J, Champion CI, Salehi S, Srivastava M, Sharma S, et al. Vault nanocapsules as adjuvants favor cell-mediated over antibody-mediated immune responses following immunization of mice. PLOS ONE 2012;7:e38553.
[27] Buehler DC, Marsden MD, Shen SH, Toso DB, Wu X, Loo JA, et al. Bioengineered vaults: self-assembling protein shell–lipophilic core nanoparticles for drug delivery. ACS Nano 2014;8:7723–32.
[28] Berger W, Steiner E, Grusch M, Elbling L, Micksche M. Vaults and the major vault protein: novel roles in signal pathway regulation and immunity. Cell Mol Life Sci 2009;66:43–61.
[29] Champion CI, Kickhoefer VA, Liu G, Moniz RJ, Freed AS, Bergmann LL, et al. A vault nanoparticle vaccine induces protective mucosal immunity. PLOS ONE 2009;4:e5409.
[30] Ogura Y, Sutterwala FS, Flavell RA. The inflammasome first line of the immune response to cell stress. Cell 2006;126:659–62.
[31] Martinon F, Tschopp J. Inflammatory caspases and inflammasomes: master switches of inflammation. Cell Death Differ 2006;14:10–22.
[32] Mariathasan S, Weiss DS, Newton K, McBride J, O'Rourke K, Roose-Girma M, et al. Cryopyrin activates the inflammasome in response to toxins and ATP. Nature 2006;440:228–32.
[33] Allen IC, Scull MA, Moore CB, Holl EK, McElvania-TeKippe E, Taxman DJ, et al. The NLRP3 inflammasome mediates in vivo innate immunity to influenza A virus through recognition of viral RNA. Immunity 2009;30:556–65.
[34] Munoz-Planillo R, Franchi L, Miller LS, Nunez G. A critical role for hemolysins and bacterial lipoproteins in *Staphylococcus aureus*-induced activation of the Nlrp3 inflammasome. J Immunol 2009;183:3942–8.
[35] Saïd-Sadier N, Ojcius DM. Alarmins, inflammasomes and immunity. Biomed J 2012;35:437–49.
[36] Halle A, Hornung V, Petzold GC, Stewart CR, Monks BG, Reinheckel T, et al. The NALP3 inflammasome is involved in the innate immune response to amyloid-β. Nat Immunol 2008;9:857–65.
[37] Martinon F, Petrilli V, Mayor A, Tardivel A, Tschopp J. Gout-associated uric acid crystals activate the NALP3 inflammasome. Nature 2006;440:237–41.
[38] Duncan JA, Gao X, Huang MT, O'Connor BP, Thomas CE, Willingham SB, et al. Neisseria gonorrhoeae activates the proteinase cathepsin B to mediate the signaling activities of the NLRP3 and ASC-containing inflammasome. J Immunol 2009;182:6460–9.
[39] Sutterwala FS, Ogura Y, Szczepanik M, Lara-Tejero M, Lichtenberger GS, Grant EP, et al. Critical role for NALP3/CIAS1/cryopyrin in innate and adaptive immunity through its regulation of caspase-1. Immunity 2006;24:317–27.
[40] Agostini L, Martinon F, Burns K, McDermott MF, Hawkins PN, Tschopp J. NALP3 forms an IL-1β-processing inflammasome with increased activity in Muckle-Wells autoinflammatory disorder. Immunity 2004;20:319–25.
[41] Martinon F, Mayor A, Tschopp J. The inflammasomes: guardians of the body. Annu Rev Immunol 2009;27:229–65.
[42] Ciraci C, Janczy JR, Sutterwala FS, Cassel SL. Control of innate and adaptive immunity by the inflammasome. Microbes Infect 2012;14:1263–70.
[43] Moayeri M, Sastalla I, Leppla SH. Anthrax and the inflammasome. Microbes Infect 2012;14:392–400.
[44] Shimada K, Crother TR, Arditi M. Innate immune responses to *Chlamydia pneumoniae* infection: role of TLRs, NLRs, and the inflammasome. Microbes Infect 2012;14:1301–7.
[45] Kickhoefer VA, Siva AC, Kedersha NL, Inman EM, Ruland C, Streuli M, et al. The 193-kD vault protein, VPARP, is a novel poly(ADP-ribose) polymerase. J Cell Biol 1999;146:917–28.
[46] Poderycki MJ, Kickhoefer VA, Kaddis CS, Raval-Fernandes S, Johansson E, Zink JI, et al. The vault exterior shell is a dynamic structure that allows incorporation of vault-associated proteins into its interior. Biochemistry 2006;45:12184–93.
[47] Kickhoefer VA, Han M, Raval-Fernandes S, Poderycki MJ, Moniz RJ, Vaccari D, et al. Targeting vault nanoparticles to specific cell surface receptors. ACS Nano 2009;3:27–36.
[48] Maxion HK, Liu W, Chang M-H, Kelly KA. The infecting dose of *Chlamydia muridarum* modulates the innate immune response and ascending infection. Infect Immun 2004;72:6330–40.
[49] Thornberry NA, Rano TA, Peterson EP, Rasper DM, Timkey T, Garcia-Calvo M, et al. A combinatorial approach defines specificities of members of the caspase family and granzyme B: functional relationships established for key mediators of apoptosis. J Biol Chem 1997;272:17907–11.
[50] Kayagaki N, Warming S, Lamkanfi M, Walle LV, Louie S, Dong J, et al. Non-canonical inflammasome activation targets caspase-11. Nature 2011;479:117–21.
[51] Ng G, Sharma K, Ward SM, Desrosiers MD, Stephens LA, Schoel WM, et al. Receptor-independent, direct membrane binding leads to cell-surface lipid sorting and Syk kinase activation in dendritic cells. Immunity 2008;29:807–18.
[52] Xu S, Huo J, Gunawan M, Su I-H, Lam K-P. Activated dectin-1 localizes to lipid raft microdomains for signaling and activation of phagocytosis and cytokine production in dendritic cells. J Biol Chem 2009;284:22005–11.
[53] Mócsai A, Ruland J, Tybulewicz VLJ. The SYK tyrosine kinase: a crucial player in diverse biological functions. Nat Rev Immunol 2010;10:387–402.

APPENDIX B

Influenza Virus Affects Intestinal Microbiota and Secondary Salmonella Infection in the Gut through Type I IFNs

PLOS | PATHOGENS

RESEARCH ARTICLE

Influenza Virus Affects Intestinal Microbiota and Secondary *Salmonella* Infection in the Gut through Type I Interferons

Elisa Deriu[1], Gayle M. Boxx[1], Xuesong He[2], Calvin Pan[3], Sammy David Benavidez[1], Lujia Cen[2], Nora Rozengurt[4], Wenyuan Shi[2], Genhong Cheng[1]*

1 Department of Microbiology, Immunology and Molecular Genetics, University of California, Los Angeles, Los Angeles, California, United States of America, **2** School of Dentistry, University of California, Los Angeles, Los Angeles, California, United States of America, **3** Department of Human Genetics, University of California, Los Angeles, Los Angeles, California, United States of America, **4** Department of Pathology and Laboratory Medicine, CURE Imaging and Stem Cell Biology Core, University of California, Los Angeles, Los Angeles, California, United States of America

* GCheng@mednet.ucla.edu

Citation: Deriu E, Boxx GM, He X, Pan C, Benavidez SD, Cen L, et al. (2016) Influenza Virus Affects Intestinal Microbiota and Secondary *Salmonella* Infection in the Gut through Type I Interferons. PLoS Pathog 12(5): e1005572. doi:10.1371/journal.ppat.1005572

Editor: Renée M. Tsolis, University of California, Davis, UNITED STATES

Received: February 5, 2016

Accepted: March 23, 2016

Published: May 5, 2016

Data Availability Statement: All relevant data are within the paper, in its Supporting Information files and in a public repository, which is available from https://dx.doi.org/10.6084/m9.figshare.3124954.v1

Funding: This work was supported by grants AI056154 and AI069120, awarded to GC from National Institute of Health. NR was supported by grant P30 DK41301, awarded to Enrique Rozengurt, from National Institute of Health (http://www.nih.gov/). The funders had no role in study design, data collection and analysis, decision to publish, or preparation of the manuscript.

Abstract

Human influenza viruses replicate almost exclusively in the respiratory tract, yet infected individuals may also develop gastrointestinal symptoms, such as vomiting and diarrhea. However, the molecular mechanisms remain incompletely defined. Using an influenza mouse model, we found that influenza pulmonary infection can significantly alter the intestinal microbiota profile through a mechanism dependent on type I interferons (IFN-Is). Notably, influenza-induced IFN-Is produced in the lungs promote the depletion of obligate anaerobic bacteria and the enrichment of Proteobacteria in the gut, leading to a "dysbiotic" microenvironment. Additionally, we provide evidence that IFN-Is induced in the lungs during influenza pulmonary infection inhibit the antimicrobial and inflammatory responses in the gut during *Salmonella*-induced colitis, further enhancing *Salmonella* intestinal colonization and systemic dissemination. Thus, our studies demonstrate a systemic role for IFN-Is in regulating the host immune response in the gut during *Salmonella*-induced colitis and in altering the intestinal microbial balance after influenza infection.

Author Summary

Influenza is a respiratory illness. Symptoms of flu include fever, headache, extreme tiredness, dry cough, sore throat, runny or stuffy nose, and muscle aches. Some people, especially children, can have additional gastrointestinal symptoms, such as nausea, vomiting, and diarrhea. In humans, there is no evidence that the influenza virus replicates in the intestine. Using an influenza mouse model, we found that influenza infection alters the intestinal microbial community through a mechanism dependent on type I interferons induced in the pulmonary tract. Futhermore, we demonstrate that influenza-induced type I interferons increase the host susceptibility to *Salmonella* intestinal colonization and

Competing Interests: The authors have declared that no competing interests exist.

dissemination during secondary *Salmonella*-induced colitis through suppression of host intestinal immunity.

Introduction

Influenza is a highly contagious viral infection that has a substantial impact on global health.

Notably, outbreaks of influenza infection are usually associated with an increased incidence or severity of secondary bacterial infections responsible for high levels of morbidity during seasonal influenza episodes. We and others have previously shown that IFN-Is play a critical role in the development of secondary bacterial pneumonia after influenza infection [1]. Since their discovery in 1957, IFN-Is have been recognized as the central antiviral cytokines in vertebrates [2]. The type I IFN family mainly consists of numerous subtypes of IFNα and a single IFNβ, whose induction appears to be ubiquitous in most cell types. Toll-like receptor (TLR)-mediated IFN-I induction plays a key role in facilitating antiviral responses [3]. IFN-Is bind to a common heterodimeric receptor, IFN-α/β receptor (IFNAR), composed of two subunits, IFNAR1 and IFNAR2. Binding activates the JAK/STAT pathway, which induces pro-inflammatory genes that inhibit viral replication and boost adaptive immunity [4], and regulates the transcription of multiple interferon-stimulated genes (ISGs) [5].

A recent study has shown that influenza infection can alter the composition of the intestinal flora, resulting in immunological dysregulation that may promote inflammatory gut disorders [6]. The mammalian gut harbors a complex microbiota that plays a key role in host health through its contribution to nutritional, immunological, and physiological functions. Intestinal commensals are required for maintaining gut homeostasis through dynamic interactions with the host's immune system [7]. Resident microbiota promote gut immune homeostasis by regulating T regulatory cells (Tregs) [8] and T helper 17 cells (Th17) [9]. The gut microbiota can inhibit infection through direct microbial antagonism or by stimulating several host effectors and injury responses [10, 11]. However, the intestinal commensals also pose an enormous challenge to the host that needs to remain "ignorant" to a selection of microbial antigens and keep the bacterial load anatomically contained, while remaining responsive to its dissemination [12]. Reciprocal interactions between gut microbiota and the host immune system shape the microbial community and influence imbalances that can lead to disease [13]. These changes are often characterized by a reduction of obligate anaerobic bacteria, and a proliferation of facultative anaerobic *Enterobacteriaceae* [14].

Furthermore, some people with pulmonary influenza infections also experience symptoms of gastrointestinal disorders, especially children [15]. Influenza RNA is rarely recovered from their stool [15], so it is unclear whether the symptoms develop from swallowed respiratory secretions or from active infection of the gastrointestinal tract.

In order to investigate the role of IFN-Is induced during influenza infection in modulating the endogenous intestinal microbiota, we established a model of influenza pulmonary infection using genetically modified animals with defective IFNAR signaling (*Ifnar1*$^{-/-}$mice). Remarkably, we found that influenza infection alters the intestinal microbial community supporting gut Proteobacteria pathobionts through a mechanism dependent on IFN-Is.

While the importance of IFN-Is in antiviral defense is well established, their role during bacterial infection is more ambiguous. Moreover, we wanted to test whether primary influenza infection can predispose the host to secondary intestinal bacterial infections. We therefore developed a model of sequential influenza pulmonary infection followed by secondary *Salmonella*-induced colitis using *Ifnar1*$^{-/-}$mice to investigate the effects of IFN-Is induced during

influenza infection on intestinal host defense against *Salmonella*. Interestingly, we found that lung induced IFN-Is enhanced the growth of *Salmonella* in the inflamed gut and increased its systemic dissemination to secondary sites. Furthermore, we found that influenza pulmonary infection resulted in a profound inhibitory effect on the intestinal antibacterial and inflammatory responses against *Salmonella* infection in a IFN-I dependent manner.

Results

Influenza-induced IFN-Is alter the intestinal microbiota

Previously, it was shown that influenza infection causes intestinal injury through microbiota-dependent inflammation [6]. Considering that IFN-Is are essential components of the host antiviral response, we hypothesized that these molecules might also mediate changes in the intestinal microbiota during viral influenza infection. To study this, we infected wild-type (WT) and *Ifnar1* knockout (*Ifnar1*$^{-/-}$) mice by non-surgical intratracheal instillation [16, 17] with a sublethal dose (200 infectious units) of influenza A/Puerto Rico/8/34 (PR8).

Mice were monitored daily for 17 days after infection. We assessed the microbiota composition in the fecal content of WT and *Ifnar1*$^{-/-}$ mice before PR8 or mock infection and at 9 day post infection (dpi) (Fig 1A) since the peak weight loss was observed at 9 dpi in WT and *Ifnar1*$^{-/-}$ mice. PR8 viral load was quantified after non-surgical intratracheal instillation at 1 dpi, and we detected live virus only in the lungs, neither in the colon content nor in the cecum tissue (S1A and S1B Fig). MiSeq Illumina analysis of microbial DNA extracted from fecal samples confirmed observations reported by others [18] that the mouse intestinal microbiota, independent of the genotype, consists of two major bacterial phyla, the Bacteroidetes and the Firmicutes (Fig 1B), with the most relevant classes being Bacteroidia and Clostridia (Fig 1C). No statistical differences were found in the fecal microbiota composition between WT and *Ifnar1*$^{-/-}$ mice, either before infection at day 0 or after mock infection at day 9. Moreover, we observed low abundance of Proteobacteria in the intestinal microbiota of the uninfected and mock-infected mice, previously reported by others [19], independent of the mouse genotype (Fig 1B). Furthermore, at day 9 post PR8 infection, Bacteroidetes and Firmicutes were still the most dominant colonizers in both mouse genotypes (Fig 1B). Our findings, however, uncovered a significant blooming of Proteobacteria at day 9 after PR8 infection only in the WT mice, whereas no significant increase was noted in the *Ifnar1*$^{-/-}$ mice, irrespective of the infection (Fig 1B). Indeed, while Proteobacteria represented 1% on average in uninfected and mock-infected mice, regardless of the genotype, they comprised approximately 15% of the total fecal microbiota in the PR8-infected WT mice ($p = 0.0340$ One-Way ANOVA after Bonferroni correction) (Fig 1B). The most striking change in the fecal microbial community of WT mice after PR8 infection was the increased abundance of the genus *Escherichia*, being however mostly undetectable in uninfected and mock-infected mice of both genotypes ($p = 0.0011$ One-Way ANOVA after Bonferroni correction) (Fig 1C).

Overall, greater Proteobacteria colonization levels after influenza infection in WT mice were not caused by differences in Proteobacteria abundance between WT and *Ifnar1*$^{-/-}$ mice prior to PR8 infection. Moreover, the thriving of Proteobacteria after PR8 infection in the WT but not *Ifnar1*$^{-/-}$ mice supports our hypothesis that influenza virus is able to alter the intestinal microbiota, and that this action is dependent on IFN-Is. In addition, using 16S quantitative PCR (qPCR) analysis we confirmed a significant increase in *Enterobacteriaceae* in the stool samples of the PR8-infected WT mice, but not in the PR8-infected *Ifnar1*$^{-/-}$ mice (Fig 1D), however no significant difference was found between WT and *Ifnar1*$^{-/-}$ mice at day 0 prior to infection (Fig 1D). Furthermore, we detected a significant lower level of *Segmented Filamentous Bacteria* (*SFB*) in the stool samples of the PR8-infected WT mice compared to the uninfected

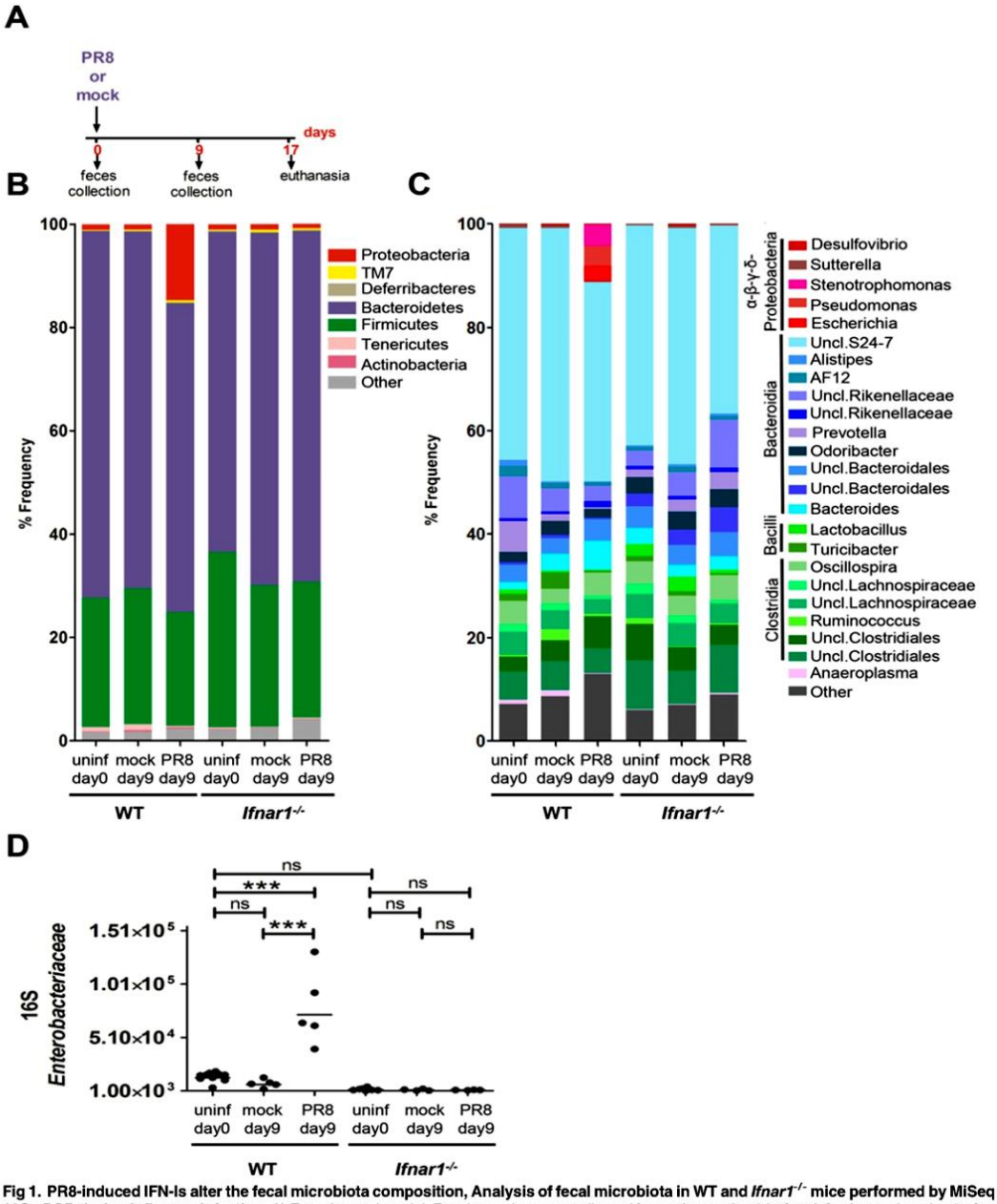

Fig 1. PR8-induced IFN-Is alter the fecal microbiota composition, Analysis of fecal microbiota in WT and *Ifnar1*$^{-/-}$ mice performed by MiSeq and 16S qPCR during influenza infection. A) Experimental model. Fecal samples were collected from mice on day 0 before infection and on day 9 after mock

and PR8 infection. Mice were euthanized at 17 dpi. B, C) The fecal microbiota from WT and *Ifnar1*$^{-/-}$ mice on day 0 before infection (n = 6 WT, n = 6 *Ifnar1*$^{-/-}$), and on day 9 after mock (n = 3 WT, n = 3 *Ifnar1*$^{-/-}$) and PR8 infection (n = 3 WT, n = 3 *Ifnar1*$^{-/-}$) was analyzed by sequencing using the Illumina MiSeq system. Graphed is the average relative abundance of each bacterial phylum (B) and genus (C); the cut-off abundance level was set at 0.5%. D) Analysis of the fecal *Enterobacteriaceae* using 16S qPCR. Fecal samples were collected from mice on day 0 before infection (n = 10 WT, n = 8 *Ifnar1*$^{-/-}$) and on day 9 after mock (n = 5 WT, n = 4 *Ifnar1*$^{-/-}$) and PR8 infection (n = 5 WT, n = 4 *Ifnar1*$^{-/-}$). Copy numbers of *Enterobacteriaceae* per μl of fecal microbial DNA is shown. Each dot represents one mouse, the geometric mean is indicated. P values were calculated by One-Way ANOVA (Bonferroni multiple comparison test). ***p < 0.001; ns, not significant. One representative experiment is shown. Abbreviations are as follows: Uncl., unclassified; uninf, uninfected.

doi:10.1371/journal.ppat.1005572.g001

WT mice (S1C Fig). *SFB* are Clostridia-correlated bacteria closely attached to the intestinal epithelium, which are able to activate a range of host defenses, including the production of antimicrobials, development of Th17 cells and increased colonization resistance to the intestinal pathogen *Citrobacter rodentium* [9]. However, uninfected WT and *Ifnar1*$^{-/-}$ mice were found similarly colonized with *SFB*; furthermore, the *SFB* abundance did not significantly change in the *Ifnar1*$^{-/-}$ mice, despite PR8 infection (S1C Fig).

In summary, our findings indicate that differences in the fecal microbiota between WT and *Ifnar1*$^{-/-}$ mice prior to influenza infection are insufficient to explain the PR8-mediated changes in specific endogenous bacterial population in WT mice.

Similar results, as observed with influenza, were obtained when synthetic stimulators of IFN-Is such as poly I:C (pIC) [20, 21] were administered to WT and *Ifnar1*$^{-/-}$ mice by non-surgical intratracheal instillation at day 0 and at day 2 (S1D Fig). Using 16S qPCR analysis we found a significant increase in *Enterobacteriaceae* at day 4 and day 5 in the fecal samples of the pIC-treated WT mice, but not in the pIC-treated *Ifnar1*$^{-/-}$ mice (S1E Fig). However, lower level of *SFB* was found at day 4 only in pIC-treated WT mice, but not in the pIC-treated *Ifnar1*$^{-/-}$ mice (S1F Fig).

Collectively, our findings highlight a critical role of type I IFN-mediated signaling induced in the lungs during pulmonary influenza infection in predisposing the host to dysbiosis. Our analysis specifically demonstrates a flourishing of resident bacteria belonging to Proteobacteria pathobionts, and a depletion of a subset of indigenous *SFB*.

Influenza-induced IFN-Is impair control of *S*. Typhimurium during acute colitis

Since we demonstrated that IFNAR1-mediated signaling increased the abundance of endogenous *Enterobacteriaceae* during influenza infection, we aimed to test whether they could similarly affect the growth of *Salmonella* Typhimurium (*S*. Typhimurium), a leading cause of acute gastroenteritis and inflammatory diarrhea, using a mouse model of acute colitis. One of the hallmarks of *S*. Typhimurium virulence in mice is its systemic manifestations resembling typhoid fever; in the typhoid model no intestinal inflammation is observed, and subsequently *Salmonella* numbers in the colon content are low and extremely variable [22, 23]. To achieve colitis, *S*. Typhimurium must be administered to mice pretreated with the antibiotic streptomycin, this results in its effective colonization of the intestinal lumen, followed by high density growth and mucosal inflammation [22]. In our colitis model, WT and *Ifnar1*$^{-/-}$ mice were treated with streptomycin 1 day prior to *S*. Typhimurium infection in order to achieve acute inflammation of the cecal mucosa. On day 0, mice were first infected with a sublethal dose of PR8 virus or PBS by non-surgical intratracheal instillation, then secondarily infected by oral gavage with 10^7 CFU of *S*. Typhimurium or given LB medium alone at 5 dpi (Fig 2A). Mice were monitored daily until euthanasia at 8 dpi. At that time point, WT mice infected with PR8, followed by *S*. Typhimurium, referred to as "secondarily infected", were noted to have significantly more weight loss than those infected only with *S*. Typhimurium (Fig 2B), and no difference in weight loss between the two groups of *Ifnar1*$^{-/-}$ mice was detected at 8 dpi. The extent

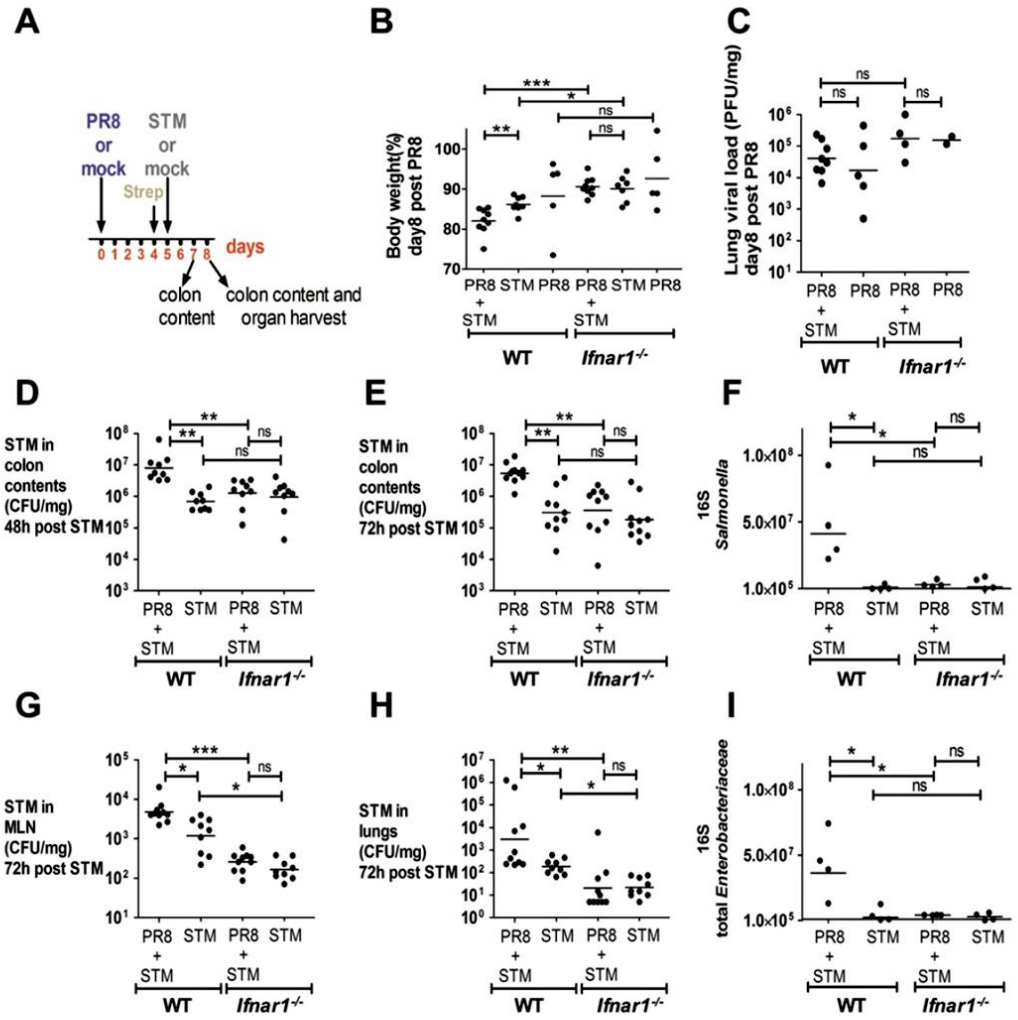

Fig 2. PR8-induced IFN-Is sensitize the host to *S.* Typhimurium infection. A) Schematic representation of the PR8-secondary *S.* Typhimurium infection model. B) Body weight loss at 8 dpi of WT and *Ifnar1*$^{-/-}$ mice in secondarily infected, *S.* Typhimurium-only and PR8-only infected mice. C) Lung viral load was measured at 8 dpi by plaque assay in secondarily infected and PR8-only infected WT and *Ifnar1*$^{-/-}$ mice. D, E) *S.* Typhimurium load in the colon content at 48 h (7 dpi) and 72 h (8 dpi) after bacterial infection. F, I) 16S copy numbers of *Salmonella* (F) and total *Enterobacteriaceae* (I) per μl of microbial DNA from colon content determined at 8 dpi. G, H) *S.* Typhimurium load in MLN and lungs at 72 h after bacterial infection. Each dot represents one mouse, the geometric mean is indicated. *P* values were calculated by two-tailed Mann-Whitney test in (B, D, E, F, G, H, I). Non-parametric Kruskal-Wallis test was used in (C). *p < 0.05, **p < 0.01, ***p < 0.001; ns, not significant. Two independent experiments are shown in (B, D, E, G, H). A representative experiment is shown in (C). A representative experiment is shown in (F, I). N of mice used in each group in (B): PR8 = 5 WT and 5 *Ifnar1*$^{-/-}$, PR8+STM = 9 WT and 9 *Ifnar1*$^{-/-}$, STM = 8 WT and 7 *Ifnar1*$^{-/-}$. N of mice used in each group in (C): PR8 = 5 WT and 2 *Ifnar1*$^{-/-}$, PR8+STM = 8 WT and 4 *Ifnar1*$^{-/-}$. N of mice used in each group in (D, E, G, H): PR8+STM = 9–10 WT and 9–10 *Ifnar1*$^{-/-}$, STM = 9–10 WT and 9–10 *Ifnar1*$^{-/-}$. N of mice used in each group in (F, I): PR8+STM = 4 WT and 4 *Ifnar1*$^{-/-}$, STM = 4 WT and 4 *Ifnar1*$^{-/-}$. Abbreviations are as follows: STM, *S.* Typhimurium.

doi:10.1371/journal.ppat.1005572.g002

of the weight loss seen in secondarily infected WT mice at 8 dpi was also greater than in secondarily infected *Ifnar1*$^{-/-}$ group (Fig 2B). Lung viral load measured by plaque assay (Fig 2C) and qPCR (S2A Fig) revealed no difference between the WT and *Ifnar1*$^{-/-}$ groups, implying that the influenza infection was not the direct cause of the weight loss. However, at 7 and 8 dpi, corresponding to 48 and 72 hours (h) post *S.* Typhimurium infection, respectively, we found a significant increase (12-fold and 18-fold, respectively) in the *S.* Typhimurium burden in the colons of the WT mice previously infected with PR8 (Fig 2D and 2E). In contrast, infection with PR8 did not enhance *S.* Typhimurium gut colonization in the *Ifnar1*$^{-/-}$ mice (Fig 2D and 2E). Using 16S qPCR analysis, we also detected a significant increase in the *Salmonella* copy number in the colon content of secondarily infected WT mice at 8 dpi compared to the *S.* Typhimurium-only infected WT mice. No difference was detected in the *Salmonella* gene copies between secondarily infected *Ifnar1*$^{-/-}$ and *S.* Typhimurium-only infected *Ifnar1*$^{-/-}$ mice at 8 dpi (Fig 2F). These results were confirmed by 16S-Denaturing Gradient Gel Electrophoresis (DGGE) analysis performed from the microbial DNA extracted from the colon content 8 dpi (S2B Fig). Likewise, at 8 dpi, a significant increase was noted in the total *Enterobacteriaceae* copy number only in the colon content of secondarily infected WT mice, compared to the *S.* Typhimurium-only infected WT mice (Fig 2I). We interpret this rise in total *Enterobacteriaceae* gene copies to represent an increase in the population of *Salmonella*, since a rise in other *Enterobacteriaceae* was not detected. This is in accordance with previous observations [24] showing no overgrowth of commensal *Enterobacteriaceae*, despite high levels of inflammation, in mice infected with *S.* Typhimurium.

Finally, we enumerated *S.* Typhimurium in the mesenteric lymph nodes (MLN) and lungs of WT and *Ifnar1*$^{-/-}$ mice at 8 dpi. Similar to our findings regarding the colonic burden, prior infection with PR8 enhanced the ability of *S.* Typhimurium to disseminate to the MLN and the lungs in WT but not *Ifnar1*$^{-/-}$ mice (Fig 2G and 2H). Indeed there was significantly less dissemination of *S.* Typhimurium overall in the *Ifnar1*$^{-/-}$ mice compared to WT mice (Fig 2G and 2H).

Similar results in *S.* Typhimurium intestinal colonization were obtained when mice were infected at day 5 with 10^3 CFU of *S.* Typhimurium, without streptomycin pretreatment (typhoid model) (S2C and S2D Fig). Indeed, as expected, *S.* Typhimurium numbers in the colon content were low and highly variable in *S.* Typhimurium-only infected WT and *Ifnar1*$^{-/-}$ mice, whereas prior infection with PR8 was still able to increase *S.* Typhimurium gut colonization in WT, but not in *Ifnar1*$^{-/-}$ mice (S2D Fig).

Overall, these results further support our hypothesis that PR8 infection predisposes mice to secondary *Salmonella* infection in a IFN-I-dependent manner.

We further tested whether pIC could elicit similar effects in our acute colitis mouse model as shown with influenza. WT and *Ifnar1*$^{-/-}$ mice were intraperitoneally (i.p.) injected with pIC or saline 1 day prior and 2 days after the oral gavage administration of 10^7 CFU of *S.* Typhimurium or LB alone (S3A Fig). Alternatively, WT and *Ifnar1*$^{-/-}$ mice were treated with pIC through non-surgical intratracheal instillation 1 day prior and 1 day after the oral gavage administration of 10^7 CFU of *S.* Typhimurium (S4A Fig). *S.* Typhimurium CFUs were measured in the colon content, MLN, lungs and spleen at 72 h post bacterial infection. We found that pIC treatment significantly increased the *S.* Typhimurium burden in the luminal colon of the WT mice, but not *Ifnar1*$^{-/-}$ mice (S3B Fig and S4B Fig). Moreover, we found that pIC enhanced *S.* Typhimurium dissemination in the WT but not in the *Ifnar1*$^{-/-}$ group (S3C–S3E Fig and S4C–S4E Fig). These findings imply that the pro-bacterial effects induced by pIC during *S.* Typhimurium infection are largely mediated by IFN-Is, and that these can potently enhance *S.* Typhimurium pathogenicity.

In summary, our studies have consistently shown that IFN-Is confer a fitness advantage to *Salmonella* in colonizing the intestine and disseminating to systemic sites.

Influenza-induced IFN-Is inhibit the antimicrobial response in *S.* Typhimurium-induced colitis

We next investigated whether IFN-Is might augment *Salmonella* intestinal colonization and dissemination through the suppression of specific well-characterized antimicrobial genes. To this end, we analyzed the expression of the following: *Ifnγ*, the gene that is of pivotal importance in host defense against intramacrophage pathogens [25], in *Salmonella*-induced colitis [26–28] and in the systemic control of *Salmonella* infections [29, 30]; *S100A9*, the gene that encodes one of the two subunits of calprotectin, an antimicrobial heterodimer that acts as a metal-sequestering protein, which can starve *Salmonella* and many other microorganisms of critical nutrients, such as zinc and manganese [24, 31]; *Lcn2*, the gene that encodes the antimicrobial peptide lipocalin-2, which sequesters iron-laden siderophores to inhibit *Enterobacteriaceae* growth [32]. We and others had already noted that transcript levels of *Ifnγ*, *S100A9*, *and Lcn2* were increased in the ceca of WT streptomycin-pretreated mice during *S.* Typhimurium infection [24, 33].

We next chose to compare transcript levels in WT and *Ifnar1*$^{-/-}$ mice, which were both previously PR8- or mock-infected, and secondarily infected with *S.* Typhimurium, following the infection model depicted in Fig 2A. At 8 dpi, cecal tissue was excised from the large intestines of WT and *Ifnar1*$^{-/-}$ mice, and transcription of the candidate antimicrobial genes was measured by qPCR. Although basal transcription of *Ifnγ*, *S100A9* and *Lcn2* was similar between mock-infected WT and mock-infected *Ifnar1*$^{-/-}$ mice (Fig 3A, 3C and 3E), the transcription of *Ifnγ and Lcn2* was significantly higher in the ceca of the *Ifnar1*$^{-/-}$ group, compared to the WT group, after infection with *S.* Typhimurium alone (Fig 3A and 3E). Moreover, PR8 infection alone did not change the induction level of these genes in the ceca of WT and *Ifnar1*$^{-/-}$ mice (Fig 3A, 3C and 3E).

However, WT mice secondarily infected with *S.* Typhimurium had a significant reduction in the transcription levels of all three genes, especially *S100A9*, compared to those only infected with *S.* Typhimurium (Fig 3A, 3C and 3E). By contrast, *Ifnar1*$^{-/-}$ mice showed no difference in the transcript levels of these genes when comparing secondarily *S.* Typhimurium-infected mice with *S.* Typhimurium-only infected mice (Fig 3A, 3C and 3E). Differences were also confirmed in WT mice at the protein level; Western Blot revealed drastically reduced production of S100A9 and Lcn2 in the ceca of the secondarily *S.* Typhimurium-infected mice compared to the *S.* Typhimurium-only infected mice (Fig 3B and 3F). As expected, *Ifnar1*$^{-/-}$ groups showed no difference in the expression of these antimicrobial peptides when comparing the two infection groups (Fig 3D and 3H). The concentration of Ifnγ in the serum of either WT and *Ifnar1*$^{-/-}$mice infected only with PR8 or PBS did not rise above basal levels (36 pg/ml for WT-PR8 and 66 pg/ml for *Ifnar1*$^{-/-}$-PR8-infected groups; Fig 3G). Yet, the serum level of Ifnγ was found drastically reduced in the secondarily infected WT group, in comparison with the *S.* Typhimurium-only infected WT group; by contrast, no disparity was detected between the same groups in the *Ifnar1*$^{-/-}$ cohort (Fig 3G).

Similar effects were observed when the i.p. pIC model instead of the PR8 infection was employed (S5 Fig). S100A9 and Lcn2 were both strongly inhibited at the transcript (S5A and S5B Fig) and protein level (S5E and S5F Fig) in the ceca of WT but not *Ifnar1*$^{-/-}$ mice following pIC treatment then *S.* Typhimurium infection. Cecal *Ifnγ* transcription levels were also reduced by pIC treatment in the WT mice infected with *S.* Typhimurium, but not in the *S.* Typhimurium-infected *Ifnar1*$^{-/-}$ mice (S5C Fig). Moreover, pIC treatment dramatically lowered the Ifnγ

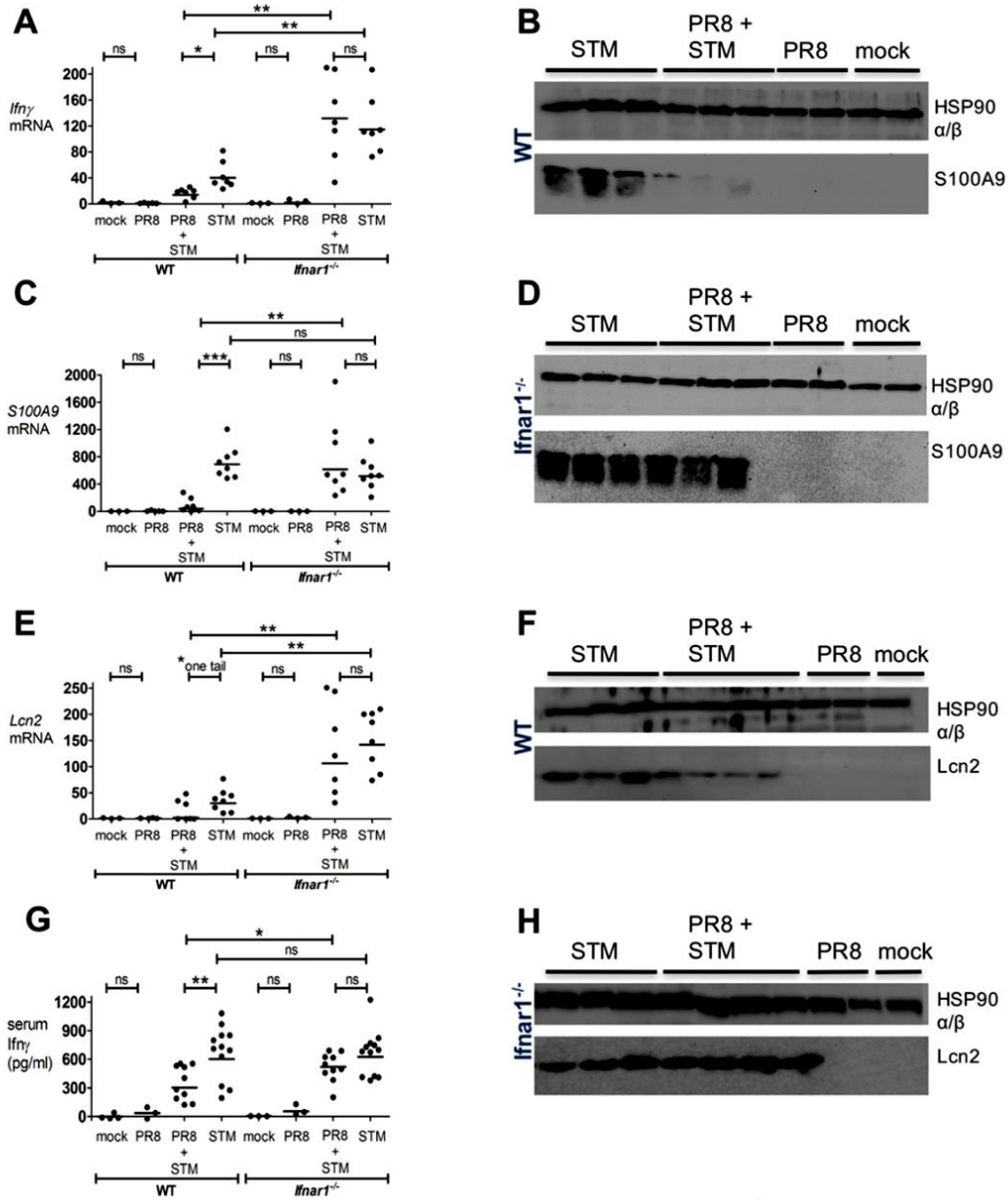

Fig 3. PR8-induced IFN-Is inhibit antimicrobial activity during *S.* Typhimurium infection. WT and *Ifnar1*$^{-/-}$ mice were infected with PR8 or PBS on day 0, followed by intragastric (i.g.) infection with *S.* Typhimurium or LB at 5 dpi. A, C, E) *Ifnγ*, *S100A9* and *Lcn2* transcript levels were detected by qPCR in the mouse cecum of WT and *Ifnar1*$^{-/-}$ at 8 dpi. G) Ifnγ level was detected by ELISA in the serum of WT and *Ifnar1*$^{-/-}$at 8 dpi. B, D) S100A9 and F, H) Lcn2 were

detected by immunoblot in the mouse cecum of WT (B, F) and *Ifnar1*$^{-/-}$ (D, H) at 8 dpi. Each dot represents one mouse, the geometric mean is indicated. *P* values were calculated by two-tailed Mann-Whitney test.*p < 0.05, **p < 0.01, ***p < 0.001; ns, not significant. Two independent experiments are shown in A, C, and E. Three independent experiments are shown in G. One representative experiment is shown in B, D, F and H. N of mice used in each group in (A, C, E, G): mock = 3–4 WT and 3 *Ifnar1*$^{-/-}$, PR8 = 3–5 WT and 3 *Ifnar1*$^{-/-}$, PR8+STM = 7–10 WT and 7–10 *Ifnar1*$^{-/-}$, STM = 7–12 WT and 7–12 *Ifnar1*$^{-/-}$. N of mice used in each group in (B, D): mock = 2 WT and 2 *Ifnar1*$^{-/-}$, PR8 = 2 WT and 2 *Ifnar1*$^{-/-}$, PR8+STM = 3 WT and 3 *Ifnar1*$^{-/-}$, STM = 3 WT and 3 *Ifnar1*$^{-/-}$. N of mice used in each group in (F, H): mock = 1 WT and 1 *Ifnar1*$^{-/-}$, PR8 = 2 WT and 2 *Ifnar1*$^{-/-}$, PR8+STM = 4 WT and 4 *Ifnar1*$^{-/-}$, STM = 3 WT and 3 *Ifnar1*$^{-/-}$.

doi:10.1371/journal.ppat.1005572.g003

serum level in the *S.* Typhimurium-infected WT mice, but not in the *S.* Typhimurium-infected *Ifnar1*$^{-/-}$ mice (S5D Fig).

All together, our findings demonstrate that IFNAR1-mediated signaling can inhibit the host antimicrobial response to *Salmonella* infection.

Influenza-induced IFN-Is downregulate the inflammatory response in the intestine of mice infected with *S.* Typhimurium

To broaden our study of the effects IFN-Is have on the level of cytokine expression in an inflammatory setting such as *Salmonella*-induced colitis, we examined the expression of the pro-inflammatory genes *Il6* and *Cxcl2*, and the anti-inflammatory genes *Il10* and *Muc2*. IL-6 and CXCL2 play important roles in macrophage activation and neutrophil function and recruitment. IL-10 and MUC2 are considered essential immunoregulators in the intestinal tract. IL-10 mainly functions to dampen excessive inflammatory responses that risk damaging the host [34, 35]. MUC2 is critical for colon protection, as *Muc-2* deficient mice spontaneously develop colitis [36, 37]. Their transcript level in the cecum was assessed in both WT and *Ifnar1*$^{-/-}$ mice at 8 dpi after PR8 or mock infection, and following a secondary *S.* Typhimurium infection. After *S.* Typhimurium infection, both pro-inflammatory genes were induced in the cecum of WT and *Ifnar1*$^{-/-}$ mice (Fig 4A and 4C).

Significantly higher transcription of *Il6* was observed in *S.* Typhimurium-only infected *Ifnar1*$^{-/-}$ mice compared to *S.* Typhimurium-only infected WT mice (Fig 4A). Interestingly, in WT but not *Ifnar1*$^{-/-}$ mice, the secondarily infected *S.* Typhimurium group showed significantly lower levels of pro-inflammatory gene transcription than the *S.* Typhimurium-only infected group (Fig 4A and 4C). By contrast, PR8 infection enhanced cecal *Il10* levels in an IFNAR1-dependent manner (Fig 4B). Basal transcript expression of *Il10* was overall similar in mock-infected WT and *Ifnar1*$^{-/-}$ mice. However, we observed a lower level of induction of *Il10* in *S.* Typhimurium-only infected *Ifnar1*$^{-/-}$ mice compared to *S.* Typhimurium-only infected WT mice (Fig 4B). We did not detect upregulation of *Muc2* in *S.* Typhimurium-only infected WT or *Ifnar1*$^{-/-}$ mice, although our samples showed a high level of variability (Fig 4D). However, in WT but not *Ifnar1*$^{-/-}$ mice, PR8 infection enhanced cecal *Muc2* levels. Furthermore, we observed an approximately 10-fold upregulation of *Muc2* in the secondarily infected WT group compared to the *S.* Typhimurium-only infected WT group (Fig 4D).

To further study the contribution of IFN-Is in the modulation of the intestinal host response during *Salmonella* infection, we examined the transcription of *Ifnβ and Ifnα4* in both the lungs and cecum of mice infected with PR8. We found their induction in the lungs but not in the cecum. We also examined the transcription level of *Cxcl10* and *Mx1*, ISGs strongly induced by IFN-Is. Strikingly, we observed approximately 10-fold upregulation of *Cxcl10* in the cecum of PR8-infected WT mice compared to mock-infected WT mice. In contrast, no difference was detected between *Ifnar1*$^{-/-}$ groups (Fig 4E). Moreover, in WT but not *Ifnar1*$^{-/-}$ mice secondarily-infected with *S.* Typhimurium, the level of induction of *Cxcl10* in the cecum was approximately 4-fold higher than *S.* Typhimurium-only infected mice (Fig 4E). Similarly, the cecal expression of *Mx1* was largely upregulated after PR8 infection in the WT mice, but not in the *Ifnar1*$^{-/-}$ mice, and as anticipated the level of induction of *Mx1* tended to be lower overall in the

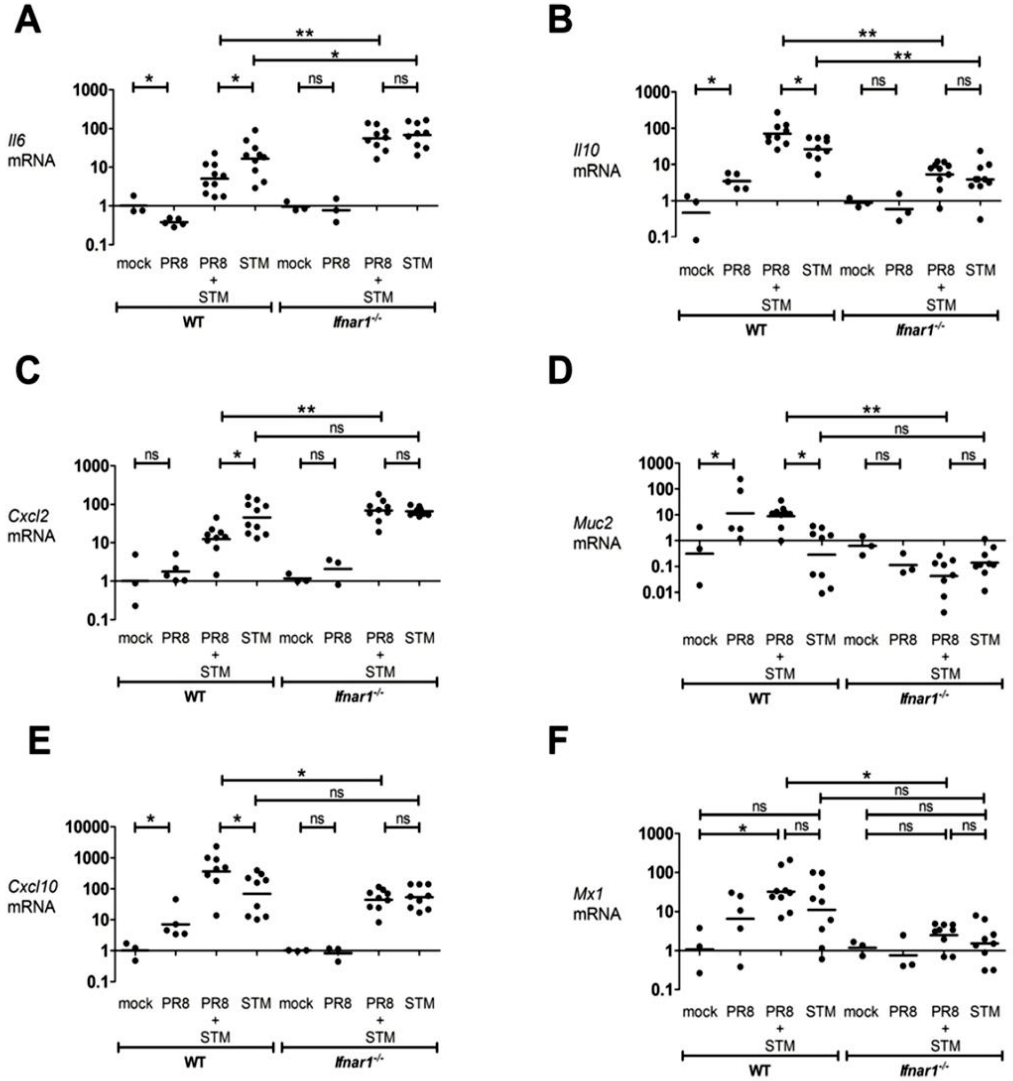

Fig 4. PR8-induced IFN-Is reduce inflammatory response in the gut during *S.* Typhimurium infection. WT and *Ifnar1*$^{-/-}$ mice were infected with PR8 or PBS on day 0, followed by i.g. infection with *S.* Typhimurium or LB at 5 dpi. (A) *Il6*, (B) *Il10*, (C) *Cxcl2*, (D) *Muc2*, (E) *Cxcl10* and (F) *Mx1* transcript levels were detected by qPCR in the cecum of WT and *Ifnar1*$^{-/-}$ mice at 8 dpi. Each dot represents one mouse, the geometric mean is indicated. *P* values were calculated by two-tailed Mann-Whitney test. *$p < 0.05$, **$p < 0.01$; ns, not significant. Two independent experiments are shown. N of mice used in each group in (A, B, C, D, E, F): mock = 3 WT and 3 *Ifnar1*$^{-/-}$, PR8 = 5 WT and 3 *Ifnar1*$^{-/-}$, PR8+STM = 8–10 WT and 8–10 *Ifnar1*$^{-/-}$, STM = 8–10 WT and 8–10 *Ifnar1*$^{-/-}$.

doi:10.1371/journal.ppat.1005572.g004

Ifnar1$^{-/-}$ mice compared to WT mice (Fig 4F). Remarkably, we observed a 12-fold upregulation of *Mx1* in the secondarily infected WT mice compared to the secondarily infected *Ifnar1*$^{-/-}$ mice (Fig 4F).

In conclusion, the dissimilar regulation of ISGs in the cecum of WT and *Ifnar1*$^{-/-}$ mice after PR8 infection suggest that type I IFN-mediated signaling significantly contributes to the host response against *S.* Typhimurium infection.

Histopathology from the cecum extracted at 8 dpi illustrates that WT and *Ifnar1*$^{-/-}$ mice develop severe inflammation 72 h after infection with *S.* Typhimurium, whereas no abnormalities are seen after PR8 or mock infection. However, WT mice infected with PR8 followed by *S.* Typhimurium infection had reduced inflammation compared to WT mice infected with *S.* Typhimurium alone (Fig 5A). Indeed, the mucosal integrity (assessed by cryptitis and epithelial erosions), inflammatory cell infiltration and submucosal edema were exacerbated in the *S.* Typhimurium-only infected WT group compared to secondarily infected WT group (Fig 5B and 5C). However, no difference in the histopathology was noted between *S.* Typhimurium-only infected *Ifnar1*$^{-/-}$ group compared to secondarily infected *Ifnar1*$^{-/-}$group (Fig 5A, 5C and 5D). Similar differences in the cecal inflammatory score detected by histopathology were noted when pretreating WT mice with pIC before *S.* Typhimurium infection (S6A–S6C Fig and S7A–S7C Fig). However, pIC did not reduce the inflammatory score in the cecum of *S.* Typhimurium-infected *Ifnar1*$^{-/-}$ mice (S6A, S6C and S6D Fig; S7A, S7C and S7D Fig).

To summarize, during *S.* Typhimurium-induced colitis, prior infection with influenza alters gut immune response promoting anti-inflammatory cytokines and reducing pro-inflammatory cytokines through an IFNAR1-dependent mechanism. The end result is a decrease, mediated by IFN-Is, of the intestinal tissue damage in mice that were first infected with influenza prior to *S.* Typhimurium infection.

Discussion

IFN-Is are primarily considered to be antiviral and immunomodulatory cytokines [38]; their effects during bacterial infection are still controversial. Although IFN-Is have been shown to protect against and limit infection with certain bacterial pathogens [39, 40], they can also impair the clearance of others [41, 42]. This suggests a complex and bacterium-specific mechanism of action.

Influenza virus is a major cause of respiratory illness in humans, with the potential to cause lung damage and sensitize the host to secondary pulmonary infections [1]. Although gastroenteritis symptoms have been reported during infection, the mechanism through which influenza virus would affect the gut is not completely clear. Our studies have shown that influenza pulmonary infection has an effect on the mouse fecal microbiota and promotes secondary infection with the intestinal pathogen, *S.* Typhimurium. Importantly, we have shown that these effects are dependent on IFN-Is, which are induced in the lungs during influenza pulmonary infection. These in turn can alter the gut microbial composition and suppress host immunity to a secondary *Salmonella* intestinal infection.

In line with a previous study [6], we found that PR8 infection and poly I:C treatment increased the relative abundance of *Enterobacteriaceae* and decreased the number of *SFB* in the fecal content of WT mice. However, we found that the relative abundance of these bacterial groups remained unchanged after PR8 infection or poly I:C treatment in mice deficient in IFN-I signaling, demonstrating that IFN-Is play an essential role in regulating their numbers. Based on these results and consistent with previous observations [43], we speculate that IFN-Is might regulate the populations of the major bacterial phyla within the intestinal tract. Moreover, our analysis showed that only particular members of the fecal microbiota were affected by PR8-induced IFN-Is. While anaerobes, such as Bacteroidetes and Firmicutes, make up the majority of the healthy microbiota, IFN-Is released during influenza infection promote the blooming of indigenous Proteobacteria pathobionts to the detriment of restricted anaerobic

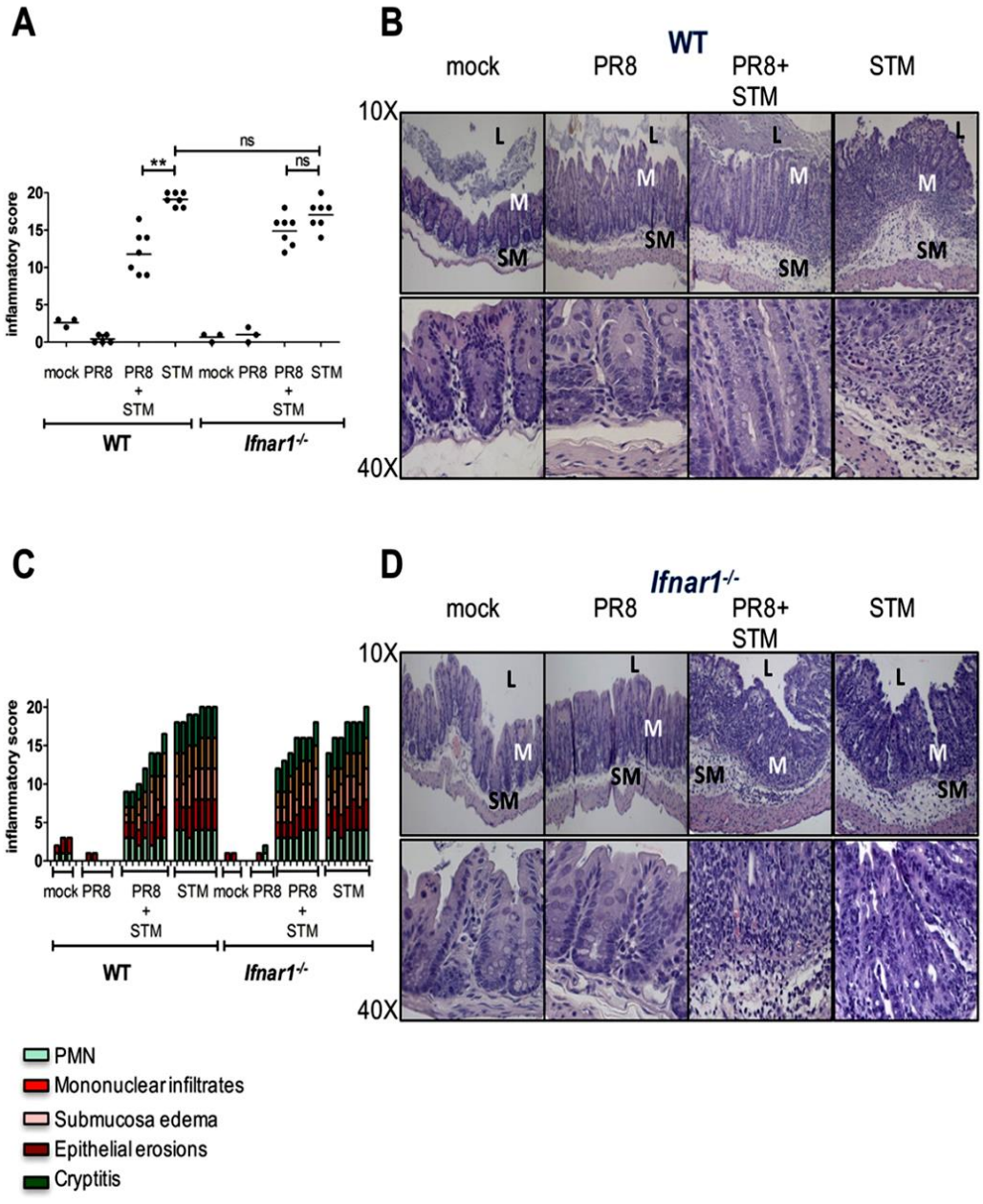
A
B
WT
mock
PR8
PR8+ STM
STM
10X
40X
L
M
SM
inflammatory score
ns
**
ns
mock PR8 PR8 + STM STM mock PR8 PR8 + STM STM
WT
Ifnar1-/-
C
D
Ifnar1-/-
PMN
Mononuclear infiltrates
Submucosa edema
Epithelial erosions
Cryptitis

Fig 5. PR8-induced IFN-Is reduce intestinal pathology during *S.* Typhimurium infection. Cecal histopathology of WT (A, B and C) and *Ifnar1*$^{-/-}$ (A, C and, D) mice. Blinded histopathology scores of cecal samples collected at 8 dpi from PR8- and mock-infected WT and *Ifnar1*$^{-/-}$ mice, administered or not with *S.* Typhimurium at 5 dpi. The score of individual mice (circles) and the geometric mean for each group (bars) are indicated in (A). *P* values were calculated by two-tailed Mann-Whitney test. **$p < 0.01$; ns, not significant. Two independent experiments are shown. N of mice used in each group in (A, C): mock = 3 WT and 3 *Ifnar1*$^{-/-}$, PR8 = 5 WT and 3 *Ifnar1*$^{-/-}$, PR8+STM = 7 WT and 7 *Ifnar1*$^{-/-}$, STM = 7 WT and 7 *Ifnar1*$^{-/-}$. A detailed scoring for the animals shown in (A) is provided; each stacked column represents an individual mouse in (C). B, D) Hematoxylin and eosin (H&E)-stained sections from representative animals for each group in WT (B) and *Ifnar1*$^{-/-}$ (D) mice. An image at lower magnification (10X) and one at higher magnification (40X) from the same section are shown. Abbreviations are as follows: L, lumen; M, mucosa; SM, submucosa.

doi:10.1371/journal.ppat.1005572.g005

commensals, leading to significant intestinal disbyosis. This is in accordance with previous findings that show that bacterial imbalance characterized by an enrichment of Proteobacteria is observed during intestinal inflammatory disorders in humans, including Crohn's disease [44] and enteropathy in human immunodeficiency virus (HIV)-infected subjects [45].

In addition, we show that influenza- and poly I:C-induced IFN-Is promote the intestinal overgrowth of the bacterial pathogen *S.* Typhimurium, which is an important component of *Enterobacteriaceae* and clinically associated with severe gastroenteritis and inflammatory diarrhea in humans [46].

Furthermore, we showed that *Ifnar1*$^{-/-}$ mice were more resistant to weight loss during *S.* Typhimurium secondary infection than WT mice, and allowed less translocation of *S.* Typhimurium across the intestinal wall. Not surprisingly, we also reported an increased resistance in *Ifnar1*$^{-/-}$ mice against single *S.* Typhimurium infection, as indicated by reduced weight loss and bacterial dissemination, as well as higher induction of specific antibacterial genes, compared to *S.* Typhimurium-only infected WT mice. This is in agreement with previous reports where *S.* Typhimurium has been shown to induce the expression of IFN-Is by macrophages [47], along with improved host survival and enhanced control of *S.* Typhimurium in *Ifnar1*$^{-/-}$ mice in a necroptosis-dependent mechanism [48]. While there were differences between *S.* Typhimurium-only infected WT and *Ifnar1*$^{-/-}$ mice, these differences were strongly exacerbated when mice were previously infected with PR8, indicating the contribution of IFN-Is produced during influenza infection to secondary *S.* Typhimurium infection.

Considering that the number of *S.* Typhimurium that disseminated systemically was greatly increased following influenza infection in WT, but not in *Ifnar1*$^{-/-}$ mice, this suggests that IFN-Is may potentially relax the intestinal barrier to allow for *Salmonella* systemic dissemination. In support of this, we found that the host inflammatory and antimicrobial responses against *S.* Typhimurium were reduced in the intestine after influenza infection in a mechanism dependent on IFNAR. Host inflammatory responses are essential to keep *Salmonella* localized to the gut and to limit the systemic spread of the pathogen. The immunosuppression mediated by IFN-Is would diminish local host surveillance, resulting in poor control of *Salmonella* in the gut and enhanced bacterial dissemination. We demonstrated that the induction of IFN-γ was decreased at the transcriptional level in the inflamed cecum and at the protein level systemically in an IFN-I-dependent manner. This is important given the key role IFN-γ plays in intestinal antibacterial immunity, host survival and resolution of *Salmonella* infection [49].

The host inflammatory response against *Salmonella* in the gut [50] includes the synthesis of antimicrobial peptides, some of which may possess a secondary function as regulatory molecules [51]. Two critical components of the mammalian nutritional immune response against *S.* Typhimurium are lipocalin-2 and calprotectin, which are both highly induced by this pathogen in the inflamed gut. Lipocalin-2 and calprotectin sequester essential nutrients from microorganisms and exert an antimicrobial effect against several bacteria, including intestinal commensals. Both antimicrobials were dramatically suppressed in the inflamed gut after PR8 infection in a mechanism that depended on IFNAR signaling. Paradoxically, we know that the metal deficiency induced by high levels of both antimicrobials can be evaded by *Salmonella*

through expression of high-affinity metal transporters [24, 52]. However, metal starvation may still have a critical defensive role against *Salmonella* by forcing infected host cells in the local microenvironment to undergo apoptosis [53, 54], thereby destroying the internalized *Salmonella*. Furthermore, both antimicrobial peptides act as crucial paracrine chemoattractants to recruit neutrophils [55, 56], which play a major role in preventing systemic dissemination of *S.* Typhimurium, as suggested by clinical and experimental data [57]. Additionally, the induction in the gut of anti-inflammatory *Il10* after influenza infection might, not only inhibit the bactericidal response of macrophages, but also cause infected macrophages to function as hosts for bacterial replication, as previously shown [58]. IL-10 has been shown to be important in the pathogenesis of *Salmonella* infection and regulation of subsequent host immune responses. IL-10 levels are elevated in susceptible strains of mice [59] suggesting that those strains producing IL-10 at high levels cannot adequately control *Salmonella* infection. Moreover, the relevance of the anti-inflammatory role mediated by IFN-Is in the gut during *Salmonella* infection was confirmed by histopathology, which underscores the concept of the double-edged sword IFN-Is represent during secondary intestinal infections. Although IFN-I-mediated effects promote *Salmonella* intestinal colonization and systemic dissemination, they also limit the damage triggered by exacerbated inflammation induced by *Salmonella* infection. Furthermore, several clinical trials could not completely define the therapeutic effects of IFN-Is in patients with ulcerative colitis, an IBD with a complex etiology that includes genetic and environmental factors leading to chronic inflammatory responses against the gut microbiota [60, 61]. This raises important questions about the potential mechanisms of action of IFN-Is in IBDs such as ulcerative colitis. Notably, IFNβ therapy markedly attenuates the course and severity of disorders such as Multiple Sclerosis (MS). Indeed, *in vitro* studies previously showed that IFNβ induced the release of the anti-inflammatory cytokine IL-10 from lymphocytes acquired from patients with MS [62, 63], which might indicate that IFNβ could eventually induce an anti-inflammatory response in the colonic mucosa as well.

Many investigators have reported a variety of both beneficial and detrimental immune functions for IFN-Is during bacterial infections, and this clearly expands the old misguided notion that IFN-Is serve "only" as antiviral cytokines. Specifically, we have examined the effects of IFN-Is induced by pulmonary influenza infection in intestinal bacterial homeostasis and during secondary enteric infection. We propose that during influenza infection, this family of cytokines alters the intestinal microbiota composition, leading to an overgrowth of pathobionts which puts the host at risk to develop intestinal bacterial disorders. This is particularly significant as IFN-Is are currently being used as anti-inflammatory therapies for several immunological disorders such as IBD and MS.

Furthermore, we propose that influenza-induced IFN-Is enhance susceptibility to *Salmonella* intestinal colonization and dissemination during secondary *Salmonella*-induced colitis through suppression of host intestinal immunity.

Our work highlights the critical importance of further studies that clarify the roles and effects IFN-Is play in balancing host susceptibility to bacterial infection and inflammatory control, as well as the potential risk associated with influenza infection in predisponing the host to *Salmonella* infections and intestinal disorders.

Materials and Methods

Bacterial strain and culture conditions

IR715 is a fully virulent, nalidixic acid-resistant derivative of *Salmonella enterica* serotype Typhimurium WT isolate ATCC 14028 [64]. The strain was cultured aerobically in Luria Bertani (LB) broth at 37°C. Bacterial strains and plasmids used in this study are listed in S1 Table.

Carbenicillin was added to final 100 mg/L as needed. To render all strains equally resistant to streptomycin, pHP45omega plasmid [65] was introduced by electroporation.

Mouse experiments

7–9 week old mice with a C57BL/6J genetic background were used in all experiments. *Ifnar1*$^{-/-}$mice were generated as previously reported [42]. The same number of males and females were used in each treatment group. Colonies of *Ifnar1*$^{-/-}$ and WT mice were maintained and housed in the same pathogen-free facilities at UCLA. The mouse studies described in this manuscript were performed under the written approval of the UCLA Animal Research Committee (ARC) in accordance to all federal, state, and local guidelines. All studies were carried out under strict accordance to the guidelines in The Guide for the Care and Use of Laboratory Animals of the National Institutes of Health and the accreditation and guidelines of the Association for the Assessment and Accreditation of Laboratory Animal Care (AALAC) International under UCLA OARC Protocol Number 2009-012-21.

Viral mouse infection and lung collection

Mice were infected with a sublethal dose (200 PFU) of the mouse-adapted influenza A/Puerto Rico/8/34 (PR8) virus strain by non-surgical intratracheal instillation [66].

Briefly, mice were anesthetized with a mixture of ketamine and xylazine (100 mg/10 mg/kg), suspended by an incisor wire on an angled stand, and then a fixed volume containing 200 PFU of PR8 in pharmaceutical grade PBS was instilled inside the trachea [66]. Following aspiration of the inoculum into the lungs, mice were maintained on warming pads and monitored until completely ambulatory. Mice were monitored daily and weight was recorded. On day 1, 8 or 17 after PR8 (or mock) infection, mice were euthanized by CO_2 asphyxiation. Lungs were excised, lobes were separated and placed in a 2 mL FastPrep homogenization tube containing lysing matrix D. Sterile DPBS was added to give a final 20% w/v suspension and homogenized using a FastPrep-24 Instrument, 6 m/s, 45 s (MP Biomedicals, Santa Ana, CA). Lung homogenate was diluted 1:10 in TRIzol Reagent (Life Technologies, Grand Island, NY) for analysis of gene expression, or serially diluted with DPBS for quantification of bacterial burden by CFU analysis and viral titer by plaque assay.

Viral titering

Viral titer was determined by plating a monolayer of MDCK cells in 6-well tissue culture treated plates, then incubating with lung homogenate, serially diluted in virus dilution buffer (PBS with 1% Pencillin/Streptomycin, 0.2% BSA, 0.005% DEAE Dextran, 1X $CaCl_2/MgCl_2$), for 1 h at 37°C. Extracellular virus was removed by gently washing the monolayer, then an overlay containing 2% low melting point agarose in virus growth medium (MEM containing BME vitamins, 10 mM HEPES, 1% Pencillin/Streptomycin, 0.15% $NaHCO_3$, 0.2% BSA, 0.0015% DEAE Dextran, 0.7 mg/ml TPCK-treated Trypsin) was applied and plates were incubated for 2 days at 37°C. The overlay was gently aspirated, then the plates were incubated with 0.3% crystal violet in 20% ethanol and plaque forming units (PFU) were enumerated.

Analysis of the fecal microbiota after influenza infection

Mice were administered 200 PFU of PR8 virus or PBS through non-surgical intratracheal instillation [66].

Mice were monitored daily at the same time until day 17, when all the mice were euthanized.

Fecal samples were collected from WT and *Ifnar1*$^{-/-}$ mice before PR8 or mock infection on day 0 and at 9 dpi, then snap frozen in liquid nitrogen. The fecal DNA was subsequently

extracted using the QIAamp DNA stool kit (Qiagen), according to the manufacturer's instructions. The fecal microbial DNA was used for 16S quantitative real-time PCR (qPCR) analysis and for Illumina MiSeq analysis.

Two μl of extracted fecal bacterial DNA was used as a template for 16S qPCR reaction with the primer pairs previous developed and presented in S2 Table. The 16S gene copy numbers per μl of DNA from each sample (one fecal pellet collected from each mouse) was determined using the plasmids described in S1 Table.

For MiSeq analysis, bacterial DNA was amplified by a two-step PCR enrichment of the 16S rDNA (V4 region) encoding sequences from each sample with primers 515F and 806R modified by addition of barcodes for multiplexing. Libraries were sequenced using an Illumina MiSeq system. Following quality filtering, the sequences were demultiplexed and trimmed before performing sequence alignments, identification of operational taxonomic units (OTU), clustering, and phylogenetic analysis using QIIME open-source software (http://qiime.org).

Secondary *S.* Typhimurium infection

Mice were infected on day 0 with 200 PFU of PR8 influenza strain or PBS through non-surgical intratracheal instillation [66]. WT and *Ifnar1*$^{-/-}$ mice were orally gavaged with 0.1 ml of a 200 mg/ml streptomycin/sterile water solution on day 4, prior to mock infection in LB or oral infection with 1×10^7 CFU of *S.* Typhimurium in LB on day 5. Colon content was collected at 48 h postbacterial infection, weighed, homogenized in 1 ml of sterile PBS, serial diluted and plated on LB agar containing appropriate antibiotics. At 72 h post-bacterial infection the cecum was harvested for mRNA, protein, and histopathology. The colon contents, spleen, lungs and mesenteric lymph nodes (MLN) were collected, serially diluted, and plated on appropriate antibiotic LB agar plates to determine bacterial counts. Lungs were harvested for mRNA isolation and plaque assay. Blood was collected by cardiac puncture, allowed to clot at room temperature; serum was isolated by centrifugation, transferred to a sterile tube and stored at -80°C until ELISA cytokine analysis. Groups of 4–6 mice were used for each experiment. Mouse weight was taken daily until euthanasia.

For the typhoid model, WT and *Ifnar1*$^{-/-}$ mice were infected on day 0 with 200 PFU of PR8 influenza strain or PBS through non-surgical intratracheal instillation [66]. Mice were gavaged with 1×10^3 CFU of *S.* Typhimurium in LB, without streptomycin pre-treatment, on day 5. The colon contents were collected at 72h post bacterial infection, serially diluted, and plated on appropriate antibiotic LB agar plates to determine bacterial counts.

Analysis of the fecal microbiota after poly I:C treatment

Polyinosinic polycytidylic acid (#tlrl-pic) was purchased from Invivogen (San Diego, CA). Mice were administered 50 μg of pIC or saline through non-surgical intratracheal instillation [66] on day 0 and on day 2. Fecal samples were collected from WT and *Ifnar1*$^{-/-}$ mice on day 0 before treatment and on day 4 and day 5, then snap frozen in liquid nitrogen. The fecal DNA was subsequently extracted using the QIAamp DNA stool kit (Qiagen), according to the manufacturer's instructions. The fecal microbial DNA was used for 16S qPCR analysis, as described above, and the copy numbers' fold increase from each mock and pIC-treated sample (one fecal pellet collected from each mouse) on day 4 and day 5 over the baseline before treatment on day 0 were calculated.

Poly I:C treatment during *S.* Typhimurium infection

In the i.p. pIC model, WT and *Ifnar1*$^{-/-}$ mice were intraperitoneal injected with 150 μg of pIC or saline on day -1, and intragastrically treated with streptomycin (0.1 ml of a 200 mg/ml

solution in sterile water) [22] on day -1. Alternatively, in the non-surgical intratracheal instillation pIC model, WT and *Ifnar1*$^{-/-}$ mice were injected with 50 μg of pIC or saline on day -1, and intragastrically treated with streptomycin (0.1 ml of a 200 mg/ml solution in sterile water) [22] on day -1. In both models, mice were then orally gavaged with a dose of 10^7 CFU of *S.* Typhimurium in 0.1 ml of LB on day 0 or mock-infected. A booster dose of 100 μg or 50 μg of pIC was administered on day 2 or on day 1 in the i.p pIC or in the non-surgical intratracheal instillation pIC models, respectively.

On day 3, corresponding to 72 h post *S.* Typhimurium infection, mice were euthanized; the cecum was collected for mRNA and protein isolation and also for histopathological analysis. Serum was separated from blood and collected for ELISA cytokine detection. CFU was enumerated from homogenates of colon content, MLN, lungs and spleen serially diluted and plated on agar plates containing the appropriate antibiotic selection.

Quantitative real-time PCR

Total RNA was extracted from mouse cecal tissue with TRIzol Reagent (Life Technologies). Reverse transcription of 1 μg of total RNA was performed with the iScript cDNA Synthesis kit (Bio-Rad). qPCR was performed using iTaq Universal Sybr Green Supermix (Bio-Rad). For analysis, target gene expression of each sample was normalized to the respective level of *L32* mRNA. Fold changes in gene expression values were then calculated using the mean from the control samples as a baseline and determined using the $\Delta\Delta$ Ct method. A list of qPCR primers used in this study is provided in S2 Table. See also S1 References.

Murine cytokine ELISA

Mouse IFNγ ELISA Ready-SET-Go! was purchased from eBioscience. Cytokine serum levels were measured according to the manufacturer's instructions.

Immunoblot

Total protein was extracted from mouse cecum tissue using TRIzol Reagent (Life Technologies, Grand Island, NY). 15 μg of total protein was resolved using 12.5% SDS-PAGE gels and transferred to PVDF membranes. The membranes were blocked with 2% nonfat dried milk and incubated at 4°C with primary antibodies. Detection of mouse HSP90 α/β was performed with primary rabbit polyclonal antibodies (Santa Cruz Biotechnology), while detection of S100A9 was performed with polyclonal goat anti-mouse S100A9 (R&D Systems). Lcn-2 was detected by polyclonal goat anti-mouse Lcn2 (R&D Systems). After overnight incubation at 4°C, the blots were washed and then incubated for 1 h at room temperature with secondary goat anti-rabbit and donkey anti-goat antibodies conjugate to horseradish peroxidase (HRP) (Southern Biotech and Santa Cruz Biotechnology, respectively). After washing, bands were developed using the SuperSignal West Pico Chemiluminescent Sustrate (Thermo Scientific) per manufacturer's instructions and visualized using Gel Doc (BioRad).

PCR-DGGE analysis

Total genomic bacterial DNA was isolated using the MasterPure DNA purification kit (Epicentre). DNA quality and quantity were determined with a Spectronic Genesys UV spectrophotometer at 260 nm and 280 nm (Spectronic Instruments, Inc. Rochester, NY). Amplification of bacterial 16S rDNA was carried out by PCR as described previously [67]. Briefly, the universal primer set Bac1 and Bac2 [68] (S2 Table) was used to amplify an approximately 300-base-pair internal fragment of the 16S rDNA. Each 50 μl PCR contained 100 ng purified

genomic DNA, 40 pmole each primer, 200 μM of each dNTP, 4.0 mM $MgCl_2$, 5 μl 10 X PCR buffer, and 2.5 U Taq DNA polymerase (Invitrogen). Cycling conditions were 94°C for 3 min, followed by 30 cycles of 94°C for 1 min, 56°C for 1 min and 72°C for 30 s, with a final extension period of 5 min at 72°C. The resulting PCR products were evaluated by electrophoresis through 1.0% agarose. DGGE was performed by use of the Bio-Rad DCode System (Hercules, CA, USA). A 40% to 60% linear DNA denaturing gradient (100% denaturant is equivalent to 7 M urea and 40% de-ionized formamide) was formed in 8% (w/v) polyacrylamide gels. Approximately 300 ng PCR product was applied per lane. The gels were submerged in 1 X TAE buffer (40 mM Tris base, 40 mM glacial acetic acid, 1 mM EDTA) and the PCR products were separated by electrophoresis for 17 h at 58°C using a fixed voltage of 60 V. After electrophoresis, the DNA bands were stained with 0.5 μg/ml ethidium bromide and DGGE profile images were digitally recorded using the Molecular Imager Gel Documentation system (Bio-Rad). DIVERSITY DATABASE Software (Bio-Rad) was used to assess the change in the relative intensity of bands corresponding to bacterial species of interest.

Identification of bacterial species from DGGE gels

The DNA bands of interest were excised from the DGGE gels and transferred to a 1.5-ml microfuge tube containing 20 μl sterile ddH_2O. Tubes were incubated at 4°C overnight before the recovered DNA samples were re-amplified with the universal primer set Bac1 and Bac2. The PCR products were purified using the QIAquick PCR purification kit (Qiagen) and sequenced at the UCLA Core DNA Sequencing Facility. The sequences obtained were subjected to nucleotide BLAST searches against the NCBI (http://blast.ncbi.nlm.nih.gov/) and Human Oral Microbiome (http://www.homd.org/index.php) databases.

Statistics

The differences between treatment groups were analyzed by non-parametric 2-tailed Mann-Whitney U test, non-parametric Kruskal-Wallis test (Dunn's Multiple Comparison Test) and One-Way Analysis of variance (ANOVA) with Bonferroni correction, as specified in each Fig legend. Data were expressed as the geometric mean or mean ± SEM, as indicated in each Fig legend, and the results were considered statistically significant when the p value was < 0.05. All calculations were performed using GraphPad Software, unless indicated otherwise.

Histopathology

Tissue samples were fixed in formalin for 24 h, processed according to standard procedures for paraffin embedding, sectioned at 4 mm, and stained with hematoxylin and eosin. The pathology score of cecal samples was determined by blinded examinations of cecal sections by a board-certified pathologist using previously published methods [22]. Each section was evaluated for the presence of neutrophils, mononuclear infiltrate, submucosal edema, epithelial erosions and cryptitis. Inflammatory changes were scored from 0 to 4 according to the following scale: 0 = none; 1 = low; 2 = moderate; 3 = high; 4 = extreme. The inflammation score was calculated as a sum of each parameter score and interpreted as follows: 0–3 = within normal limits; 4–8 = mild; 9–14 = moderate; 15–20 = severe.

Ethics statement

The mouse studies described in this manuscript were performed under the written approval of the UCLA Animal Research Committee (ARC) in accordance to all federal, state, and local guidelines. All studies were carried out under strict accordance to the guidelines in The Guide

for the Care and Use of Laboratory Animals of the National Institutes of Health and the accreditation and guidelines of the Association for the Assessment and Accreditation of Laboratory Animal Care (AALAC) International under UCLA OARC Protocol Number 2009-012-21. Influenza infections were performed under ketamine/xylazine anesthesia and all efforts were made to minimize animal pain and discomfort.

Supporting Information

S1 Fig. Changes in the fecal microbiota after PR8 infection and poly I:C treatment are mediated by IFN-Is. A and B) WT and *Ifnar1*$^{-/-}$ mice (n = 4 WT, n = 4 *Ifnar1*$^{-/-}$) were infected with PR8 (n = 3 WT, n = 3 *Ifnar1*$^{-/-}$) or PBS (n = 1 WT, n = 1 *Ifnar1*$^{-/-}$) on day 0 through non-surgical intratracheal instillation. Viral titer was determined by plaque assay in lungs and colon content on day 1 after PR8 infection (A). The levels of the influenza virus–derived matrix M protein gene in both lung and cecum tissues were quantified by qPCR on day 1 after infection (B). C) Analysis of the *Segmented Filamentous Bacteria* (*SFB*) using 16S rRNA gene qPCR from fecal samples collected from mice on day 0 before infection (n = 9 WT, n = 8 *Ifnar1*$^{-/-}$), on day 9 after mock (n = 4 WT, n = 4 *Ifnar1*$^{-/-}$) and PR8 infection (n = 5 WT, n = 4 *Ifnar1*$^{-/-}$). Displayed are copy numbers of *SFB* per μl of fecal microbial DNA. Each dot represents one mouse, the geometric mean is indicated. D, E and F) Mice were treated with pIC (n = 4 WT, n = 3 *Ifnar1*$^{-/-}$) or saline (n = 4 WT, n = 3 *Ifnar1*$^{-/-}$) through non-surgical intratracheal instillation on day 0 and on day 2. Mice were euthanized on day 9. Fecal samples were collected from WT and *Ifnar1*$^{-/-}$ mice on day 0 before treatment and on day 4 and day 5 after treatment (D). Analysis of the fecal *Enterobacteriaceae* (E) and *SFB* (F) using 16S qPCR. Data are expressed as copy numbers' fold increase of mock- and pIC-treated on day 4 and day 5 over the baseline before treatment on day 0. Data are expressed as mean ± SEM. P values were calculated by Kruskal-Wallis (Dunn's multiple comparison test) in (C) and by two-tailed Mann-Whitney test in (E and F). *p value < 0.05, **$p < 0.01$; ns, not significant. One representative experiment is shown. Abbreviations are as follows: n.d., not detected.
(TIF)

S2 Fig. Influenza-induced IFN-Is enhance host sensitivity to secondary *S.* Typhimurium infection. A) Lung PR8 was measured by qPCR at 8 dpi, and its relative expression to *L32* was calculated in WT and *Ifnar1*$^{-/-}$ mice that were infected with either PR8-only or secondarily infected with *S.* Typhimurium. One representative experiment is shown. N of mice used in each group in (A): PR8 = 5 WT and 2 *Ifnar1*$^{-/-}$, PR8+STM = 10 WT and 4 *Ifnar1*$^{-/-}$. *P* values were calculated in (A) using non-parametric Kruskal-Wallis test (Dunn's multiple comparison test). B) Relative abundance of *Salmonella* in colon content of WT (left) and *Ifnar1*$^{-/-}$ (right) mice revealed by PCR-Denaturing Gradient Gel Electrophoresis (DGGE). Red arrows indicate the *Salmonella* band; mock: mock-infected mice on day 0; PR8: mice infected with PR8 virus on day 0; PR8+STM: mice infected with PR8 virus on day 0, followed by *S.* Typhimurium administration on day 5; STM: mice infected with *S.* Typhimurium on day 5. All the mice illustrated were streptomycin-treated by oral gavage on day 4. The luminal content used to isolate the bacterial DNA was extracted at the end of the experiment on day 8. C) Schematic representation of the secondary *S.* Typhimurium infection model in absence of streptomycin pretreatment (typhoid model). WT and *Ifnar1*$^{-/-}$ mice were previously infected with PR8 or PBS on day 0, then infected with 10^3 CFU of *S.* Typhimurium or LB alone on day 5. D) *S.* Typhimurium load in the colon content at 72 h (8 dpi) after bacterial infection in the typhoid model. *P* values were calculated by two-tailed Mann-Whitney test.*$p < 0.05$; ns, not significant. One representative experiment is shown. N of mice used in each group in (D): PR8+STM = 8 WT

and 6 *Ifnar1*$^{-/-}$, STM = 8 WT and 6 *Ifnar1*$^{-/-}$.
(TIF)

S3 Fig. Poly I:C-induced IFN-Is promote S. Typhimurium intestinal colonization and systemic dissemination (i.p. model). A) Schematic of the i.p. pIC model. B, C, D, E) Colon content, MLN, lungs and spleen were harvested 72 h (day 3) post bacterial infection for enumeration of *S.* Typhimurium. *P* values were calculated by two-tailed Mann-Whitney test. *p value < 0.05, **p value < 0.01; ns, not significant. Data from two indipendent experiments are shown in (B, C, D and E). N of mice used in each group in (B): pIC +STM = 8 WT and 8 *Ifnar1*$^{-/-}$, STM = 8 WT and 8 *Ifnar1*$^{-/-}$. N of mice used in each group in (C, D, E): pIC +STM = 5–6 WT and 5 *Ifnar1*$^{-/-}$, STM = 5–6 WT and 5 *Ifnar1*$^{-/-}$.
(TIF)

S4 Fig. Poly I:C-induced IFN-Is promote S. Typhimurium intestinal colonization and systemic dissemination (non-surgical intratracheal instillation model). A) Schematic of the non-surgical intratracheal instillation pIC model. B, C, D, E) Colon content, MLN, lungs and spleen were harvested 72 h (day 3) post bacterial infection for enumeration of *S.* Typhimurium. *P* values were calculated by two-tailed Mann-Whitney test *p value < 0.05, **p value < 0.01; ns, not significant. Data from a representative experiment is shown. N of mice used in each group in (B, C, D, E): pIC +STM = 5 WT and 5 *Ifnar1*$^{-/-}$, STM = 5 WT and 5 *Ifnar1*$^{-/-}$.
(TIF)

S5 Fig. Poly I:C-induced IFN-Is inhibit host immunity during S. Typhimurium infection. A, B, C) *S100A9*, *Lcn2* and *Ifnγ* transcript levels were detected by qPCR in the i.p. pIC model from cecum of WT and *Ifnar1*$^{-/-}$mice 72 h post infection. D) Serum Ifnγ protein was assessed by ELISA in the i.p. pIC model from cecum of WT and *Ifnar1*$^{-/-}$mice 72 h post infection. E, F) HSP90α/β, Lcn2 and S100A9 were detected by immunoblot in the i.p. pIC model from cecum of WT (E) and *Ifnar1*$^{-/-}$(F) mice 72 h post infection from a representative experiment. Each dot represents one mouse, the geometric mean is indicated. *P* values were calculated by two-tailed Mann-Whitney test. *p value < 0.05, **p value < 0.01, ***p value < 0.001; ns, not significant. N of mice used in each group in (A, B, C, D): mock = 3 WT and 3 *Ifnar1*$^{-/-}$, pIC = 3–5 WT and 3–5 *Ifnar1*$^{-/-}$, pIC+STM = 7–10 WT and 7–10 *Ifnar1*$^{-/-}$, STM = 7–10 WT and 7–10 *Ifnar1*$^{-/-}$. N of mice used in each group in (E, F): mock = 1 WT and 1 *Ifnar1*$^{-/-}$, pIC = 4WT and 4 *Ifnar1*$^{-/-}$, pIC+STM = 5 WT and 5 *Ifnar1*$^{-/-}$, STM = 3 WT and 3 *Ifnar1*$^{-/-}$. The samples showed were pooled from two independent experiments in (A, B, C and D) or used from one representative experiment in (E, F).
(TIF)

S6 Fig. Poly I:C reduces cecal histopathology in WT mice, but not in *Ifnar1*$^{-/-}$ mice during *S.* Typhimurium infection (i.p. model). Blinded histopathology scores of cecal samples from WT (A, B and C) and *Ifnar1*$^{-/-}$ (A, C and, D) mice at 72 h post *S.* Typhimurium or mock infection, i.p. pIC- or mock- treated. The score of individual mice (circles) and the geometric mean for each group (bars) are indicated in (A). *P* values were calculated by two-tailed Mann-Whitney test. **p < 0.01; ns, not significant. One representative experiment is shown. N of mice used in each group in (A, C): mock = 3 WT and 3 *Ifnar1*$^{-/-}$, pIC = 3 WT and 2 *Ifnar1*$^{-/-}$, pIC+STM = 5 WT and 5 *Ifnar1*$^{-/-}$, STM = 5 WT and 5 *Ifnar1*$^{-/-}$. A detailed scoring for the animals shown in (A) is provided; each stacked column represents an individual mouse in (C). B and D) Hematoxylin and eosin (H&E)-stained sections from representative animals for each group in WT (B) and *Ifnar1*$^{-/-}$ (D) mice. Abbreviations are as follows: L, lumen; M, mucosa; SM, submucosa.
(TIF)

S7 Fig. Poly I:C reduces cecal histopathology in WT mice, but not in *Ifnar1*$^{-/-}$ mice during *S.* Typhimurium infection (non-surgical intratracheal instillation model). Blinded histopathology scores of cecal samples from WT (A, B and C) and *Ifnar1*$^{-/-}$ (A, C and D) mice at 72 h post *S.* Typhimurium or mock infection, treated or not with pIC through non-surgical intratracheal instillation. The score of individual mice (circles) and the geometric mean for each group (bars) are indicated in (A). *P* values were calculated by two-tailed Mann-Whitney test. $^{*}p < 0.05$; ns, not significant. One representative experiment is shown. N of mice used in each group in (A, C): mock = 2 WT and 2 *Ifnar1*$^{-/-}$, pIC = 3 WT and 3 *Ifnar1*$^{-/-}$, pIC+STM = 5 WT and 5 *Ifnar1*$^{-/-}$, STM = 5 WT and 5 *Ifnar1*$^{-/-}$. A detailed scoring for the animals shown in (A) is provided; each stacked column represents an individual mouse in (C). B and D) Hematoxylin and eosin (H&E)-stained sections from representative animals for each group in WT (B) and *Ifnar1*$^{-/-}$ (D) mice. Abbreviations are as follows: L, lumen; M, mucosa; SM, submucosa.
(TIF)

S1 Table. Strains and plasmids used in this study.
(DOCX)

S2 Table. Real-time qPCR primers used in this study.
(DOCX)

S1 References. Supplemental references cited only in the supporting information files.
(DOCX)

Acknowledgments

We would like to acknowledge Manuela Raffatellu and her lab for the gift of *Salmonella* Typhimurium strain, plasmids and precious suggestions, Natalie Quanquin for remarkable help with editing the manuscript, Maxime Chapon for helpful discussions, UCLA Genotyping and Sequencing Core for processing samples for Illumina MiSeq analysis, and CURE (Digestive Diseases Research Center), whose services were provided by the Imaging and Stem Cell Biology Core (ISCB).

Author Contributions

Conceived and designed the experiments: ED GMB GC. Performed the experiments: ED GMB XH SDB LC. Analyzed the data: ED GMB XH CP NR GC. Contributed reagents/materials/analysis tools: WS. Wrote the paper: ED.

References

1. Shahangian A, Chow EK, Tian X, Kang JR, Ghaffari A, Liu SY, et al. Type I IFNs mediate development of postinfluenza bacterial pneumonia in mice. J Clin Invest. 2009; 119(7):1910–20. Epub 2009/06/03. doi: 10.1172/JCI35412 PMID: 19487810; PubMed Central PMCID: PMC2701856.
2. Fensterl V, Sen GC. Interferons and viral infections. Biofactors. 2009; 35(1):14–20. Epub 2009/03/26. doi: 10.1002/biof.6 PMID: 19319841.
3. Doyle S, Vaidya S, O'Connell R, Dadgostar H, Dempsey P, Wu T, et al. IRF3 mediates a TLR3/TLR4-specific antiviral gene program. Immunity. 2002; 17(3):251–63. Epub 2002/10/02. PMID: 12354379.
4. Tough DF, Borrow P, Sprent J. Induction of bystander T cell proliferation by viruses and type I interferon in vivo. Science. 1996; 272(5270):1947–50. Epub 1996/06/28. PMID: 8658169.
5. Schneider WM, Chevillotte MD, Rice CM. Interferon-stimulated genes: a complex web of host defenses. Annu Rev Immunol. 2014; 32:513–45. Epub 2014/02/22. doi: 10.1146/annurev-immunol-032713-120231 PMID: 24555472; PubMed Central PMCID: PMC4313732.
6. Wang J, Li F, Wei H, Lian ZX, Sun R, Tian Z. Respiratory influenza virus infection induces intestinal immune injury via microbiota-mediated Th17 cell-dependent inflammation. J Exp Med. 2014; 211

(12):2397–410. Epub 2014/11/05. doi: 10.1084/jem.20140625 PMID: 25366965; PubMed Central PMCID: PMC4235643.

7. Turnbaugh PJ, Hamady M, Yatsunenko T, Cantarel BL, Duncan A, Ley RE, et al. A core gut microbiome in obese and lean twins. Nature. 2009; 457(7228):480–4. Epub 2008/12/02. doi: 10.1038/nature07540 PMID: 19043404; PubMed Central PMCID: PMC2677729.
8. Round JL, Mazmanian SK. Inducible Foxp3+ regulatory T-cell development by a commensal bacterium of the intestinal microbiota. Proc Natl Acad Sci U S A. 2010; 107(27):12204–9. Epub 2010/06/23. doi: 10.1073/pnas.0909122107 PMID: 20566854; PubMed Central PMCID: PMC2901479.
9. Ivanov II, Atarashi K, Manel N, Brodie EL, Shima T, Karaoz U, et al. Induction of intestinal Th17 cells by segmented filamentous bacteria. Cell. 2009; 139(3):485–98. Epub 2009/10/20. doi: 10.1016/j.cell.2009.09.033 PMID: 19836068; PubMed Central PMCID: PMC2796826.
10. Scales BS, Huffnagle GB. The microbiome in wound repair and tissue fibrosis. J Pathol. 2013; 229 (2):323–31. Epub 2012/10/09. doi: 10.1002/path.4118 PMID: 23042513; PubMed Central PMCID: PMC3631561.
11. Pfefferle PI, Renz H. The mucosal microbiome in shaping health and disease. F1000Prime Rep. 2014; 6:11. Epub 2014/03/05. doi: 10.12703/P6-11 PMID: 24592323; PubMed Central PMCID: PMC3914505.
12. Round JL, Mazmanian SK. The gut microbiota shapes intestinal immune responses during health and disease. Nat Rev Immunol. 2009; 9(5):313–23. Epub 2009/04/04. doi: 10.1038/nri2515 PMID: 19343057; PubMed Central PMCID: PMC4095778.
13. Garrett WS, Lord GM, Punit S, Lugo-Villarino G, Mazmanian SK, Ito S, et al. Communicable ulcerative colitis induced by T-bet deficiency in the innate immune system. Cell. 2007; 131(1):33–45. Epub 2007/10/10. doi: 10.1016/j.cell.2007.08.017 PMID: 17923086; PubMed Central PMCID: PMC2169385.
14. Winter SE, Winter MG, Xavier MN, Thiennimitr P, Poon V, Keestra AM, et al. Host-derived nitrate boosts growth of E. coli in the inflamed gut. Science. 2013; 339(6120):708–11. Epub 2013/02/09. doi: 10.1126/science.1232467 PMID: 23393266; PubMed Central PMCID: PMC4004111.
15. Dilantika C, Sedyaningsih ER, Kasper MR, Agtini M, Listiyaningsih E, Uyeki TM, et al. Influenza virus infection among pediatric patients reporting diarrhea and influenza-like illness. BMC Infect Dis. 2010; 10:3. Epub 2010/01/08. doi: 10.1186/1471-2334-10-3 PMID: 20053294; PubMed Central PMCID: PMC2820480.
16. Zheng D, Limmon GV, Yin L, Leung NH, Yu H, Chow VT, et al. A cellular pathway involved in Clara cell to alveolar type II cell differentiation after severe lung injury. PLoS One. 2013; 8(8):e71028. doi: 10.1371/journal.pone.0071028 PMID: 23940685; PubMed Central PMCID: PMCPMC3734298.
17. Yin L, Xu S, Cheng J, Zheng D, Limmon GV, Leung NH, et al. Spatiotemporal quantification of cell dynamics in the lung following influenza virus infection. J Biomed Opt. 2013; 18(4):046001. doi: 10.1117/1.JBO.18.4.046001 PMID: 23545853.
18. Winter SE, Thiennimitr P, Winter MG, Butler BP, Huseby DL, Crawford RW, et al. Gut inflammation provides a respiratory electron acceptor for Salmonella. Nature. 2010; 467(7314):426–9. Epub 2010/09/25. doi: 10.1038/nature09415 PMID: 20864996; PubMed Central PMCID: PMC2946174.
19. Peterson DA, Frank DN, Pace NR, Gordon JI. Metagenomic approaches for defining the pathogenesis of inflammatory bowel diseases. Cell Host Microbe. 2008; 3(6):417–27. Epub 2008/06/11. doi: 10.1016/j.chom.2008.05.001 PMID: 18541218; PubMed Central PMCID: PMC2872787.
20. Mattei F, Schiavoni G, Belardelli F, Tough DF. IL-15 is expressed by dendritic cells in response to type I IFN, double-stranded RNA, or lipopolysaccharide and promotes dendritic cell activation. J Immunol. 2001; 167(3):1179–87. Epub 2001/07/24. PMID: 11466332.
21. Tian X, Xu F, Lung WY, Meyerson C, Ghaffari AA, Cheng G, et al. Poly I:C enhances susceptibility to secondary pulmonary infections by gram-positive bacteria. PLoS One. 2012; 7(9):e41879. Epub 2012/09/11. doi: 10.1371/journal.pone.0041879 PMID: 22962579; PubMed Central PMCID: PMC3433467.
22. Barthel M, Hapfelmeier S, Quintanilla-Martinez L, Kremer M, Rohde M, Hogardt M, et al. Pretreatment of mice with streptomycin provides a Salmonella enterica serovar Typhimurium colitis model that allows analysis of both pathogen and host. Infect Immun. 2003; 71(5):2839–58. Epub 2003/04/22. PMID: 12704158; PubMed Central PMCID: PMC153285.
23. Behnsen J, Jellbauer S, Wong CP, Edwards RA, George MD, Ouyang W, et al. The cytokine IL-22 promotes pathogen colonization by suppressing related commensal bacteria. Immunity. 2014; 40(2):262–73. Epub 2014/02/11. doi: 10.1016/j.immuni.2014.01.003 PMID: 24508234; PubMed Central PMCID: PMC3964146.
24. Liu JZ, Jellbauer S, Poe AJ, Ton V, Pesciaroli M, Kehl-Fie TE, et al. Zinc sequestration by the neutrophil protein calprotectin enhances Salmonella growth in the inflamed gut. Cell Host Microbe. 2012; 11 (3):227–39. Epub 2012/03/20. doi: 10.1016/j.chom.2012.01.017 PMID: 22423963; PubMed Central PMCID: PMC3308348.

25. Nairz M, Fritsche G, Brunner P, Talasz H, Hantke K, Weiss G. Interferon-gamma limits the availability of iron for intramacrophage Salmonella typhimurium. Eur J Immunol. 2008; 38(7):1923–36. Epub 2008/06/27. doi: 10.1002/eji.200738056 PMID: 18581323.

26. Spees AM, Kingsbury DD, Wangdi T, Xavier MN, Tsolis RM, Baumler AJ. Neutrophils are a source of gamma interferon during acute Salmonella enterica serovar Typhimurium colitis. Infect Immun. 2014; 82(4):1692–7. Epub 2014/01/15. doi: 10.1128/IAI.01508-13 PMID: 24421037; PubMed Central PMCID: PMC3993401.

27. Harrington L, Srikanth CV, Antony R, Shi HN, Cherayil BJ. A role for natural killer cells in intestinal inflammation caused by infection with Salmonella enterica serovar Typhimurium. FEMS Immunol Med Microbiol. 2007; 51(2):372–80. doi: 10.1111/j.1574-695X.2007.00313.x PMID: 17727655; PubMed Central PMCID: PMCPMC3205980.

28. Rhee SJ, Walker WA, Cherayil BJ. Developmentally regulated intestinal expression of IFN-gamma and its target genes and the age-specific response to enteric Salmonella infection. J Immunol. 2005; 175 (2):1127–36. PMID: 16002714.

29. Ramarathinam L, Shaban RA, Niesel DW, Klimpel GR. Interferon gamma (IFN-gamma) production by gut-associated lymphoid tissue and spleen following oral Salmonella typhimurium challenge. Microb Pathog. 1991; 11(5):347–56. PMID: 1816488.

30. Nauciel C, Espinasse-Maes F. Role of gamma interferon and tumor necrosis factor alpha in resistance to Salmonella typhimurium infection. Infect Immun. 1992; 60(2):450–4. PMID: 1730475; PubMed Central PMCID: PMCPMC257648.

31. Corbin BD, Seeley EH, Raab A, Feldmann J, Miller MR, Torres VJ, et al. Metal chelation and inhibition of bacterial growth in tissue abscesses. Science. 2008; 319(5865):962–5. Epub 2008/02/16. doi: 10.1126/science.1152449 PMID: 18276893.

32. Flo TH, Smith KD, Sato S, Rodriguez DJ, Holmes MA, Strong RK, et al. Lipocalin 2 mediates an innate immune response to bacterial infection by sequestrating iron. Nature. 2004; 432(7019):917–21. Epub 2004/11/09. doi: 10.1038/nature03104 PMID: 15531878.

33. Deriu E, Liu JZ, Pezeshki M, Edwards RA, Ochoa RJ, Contreras H, et al. Probiotic bacteria reduce salmonella typhimurium intestinal colonization by competing for iron. Cell Host Microbe. 2013; 14(1):26–37. Epub 2013/07/23. doi: 10.1016/j.chom.2013.06.007 PMID: 23870311; PubMed Central PMCID: PMC3752295.

34. Kuhn R, Lohler J, Rennick D, Rajewsky K, Muller W. Interleukin-10-deficient mice develop chronic enterocolitis. Cell. 1993; 75(2):263–74. Epub 1993/10/22. PMID: 8402911.

35. Rennick DM, Fort MM, Davidson NJ. Studies with IL-10-/- mice: an overview. J Leukoc Biol. 1997; 61 (4):389–96. Epub 1997/04/01. PMID: 9103224.

36. Van der Sluis M, De Koning BA, De Bruijn AC, Velcich A, Meijerink JP, Van Goudoever JB, et al. Muc2-deficient mice spontaneously develop colitis, indicating that MUC2 is critical for colonic protection. Gastroenterology. 2006; 131(1):117–29. Epub 2006/07/13. doi: 10.1053/j.gastro.2006.04.020 PMID: 16831596.

37. Shan M, Gentile M, Yeiser JR, Walland AC, Bornstein VU, Chen K, et al. Mucus enhances gut homeostasis and oral tolerance by delivering immunoregulatory signals. Science. 2013; 342(6157):447–53. Epub 2013/09/28. doi: 10.1126/science.1237910 PMID: 24072822; PubMed Central PMCID: PMC4005805.

38. McNab F, Mayer-Barber K, Sher A, Wack A, O'Garra A. Type I interferons in infectious disease. Nat Rev Immunol. 2015; 15(2):87–103. Epub 2015/01/24. doi: 10.1038/nri3787 PMID: 25614319.

39. Ishihara T, Aga M, Hino K, Ushio C, Taniguchi M, Iwaki K, et al. Inhibition of chlamydia trachomatis growth by human interferon-alpha: mechanisms and synergistic effect with interferon-gamma and tumor necrosis factor-alpha. Biomed Res. 2005; 26(4):179–85. Epub 2005/09/13. PMID: 16152734.

40. Plumlee CR, Lee C, Beg AA, Decker T, Shuman HA, Schindler C. Interferons direct an effective innate response to Legionella pneumophila infection. J Biol Chem. 2009; 284(44):30058–66. Epub 2009/09/02. doi: 10.1074/jbc.M109.018283 PMID: 19720834; PubMed Central PMCID: PMC2781560.

41. Berry MP, Graham CM, McNab FW, Xu Z, Bloch SA, Oni T, et al. An interferon-inducible neutrophil-driven blood transcriptional signature in human tuberculosis. Nature. 2010; 466(7309):973–7. Epub 2010/08/21. doi: 10.1038/nature09247 PMID: 20725040; PubMed Central PMCID: PMC3492754.

42. O'Connell RM, Saha SK, Vaidya SA, Bruhn KW, Miranda GA, Zarnegar B, et al. Type I interferon production enhances susceptibility to Listeria monocytogenes infection. J Exp Med. 2004; 200(4):437–45. Epub 2004/08/11. doi: 10.1084/jem.20040712 PMID: 15302901; PubMed Central PMCID: PMC2211937.

43. Kawashima T, Kosaka A, Yan H, Guo Z, Uchiyama R, Fukui R, et al. Double-stranded RNA of intestinal commensal but not pathogenic bacteria triggers production of protective interferon-beta. Immunity. 2013; 38(6):1187–97. Epub 2013/06/25. doi: 10.1016/j.immuni.2013.02.024 PMID: 23791646.

44. Frank DN, St Amand AL, Feldman RA, Boedeker EC, Harpaz N, Pace NR. Molecular-phylogenetic characterization of microbial community imbalances in human inflammatory bowel diseases. Proc Natl Acad Sci U S A. 2007; 104(34):13780–5. Epub 2007/08/19. doi: 10.1073/pnas.0706625104 PMID: 17699621; PubMed Central PMCID: PMC1959459.

45. Vujkovic-Cvijin I, Dunham RM, Iwai S, Maher MC, Albright RG, Broadhurst MJ, et al. Dysbiosis of the gut microbiota is associated with HIV disease progression and tryptophan catabolism. Sci Transl Med. 2013; 5(193):193ra91. Epub 2013/07/12. doi: 10.1126/scitranslmed.3006438 PMID: 23843452; PubMed Central PMCID: PMC4094294.

46. Hohmann EL. Nontyphoidal salmonellosis. Clin Infect Dis. 2001; 32(2):263–9. doi: 10.1086/318457 PMID: 11170916.

47. Sing A, Merlin T, Knopf HP, Nielsen PJ, Loppnow H, Galanos C, et al. Bacterial induction of beta interferon in mice is a function of the lipopolysaccharide component. Infect Immun. 2000; 68(3):1600–7. PMID: 10678979; PubMed Central PMCID: PMCPMC97320.

48. Robinson N, McComb S, Mulligan R, Dudani R, Krishnan L, Sad S. Type I interferon induces necroptosis in macrophages during infection with Salmonella enterica serovar Typhimurium. Nat Immunol. 2012; 13(10):954–62. Epub 2012/08/28. doi: 10.1038/ni.2397 PMID: 22922364; PubMed Central PMCID: PMC4005791.

49. Gordon MA, Jack DL, Dockrell DH, Lee ME, Read RC. Gamma interferon enhances internalization and early nonoxidative killing of Salmonella enterica serovar Typhimurium by human macrophages and modifies cytokine responses. Infect Immun. 2005; 73(6):3445–52. Epub 2005/05/24. doi: 10.1128/IAI.73.6.3445–3452.2005 PMID: 15908373; PubMed Central PMCID: PMC1111838.

50. Broz P, Ohlson MB, Monack DM. Innate immune response to Salmonella typhimurium, a model enteric pathogen. Gut Microbes. 2012; 3(2):62–70. doi: 10.4161/gmic.19141 PMID: 22198618; PubMed Central PMCID: PMCPMC3370950.

51. Liang SC, Tan XY, Luxenberg DP, Karim R, Dunussi-Joannopoulos K, Collins M, et al. Interleukin (IL)-22 and IL-17 are coexpressed by Th17 cells and cooperatively enhance expression of antimicrobial peptides. J Exp Med. 2006; 203(10):2271–9. Epub 2006/09/20. doi: 10.1084/jem.20061308 PMID: 16982811; PubMed Central PMCID: PMC2118116.

52. Raffatellu M, George MD, Akiyama Y, Hornsby MJ, Nuccio SP, Paixao TA, et al. Lipocalin-2 resistance confers an advantage to Salmonella enterica serotype Typhimurium for growth and survival in the inflamed intestine. Cell Host Microbe. 2009; 5(5):476–86. Epub 2009/05/21. doi: 10.1016/j.chom.2009.03.011 PMID: 19454351; PubMed Central PMCID: PMC2768556.

53. Devireddy LR, Teodoro JG, Richard FA, Green MR. Induction of apoptosis by a secreted lipocalin that is transcriptionally regulated by IL-3 deprivation. Science. 2001; 293(5531):829–34. Epub 2001/08/04. doi: 10.1126/science.1061075 PMID: 11486081.

54. Li C, Chen H, Ding F, Zhang Y, Luo A, Wang M, et al. A novel p53 target gene, S100A9, induces p53-dependent cellular apoptosis and mediates the p53 apoptosis pathway. Biochem J. 2009; 422(2):363–72. Epub 2009/06/19. doi: 10.1042/BJ20090465 PMID: 19534726.

55. Schroll A, Eller K, Feistritzer C, Nairz M, Sonnweber T, Moser PA, et al. Lipocalin-2 ameliorates granulocyte functionality. Eur J Immunol. 2012; 42(12):3346–57. Epub 2012/09/12. doi: 10.1002/eji.201142351 PMID: 22965758.

56. Simard JC, Girard D, Tessier PA. Induction of neutrophil degranulation by S100A9 via a MAPK-dependent mechanism. J Leukoc Biol. 2010; 87(5):905–14. Epub 2010/01/28. doi: 10.1189/jlb.1009676 PMID: 20103766.

57. Santos RL, Raffatellu M, Bevins CL, Adams LG, Tukel C, Tsolis RM, et al. Life in the inflamed intestine, Salmonella style. Trends Microbiol. 2009; 17(11):498–506. Epub 2009/10/13. doi: 10.1016/j.tim.2009.08.008 PMID: 19819699; PubMed Central PMCID: PMC3235402.

58. Lee KS, Jeong ES, Heo SH, Seo JH, Jeong DG, Choi YK. IL-10 suppresses bactericidal response of macrophages against Salmonella Typhimurium. J Microbiol. 2011; 49(6):1050–3. Epub 2011/12/29. doi: 10.1007/s12275-011-1043-z PMID: 22203573.

59. Pie S, Matsiota-Bernard P, Truffa-Bachi P, Nauciel C. Gamma interferon and interleukin-10 gene expression in innately susceptible and resistant mice during the early phase of Salmonella typhimurium infection. Infect Immun. 1996; 64(3):849–54. PMID: 8641791; PubMed Central PMCID: PMCPMC173847.

60. Nikolaus S, Rutgeerts P, Fedorak R, Steinhart AH, Wild GE, Theuer D, et al. Interferon beta-1a in ulcerative colitis: a placebo controlled, randomised, dose escalating study. Gut. 2003; 52(9):1286–90. Epub 2003/08/13. PMID: 12912859; PubMed Central PMCID: PMC1773804.

61. Musch E, Andus T, Malek M, Chrissafidou A, Schulz M. Successful treatment of steroid refractory active ulcerative colitis with natural interferon-beta—an open long-term trial. Z Gastroenterol. 2007; 45(12):1235–40. Epub 2007/12/15. doi: 10.1055/s-2007-963378 PMID: 18080224.

62. Rudick RA, Ransohoff RM, Peppler R, VanderBrug Medendorp S, Lehmann P, Alam J. Interferon beta induces interleukin-10 expression: relevance to multiple sclerosis. Ann Neurol. 1996; 40(4):618–27. Epub 1996/10/01. doi: 10.1002/ana.410400412 PMID: 8871582.

63. Billiau A. Anti-inflammatory properties of Type I interferons. Antiviral Res. 2006; 71(2–3):108–16. Epub 2006/04/22. doi: 10.1016/j.antiviral.2006.03.006 PMID: 16626815.

64. Stojiljkovic I, Baumler AJ, Heffron F. Ethanolamine utilization in Salmonella typhimurium: nucleotide sequence, protein expression, and mutational analysis of the cchA cchB eutE eutJ eutG eutH gene cluster. J Bacteriol. 1995; 177(5):1357–66. Epub 1995/03/01. PMID: 7868611; PubMed Central PMCID: PMC176743.

65. Prentki P, Krisch HM. In vitro insertional mutagenesis with a selectable DNA fragment. Gene. 1984; 29 (3):303–13. Epub 1984/09/01. PMID: 6237955.

66. Rayamajhi M, Redente EF, Condon TV, Gonzalez-Juarrero M, Riches DW, Lenz LL. Non-surgical intratracheal instillation of mice with analysis of lungs and lung draining lymph nodes by flow cytometry. J Vis Exp. 2011;(51:). doi: 10.3791/2702 PMID: 21587154; PubMed Central PMCID: PMCPMC3280633.

67. Li Y, Ku CY, Xu J, Saxena D, Caufield PW. Survey of oral microbial diversity using PCR-based denaturing gradient gel electrophoresis. J Dent Res. 2005; 84(6):559–64. Epub 2005/05/26. PMID: 15914595.

68. Sheffield VC, Cox DR, Lerman LS, Myers RM. Attachment of a 40-base-pair G + C-rich sequence (GC-clamp) to genomic DNA fragments by the polymerase chain reaction results in improved detection of single-base changes. Proc Natl Acad Sci U S A. 1989; 86(1):232–6. Epub 1989/01/01. PMID: 2643100; PubMed Central PMCID: PMC286438.